

**Pore Scale Investigations on the Dynamics of SAGD Process and Residual Oil Saturation
Development**

by

Francisco Javier Argüelles-Vivas

A thesis submitted in partial fulfillment of the requirements for the degree of

Doctor of Philosophy

in

Petroleum Engineering

Department of Civil and Environmental Engineering
University of Alberta

© Francisco Javier Argüelles-Vivas, 2015

ABSTRACT

Since its invention, steam assisted gravity drainage (SAGD) demonstrated to be a viable technology to recover heavy oil and bitumen from oil sands. However, the field experience over the last two decades indicated that, oil recovery factor is below the expected values determined from the scaled physical lab models. Knowing that the reduction of the high cost of steam is quite difficult, efforts should be made towards the improvement of the recovery factor (or reducing the residual oil saturation, S_{or}). Thus, the analysis of the development of S_{or} at the macro and micro scales turns out to be a critical problem.

S_{or} is impacted by the dynamics of the SAGD process, reservoir properties and operational conditions. The objective of this dissertation is to systematically investigate the physical reasons behind the formation of S_{or} at the micro scale focusing on the effects of the dynamics of SAGD and characteristics of the reservoir. This research begins with a study on S_{or} development in capillary tubes considering variable temperatures. Then, Computational Fluid Dynamics (CFD) approach is used to investigate the development of S_{or} at temperature and pressure conditions that are difficult to reproduce through physical experiments. Using the observations through these analyses and data, the effects of a temperature gradient on the flow dynamics, oil recovery and relative permeabilities are investigated analytically for single and bundle of cylindrical capillaries. Finally, the dynamics of the SAGD process and the development of S_{or} are studied through 2-D glass bead models visually.

The results show that the S_{or} is a dynamic property that depends on the balance of the acting forces, the temperature and the temperature gradient. A detailed analysis is carried out starting from the physics in a pore. The displacement and trapping mechanisms during the formation of

the steam chamber are elucidated and it is demonstrated how those affect the residual oil saturation development. It is also shown how the pore size, the heterogeneities and the wettability are responsible for low oil recovery factors to a great extent.

Dedicated to my wonderful family,

My grandma Carmen, my mom Maria del Carmen, my dad Homegar, my brother Homegar and family, my sister Carmen and my lovely twin Isabel

and,

To the love of my life *Adriana Bustos – Cruz*

ACKNOWLEDGMENTS

First of all, I want to thank my supervisor Dr. Tayfun Babadagli for his valuable advice and support through my PhD studies. I am thankful for your willingness to help me whenever I knocked on your door, regardless of the day -weekdays, weekends, holidays- or if it were a non-scheduled meeting. I respect your professionalism and knowledge, and seriousness with the students and research. My sincerest gratitude for all of your guidance, Dr. Babadagli.

I am thankful for the love and support of my great family. Thank you to my parents Maria Del Carmen Vivas Fayad and Homegar Arguelles Salazar, and my grandma Carmen Fayad Serna for all the efforts and sacrifices made so that I could have a good life and education. I am also thankful to my brother Homegar and family and my sisters Carmen and Isabel for your love and support.

I am especially grateful to Adriana Bustos – Cruz, my love and life partner. Thank you for your love, support and patience during all of these years. Thanks also for your understanding my decision to come to Canada and for waiting for me while I went through this long journey to achieve this dream. I am very lucky that you love me. I love you so much.

I would also like to thank my committee members Dr. Ergun Kuru, Dr. Ryosuke Okuno, Dr. Huazhou Li, Dr. Anthony Young and the external examiner Dr. Hemanta Sarma for your time to read, discuss and comment on my thesis. I am also thankful to my candidacy committee members Dr. Qingxia Liu and Dr. Zaher Hashisho for your time and suggestions on how to improve my research.

I am grateful for the financial support of CONACYT (National Council of Science and Technology-Mexico) during my graduate studies at the University of Alberta. This research was conducted under Dr. Babadagli's NSERC Industrial Research Chair in Unconventional Oil Recovery (industrial partners are CNRL, SUNCOR, Petrobank (Touchstone Exploration), Sherritt Oil, APEX Engineering, PEMEX, Saudi Aramco, and Husky Energy).

I am thankful to the following people who enriched my investigation with their comments and discussions: Dr. Zhenghe Xu from the Department of Chemical and Materials Engineering, Dr.

Carlos Lange, from the Department of Mechanical Engineering (who let me partake in the CFD course, and for treating me as a student and providing consultancy when needed), my cousin, Dr. Cesar Ortega Vivas, and my Mexican friends Dr. Carlos Amir Escalante Velazquez and Victor Matías Perez.

My gratitude to the EOGRRRC lab technicians, especially to Mihaela Istratescu for being so helpful and kind in the last stage of my research and to whom I now consider a good friend. Thanks also to Anna Zhang, Todd Kinee and Lixing Lin. Thanks to Pamela Keegan for editing my papers and thesis.

My gratitude is extended to all past and current EOGRRRC members. I want to mention my Mexican friends Jose Ramon Mayorquin-Ruiz and Hector Leyva-Gomez and their families for always making me feel as though I were an old friend. Thanks for all your support through these years. I always felt safe knowing that I could ask you for help if I needed it. Thanks to my friends Yousef Hamedi, Varun Pathak, Ekaterina Stalgorova, Hannes Hofmann, Mohammedalmojtaba Mohammed, Khosrow Naderi, Achinta Bera and Andrea Marciales-Ramirez. I will remember all of you as a part of this adventure.

Finally, thanks to all the friends who I met in Canada and my old friends in Mexico for letting me to be part of your lives.

TABLE OF CONTENTS

Chapter 1 : Introduction	1
1.1 Background.....	2
1.2 Residual Oil Saturation in SAGD	3
1.3 Dynamics of SAGD at pore scale	5
1.4 Statement of the problem and objectives.....	7
1.5 Outline	9
1.6 References.....	10
Chapter 2 : Drainage Type Oil and Heavy-Oil Displacement in Circular Capillary Tubes: Two- and Three-Phase Flow Characteristics and Residual Oil Saturation Development in the Form of Film at Different Temperatures	12
2.1 Introduction.....	14
2.2 Experimental Work.....	17
2.2.1 <i>Setup</i>	17
2.2.2 <i>Fluids and their properties with respect to temperature</i>	18
2.2.3 <i>Experimental details</i>	20
2.3 Results and discussion	22
2.3.1 <i>Analysis of film thickness in horizontal displacements</i>	23
2.3.2 <i>Residual oil saturation behavior in horizontal and vertical displacements</i>	30
2.4 Conclusions.....	42
2.5 References.....	44
Chapter 3 : Residual Liquids Saturation Developments During Two and Three Phase Flow under Gravity in Square Capillaries at Different Temperatures	48
3.1 Introduction.....	49
3.1.1 <i>Statement of the problem</i>	49
3.1.2 <i>Background and solution methodology</i>	50

3.2	Experimental Work	52
3.2.1	<i>Set up</i>	52
3.2.2	<i>Fluid properties</i>	52
3.2.3	<i>Capillary tubes</i>	53
3.2.4	<i>Experimental procedure</i>	53
3.3	Results and Discussion	55
3.3.1	<i>Two phase flow system: Air – heavy oil</i>	56
3.3.1.1	<i>Gravity drainage experiments at different trapping numbers and temperatures</i>	56
3.3.1.2	<i>Effects of travel distance by the liquid phase (heavy oil) on S_{or} during FFGD</i>	59
3.3.1.3	<i>Effects of oil slug length on S_{or} during FFGD</i>	60
3.3.1.4	<i>Effects of characteristic length of square capillaries on S_{or} during FFGD</i>	61
3.3.1.5	<i>Layer thickness of S_{or} in FFGD experiments</i>	62
3.3.2	<i>Three phase flow system: Air – heavy oil – water</i>	64
3.3.2.1	<i>Gravity drainage experiments at different trapping numbers and temperatures</i>	64
3.3.2.2	<i>Effects of fluid distribution on the residual liquids saturation during Free Fall Gravity Drainage (FFGD)</i>	68
3.3.2.3	<i>Effects of wettability on the residual liquids saturation during FFGD</i>	73
3.4	Conclusions and remarks	74
3.5	References.....	76
3.6	Appendix.....	80
 Chapter 4 : Gas-Heavy Oil Displacement in Capillary Media at High Temperatures: A CFD Approach to Model Microfluidics Experiments		82
4.1	Introduction.....	83
4.2	Numerical modeling in CFX.....	87
4.2.1	<i>Multiphase flow equations</i>	87
4.2.2	<i>Surface Tension and Wettability Model</i>	88
4.2.3	<i>Volume of Fluid Method (VOF)</i>	89

4.3	Solution methodology.....	89
4.3.1	<i>Body diagram of the problem and geometry</i>	89
4.3.2	Meshing.....	91
4.3.3	<i>Fluids and properties</i>	92
4.3.4	<i>Boundary conditions</i>	92
4.3.5	<i>Simulations cases</i>	93
4.3.6	<i>Solver solution technique</i>	93
4.4	Results and Discussion.....	94
4.4.1	<i>Development of S_{or} along the square capillary</i>	94
4.4.2	<i>Visualization of the S_{or} formation</i>	99
4.4.3	<i>Change of S_{or} with time</i>	101
4.4.4	<i>Wettability effects</i>	102
4.5	Conclusions.....	102
4.6	References.....	103

Chapter 5 : Analytical Solutions and Derivation of Relative Permeabilities for Water–Heavy Oil Displacement and Gas–Heavy Oil Gravity Drainage Under Non-Isothermal Conditions 105

5.1	Introduction.....	106
5.2	Theoretical work: development of non – isothermal models.....	109
5.2.1	<i>Non-isothermal water–heavy oil displacement</i>	109
5.2.2	<i>Non-isothermal gas–heavy oil gravity drainage</i>	113
5.3	Results and Discussion: Application of non-isothermal models.....	116
5.3.1	<i>Fluid properties</i>	117
5.3.2	<i>Non – isothermal water – heavy oil displacements</i>	118
5.3.3	<i>Non – isothermal gas – heavy oil gravity drainage displacements</i>	121
5.3.4	<i>Effects of non – isothermal conditions on relative permeability curves</i>	123
5.3.5	<i>Limitations of the model, potential improvements and considerations for field scale modeling</i>	130
5.4	Conclusions.....	131

5.5 Nomenclature.....	132
5.6 References.....	134
Chapter 6 : Pore Scale Investigations on the Dynamics of Gravity Driven Steam Displacement Process for Heavy Oil Recovery and Development of Residual Oil Saturation: A 2-D Visual Analysis.....	139
6.1 Introduction.....	140
6.2 Background of Residual Oil Saturation Development in SAGD	141
6.3 Experimental Work.....	145
6.3.1 Models and materials	145
6.3.2 Setup	147
6.3.3 Procedure	148
6.4 Results and discussion	148
6.4.1 Dynamics of S_{or} and trapping mechanisms during the lateral expansion of steam chamber	148
6.4.2 Dynamics of S_{or} and trapping mechanisms during half symmetric SAGD chamber growth	153
6.4.3 Shape of the steam chamber	161
6.4.4 Effects on porous medium characteristics on S_{or}	162
6.4.4.1 Effects on permeability on S_{or}	162
6.4.4.2 Effects of pore scale heterogeneities on S_{or}	164
6.4.4.2.1 Small glass beads surrounded by big glass beads.....	164
6.4.4.2.2 Big glass beads surrounded by small glass beads.....	167
6.4.4.3 Effects of wettability	169
6.5 Conclusions.....	170
6.6 References.....	174
Chapter 7 : Summary, Contributions and Recommendations	176
7.1 Summary of the research	177
7.2 Limitations and applicability of this research.....	177

7.3 Scientific and practical contributions to the literature and industry	180
7.4 Suggested future work	185
BIBLIOGRAPHY	186

LIST OF TABLES

Table 2-1: Fluid properties.....	20
Table 3-1: Fluids properties (taken from [5], except σ_{ow})	53
Table 4-1: Mesh information for the simulations runs.	91
Table 4-2: Air and heavy oil properties used in the simulations runs.	92
Table 4-3: Simulation cases and dimensionless numbers.....	93

LIST OF FIGURES

Figure 1-1: SAGD concept.	5
Figure 2-1: Experimental set-up: a) horizontal displacements; b) vertical displacements.	18
Figure 2-2: Kerosene viscosity behavior with respect to temperature.....	18
Figure 2-3: Surface tension behavior for air-kerosene and air-heavy oil A systems.....	19
Figure 2-4: Heavy oil A viscosity behavior with respect to temperature	19
Figure 2-5: Evolution of the contact angle between air-heavy oil A – pyrex glass at different temperatures.....	20
Figure 2-6: Graphical description of the residual oil saturation measurements.	21
Figure 2-7: Comparison of kerosene film thickness with Bretherton model in a capillary tube ..	24
of $r=0.025$ cm.....	24
Figure 2-8: Comparison of heavy oil film thickness with Bretherton model in a capillary tube .	27
Figure 2-9: Comparison of fraction of fluid left behind (kerosene) in a capillary tube of $r=0.025$ cm.....	29
Figure 2-10: Comparison of fraction of fluid left behind (heavy oil) in a capillary tube of $r=0.025$ cm.....	29
Figure 2-11: Residual oil saturation (kerosene) vs. capillary number in a circular capillary tube showing the different injection rates.....	31
Figure 2-12: Residual oil saturation (kerosene) vs. capillary number in a circular capillary tube showing the effect of 1.5% of water saturation at $T=23.5$ °C.....	34
Figure 2-13: Residual oil saturation (kerosene) vs. capillary number in a circular capillary tube showing the effect of 1.5% of water saturation at $T=85$ °C.....	34
Figure 2-14: Residual oil saturation in the presence of initial water saturation.	35
Figure 2-15: Spreading of kerosene (red fluid) over water a) $T=23.5$ °C, b) $T=85$ °C.....	35
Figure 2-16: Residual oil saturation (heavy oil) vs. capillary number in a circular capillary tube showing different injection rates.....	36
Figure 2-17: Air-heavy oil A displacement at 47.55 cc/hr showing the residual oil saturation and the formation of collars and lenses at different times of the process.....	37
Figure 2-18: Residual oil saturation (heavy oil) vs. capillary number during a gravity drainage in a capillary tube of $r=0.025$ cm.	39
Figure 2-19: Comparison of residual oil saturation (heavy oil) vs. capillary number in a circular capillary in vertical displacements for two different radii.....	39
Figure 2-20: Comparison of residual oil saturation (heavy oil) vs. trapping number in a circular capillary tube for vertical displacements for two different radii.....	41
Figure 2-21: Comparison of residual oil saturation (heavy oil) vs. capillary number in a circular capillary tube for horizontal and vertical displacements.	42
Figure 3-1: Experimental Setup [5]. ... 52	52
Table 3-1: Fluids properties (taken from [5], except σ_{ow})	53

Figure 3-2: Cross sectional area of a circular capillary tube with $D=0.03$ cm (left) and square capillary tube with $W=0.03$ cm.....	53
Figure 3-3: Description of the residual oil saturation measurements (taken and modified from Ref. [5]).....	54
Figure 3-4: Residual oil saturation (heavy oil) vs. trapping number in a square capillary tube ($W=0.03$ cm) at high temperatures.	56
Figure 3-5: Comparison of the residual oil saturations in the square ($W=0.03$ cm) and circular ($D=0.032$ cm) capillary tubes (data of the circular tube experiments taken from Argüelles - Vivas and Babadagli [5]).....	58
Figure 3-6: Pictures of the square capillary tube ($W=0.03$ cm): a) before the displacement, b) rear meniscus of the oil slug in FFGD at 85 °C, c) oil layers in the angular zones 4 cm behind the rear meniscus, d) oil layer in the angular zones at 37 cm behind the rear meniscus.	59
Figure 3-8: Effects of the travel distance on the oil slug on the S_{or} during FFGD experiments...	60
Figure 3-9: Effects of the slug size on the S_{or} during FFGD experiments.....	60
Figure 3-10: Effects of characteristic length (or width) through Bond number on S_{or}	61
Figure 3-11: Measurements of layer thickness in a square capillary tube ($W=0.03$ cm)	63
Figure 3-12: Average layer thickness in square capillary tube of $W=0.03$ cm during a free fall gravity drainage at $T=55$ °C.....	63
Figure 3-13: Average layer thickness in square capillary tube of $W=0.03$ cm during a free fall gravity drainage at $T=85$ °C.....	64
Figure 3-14: Comparison of residual oil saturation between air – heavy oil and air-heavy oil – initial water systems at $T=55$ °C in a square capillary ($W=0.03$ cm).	65
Figure 3-15: Comparison of residual oil saturation between air – heavy oil and air-heavy oil – initial water systems at $T=85$ °C in a square capillary ($W=0.03$ cm).	65
Figure 3-16: Total oil and water saturation during air-heavy oil – water gravity drainage experiments at $T=55$ °C in a square capillary ($W=0.03$ cm).	66
Figure 3-17: Total oil and water saturation during air-heavy oil – water gravity drainage experiments at $T=85$ °C in a square capillary ($W=0.03$ cm).	66
Figure 3-18: Water saturation during air-heavy oil – water gravity drainage experiments at $T=55$ °C and $T=85$ °C in a square capillary ($W=0.03$ cm).	67
Figure 3-19: Photos of water and oil in a square capillary ($W=0.03$ cm) after a FFGD at 55 °C for air – heavy oil – water system: a) rear meniscus b) oil slug over water saturation.....	68
Figure 3-20: Different fluid distribution during FFGD experiments in square capillary ($W=0.03$ cm).	69
Figure 3-21: Residual oil saturation under different fluid configurations in square capillary tubes ($W=0.03$ cm).....	70
Figure 3-22: Residual water saturation under different fluid configurations in square capillary tubes ($W=0.03$ cm).	70
Figure 3-23: Engulfment of water in heavy oil: a) $T=25$ °C, b) $T=55$ °C, c) $T=85$ °C.....	71

Figure 3-24: Photos of water and oil in a square capillary (W=0.03 cm) after a FFGD for air-water – heavy oil configuration at T=55 °C.....	72
Figure 3-25: Residual oil saturation in WW AND OW square capillary tubes (W=0.03 cm) for FFGD experiments.....	73
Figure 3-26: Residual water saturation in WW AND OW square capillary tubes (W=0.03 cm) for FFGD experiments.....	74
Figure 4-1: Body diagram and selection of geometry.	90
Figure 4-2: Profile of the air -heavy oil displacements and zones of the interface: a) constant thickness region, b) transition zone, c) cap region.....	91
Figure 4-3: Boundary conditions for the simulations cases.....	92
Figure 4-4: Residual oil saturation in cross sectional planes along the square capillary at 55 °C. (UG: Uniform Grid, 10L 1.1GR:10 Inflation layers with 1.1 Growth Rate, 10L 1.1GR:10 Inflation layers with 1.2 Growth Rate, 15L 1.1GR:15 Inflation layers with 1.1 Growth Rate, 15L 1.2GR:15 Inflation layers with 1.2 Growth Rate, 23L 1.1GR:23 Inflation layers with 1.1 Growth Rate).....	95
Figure 4-5: Residual oil saturation in cross sectional planes along the square capillary at 85 °C. (UG: Uniform Grid, 10L 1.1GR:10 Inflation layers with 1.1 Growth Rate, 10L 1.1GR:10 Inflation layers with 1.2 Growth Rate, 15L 1.1GR:15 Inflation layers with 1.1 Growth Rate, 15L 1.2GR:15 Inflation layers with 1.2 Growth Rate, 23L 1.1GR:23 Inflation layers with 1.1 Growth Rate).....	96
Figure 4-6: Comparison of the S_{or} in a cross sectional plane at $2.5E-4$ for the tested grids at 85 °C. (red color is heavy oil, the rest is air: I: Uniform Grid, II: 10 Inflation layers with 1.1 Growth Rate, III: 10 Inflation layers with 1.2 Growth Rate, IV: 15 Inflation layers with 1.1 Growth Rate, V: 15 Inflation layers with 1.2 Growth Rate, VI: 23 Inflation layers with 1.1 Growth Rate).....	97
Figure 4-7: Residual oil saturation in cross sectional planes along the square capillary at 200 °C. (UG: Uniform Grid, 10L 1.1GR:10 Inflation layers with 1.1 Growth Rate, 10L 1.1GR:10 Inflation layers with 1.2 Growth Rate, 15L 1.1GR:15 Inflation layers with 1.1 Growth Rate, 15L 1.2GR:15 Inflation layers with 1.2 Growth Rate, 23L 1.1GR:23 Inflation layers with 1.1 Growth Rate).....	98
Figure 4-8: 3D and 2D air - heavy oil displacements at 55, 85, and 200 °C.	100
Figure 4-9: Change of S_{or} with respect to time in a cross sectional plane located at the middle of the square capillary for 55, 85, and 200 °C.....	101
Figure 4-10: Change of S_{or} with respect to the contact angle at different temperatures.....	102
Figure 5-1: Non-isothermal water–heavy oil displacement in a single capillary tube.	109
Figure 5-2: Non-isothermal gas–heavy oil gravity drainage displacement in a single capillary tube.....	113
Figure 5-3: Viscosity behavior with respect to temperature: a) heavy oil viscosity, b) water viscosity.	117
Figure 5-4: Interfacial tension behavior with respect to temperature: a) water–heavy oil, b) air–heavy oil.....	118

Figure 5-5: Location of the water–heavy oil interface in a capillary tube of $R = 0.00005$ m for isothermal and non-isothermal cases.	118
Figure 5-6: Dimensionless velocity of the water–heavy oil interface in a capillary tube of $R = 0.00005$ m for isothermal and non-isothermal cases.	119
Figure 5-7: Location of the water-heavy oil interface in a capillary tube of $R = 0.00005$ m in a spontaneous imbibition process for isothermal and non-isothermal cases.	119
Figure 5-8: An illustrative example of the effects of: a) positive temperature gradient, b) negative temperature gradient.	120
Figure 5-9: Positions of water – heavy oil interfaces in a bundle of capillary tube for isothermal and non-isothermal cases: a) 10000 s b) 40000 s.	121
Figure 5-10: Location of the gas–heavy oil interface in a capillary tube of $R = 0.00005$ m for isothermal and non-isothermal cases.	121
Figure 5-11: Dimensionless velocity of the gas–heavy oil interface in a capillary tube of $R = 0.00005$ m for isothermal and non-isothermal cases.	122
Figure 5-12: Positions of gas–heavy oil interfaces in a bundle of capillary tubes for isothermal and non-isothermal cases: a) $t = 1000$ s, b) 3000 s.	122
Figure 5-13: Representation of oil sands as bundles of capillaries tubes during gas and water injection.....	123
Figure 5-14: Water –heavy oil relative permeability curves at isothermal and non–isothermal conditions for a bundle of parallel and non-interconnected capillary tubes.	126
Figure 5-15: Gas–heavy oil relative permeability curves at isothermal and non-isothermal conditions for a bundle of parallel and non-interconnected capillary tubes.	127
Figure 6-1: Theorized SAGD concept.	143
Figure 6-2: Relationship of S_{or} in capillaries with SAGD (Figure in left side taken from Mohammadzadeh and Chatzis, 2009; 2010; 2012).....	144
Figure 6-3: Emulsion formation observed by Arguelles and Babadagli (2015, Figure in left side) and Mohammadzadeh and Chatzis (2009, Figure in right side,) at different scales.	145
Figure 6-4: Framework and glass beads model to carry out the steam injection experiments. ..	146
Figure 6-5: Heavy oil viscosity behavior with temperature.....	147
Figure 6-6: Experimental system a) oven with container, b)steam lines, c) temperature controller, d) inlet valve and manometer, e) a vacuum chamber, f) glass beads model, g) production port, h)data acquisition system, and i) a camera to record pore scale events.....	147
Figure 6-7: Steam chamber lateral growth (s: steam, w: water, o: oil).....	149
Figure 6-8: Temperature profiles during the lateral expansion of the steam chamber experiment.	150
Figure 6-9: Dynamics at pore scale during the lateral expansion of SAGD (s: steam, w: water, o: oil).	150
Figure 6-10: (a) Direct steam displacement and flow of film; (b) existence of films, water (w), trapped blobs and steam (s) within steam chamber (s: steam, w: water).....	152
Figure 6-11: Shapes of residual oil: (a) films connected by blobs, (b) islands of oil and blobs.	153

Figure 6-12: Half symmetric SAGD chamber growth (s: steam, w: water, o: oil).....	154
Figure 6-13: The birth of the steam chamber (s: steam, w-o: water in oil emulsion).....	155
Figure 6-14: Early spreading of the steam chamber showing irregular interface at pore scale (s: steam, w: water, w-o: water in oil emulsion).....	156
Figure 6-15: Residual oil saturation formation during the upward and outward growing of the steam chamber (s: steam, w: water, w-o: water in oil emulsion).....	156
Figure 6-16: Residual oil saturation formation during the expansion of the steam chamber (s: steam, w: water, w-o: water in oil emulsion).....	157
Figure 6-17: Sequence of capillary (hydraulic) continuity lost in the ceiling part of the steam chamber (s: steam).....	159
Figure 6-18: Capillary tube experiment where there is not hydraulic continuity and thus there is not counter-current flow.	160
Figure 6-19: Capillary tube experiment where hydraulic continuity exists and there is counter-current flow.	161
Figure 6-20: Permeability effects on S_{or} during lateral expansion of steam chamber: (a) 3 mm model (2 hours), (b1) 1 mm model (2 hours) and (b2) 1 mm model (7 hours). (s: steam, w: water, o: oil).....	163
Figure 6-21: Close up of the S_{or} shapes of (a) 3 mm model and (b) 1 mm model of Figure 6-20.	164
Figure 6-22: Sequence of stages during the lateral expansion of steam in a model of small beads clusters surrounded by big beads (s: steam, w:water, o:oil).	165
Figure 6-23: Final state of the residual oil saturation in the model of small beads clusters surrounded by big beads.	167
Figure 6-24: Sequence of stages during the lateral expansion of steam in a model of big beads clusters surrounded by small beads (w: water).	167
Figure 6-25: Final state of the residual oil saturation in the model of big beads clusters surrounded by small beads (w: water).	168
Figure 6-26: Wettability effects on S_{or} : (a) 3 mm water wet model, (b) 3 mm strongly oil wet model, and (c) 2 mm mixed wettability model.	169
Figure 6-27: Close up of the S_{or} shapes for the wettability cases shown in Figure 6-26.....	170

Chapter 1: Introduction

1.1 Background

Due to increasing world energy demand and continuous depletion of conventional oil reservoirs, heavy oil and bitumen fields have become critically important in meeting future energy needs. Techniques considered for heavy-oil and bitumen recovery can be categorized as (1) thermal methods and (2) miscible injection. While miscible injection has not become a commercial application yet, thermal methods, especially Steam Assisted Gravity Drainage (SAGD), has been widely applied to produce heavy oil and bitumen in Canada since the late 80s and more recently in Venezuela.

The concept of SAGD was developed by Butler in the late 1970s (Al-Bahlani and Babadagli, 2009). It basically consists of injecting steam at a constant pressure through an upper horizontal well located near the bottom part of the pay zone and producing oil in another horizontal well located around 5-10 meters below the injection well. Steam rises to the upper part of the reservoir forming a growing steam chamber and condenses in its perimeter due to heat transfer (mainly by conduction). Then, water and mobile oil flow to the production well due to the interplay of gravity and capillary forces (Butler, 1994; Al-Bahlani and Babadagli, 2009; Mohammadzadeh and Chatzis, 2009 and 2010). As the oil is being produced, the steam chamber grows up vertically and laterally (Butler, 1994). Mohammadzadeh and Chatzis (2009) explained that SAGD process advances through four subsequent stages based on the steam chamber growing, the following occur: a) communication between injector and producer wells, b) vertical development of steam chamber, c) lateral expansion of steam chamber, and d) falling-down of steam chamber driving to depletion.

Although SAGD was conceived to recover heavy oil or bitumen more efficiently than steam drive processes, there are still many challenges to tackle at the micro and macro scales to make the process technically and economically feasible (Al-Bahlani and Babadagli, 2009). Al-Bahlani and Babadagli (2009) published a review of these challenges involved in SAGD. These can be classified in five categories: (1) mechanics of SAGD, (2) reservoir properties, (3) SAGD operation, (4) numerical modeling, and (5) improvements.

One of the critical issues that has received very little attention, although it is one of the most important variables in the economics of the process, is the development of residual oil saturation

(S_{or}). S_{or} is a dynamic property that can dictate the continuation or discontinuation of a SAGD operation. It is influenced by the mechanics of SAGD, the reservoir properties, and the field operation. Actually, nowadays, it is known that the oil recovery factor of completed SAGD projects at field scale is not that expected.

In this thesis, the focus is to investigate the impact of the dynamics of SAGD and the nature of the reservoir on the formation of residual oil saturation at the micro scale. Experimental, analytical, and numerical tools are used for this purpose.

1.2 Residual Oil Saturation in SAGD

Recently, it was concluded through an analysis of field performance of SAGD projects (Jimenez, 2008) that geology and reservoir properties are by far the most dominant features for a successful SAGD operation. According to this data, the highest ultimate recoveries of the SAGD projects at the field scale have been between around 60–70% OOIP assuming that the above mentioned features are suitable. However, the average recovery factor is only around 30-40%. Jimenez (2008) also stated that concerns on geology and reservoir properties include reservoir thickness, shale barriers, porosity, and oil saturation. He did not observe enough evidence to suggest that k_v/k_h played a significant role as long as the vertical continuity exists and permeability is high.

Baker et al. (2010) concluded through available production, injection pressure, seismic and temperature logs for two different SAGD projects that oil recovery of a thermal project is highly dependent on the displacement and volumetric sweep efficiency and that heterogeneity and fluid dynamics strongly affect the shape of the steam chamber. Volumetric sweep efficiency is a macroscopic parameter that is dependent on flooding pattern design, number of injectors, reservoir continuity, and reservoir heterogeneity whereas displacement efficiency is a microscopic parameter that involves the interplay among the capillary, gravity and viscous forces at pore scale. The effects of capillary forces are the most difficult to understand since they involve wettability and interfacial tensions, particle size, particle size distribution, microscopic heterogeneities, and pore structure issues.

Although it is recognized that the average macroscopic behaviour of flow in porous media is a result of microscopic transport mechanisms, there is a lack of experimental and theoretical works

of the mechanics of SAGD at the pore scale. In general, the consensus on the reasons behind low recovery factor is related to (a) the nature of the reservoir, (b) the dynamics of fluid flow in the porous medium, and (c) the technical problems due to facilities and engineering designs.

In the original idea of SAGD, Butler (1991) assumed that as the steam chamber grows up and the oil and condensates are produced, the oil zone is swept immediately reaching the residual oil saturation. Moreover, for theoretical works, it is necessary to know the mobile oil and the average residual oil saturations accurately, which are initially estimated using an equation developed by Cardwell and Parsons (1949) based on the theory of air-liquid free fall gravity drainage:

$$\hat{S}_{or} = \frac{(b-1)}{b} \left(\frac{v_s \phi Z}{bkgt} \right)^{1/(b-1)} \quad (1)$$

Where \hat{S}_{or} is the average residual oil saturation after time t , Z is the drainage height, k is the absolute permeability, b is an exponent for relative permeability, and v_s is the kinematic viscosity of the oil at the steam temperature. b is typically set equal to 3.5, which a fitting value for published data of unconsolidated sand packs (Cardwell and Parsons, 1949). However, this abstract expression requires the estimation of parameters, which requires extensive experimental analyses. Hence, Eq. 1 is limited in incorporating the complex nature of the evolution of the residual oil saturation during SAGD.

Butler (1994) noticed that most of the oil drained in the chamber edges rather than through it. He stated that this occurs because the residual saturation in the steam chamber is very low to promote flow of oil and also, as the water condensates, it is kept between steam and oil by surface tension supporting the oil drainage at the edges of the chamber. Pooladi-Darvish and Mattar (2002) explained that high residual oil saturation is caused because high pressure steam injection has less latent heat and, as a consequence, more heat will abandon the reservoir through the produced fluids at higher temperatures. This also results in more heat left in SAGD chamber where the oil no longer exists. **Figure 1-1** schematically displays the theorized SAGD concept.

Walls et al. (2003) studied the residual oil saturation in the steam chamber through relative permeability curves. They did a sensitivity study on the shapes and the end points of relative

permeability curves firstly and then matched the oil-gas relative permeability curves with the residual oil saturation determined theoretically. They stated that water relative permeability and oil relative permeability in the gas-oil system are the critical parameters to determine the magnitude and shape of the oil saturation behaviour as a function of time. Also, they pointed out that residual oil saturation increases at lower SAGD operating pressures.

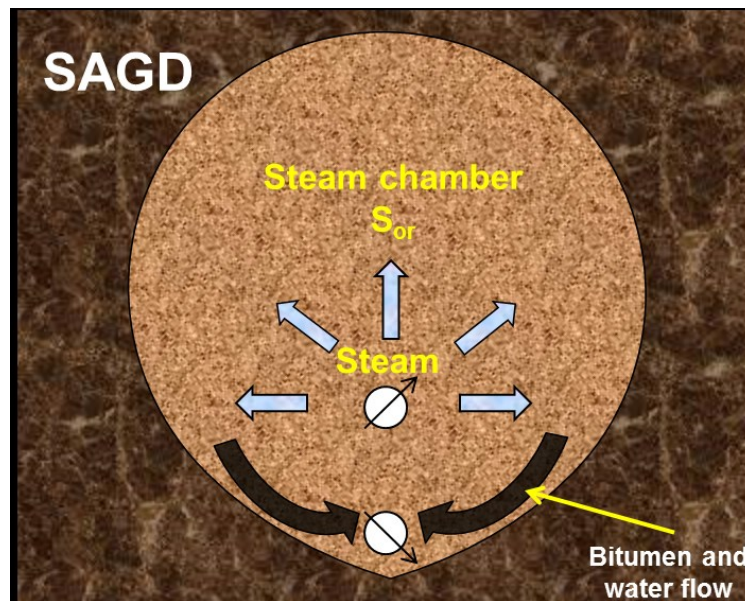


Figure 1-1: SAGD concept.

Mohammadzadeh and Chatzis (2012) also calculated the ultimate recovery using two approximations: 1) Weighting of the micromodel before and after the experiment and 2) tracking of the interface during the SAGD process. The matching was good between both methods. An important conclusion was that higher permeability and lower bitumen viscosity yields higher oil recovery factor.

1.3 Dynamics of SAGD at pore scale

More recently, Mohammadzadeh and Chatzis (2009; 2010) studied the SAGD process at the pore scale using glass micromodels saturated with heavy oil within a vacuum chamber to minimize heat losses. They focused on analyzing the lateral steam chamber expansion, steam fingering, fluid flow regimes, drainage mechanisms, and emulsification phenomenon. With their experimental design (lateral steam injection using a line-source scheme by a channel), they showed the lateral expansion of the chamber in the early stage of the SAGD through pictures.

According to their micromodel observations, there are three fluid regions in a SAGD process at the pore scale: (1) steam chamber, where steam is the dominant existing phase, (2) bitumen filled pores, which is the inactive region where the viscosity of bitumen is too high to gain mobilization, and (3) mobilized region, where three phase flow, namely mobile oil, steam and water occurs and is located between the steam chamber and the bitumen saturated pores.

Focusing on the mobilized oil region, Mohammadzadeh and Chatzis (2009) pointed out two simultaneous drainage mechanisms responsible of oil mobilization: 1) Capillary drainage displacement and 2) film-flow drainage displacement. In the capillary drainage mechanism, a small amount of mobile oil (a volume covering 1-5 pores) pertaining to the mobilized oil region, is displaced directly by the steam phase, which is the non-wetting fluid, with the assistance of gravity and with the presence of negligible viscous force. Also, due to periodic steam condensation, a water slug can be formed, which is displaced by the non-wetting steam, aiding the mixing of water and oil in the pores of the mobilized region (Mohammadzadeh and Chatzis, 2009 and 2010).

In the case of film-flow drainage displacement, Mohammadzadeh and Chatzis (2009) observed that the high local mixing in the mobilization zone does not let an extended hydraulic continuity of the films causing a poor contribution of the films flow to the total drainage. Also, they observed that the film flow rate contributing to the drainage rate is lower than that of capillary drainage displacement and could be important if such films keep their hydraulic continuity. In summary, mobile oil saturated pores are swept by interplay of direct drainage displacement by water condensate as well as steam and film flow drainage displacement (Mohammadzadeh and Chatzis, 2009 and 2010).

The emulsification phenomenon at the interface caused by local steam condensation was also proven through the visual experiments. Mohammadzadeh and Chatzis (2009) explained that due to the non-spreading characteristic of water on oil (negative spreading coefficient), very fine droplets of condensate are buried within the bulk oil behind the nominal interface resulting in water in oil emulsification. Sasaki et al. (2002) observed through their experimental SAGD study the emulsification phenomenon using high resolution optical-fiber scope. Furthermore, emulsification of oil during a steamflooding was firstly observed by Kong et al. (1992) in a Hele-

Shaw cell.

Mohammadzadeh and Chatzis (2012) quantified the performance of SAGD determining the interface advancement velocity and ultimate recovery factor based on the previous experimental work (Mohammadzadeh and Chatzis, 2009 and 2010). They provided a heat transfer analysis for the laboratory scaled SAGD and observed that the velocity of horizontal interface advancement remains constant during the SAGD process within each particular cell block along the height of each individual micromodel. These results were analyzed using an analytical model developed by Butler (1987) and a good agreement was obtained. With the experimental design that minimized the convective heat transfer, Mohammadzadeh and Chatzis (2012) also found that radiation is the sole heat transfer mechanism responsible for heat losses from the micromodels to the surroundings. The heat loss analysis was also used to calculate the net cumulative steam-oil ratio, cSOR, in order to estimate the consumed volume of steam to offset the radiation heat loss from the model to the surroundings.

1.4 Statement of the problem and objectives

As it is shown in the literature review, studies conducted to clarify the mechanisms responsible for the development of S_{or} in non-isothermal oil recovery processes are very limited, especially for SAGD. In addition to this, these published works focusing on S_{or} are based on numerical models, which do not necessarily take into account the underlying physics of flow phenomena involved in the process at the pore scale. Furthermore, data fed to the reservoir simulators such as relative permeabilities, residual saturations, and mobile oil is based on liquid-gas and liquid-liquid systems for isothermal applications where the flow dynamics is different from that of non-isothermal methods.

Estimations of S_{or} are characteristically carried out using the free fall gravity drainage theory for air-liquid systems. Matching the field and lab results with numerical simulator based on those models does not represent the physics behind the non-isothermal processes. This is mainly due to a lack of research and understanding of the pore scale activity, which is the elementary cell in the average behaviour of a porous medium. In other words, a deep and systematic study of the behaviour of non-isothermal processes at pore scale has not been carried out as in the case of isothermal water and gas flooding.

Hence, the main objectives of this research can be summarized as follows:

1. To explain how the isothermal and non-isothermal conditions, the fluid dynamics and the nature of the porous medium affect the development of residual oil saturation at pore scale.
2. To describe visually the mechanics of SAGD and the development of S_{or} at pore scale.
3. To achieve a clear understanding of pore scale events in order to distinguish which flow mechanisms are dominant and relevant to be incorporated in the development of new mathematical models and in the determination of relative permeabilities for SAGD.

To accomplish these objectives the following aspects are investigated:

1. The development of residual heavy oil saturation in single pores must be clarified. It is not known how the S_{or} varies under the interplay of gravity, viscous and capillary forces during two phases (gas-heavy oil) and three phases (gas-water-heavy oil) at high temperature conditions. Cylindrical and angular pores are used to mimic the pores and crevices of oil sands.
2. During the application of thermal methods as SAGD non-isothermal conditions exists rather than high and constant temperature conditions. The existence of a temperature gradient must be investigated at pore scale to determine if it could modify the flow dynamics, the oil recovery, and thus the trapping of oil.
3. The dynamics of SAGD and the trapping mechanisms need to be visualized to have a better understanding about how the S_{or} is distributed in the reservoirs and what their geometrical shapes are. The trapping mechanisms during lateral expansion of steam chamber and the simultaneous vertical and lateral expansion of the steam chamber must be explained at the pore scale.
4. It is not known how the pore structure, the pore and particle size distribution (heterogeneities), and the wettability influence the development of S_{or} in the SAGD process. These aspects must be clarified.

1.5 Outline

This is a paper-based thesis. Five papers presented at conferences and/or published in (or submitted to) different journal publications comprehend the five chapters of this thesis. Each chapter has its own introduction, literature review, conclusions, and references. In addition to a short introductory chapter (chapter 1), a chapter to summarize the contributions is included at the end of the thesis.

In chapter 2, air-heavy oil and air-heavy oil-water displacements were carried out in cylindrical capillary tubes under different temperature conditions. The interplay between capillary, gravity and viscous forces was analyzed. The effects of spreading coefficient, wettability, and pore size were also evaluated. This work was extended in chapter 3 and the liquid retention characteristics in square capillary tubes during two and three phase gravity drainage experiments were investigated at different temperatures using heavy crude oil, water, and air.

In chapter 4, the retention of heavy oil, that is, the S_{or} , was investigated using a CFD approach at temperature and pressure conditions that are very difficult to generate at the microscopic scale in laboratory experiments.

In chapter 5, a fundamental analysis of the water-heavy oil displacement and gas-heavy oil gravity drainage under a temperature gradient using a cylindrical capillary tube model was conducted. The momentum equations for both processes were developed and the exact solutions were obtained. The dynamics of displacement, the rate of heavy oil recovery, and the relative permeability curves were investigated with these models.

Chapter 6 is dedicated to the visual analysis of SAGD process at the pore scale. The influence of the dynamics of SAGD and the properties of the reservoir on the development of residual oil saturation was investigated. Drainage and trapping mechanisms of heavy oil were described and, a detailed analysis of counter-current flow and dynamics of the ceiling part was provided.

Chapter 7 summarizes the contributions of this dissertation to the literature and industry.

1.6 References

1. Al-Bahlani, A.M. and Babadagli, T. 2009. *SAGD Laboratory Experimental and Numerical Simulation Studies: A Review of Current Status and Future Issues*. J. Petr. Sci. and Eng., **68** (3-4): 135-150.
2. Baker, R.O., Rodrigues, K., Sandhu, K.S. and Jong, E.S.W. 2010. *Key Parameters in Steam Chamber Development*. SPE 138113-MS presented at the Canadian Unconventional Resources and International Petroleum Conference, Calgary, Alberta, Canada. October 19-21.
3. Butler, R.M. 1987. *Rise of Interfering Steam Chambers*. JCPT. Paper 87-03-07.
4. Butler, R.M. 1991. *Thermal Recovery of Oil and Bitumen*. Prentice Hall Inc., New Jersey, 285-359.
5. Butler, R.M. 1994a. *Steam-Assisted Gravity Drainage: Concept, Development, Performance and Future*. JCPT **32** (2).
6. Cardwell, W.T. and Parsons, R.L. 1949. *Gravity Drainage Theory*. Trans. AIME **179**: 199-211.
7. Jimenez, J. 2008. *The Field Performance of SAGD Projects in Canada*. Paper IPTC 12860 presented at the Int. Petroleum Tech. Conf., Kuala Lumpur, Malaysia, 3-5 Dec.
8. Kong, X., Haghghi, M. and Yortsos, Y.C. 1992. *Visualization of steam displacement of heavy oils in a Hele-Shaw cell*. Fuel **71**: 1465-1471.
9. Mohammadzadeh, O. and Chatzis, I. 2009. *Pore-Level Investigation of Heavy Oil Recovery Using Steam Assisted Gravity Drainage (SAGD)*. Paper IPTC 13403 presented at the Int. Petroleum Tech. Conf., Doha, Qatar, 7-9 Dec.
10. Mohammadzadeh, O. and Chatzis, I. 2010. *Pore-Level Investigation of Heavy Oil Recovery Using Steam Assisted Gravity Drainage (SAGD)*. Oil & Gas Science and Technology – Rev. IFP Energies Nouvelles. **65** (6): 839-857.
11. Mohammadzadeh, O., Rezaei, N. and Chatzis, I. 2012. *SAGD Visualization Experiments: What Have We Learned From the Pore-Level Physics of This Process?* Paper WHOC12-421 presented at the World Heavy Oil Congress, Aberdeen, Scotland.
12. Pooladi-Darvish, M. and Mattar, L. 2002. *SAGD Operations in the presence of overlaying gas cap and water layer-effect of shale layers*. JCPT **41** (6).

13. Sasaki, K., Akibayashi, S., Yazawa, N. and Kaneko, F. 2002. *Microscopic visualization with high resolution optical-fiber scope at steam chamber interface on initial stage of SAGD process*. SPE 75241, SPE/DOE Imp. Oil Rec. Sym., Tulsa USA.
14. Walls, E., Palmgren, S. and Kisman, K. 2003. *Residual oil saturation inside the steam chamber during SAGD*. JCPT **42** (1).

Chapter 2 : Drainage Type Oil and Heavy-Oil Displacement in Circular Capillary Tubes: Two- and Three-Phase Flow Characteristics and Residual Oil Saturation Development in the Form of Film at Different Temperatures

A version of this chapter was presented at the SPE Canadian Unconventional Resources Conference held in Calgary, Alberta, Canada, 15-17 November 2011, and was also published in Journal of Petroleum Science and Engineering (2014, volume 118, 61-73).

It is still uncertain to what extent pore scale mechanisms, such as the counter and co-current nature of multiphase flow, the trapping mechanisms, the distribution of phases, and heat transfer mechanisms affect the process of isothermal and non-isothermal gravity drainage dominated oil and heavy-oil recovery. This type of processes is encountered during gas injection into oil reservoirs for enhanced oil recovery under isothermal conditions. Steam injection in thick reservoirs where gravity displacement is an effective mechanism and steam assisted gravity drainage (SAGD) are well-known examples of a non-isothermal gravity dominated heavy-oil recovery applications. It is commonly observed that field scale applications of the latter yield less recovery than estimated. One may also encounter this type process in the removal of any crude oil contamination in shallow zones where steam injection is used for cleaning. All these require in-depth analysis of the problem at the pore scale to account for the residual oil saturation (S_{or}) in the swept zone.

In this paper, we used a single capillary tube (radius < 0.03 cm) to mimic an elementary volume in the swept area during gravity dominated displacement applications and studied the flow characteristics of two and three phase flow with emphasis on film development. We carried out two-phase (air-oil) and three phase (air-oil-initial water saturation) flow displacements in a capillary tube under different temperature conditions, varying the air injection rate and the capillary properties. Detailed visualization experiments were carried out to analyze: (1) The effects of heavy oil viscosity, wettability and spreading coefficient on displacements at different temperature conditions, (2) the interplay among capillary, gravity and viscous (air injection rates) forces and wettability using different capillary size (pore size), and (3) the residual oil saturation in the form of film development and phase distribution in the capillaries (mainly the thicknesses of the wetting and non-wetting phases).

The experimental observations suggest that for heavy oil there is a threshold capillary number around $1.0E-2$ over which the oil recovery (and therefore the residual oil saturation) is very sensitive to the capillary number, i.e., the injection rate, interfacial tension, wettability and temperature. At lower capillary numbers (typical range for oil reservoirs) temperature and hence viscosity do not have a significant influence in the residual oil saturation of the processed and crude oils; for horizontal displacement the residual oil saturation is a function of the capillary

forces and for gravity drainage experiments it depends of the competition between capillary and gravity forces (Bond number).

2.1 Introduction

Determination of the remaining or residual oil saturation during complex displacement processes such as three phase flow under isothermal and non-isothermal conditions is still a challenge. This is partly due to an incomplete understanding of the displacement mechanisms at the pore scale. Numerous efforts have been made to determine the magnitude and the distribution of the residual oil saturation in some processes such as waterflooding in reservoirs under water wet conditions at ambient conditions (Chatzis et al., 1983; Chatzis et al., 1988; Oshita et al., 2000; Kamath et al., 2001; Yang et al., 2013).

More recently, a visual analysis of the steam assisted gravity drainage process (SAGD) was carried out to clarify the physics of the process at the pore scale using micromodels (Mohammadzadeh and Chatzis, 2009). The residual oil development during such processes is more crucial as the process efficiency is very critical due to low production caused by the nature of oil and rock and the high cost of steam injection. It was recently shown that the highest ultimate recovery reached during the SAGD process is only 60% (the average in the Albertan applications yielded 35-40% ultimate recovery), which is way below expectations to make the process efficient (Jimenez, 2008; Al-Bahlani and Babadagli, 2009). Hence, one needs to distinguish the reasons for low oil production in such processes and to clarify to what extent it is related to pore scale dynamics. In cases of relatively inexpensive processes, such as gas injection (Hagoort, 1980; Chatzis et al., 1988) or the double displacement process where gravity drainage is the dominant production mechanism (a double displacement generally occurs when gas is injected in a reservoir after a waterflooding: gas displaces oil and this in turn displaces water), determination of residual oil saturation is also critical as the target oil is not abundant in this type of tertiary recovery application and thereby, the efficiency of the process is highly sensitive to the ultimate recovery.

In this regard, one may start with the 'simplest' way of the determination of the residual liquid saturation left behind in a circular capillary tube during a gas-oil displacement. In a pioneering work, Fairbrother and Stubbs (1935) found that in a capillary tube, an air bubble flows faster

than liquid being displaced due to the adhesion of a thin film on the walls of the tube. The magnitude of the residual liquid left behind was found to be a function of the balance between the viscous forces and the capillary forces. This was expressed through the capillary number, Ca , as follows:

$$Ca = \frac{\mu U_b}{\sigma} \quad (1)$$

Where μ is the viscosity of the displaced fluid, U_b is the bubble velocity and σ is the surface tension air –liquid. They introduced an empirical equation to determine the fraction of the liquid supported on the surface of the tube and was related to the capillary number:

$$W = \frac{U_b - U_m}{U_b} = Ca^{1/2} \quad (2)$$

Where U_m is the average velocity of the liquid. This correlation is useful for $1.0E-3 < Ca < 1.0E-2$. Taylor (1961) found that Eq. (2) can be extended to $Ca=0.09$ and that W approaches an asymptotic value of 0.56. Later, Bretherton (1961) proposed an equation to predict the film thickness surrounding the bubble as follows using the lubrication theory and assuming that the bubble profile is of constant curvature except very near the wall, where the meniscus is deformed by viscous forces:

$$\frac{h}{r} = 0.643(3Ca)^{2/3} \quad (3)$$

Through his own experiments, Bretherton found that Eq. (3) applies for $Ca > 1.0E-4$. At lower gas velocities, the experimental film thickness surpassed the theoretical value and at the very lowest capillary numbers ($Ca < 1.0E-6$) the difference between experimental results and the two-third power law involve a factor of 8. Following the work of Bretherton, Cox (1962) solved the Stokes equation using a stream function for $2 < Ca < 10$ and presented experimental results indicating that the ultimate value of W was about 0.6. Park and Homsy (1984) formalized the Bretherton model through perturbation techniques and Ratulowski and Chang (1989) extended it to higher capillary numbers using a composite lubrication equation. Chen (1986) measured the film thickness through a conductimetric technique and found that it decreased as the capillary number

diminished until it approaches a constant value at low Ca . He found a deviation from Bretherton theory and argued that such deviation was due to the roughness of the tube wall. Ratulowski and Chang (1990) investigated the Marangoni effects due to impurities in the liquid during the movement of long air bubbles in capillaries. They stated that Marangoni effects could explain the underestimation of the film thickness of the Bretherton model at low air bubble velocity. Berg (2010) did an analysis of the implications of Marangoni effects in different situations and the emergence of such effects due to variations of surface or interfacial tension as well as of temperature gradients.

Schwartz et al. (1986), through experimental research for very small capillary numbers, $Ca < 1.0E-5$, explained some of the discrepancies of the literature with respect to the dependence of the deposited film thickness on bubble length. They found that for the bubbles of length many times greater than the tube radius, the ratio of film thickness to tube radius is a function of the capillary number. For bubble length less than 20 times that of the tube radius, there is good agreement with the Bretherton theory over two orders of magnitude of the bubble velocity.

More recently, the research in this topic has focused on solving the equations of motion (generally reduced to the Stokes equation for slow motion) through different numerical techniques covering different capillary number ranges (Reinelt and Saffman, 1997; Shen and Udell, 1985; Martinez and Udell, 1989). The work of Giavedoni and Saita (1997) covered the widest capillary number range, $5.0E-5 < Ca < 10$, and observed an excellent agreement with the Bretherton's theory for $Ca \leq 1.0E-3$. However, it is still a challenge to model the low velocity region due to the complexity of solving the thin-film region (Dong and Chatzis, 2004). Low capillary numbers ($Ca < 1.0E-4$) are characteristic of oil reservoirs (Dullien, 1992; Schwartz et al., 1986).

While the previous works focused on solving the problem of the residual liquid saturation for high capillary numbers and ambient conditions, we focused on the analysis of the effects of different high temperature conditions on the residual oil saturation (film thickness) in gas – oil displacements at low capillary numbers. In practice, this is a way to approximate non-isothermal heavy-oil recovery processes such as SAGD or steam injection in thick reservoirs.

We are aware that, in steam based heavy-oil recovery methods, the process is a complex multiphase flow problem where it is possible to find steam, condensed water, oil, water in oil emulsions and organic depositions in a single pore at the same time, depending on the temperature gradient, the stage of the process and the thermodynamic behavior. For sake of minimization of this complexity, we started from the simplest way to determine the residual oil saturation as a thin film having a liquid phase (heavy-oil) and a gas phase (air) in a circular capillary tube. Also, although it was recognized that circular capillary tubes are not the best option to mimic the network of pores in a real reservoir (Blunt et al., 1995; Dong and Chatzis, 2004) due to its low retention power, we used this approach on the basis of their availability for relatively small diameters and ease of use in visualization, especially with heavy crude oil. We believe that, as a starting attempt, this research contributes to a better understanding of the behavior of residual oil in gas/steam-oil displacements where there is a significant temperature gradient. To the best of our knowledge, there is not this kind of experimental and quantitative pore scale studies (capillary tubes) in the literature focus on high temperature heavy oil recovery applications.

2.2 Experimental Work

2.2.1 Setup

An experimental set up was designed for horizontal displacements as shown in **Figure 2-1**. A Pyrex circular capillary tube ($r=0.0254$ cm) was placed in a leveler which had a millimeter ruler along the circular capillary to measure the change of slug length during the air – liquid displacement. A heating tape covering half of the cylindrical body of the capillary tube was attached along the capillary tube to perform high temperature displacements. The constant heating rate and temperature were monitored by a temperature controller (Cole Parmer DigiSense[®] Temperature controller R/S). A camera (Canon EO7D) with a macro lens (Canon EF100mm f/2.8L Macro IS USM) was used to take snapshot photos and videos of the flow (film formation, slug flow, and formation and film breaking). The displacements were carried out using a syringe pump (Kent Scientific Corporation) which provided a wide interval of flow rates. The whole setup was placed on a vibration free table to eliminate external forces other than the gas injection rate.

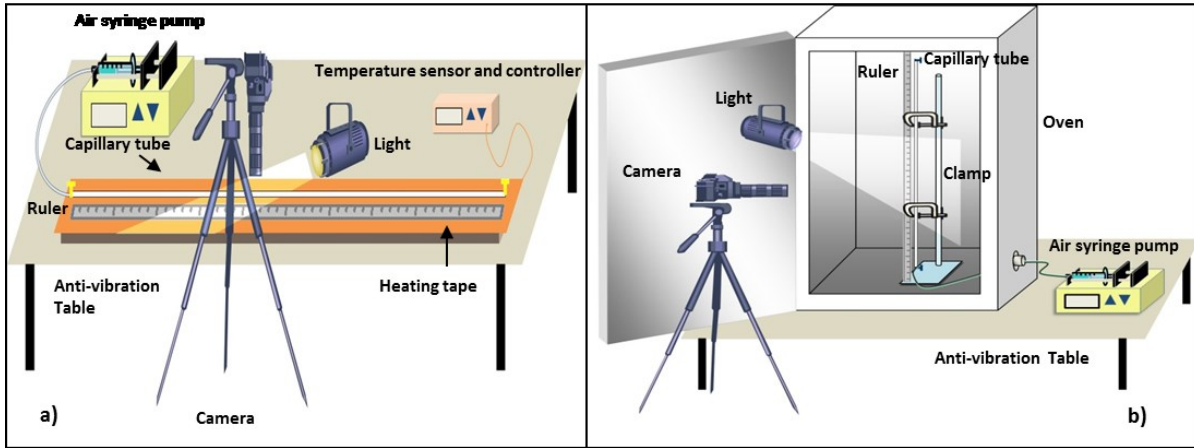


Figure 2-1: Experimental set-up: a) horizontal displacements; b) vertical displacements.

For the case of vertical displacements an oven was used because temperature stabilization using heating tape was not practically possible. The temperature inside the oven was kept constant during the experiments. Figure 1b shows the setup for the vertical experimental runs.

2.2.2 Fluids and their properties with respect to temperature

For all experiments air was used as the gas phase and Kerosene dyed with orange colorant and heavy crude oil were selected as the oil phases. For the experiments with initial water saturation, distilled water was used.

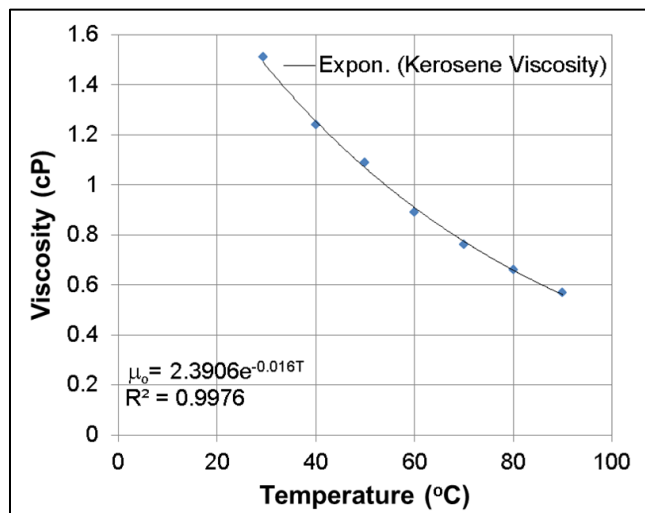


Figure 2-2: Kerosene viscosity behavior with respect to temperature.

Figure 2-2 shows the viscosity behavior of the kerosene with respect to the temperature. The air - kerosene surface tension behavior with respect to the temperature is given in **Figure 2-3**. Contact

angles of kerosene-air-glass and kerosene-water-glass were measured for the temperature range of 23.5 and 90.5 °C and no significant change with respect to temperature was observed.

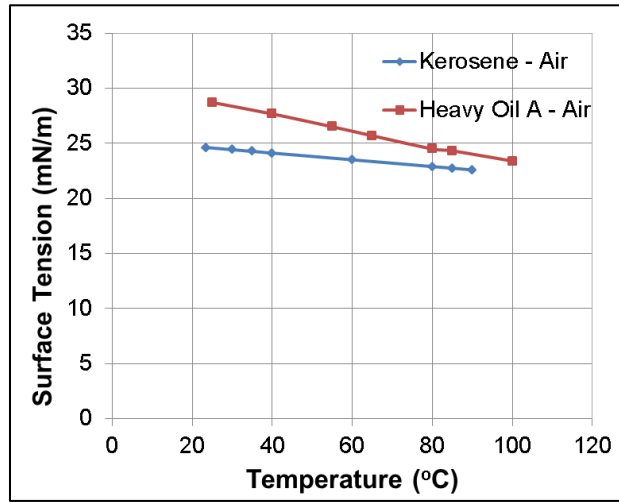


Figure 2-3: Surface tension behavior for air-kerosene and air-heavy oil A systems.

For air-crude oil displacements, a heavy oil labeled as “heavy-oil A” was used (see **Table 2-1**). **Figure 2-3** and **Figure 2-4** show the surface tension and viscosity behavior of the “heavy oil A” with respect to temperature, respectively. Contact angles between “heavy oil A” and air (on the glass) were measured between the range of 23 and 85 °C (**Figure 2-5**) at different temperatures.

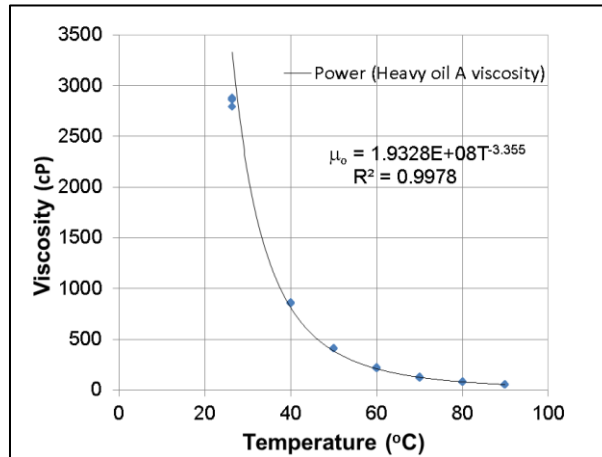


Figure 2-4: Heavy oil A viscosity behavior with respect to temperature

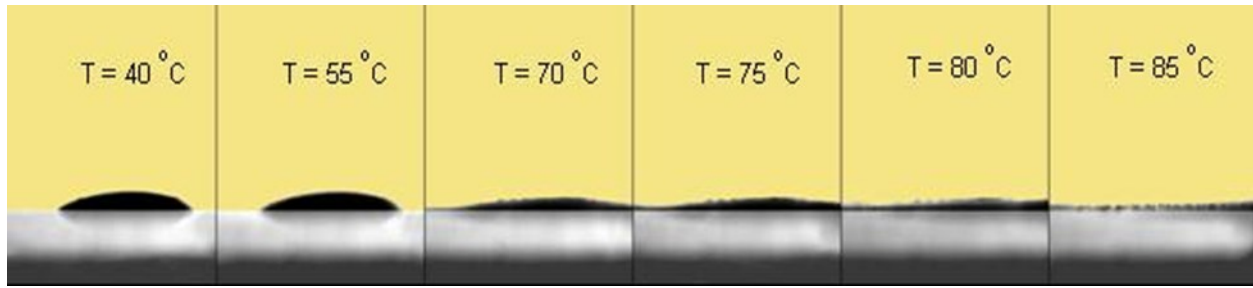


Figure 2-5: Evolution of the contact angle between air-heavy oil A – pyrex glass at different temperatures

The viscosity measurements were conducted using a viscometer (BrookField DV-II+ Pro, viscosity accuracy of $\pm 1.0\%$, viscosity repeatability of $\pm 0.2\%$). The surface/interfacial tensions and the contact angle measurements were obtained using the Pendant Drop Interfacial Tension Cell (Model IFT-10, TEMCO, Inc). The uncertainty for surface and interfacial tensions was ± 0.5 mN/m. **Table 2-1** shows the fluid properties at the temperatures inside the capillary tube during the experimental runs. Temperature measurements had a precision of ± 1.0 °C.

Table 2-1: Fluid properties.

Fluid	T °C	σ_{a-o} (mN/m)	σ_{ow} (mN/m)	θ_{a-o-s} (°)	θ_{w-o-s} (°)	μ_o (cP)
Kerosene	23.5	24.6	41.1	30	23.7	1.64
	85	22.8	38.0	30	23.7	0.61
Heavy Oil A	55	26.5	-	24.3	-	289.8
	85	24.3	-	0	-	67.3

a: air, o: oil, w: water s: glass surface

2.2.3 Experimental details

a) Horizontal displacements

“Air – kerosene – capillary tube” and “air – kerosene – water - capillary tube” systems

Two different temperature conditions were selected. One set of experiments was performed at room temperature ($T=23.5$ °C). The second set was carried out at high temperature conditions. In the latter, a constant heating rate and temperature of 100 °C were maintained in the outer diameter of the capillary tube covering half of its cylindrical body so that an average temperature gradient of 30 °C was maintained from the heated half to the top of the other half of the capillary

tube. The wall thickness was 0.175 cm. An average temperature inside the capillary tube was estimated to be 85 °C.

For air-kerosene displacements, a small liquid slug (5 cm, approximately) was placed inside the capillary tube and it was allowed to reach the temperature of the test. Then, air at room temperature was injected through the inlet valve of the system. The slug was moved 50 cm (measured from the outward side of the meniscus). The camera was used to record the flow (film formation, slug flow and film breaking) during the displacement and for a better determination of the lengths of the slugs through image processing. The average residual oil saturation left behind during the displacement was determined by dividing the difference between the initial and final lengths of the liquid slug by the distance that the liquid slug was drained by an endless air bubble. This procedure to measure residual oil saturations is illustrated in **Figure 2-6**. This approximation to measure the average residual liquid saturation was proposed by others (Bretherton, 1961; Schwartz et al., 1986; Chatzis et al., 1988; Dong and Chatzis, 2004). The average velocity of the liquid slug was calculated by dividing the distance traveled by the travel time.

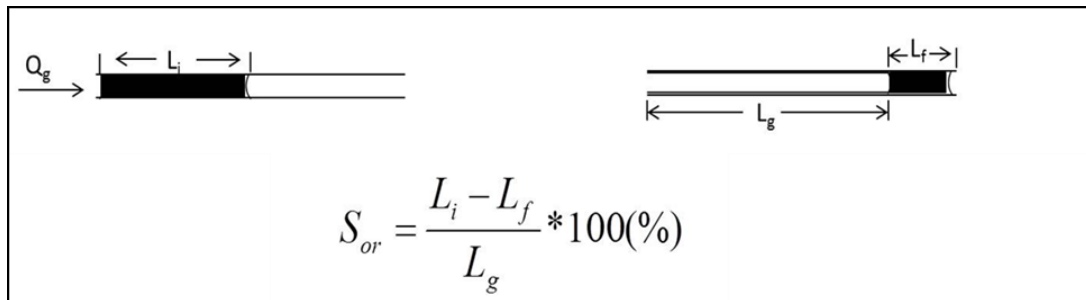


Figure 2-6: Graphical description of the residual oil saturation measurements.

For air – kerosene – water capillary tube displacements, we studied the effects of the initial water saturation inside the tube (which was estimated to be an average value of 1.5 %). After each experimental run with kerosene, the capillary tube was cleaned with a sulfuric chromic solution and methanol and then dried with air for the next experiment.

“Air – heavy oil A – capillary tube” system

For the experiments with heavy oil A, toluene, and methanol were used as the cleaning agents. Two different temperature conditions were selected. Both sets of experiments were made at high

temperature conditions. Similar to the kerosene experiments given in the previous section, a constant heating rate and constant temperature were maintained at the outer diameter of the capillary tube covering half of its cylindrical body, being 100 and 70 °C for the first and second set of experiments, respectively. A temperature gradient of 30 °C was kept between the heated half and the top of the other half of the capillary tube. Averages temperatures of 55 and 85 °C were estimated inside the capillary tube for both set of experiments, respectively. The displacements were performed as described in the air-kerosene section.

Quite a number of displacements for all systems were carried out at different gas injection rates to cover a wide range of capillary numbers possibly existing in oil reservoirs.

b) Vertical displacements – Gravity drainage

“Air - heavy oil A - capillary tube” system

Gravity drainage (free – fall and forced) experiments were carried out using two different radii ($r=0.025$ and 0.0165 cm) at high temperature conditions. For each radius, two sets of experiments were performed, at 55 and 85 °C. Also, the displacements were performed as described in the air – kerosene section but, instead of injecting the air through the inlet to displace the liquid slug, the air was sucked using the syringe pump through the outlet valve.

2.3 Results and discussion

We use the following definition for the capillary number (Ca) in the gas-oil displacements:

$$Ca = \frac{v_a \mu_o}{\sigma_{o-a} \cos \theta} \quad (4)$$

Where v_a is the air velocity, μ_o is the viscosity of the oil phase, σ_{o-a} is the surface tension of the oil and θ is the contact angle measured through the wetting phase. In the literature (Fairbrother and Stubbs, 1935; Bretherton, 1961; Giavedoni and Saita, 1997) the contact angle between the liquid slug and the solid was found to be 0. Hence, $\cos \theta=1$. However, in some of our systems the contact angle is different from zero as mentioned earlier.

Also, we calculated the Bond number (Bo) for the gravity drainage experiments. The Bond number is defined as:

$$Bo = \frac{\Delta\rho g L^2}{\sigma_{o-a} \cos \theta} \quad (5)$$

where $\Delta\rho$ is the density difference between the oil and the air, g is the gravitational constant, L is the characteristic length, σ_{o-a} is the surface tension of the oil and θ is the contact angle measured through the wetting phase. The characteristic length of the circular capillary tubes was their radii.

2.3.1 Analysis of film thickness in horizontal displacements

We determined the film thickness of horizontal displacements at low capillary numbers since the diameter of the capillary tube and the percentage of the area occupied by the residual oil saturation are known. Also, selecting a circular tube for the experiment, we assumed that the film thickness had a circular shape, which was supported by the fact that residual oil saturation was homogeneously distributed as observed during the experimental runs.

Based on these assumptions, the dimensionless film thickness is defined as the ratio of the film thickness (b) and the radius of the capillary tube (r):

$$h_{\infty} = \frac{b}{r} \quad (6)$$

The equation to calculate the dimensionless film thickness for the air – kerosene and air – heavy oil displacements is defined as follows:

$$h_{\infty} = \frac{r - \sqrt{\left(1 - \frac{S_{or}}{100}\right) A_T}}{r} \quad (7)$$

Where S_{or} is the residual oil saturation given in percentage and A_T is the total cross sectional area of the capillary tube. The term within the square root is the difference between the total cross sectional area of the tube and the area occupied by the thin film assuming that the film has a circular shape. **Figure 2-7** shows a comparison of dimensionless film thicknesses for air-

kerosene displacements at different temperatures with the classical Bretherton model (equation 3). The Bretherton model was used in many studies, especially the numerical ones, as a base case for comparative analysis. In such an attempt, Giavedoni and Saita (1997) observed a good match with the Bretherton theory for $Ca < 1E-3$ up to $Ca < 5E-5$ but they noticed that there was a significant deviation from it for larger capillary numbers.

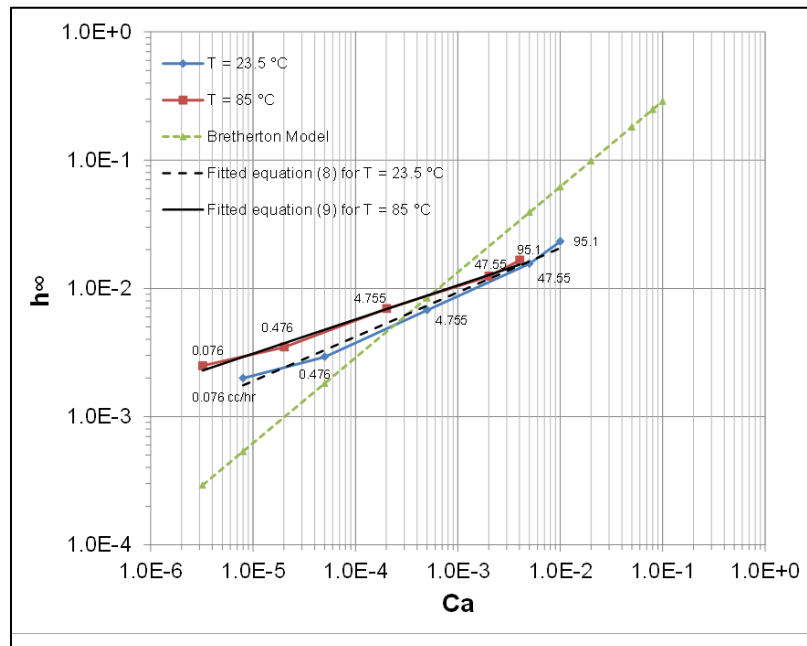


Figure 2-7: Comparison of kerosene film thickness with Bretherton model in a capillary tube of $r=0.025$ cm.

One may infer from **Figure 2-7** that air-kerosene results do not match well with the Bretherton model at low capillary numbers. The region which could be considered in agreement with the Bretherton model corresponds to $3E-4 \leq Ca \leq 5E-4$. For $Ca=3E-4$, the absolute errors compared to the Bretherton model are around 29.7% and 2.29% at 85° C and 55° C, respectively. On the other hand, for $Ca=5E-4$, the absolute errors are around 5.7 % and -13.16% at 85° C and 55° C, respectively. The Bretherton model underestimates the film thickness for both temperatures for $Ca < 2E-4$ while we observe overestimation for $Ca > 5E-4$. Actually, Bretherton (1961) stated that his theory applies well for $1E-4 < Ca < 3E-3$.

Bretherton (1961) also found that equation (3) underestimated the film thickness in his experimental results for $Ca < 1E-4$. Although he did not have any strong evidence, he attributed such deviation at low capillary numbers to the possible effects of the roughness of the capillary

tube, surface-active impurities, which cause a hardening of the free surface and the disjoining pressure, which could be very significant in case of thin films.

Later, Chen (1986) and Schwartz et al (1986) observed similar deviations from the Bretherton model. The former explained it through the roughness of his capillary tubes showing photographs of the wall of the tube. However, Bretherton found that aniline and benzene had different film thicknesses at low capillary numbers. Hence, if the roughness caused the film to approach a constant value as the capillary number decreases, like the case in Chen 's results (1986), the asymptotic value should not depend of the wetting liquid as pointed out by Ratulowski and Chang (1990). On the other hand, Schwartz et al. (1986) attributed the deviation to the length of the air bubbles. The results for long bubbles were closer to the Fairbrother and Stubb (1935) correlation than the Bretherton equation. For bubble lengths less than about 20 times of the tube radii, a good match was obtained with the Bretherton theory.

The most approved explanation about the deviation of the experimental results from the Bretherton theory at low capillary numbers is the presence of surface active impurities (traces of surfactants) in the displaced liquid (Bretherton, 1961; Schwartz et al., 1986; Hirasaki and Lawson, 1985; Ginley and Radke, 1989; Ratulowski and Chang, 1990).

An acceptable hypothesis to explain our results, at least in part, is that of proposed by Ratulowski and Chang (1990). They explained that, for an augmentation in the film thickness, it is necessary to have a concentration gradient of surfactant in the bulk liquid overcoming the effects of surface convection. This gradient provokes a decrease in the surface concentration from the bubble nose to the flat film. Due to a smaller surfactant concentration in the film, a larger surface tension exists in this region, causing a surface pulling in the direction of the film, and as a consequence, a greater amount of liquid flows to the film producing a thicker film than in a case without surface active impurities. Ratulowski and Chang (1990) affirmed that this phenomenon does not occur at higher capillary numbers since the velocity and thereby surface convection, dominate the flow so that the surface concentration gradient does not cause enough pulling force to modify the flow field.

If we assume that kerosene contains some active surface impurities (it is generally a mixture of alkanes from C_{10} to C_{16}) the Ratulowsky and Chang's hypothesis fits well even though they did

not mention the Marangoni effects caused by temperature. For $Ca < 2E-4$, there was an increase in the film thickness for both temperatures being larger at higher temperature (see **Figure 2-7**). In the 23.5 °C experiment, air and kerosene were at the same temperature, but the air was entering the tube at room temperature in the 85 °C experiment, so that there was probably a larger temperature gradient in the flat film than in the interface near nose bubble, which could promote the Marangoni effects. In this sense, the surface pulling directed to the film was exacerbated increasing the film thickness for the experiment at 85 °C. Other valid explanation could be possible viscosity reduction at higher temperatures, i.e., in the case of kerosene, its viscosity at 85 °C was 2.69 times smaller than at 23.5 °C and it is known that the flow rate in a film is inversely proportional to the viscosity yielding more fluid flow through the transitional zone of the interface to the flat film.

We fitted equations for the air – kerosene displacements at both temperatures:

For $T=23.5$ °C,

$$h_{\infty} = 0.1015Ca^{0.346} \quad (8)$$

For $T=85$ °C,

$$h_{\infty} = 0.0677Ca^{0.2668} \quad (9)$$

Analyzing the air-heavy oil displacements at different temperatures is more complicated as inferred from **Figure 2-8**. For all range of capillary numbers, the Bretherton equation overestimates the film thickness, which means that the Bretherton model is not suitable to represent heavy oil film thickness. In the case of heavy oil, the Marangoni effect could be more pronounced due to the effects of surface-active compounds which exists naturally in a heavy oil sample (mainly in the asphaltene fraction). Also, because air was injected at room temperature, there was a temperature gradient in the flat film and in the nose bubble in the air-kerosene experiments.

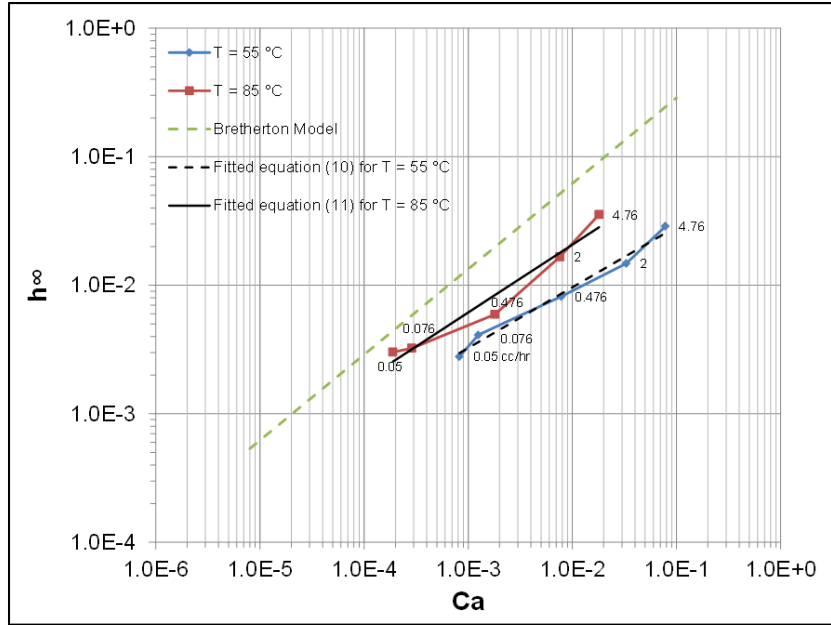


Figure 2-8: Comparison of heavy oil film thickness with Bretherton model in a capillary tube of $r=0.025$ cm.

The trend observed makes sense because the film thickness increases at higher temperature for the air-kerosene experiments (looking at the same Ca). However, it is likely that the surface pulling caused by a surfactant concentration gradient was less effective in these cases because the surfactant concentration must be higher in the heavy oil than in the kerosene and as a consequence, the gradient between the flat zone and the nose bubble is smaller. In this case, we believe that the limiting factor to increase the film thickness was the viscosity of the heavy oil, which was 289.8 cP at 55 °C and 67.3 cP at 85 °C. These values are noticeably larger than those of kerosene so that the flow rate through the films should be much smaller. The surface pulling directed toward the film due to surface gradient of surfactant and the surface tension gradient due to temperature variations cannot overcome the effects of oil viscosity on the flow rate directed toward the film and the surface convection during the oil slug displacement.

It is also possible to explain the deviations from the Bretherton model and the others' works in a simpler manner from a more macroscopic point of view. To obtain the same capillary number at higher temperatures, it is necessary to increase the air velocity due to the viscosity reduction. In this case, the liquid slug will move faster and the perturbation of the air-liquid interface will be larger promoting more fingering of the air over the liquid slug, and as a consequence, a thicker film will be formed. For instance, if we look at the heavy oil experiments of $Ca=7.7E-3$ in

Figure 2-8, we observe that it was necessary to apply 2 cc/hr of gas injection rate at 85 °C and just 0.476 cc/hr at 55 °C because the oil viscosity at the former temperature was 67.3 cP and 289.8 cP for the latter. The oil slug at 85 °C moved about 28 times faster than at 55 °C, hence the displacement was more homogeneous and the interface was flatter at the lower temperature. Based on this, it makes sense that heavy oil film thicknesses are smaller than those of kerosene. For instance, looking at $Ca=2E-4$ at 85 °C in **Figure 2-7** and **Figure 2-8**, we measure the dimensionless film thickness of oil as 0.0069 and 0.003 for kerosene and heavy-oil, respectively. However, the air injection rate for heavy oil and kerosene experiments was 0.05 and 4.755 cc/hr, respectively. That means the kerosene slug moved 100 times faster than the oil slug at the same temperature and this resulted in more homogeneous displacement and flatter interface for the heavy-oil case.

Fitted equations for air – heavy oil at both temperatures are presented below:

For $T=55$ °C,

$$h_{\infty} = 0.0849Ca^{0.472} \quad (10)$$

For $T=85$ °C,

$$h_{\infty} = 0.236Ca^{0.5283} \quad (11)$$

A comparison of the fractional fluid (kerosene and heavy oil) left behind with the Bretherton model and the empirical correlation of Fairbrother and Stubb (equation 2) are shown in **Figure 2-9** and **Figure 2-10**.

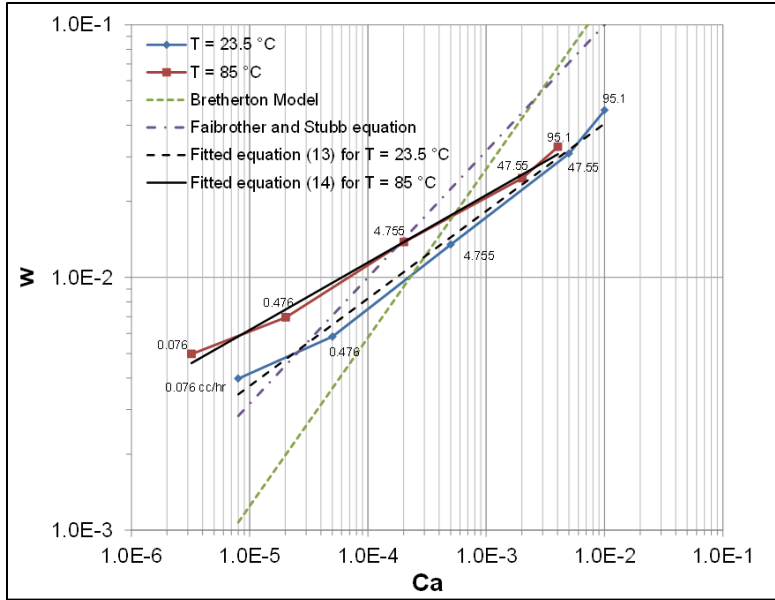


Figure 2-9: Comparison of fraction of fluid left behind (kerosene) in a capillary tube of $r=0.025$ cm.

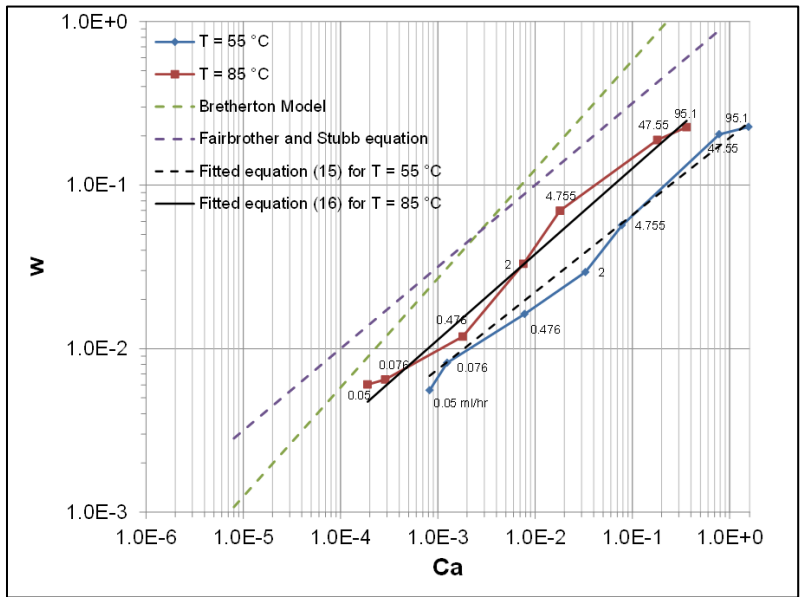


Figure 2-10: Comparison of fraction of fluid left behind (heavy oil) in a capillary tube of $r=0.025$ cm.

In this analysis, the Bretherton equation defined for the fractional fluid left behind was used:

$$W = 1.29(3Ca)^{\frac{2}{3}} \quad (12)$$

For $Ca > 3E-3$, a better agreement with the empirical correlation of Fairbrother and Stubbs (1935) was obtained in case of kerosene (Figure 9) compared to the Bretherton's equation whereas no match was obtained for the heavy-oil case (Figure 10) with neither of the models. We propose

the next fitted equations for the fraction of kerosene and heavy oil left behind as residual liquid saturation:

For Air – kerosene at T=23.5 °C,

$$W = 0.1998 Ca^{0.346} \quad (13)$$

For Air – kerosene at T=85 °C,

$$W = 0.1338 Ca^{0.2668} \quad (14)$$

For Air – heavy oil at T=55 °C,

$$W = 0.1946 Ca^{0.472} \quad (15)$$

For Air – heavy oil at T=85 °C,

$$W = 0.4216 Ca^{0.5283} \quad (16)$$

2.3.2 Residual oil saturation behavior in horizontal and vertical displacements

i) Horizontal displacements

“Air – kerosene – capillary tube system”

Figure 2-11 shows the residual oil saturation vs. capillary number for experiments at room (T=23.5 °C) and a high temperature (T=85 °C). One may infer the following from this graph:

- a) For the same gas injection rate at different temperatures, different capillary numbers were obtained due mainly to change in oil viscosity. Hence, to compare the curves at different temperatures, we have to obtain the residual oil saturations from the graph using the capillary numbers at the same air flow rate. Based on this approach, a lower residual oil saturation value is obtained at the same gas injection rate for the higher temperature case when $Ca > 1.0E-3$. This is due to the fact that the viscous forces opposing the movement of the liquid are reduced at higher temperatures. Consequently, gas can push the liquid

slug easier and overcome the capillary forces that retain the wetting liquid. For this system, the capillary forces did not present a significant change with respect to the temperature.

- b) The difference between the residual oil saturation of the room temperature and high temperature cases was more pronounced when higher air injection rates were applied. However, with decreasing air velocity, this difference was diminished significantly. For $Ca < 1.0E-3$ the residual oil saturation was practically independent of the temperature of the system. This is due to the fact that the viscous forces are negligible over the movement of the liquid slug at these low capillary numbers because the momentum transfer coming from the gas is insignificant compared to the capillary forces, which dominate the process. As explained earlier, these properties did not change significantly with increasing temperature. The contact angle of the air-kerosene-glass system measured through the liquid was estimated to be 30° in the range of 23.5 and 90.5 °C and the surface tension change was negligible (see **Figure 2-3**).

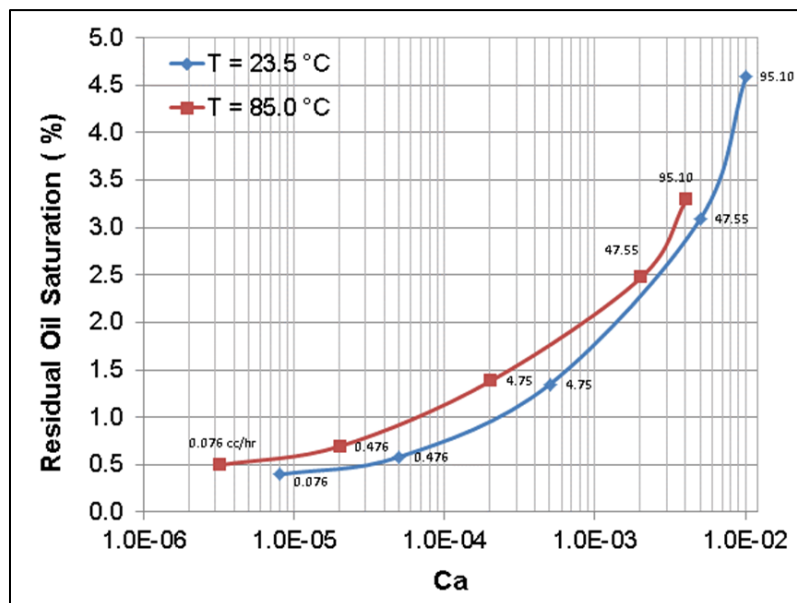


Figure 2-11: Residual oil saturation (kerosene) vs. capillary number in a circular capillary tube showing the different injection rates.

After the displacement of a liquid by gas in a capillary tube, the formation of a film can be predicted. However, different types of films can be formed according to the different forces influencing the interaction of the solid and the flowing liquid. The molecular forces could also

be determinant when the film is thin (Berg, 2010) and very low capillary numbers are present (Teletzke et al. 1988). Important aspects of films are their type, stability and homogeneity. These factors can be explained through the concept of “disjoining pressure $\Pi(t)$ introduced by Derjaguin (Rusanov, 2006):

$$\Pi(t) = p^\beta - p^\alpha \quad (17)$$

Where p^β is the equilibrium pressure in the film, p^α is the equilibrium pressure in the bulk phase and t is the thickness of the film. $\Pi(t)$ depends on the material of the film, the adjoining bulk phases and the interface between them. The disjoining pressure quantifies the pressure difference existing between a thin film and the adjoining bulk phase of the same fluid under the same thermodynamic condition.

In general, the disjoining pressure is the summation of the different interaction forces between the film and the neighboring phases (Adamson and Gast, 1997; Berg, 2010):

$$\Pi_{total}(t) = \Pi_{vdw}(t) + \Pi_H(t) + \Pi_{el}(t) + \Pi_{steric}(t) + \dots \quad (18)$$

Where $\Pi_{vdw}(t)$ denotes the van der Waals forces, $\Pi_H(t)$ hydrogen bonding, $\Pi_{el}(t)$ electrostatic forces, $\Pi_{steric}(t)$ steric interactions. Thus, as mentioned earlier, depending of the interacting forces contributing to the disjoining pressure, different type of films will be formed.

Berg (2010) explained that, in general, the function $\Pi_{total}(t)$ is usually one of the four isotherms that are defined as type I, II, III and IV. Types I and II correspond to van der Waals liquids on solid or liquid substrates but for Type I spontaneous thickening of the film can be predicted since the effective Hamaker constant is negative and for Type II spontaneous thinning is expected as the effective Hamaker constant is positive. Type III and IV are isothermals for films where it is possible to have a thin film with bulk liquid and thin film with a thick thin film respectively. In both cases, there are positive and negative contributions to the disjoining pressure.

For the cases of air – kerosene displacements a formation of a very thin film was observed through the change of color of the glass surface from transparency to the orange color of the dyed kerosene. This oil is made up of a mixture of alkanes from C_{10} to C_{16} approximately. Using the Hamaker constant of kerosene, $A_{KK}=5.17E-20$ J (through equation 7.44 from Berg, 2010) at

$T=23.5\text{ }^{\circ}\text{C}$ and taking a Hamaker constant of $A_{PP}=1.15\text{E-}19\text{ J}$ for Pyrex glass (Gregory, 1969), we have an effective Hamaker constant of $A_{\text{effective}}=-2.54\text{E-}20\text{ J}$. According to previous classification, kerosene will form a thick film, at least at the lowest capillary numbers, where the molecular forces become critically important.

Considering that the film is Type I and homogeneous, and the Hamaker constant is negative and the film is “thick” enough, one can estimate the thickness of such film as the diameter of the tube and the percentage of the area occupied by the residual oil saturation are known (see equation 7). For example, for $Ca=8.01\text{E-}6$ at $23.5\text{ }^{\circ}\text{C}$, the film thickness was $5.05\text{E-}5\text{ cm}$ and for $Ca=3.22\text{E-}6$ at $85\text{ }^{\circ}\text{C}$ the film thickness was $6.32\text{E-}5\text{ cm}$. For both capillary numbers, the gas flow rate was 0.076 cc/hr .

“Air – kerosene – capillary tube system with initial water saturation”

We placed an average of 1.5% of water saturation for all of the experiments as a film on the surface of the tube. In the calculations of the capillary numbers, we used the surface tension of the kerosene and considered a contact angle equal to zero because kerosene spread completely onto water. It should be mentioned that although all the experiments had the same average water saturation, we observed that its distribution was not always exactly the same along the capillary tube. We saw small separated collars distributed along the capillary tube and the rest of the regions of the tube was covered by a very thin film of water. Probably, the water on Pyrex glass surface formed films corresponding to Type III (thin film with bulk liquid) or Type IV (thin thin film with thick thin film). Churaev and Derjaguin (1985) calculated isotherms of disjoining pressure of films of water on quartz corresponding to Type III and Type IV.

Figure 2-12 and Figure 2-13 show the residual oil saturation vs. capillary number for experiments at $T=23.5\text{ }^{\circ}\text{C}$ and at $T=85\text{ }^{\circ}\text{C}$ inside the capillary tube with and without initial water saturation, respectively. Comparing the experiments at the same temperature, we observe that the presence of water caused an augmentation in the residual oil saturation. Also, for the curve at the higher temperature, it was observed that as the capillary number becomes smaller, the difference in the residual oil saturation is reduced.

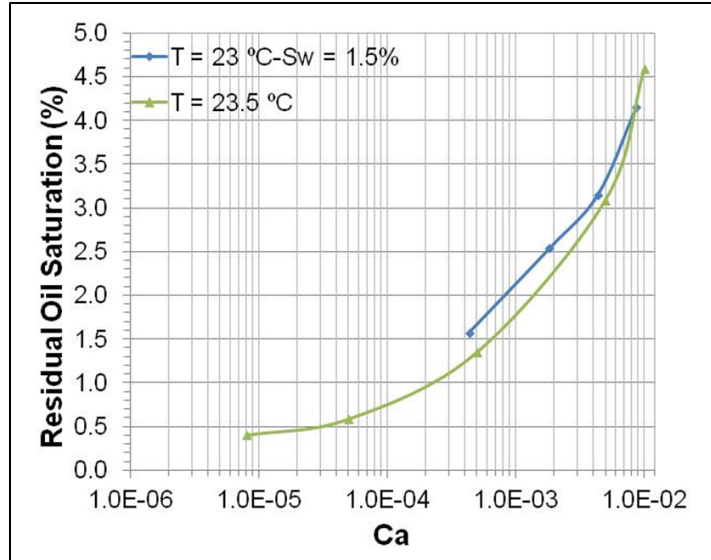


Figure 2-12: Residual oil saturation (kerosene) vs. capillary number in a circular capillary tube showing the effect of 1.5% of water saturation at $T=23.5\text{ }^{\circ}\text{C}$.

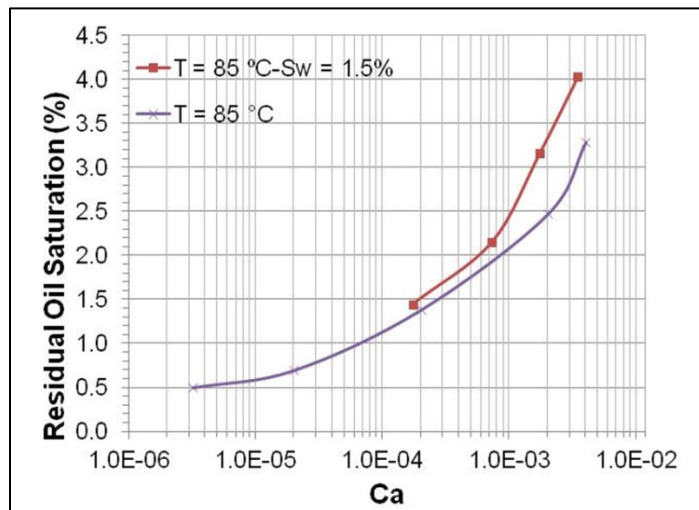


Figure 2-13: Residual oil saturation (kerosene) vs. capillary number in a circular capillary tube showing the effect of 1.5% of water saturation at $T=85\text{ }^{\circ}\text{C}$.

The reason for increasing the residual oil saturation in the system with an initial water saturation could be attributed to the fact that the spreading coefficient of the kerosene on water is positive (calculated as 6.13 mN/m at $T=23.5\text{ }^{\circ}\text{C}$ and 0.444 mN/m at $T=85\text{ }^{\circ}\text{C}$) meaning that a thin film of kerosene can be formed and retained over the surface during and after the displacement. Furthermore, we noticed that there was a higher kerosene accumulation around the collars of water compared to that on the glass surface for the air – kerosene systems at room and high temperature (**Figure 2-14**). The greatest change in the residual oil saturation was observed for the high temperature air–kerosene–water system. To corroborate these observations, we

conducted two simple experiments by putting a drop of water and a drop of kerosene on the Pyrex glass surface next to each other. The kerosene drop immediately moved around the water drop with more accumulation of kerosene between the glass and the water drop.

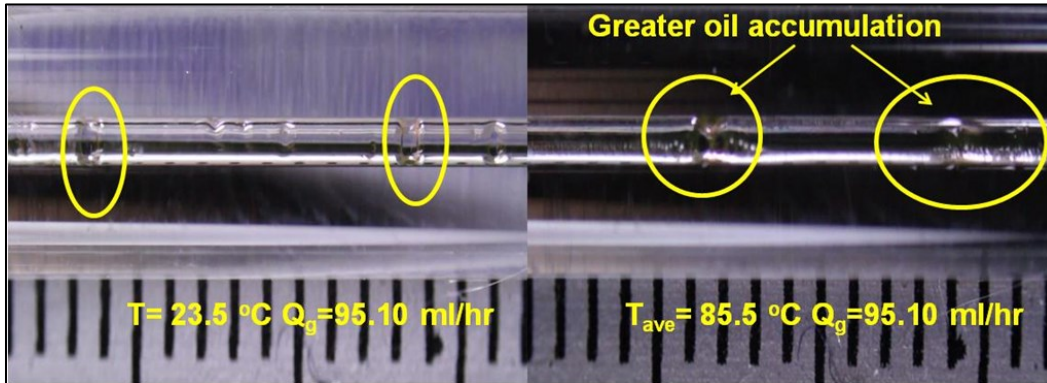


Figure 2-14: Residual oil saturation in the presence of initial water saturation.

We repeated the same experiment at a non-isothermal (high temperature) condition and we observed that the kerosene drop not only moved around the water drop but also went over it. Also, the spreading was much faster at high temperature (even though the spreading coefficient was smaller at a high temperature) as it is shown in **Figure 2-15**.

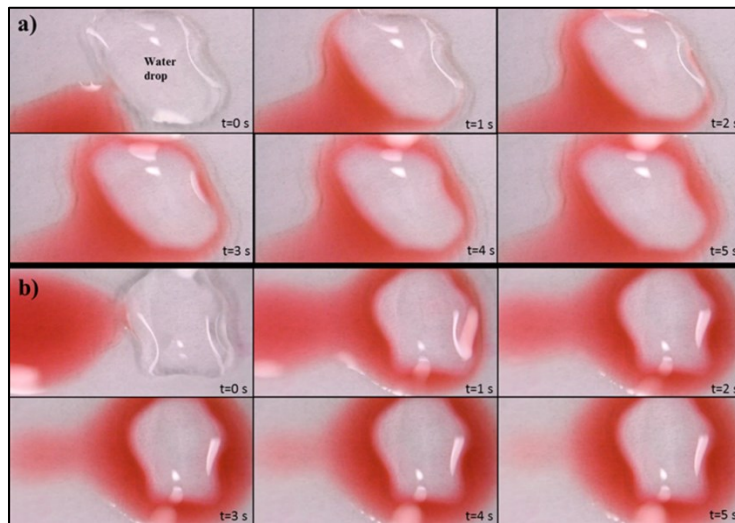


Figure 2-15: Spreading of kerosene (red fluid) over water a) $T=23.5\text{ }^{\circ}\text{C}$, b) $T=85\text{ }^{\circ}\text{C}$.

“Air – heavy oil – capillary tube system”

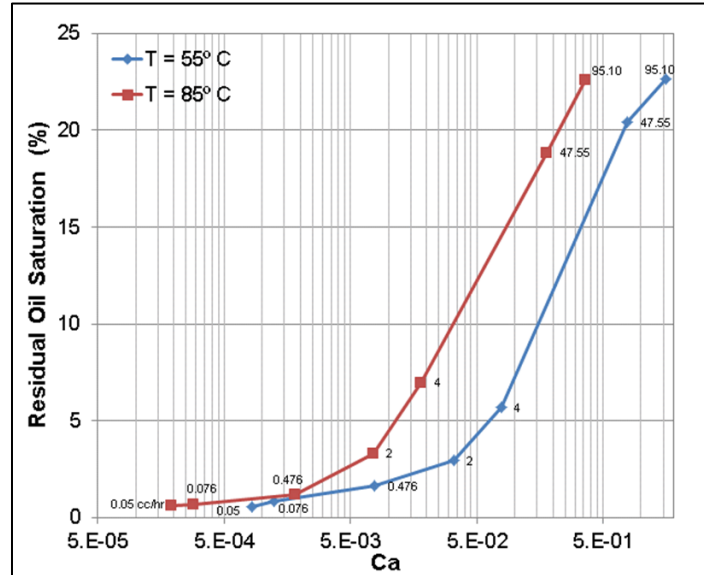


Figure 2-16: Residual oil saturation (heavy oil) vs. capillary number in a circular capillary tube showing different injection rates.

Figure 2-16 shows the residual oil saturation vs. capillary number for the “air–heavy oil A” system for two sets of measurements at two different temperatures (55 and 85 °C). One can infer the following through the analysis of this graph:

- 1) For $Ca > 3.5E-1$, the residual oil saturation reached a value around 20% regardless of the temperature and the capillary number of the experiment. For example, for $Q_g = 95.10$ cc/hr, the Ca were 1.56 and 3.61E-1 at $T_{ave} = 55$ °C and $T_{ave} = 85$ °C, respectively. However, more experiments for $Ca > 2.0$ are necessary to investigate the limit value of residual oil saturation using heavy oil. An asymptotic value of around 50% was reported experimentally (Taylor, 1960; Cox, 1962) and numerically (Giavedoni and Saita, 1997; Martinez and Udell, 1989).

It is worth mentioning that the determination of the residual oil saturation for real heavy oil was rather difficult at high capillary numbers. The approximation we used to obtain it was to bring the length of the liquid slug to zero in order to have an estimation of the traveled distance by the air because visualization through black oil was highly difficult. An interesting flow phenomenon we observed is that once the gas displaced all the liquid slug, a formation of collars was seen first (**Figure 2-17**) due to the drag forces of the air, then the collars attached to each other to form a

lens, which started to flow and broke down again (this occurred if the same gas velocity was kept). However the drag force needed to form the collars and the lens from films seems to be out of the range of capillary numbers typically observed in an oil reservoir. This phenomenon was studied by Gauglitz and Radke (1988) in detail using a viscous solution of glycerol in water.

- 2) For $Ca \leq 1.0E-2$, the temperature had much less influence on the residual oil saturation. A decrease in the difference between those residual oil saturation was observed for both sets of experiments. In this zone, the displacement was controlled predominantly by the capillary forces. We also observed that the final residual saturation at lower capillary numbers ($Ca \leq 8E-3$) was around 0.5%. However, the region below $1.0E-5$ must be analyzed to confirm this. We also observed a difference in the contact angle, from 24.3° at $T=55^\circ\text{C}$ to 0° at $T=85^\circ\text{C}$ and this change did not affect the residual oil saturation at low capillary numbers.

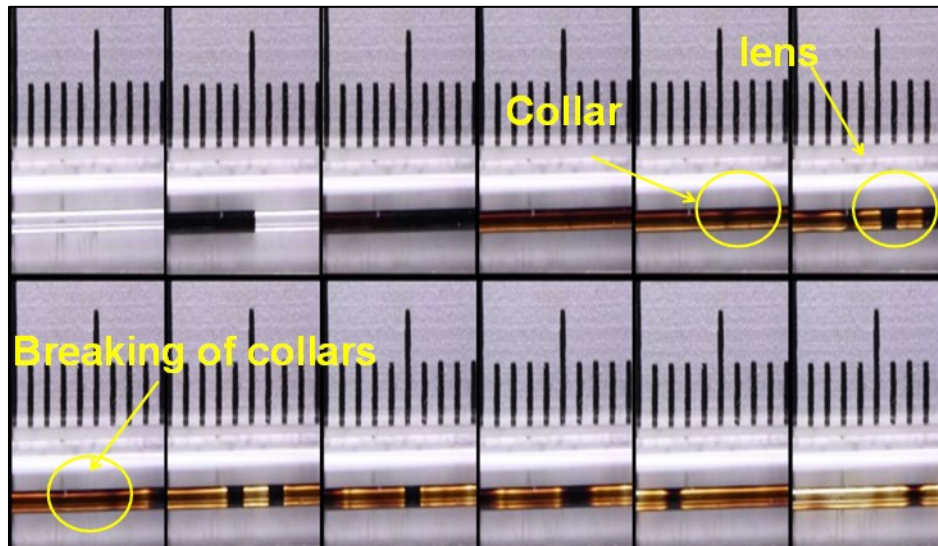


Figure 2-17: Air-heavy oil A displacement at 47.55 cc/hr showing the residual oil saturation and the formation of collars and lenses at different times of the process.

In horizontal air – heavy oil displacement cases, we observed the formation of homogeneous films for all the capillary numbers and these were very stable at low capillary numbers. For $Ca=8.22E-4$ at $T=55^\circ\text{C}$ the film thickness was $7.07E-5$ cm and for $Ca=1.9E-4$ at $T=85^\circ\text{C}$ the film thickness was $7.67E-5$ cm. The air flow rate for these Ca 's was 0.05 cc/hr.

ii) *Vertical displacements*

Free fall and forced gravity drainage displacements were carried at 55 °C and 85° C using two different radii for “Air - heavy oil A - capillary tube” system. **Figure 2-18** shows the results for $r=0.025$ cm during forced gravity drainage experiments. Some observations derived from this graph are as follows:

- a) For $Ca \leq 3.29E-2$, the temperature does not have a significant effect on the residual oil saturation, being almost equal at 55 and 85° C. For this capillary number region ($Ca \leq 3.29E-2$) the capillary and gravity forces are dominant over the viscous forces.
- b) For $Ca \leq 1.0E-03$ the residual oil saturation approximates to an asymptotic value of around 4%, being just a function of the competition between capillary and gravity forces. It seems that this is the minimum amount of heavy oil that this capillary tube can retain.
- c) To corroborate the previous statement, we carried out free fall gravity drainage experiments [$Ca=0$ and $Bo=0.023$ ($T=85^\circ C$) and $Bo=0.024$ ($T=55^\circ C$)]. We found residual oil saturation equal to 4.36% at 85° C and 4.2% at 55° C. Having these value very close to those for $Ca < 1E-3$, one may conclude that the viscous forces and thereby the deformation of the original interface between air and heavy oil do not affect the amount of residual oil saturation for this capillary number zone. Hence, the minimum amount of residual oil just depends on the Bond number.
- d) In the middle zone of the capillary number ($Ca > 3.29E-2$), the residual oil saturation is predominantly dependent on the temperature and therefore, the viscous and capillary forces compete to dominate the process.
- e) For a gas flow rate of 47.5 cc/hr for both temperatures, we found a residual saturation value of ~19 %.

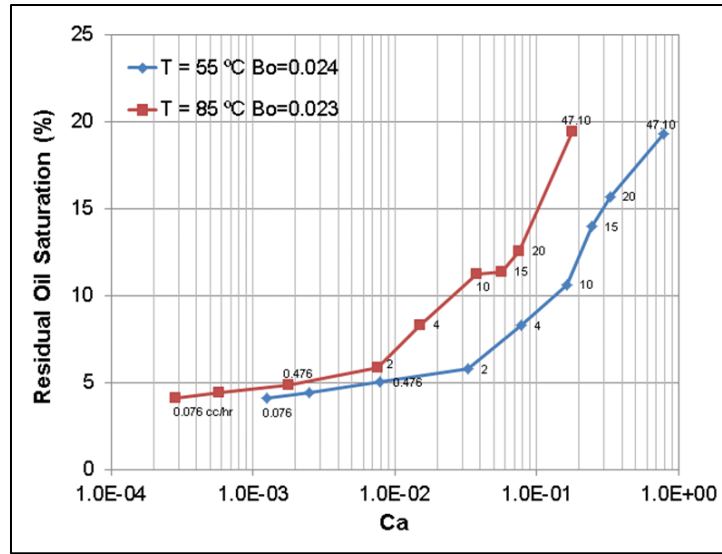


Figure 2-18: Residual oil saturation (heavy oil) vs. capillary number during a gravity drainage in a capillary tube of $r=0.025$ cm.

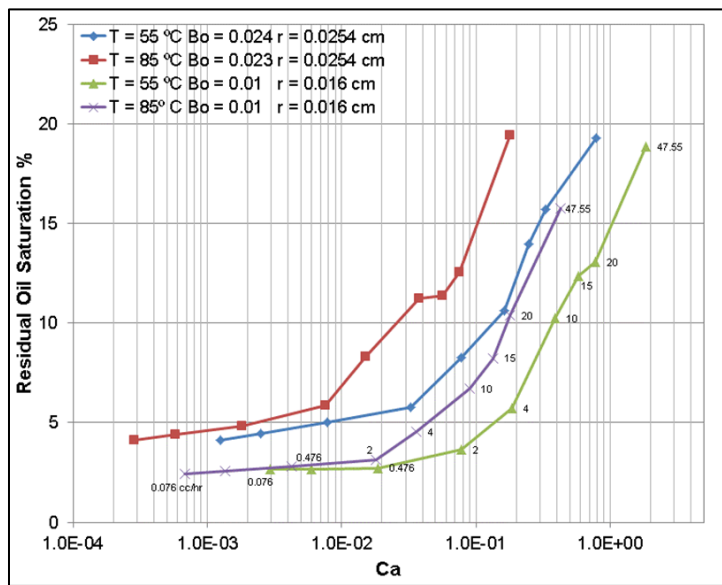


Figure 2-19: Comparison of residual oil saturation (heavy oil) vs. capillary number in a circular capillary in vertical displacements for two different radii.

Figure 2-19 shows a comparison of vertical displacement experiments for both radii ($r=0.025$ cm and 0.0165 cm). Similar observations were made out of the analysis of this graph looking at curve for $r=0.0165$ cm:

- a) For $Ca \leq 1.7E-2$, the temperature does not have a significant effect on the residual oil saturation.

- b) For $Ca \leq 1.0E-03$, the residual oil saturation is approximately 2.5%. For $Ca=0$, the residual oil saturation were 2.6% and 2.7% at 55° C and 85° C, respectively.
- c) Also, in the middle region of the graph ($Ca > 1.7E-2$) the residual oil saturation depends on the competition between capillary and viscous forces.

Another way to analyze the behavior of residual oil saturation in steam assisted gravity drainage displacement is to use a dimensionless number which shows the competition between the viscous, gravity and capillary forces. Jin (1995) derived a new generalized dimensionless number called the trapping number and it has been applied to study oil removal (through surfactant remediation) in contaminated soils (Jin, 1995; Pennel et al., (1996) and condensate removal in gas-condensate reservoirs (Pope et al, 2000) later).

For air – heavy oil gravity drainage experiments we define the trapping number as:

$$N_T = Ca + Bo \quad (19)$$

$$N_T = \frac{v_a \mu_o + \Delta \rho g L^2}{\sigma_{o-a} \cos \theta} \quad (20)$$

Figure 2-20 shows the residual oil saturation versus trapping number for both radii. An advantage of this graph with respect to those of capillary number is that it is possible to include the values for free fall gravity drainage experiments for which $Ca = 0$ and to observe how the residual oil tends to a limit value.

When using the trapping number to analyze our experimental data, we observe that:

- a) For $N_T \leq 5.7E-2$ and $r=0.025$ cm and for $N_T \leq 2.7E-2$ and $r = 0.0165$, the temperature does not show a significant effect on the residual oil saturation, the capillary and gravity forces are dominant over the viscous forces. Above these trapping numbers, the residual oil saturation depends on the temperature and the competition between viscous and capillary forces.
- b) For $Ca=0$, $N_T=Bo$ so that the minimum residual oil saturation just depends on the Bond number.

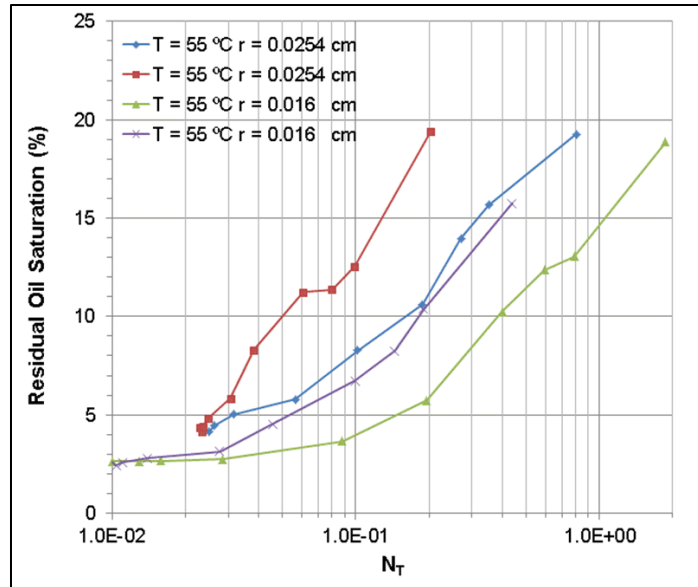


Figure 2-20: Comparison of residual oil saturation (heavy oil) vs. trapping number in a circular capillary tube for vertical displacements for two different radii.

The residual oil saturation was around 20% for both capillary tubes at a gas flow rate of 47.5 cc/hr. This means that the influence of the capillary tube size and gravity forces on the residual oil saturation is noticeable diminished at high capillary numbers. This is also true when we compare those results of vertical displacements with the horizontal case for air – heavy oil (**Figure 2-21**). Notice that, in the case of gravity drainage experiments, these residual oil saturations are not the final ones and they could be produced as drainage of films, which is a different and very slow process compared to the gravity assisted drainage.

It is worth mentioning that there exist differences in the conditions of this research with respect to those previous investigations by Taylor (1961) and Bretherton (1961). While they were working with simpler fluids (with respect to chemical composition), at constant (room) temperature and comparing the behavior between different fluids, we worked with kerosene and heavy oil at high temperature conditions and comparing the behavior of each fluid itself with respect to the temperature. Bretherton (1961) attempted to develop a model considering that, at the same capillary number; different fluids would result in the same film thickness left behind. Taylor (1961) used fluids of different viscosities (glycerin, mixtures of water and syrup and a lubricating oil) at the same temperatures to obtain approximately the same Ca and he observed a good match in certain regions of Ca , except for $Ca > 1.1$ where he just tested glycerin. Schwartz et al (1986) used water and they found thicker films than those of aniline and benzene

(Bretherton's fluids), especially at low capillary numbers. They had a good match with the Bretherton equation when long air bubbles were used at relative large capillary numbers.

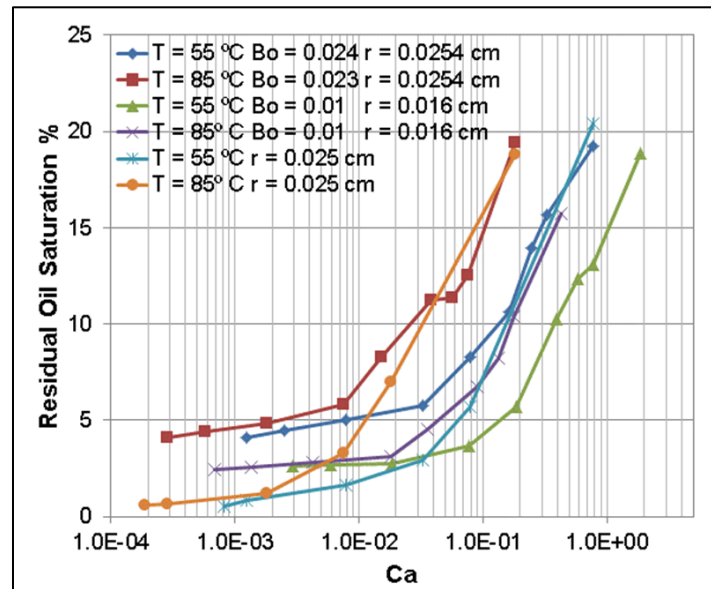


Figure 2-21: Comparison of residual oil saturation (heavy oil) vs. capillary number in a circular capillary tube for horizontal and vertical displacements.

In this research, we paid special attention to the effects of temperature conditions considering high temperature oil recovery applications such as SAGD, steam flooding, or gas injection. Based on this, we compared both curves of a fluid looking at the same air injection rate at different temperatures rather than comparing them with respect to the same capillary number as other researchers did. When we analyze **Figure 2-7** and **Figure 2-8**, it can be seen that the film thicknesses at different temperature are practically the same when they are compared with respect to the same gas injection rate for a certain capillary number range. We found that, if we compared them for the same capillary number, the film thicknesses are different being larger at higher temperatures. These observations are noticeably different from the other investigations cited in this paper.

2.4 Conclusions

This study experimented and quantitatively analyzed residual oil saturation development in isothermal (gas injection) and non-isothermal (steam injection) oil or heavy-oil recovery processes in the form of film. A relatively simplified experimental system (circular tubes) was adopted to create a realistic capillary medium comparable with high permeability heavy-oil

reservoirs or shallow zones where oil contamination may occur. The effects of injection (or flow) rate and temperature on the development of residual oil saturation were clarified to lead further studies in this area. Also, the two- and three phase flow characteristics of oil (and heavy-oil)-water-gas systems at elevated temperatures were experimentally identified. The following specific conclusions can be withdrawn from this research:

Air-kerosene displacements

1. Correlations were proposed for the behavior of film thickness and residual liquid saturation as fractional fluid at 23.5 °C and 85 °C.
2. The displacement of kerosene by air shows that, for $Ca < 1.0E-3$, the residual oil saturation is practically independent of the temperature of the system, being a function of the capillary forces. For higher values of the capillary number, the residual oil saturation is predominantly dependent on the temperature and highly dependent on the gas injection rate.
3. Initial water saturation results in an increase in the amount of retained oil, especially at high temperatures for air kerosene horizontal displacements.

Air – heavy oil horizontal displacements

1. Equations were proposed for the behavior of film thickness and residual oil saturation as fractional fluid at 55 °C and 85 °C.
2. For low capillary numbers ($Ca < 1.0E-2$), in the region for fluid flow in oil reservoirs, the residual oil saturation is not practically affected by temperature and gas flow rate, being just a function of the capillary forces.
3. At higher capillary numbers, in the middle region zone ($Ca > 1.0E-2$), the residual oil saturation is dependent of the temperature and gas flow rate, and therefore of the competition between capillary and viscous forces.

Air – heavy oil vertical displacements

1. In the case of vertical displacements for $0 \leq Ca \leq 1E-3$, the residual oil saturation tends a limit value, which it seems to depend just of the Bond number for each case. Also, this limit value decreases as the radius of the capillary tube diminishes.
2. At higher capillary numbers, in the middle region zone ($Ca > 3.29E-2$ for $r=0.025$ cm and $Ca > 1.7E-2$ for $r=0.0165$ cm) the residual oil, saturation is a function of the competition between capillary and viscous forces.

This study is expected to shed light to further research in the following subjects:

1. This study used circular capillary tubes. Although its size is representative of high permeability oil sands reservoirs, the shape of it can be changed. Initial attempts were made in Arguelles and Babadagli (2012) where square capillaries were used. This can also be extended to 2-D porous media in which the residual oil saturation would develop not only in the form of a film but also due to capillary entrapment.
2. The temperature effect was one of the main points considered in this study and its effects on the two- and three-phase flow of oil-water-gas systems as well as film development were clarified. This could be useful in low temperature or “no temperature” applications such as reclamation of oil contaminated -shallow- areas or immiscible gas injection (double displacement). For gravity drainage type steam applications such as SAGD, higher temperature experiments can be conducted. The -positive and negative- effects of temperature on the gas (or steam type) injection processes are clarified and quantified in this study. Real steam conditions ($T > 200$ °C) can be further tested for this type of capillary or 2-D porous media systems.

2.5References

1. Adamson, A.W., and Gast, A. P. 1997. Physical Chemistry of Surfaces. A Wiley – Interscience Publication, USA.
2. Al-Bahlani, A.M. and Babadagli, T. 2009. SAGD Laboratory Experimental and Numerical Simulation Studies: A Review of Current Status and Future Issues. *J. Petr. Sci. and Eng.*, **68**(3-4): 135-150.

3. Arguelles, F. and Babadagli, T. 2012. Pore Scale Modeling of Gravity Drainage Dominated Flow under Isothermal and Non-Isothermal Conditions. Paper SPE 153591 presented at the SPE Latin American and Carib. Petr. Eng. Conf. (LACPEC), Mexico City, Mexico, April 16-18.
4. Berg, J. 2010. An Introduction to Interfaces & Colloids, The Bridge to Nanoscience. World Scientific Publishing Co. Pte. Ltd, Singapore.
5. Blunt, M., Zhou, D. and Fenwick, D. 1995. Three-Phase Flow and Gravity Drainage in Porous Media. *Transport in Porous Media* **20**:77-103.
6. Bretherton, F.P. 1961. The Motion of Long Bubbles in Tubes. *Journal of Fluid Mechanics*. **10**: 166-188.
7. Chatzis, I., Kantzas, A. and Dullien, F.A.L. 1988. On the investigation of gravity assisted inert gas injection using micro-models, long Berea sandstone cores, and computer assisted tomography. Paper SPE 18284 presented at the SPE Annual Tech. Conf. and Exh., Houston, TX.
8. Chatzis, I., Kuntamukkula, M. and Morrow, N. 1988. Effect of Capillary Number on the Microstructure of Residual Oil in Strongly Water Wet Sandstones. *Soc. Pet. Eng. Reservoir Eng.* **3**(3): 902-912.
9. Chatzis, I., Morrow, N.R. and Lim, H.T. 1983. Magnitude and Detailed Structure of Residual Oil Saturation. Paper SPE 10681 presented at the 1982 SPE/DOE Enhanced Oil Recovery Symposium, Tulsa, OK.
10. Chen, J. D. 1986. Measuring the film thickness surrounding a bubble inside a capillary. *Journal of Colloid and Interface Science*. **109**: 34-39.
11. Churaev, N. V. and Derjaguin, B.V. 1985. Inclusion of Structural Forces in the Theory of Stability of Colloids and Films. *Journal of Colloid and Interface Science*. **103** (2): 542-553.
12. Cox, B.G. 1962. On Driving a Viscous Fluid Out of a Tube. *Journal of Fluid Mechanics*. **14**:81-96.
13. Dong, M. and Chatzis, I. 2004. An Experimental Investigation of Retention of Liquids in Corners of a Square Capillary. *Journal of Colloid and Interface Science*. **273**: 306-312.
14. Dong, M. 1995. A study of Film Transport in Capillaries with an Angular Cross-Section. *Ph.D. thesis*, University of Waterloo.
15. Dullien, F.A.L. 1992. Porous Media: Fluid Transport and Pore Structure. *Academic Press*, San Diego.
16. Fairbrother, F. and Stubbs, J. 1935. Studies in Electroendosmosis. Part VI. The 'Bubble Tube' Method of Measurement. *Journal of Chemical Society*. **1**: 527-529.
17. Gauglitz, P. A. and Radke, C.J. 1988. An Extended Evolution Equation for Liquid Film Breakup in Cylindrical Capillaries. *Chemical Engineering Science*. **43** (7): 1457-1465.
18. Giavedoni, M.D. and Saita, F.A. 1997. The Axisymmetric and Plane Cases of a Gas phase Steadily Displacing a Newtonian liquid – A simultaneous solution of the governing equations. *Phys. Fluids*, **9**(8): 2420-2428.
19. Ginley, G.M. and Radke, C.J. 1989. The Influence of Soluble Surfactants on the Flow of the Long Bubbles through a Cylindrical Capillary. *ACS Symposium Series*, **396**: 480-501.

20. Gregory, J. 1969. The Calculation of Hamaker Constants. *Advan. Colloid Interface Sci.* **2**: 396-417.
21. Hagoort, J. 1980. Oil Recovery by Gravity Drainage. Paper SPE 7424 presented at the SPE 53rd Annual Fall Tech. Conf. and Exh., Houston, TX, Oct. 1-3.
22. Hirasaki, G.J. and Lawson, J.B. 1985. Mechanisms of Foam Flow in Porous Media: Apparent Viscosity in Smooth Capillaries. *SPEJ*, **25**: 176-190.
23. Jimenez, J. 2008. The Field Performance of SAGD Projects in Canada. Paper IPTC 12860 presented at the Int. Petroleum Tech. Conf., Kuala Lumpur, Malaysia, 3-5 Dec.
24. Jin, M. 1995. A Study of Non-Aqueous Phase Liquid Characterization and Surfactant Remediation. PhD dissertation, The U. of Texas. Austin, Texas.
25. Kamath, J., Nakagawa, F., Meyer, R., Kabir, S. and Hobbet, R. 2001. Laboratory Evaluation of Waterflood Residual Oil Saturation in Four Carbonate Cores. Paper SCA 2001-12. Proc. SCA Symposium Technical Programme, Edinburgh, Scotland, September 16-19.
26. Martinez, M.J. and Udell, K.S. 1989. Boundary Integral Analysis of the Creeping flow of Long Bubbles in Capillaries. *Journal of Applied Mechanics*. **56**: 211-217.
27. Mohammadzadeh, O. and Chatzis, I. 2009. Pore-Level Investigation of Heavy Oil Recovery Using Steam Assisted Gravity Drainage (SAGD). Paper IPTC 13403 presented at the Int. Petroleum Tech. Conf., Doha, Qatar, 7-9 Dec.
28. Oshita, T., Okabe, H. and Namba. 2000. Early Water Breakthrough – X-ray CT Visualizes How It happens in Oil-Wet Cores. Paper SPE 59426 presented at the 2000 SPE Asia Pacific Conference on Integrated Modeling for Asset Management, Yokohama, Japan, April 25-26.
29. Park, C.W. and Homsy, G.M. 1984. Two Phase Displacement in Hele-Shaw cell: Theory. *Journal of Fluid Mechanics*. **139**: 291-308.
30. Pennell, K. D., Pope, G. A. and Abriola, L.M. 1996. Influence of Viscous and Buoyancy Forces on the Mobilization of Residual Tetrachloroethylene during Surfactant Flushing. *Environmental Science & Technology*. **30** (4): 1328-1335.
31. Pope, G.A., Wu, W., Narayanaswamy, G., Delshad, M., Sharma, M.M. and Wang, P. 2000. Modeling Relative Permeability Effects in Gas-Condensate Reservoirs With a New Trapping Model. *SPE Reservoir Eval. & Eng.* **3** (2): 171-178.
32. Ratulowski, J. and Chang, H.C. 1989. Transport of Gas Bubbles in Capillaries. *Phys. Fluids A* **1**(10): 1642-1655.
33. Ratulowski, J. and Chang, H.C. 1990. Marangoni Effects of Trace Impurities on the Motion of Long Gas Bubbles in Capillaries. *Journal of Fluid Mechanics*. **210**: 303-328.
34. Reinelt, D.A. and Saffman, P.G. 1985. The Penetration of a Finger into a Viscous Fluid in a Channel and Tube. *SIAM J. Sci. Stat. Comput.* **6** (3): 542-561.
35. Rusanov, A. I. 2007. Equilibrium Thin Liquid Films. *Colloid Journal*. **69** (1): 39-49.
36. Schwartz, L.W., Princen, H.M. and Kiss, A.D. 1986. On the motion of Bubbles in Capillary Tubes. *Journal of Fluid Mechanics*. **172**: 259-275.
37. Shen, E. I. and Udell, K. S. 1985. A Finite Element Study of Low Reynolds Number Two-Phase Flow in Cylindrical Tubes. *Journal of Applied Mechanics*. **52**: 253-256.

38. Taylor, G.I. 1960. Deposition of a Viscous Fluid on the Wall of a Tube. *Journal of Fluid Mechanics*. **10**: 161-165.
39. Teletzke, G. F., Davis, H.T. and Scriven L. E. 1988. Wetting Hydrodynamics. *Revue Phys. Appl.* **23**: 989-1007.
40. Yang, P., Guo, H. and Yang, D. 2013. Determination of Residual Oil Distribution during Waterflooding in Tight Oil Formations with NMR Relaxometry Measurements. *Energy & Fuels*. **27**(10): 5750-5756.

Chapter 3 : Residual Liquids Saturation Developments During Two and Three Phase Flow under Gravity in Square Capillaries at Different Temperatures

A version of this chapter was presented at the SPE Latin American and Caribbean Petroleum Engineering Conference held in Mexico City, Mexico, 16-18 April 2012, and was also published in International Journal of Heat and Fluid Flow (2015, volume 52, 1-14).

An experimental study on heavy oil with air (two phase flow) and water and air (three phase flow) at different temperatures was carried out in square capillaries under gravity drainage conditions. Fluid retention characteristics (in the corners of capillaries) were determined and evaluated using the trapping number (N_T). In air-heavy oil systems, when $N_T < 2.7E-2$, the residual oil saturation (S_{or}) was constant and equal at 55 and 85°C. The S_{or} was controlled by capillary forces regardless of viscous and gravity forces, including free fall gravity drainage (FFGD). For higher N_T , the S_{or} was a function of competition between gravity, viscous and capillary forces. The S_{or} was always higher at 55°C compared to 85°C for the same gas injection rate and the difference increased as the N_T augmented. FFGD experiments demonstrated that heavy oil retention depended on the Bond number and increased linearly as the Bond number increased.

In the three phase systems (air-heavy oil-water) the oil retention did not diminish with the presence of water, which was also constant for the entire interval of N_T at 55 and 85°C. High viscous forces originated from heavy oil were responsible for no change in the S_{or} . However, due to the water-wet nature of the capillary tubes, water was not completely swept. More S_{or} and residual water saturation were observed in air-water-heavy oil configuration, especially at 85 °C, due to the unfavorable viscosity ratio oil/water and the negative spreading coefficient of water in oil in the presence of air. Finally, the change of wettability from water wet to oil wet did not modify the S_{or} but the water saturation decreased slightly for air-heavy oil-water systems.

3.1 Introduction

The application of improved recovery methods has become a recurrent practice these days due to the world reserves depletion and the high prices of crude oil. However, the decision to apply certain recovery techniques depends, to a great extent, on the remaining or residual oil saturation (S_{or}) in the reservoir. Although different approaches have been proposed to estimate the S_{or} and

3.1.1 Statement of the problem

In reference to isothermal and non-isothermal gravity drainage processes for heavy-oil recovery, pore scale studies conducted to clarify the mechanisms responsible for the formation of residual oil saturation are very limited, especially for the latter [1]. To mimic the behavior of S_{or} in a

single pore of a petroleum reservoir, displacements of oil by other phase can be carried out in lab using circular and non-circular capillary tubes. Argüelles and Babadagli [5] proposed an approach to determine the Sor in a circular capillary tube. They analyzed the dynamics of residual oil saturation development (in the form of films) during gas-heavy oil displacement by gravity drainage at different high temperature conditions and low capillary numbers (Ca).

However, as also discussed in that research of Argüelles and Babadagli [5] and a few others, circular capillary tubes are highly idealized to represent the realistic pore structure of oil reservoirs due to their low liquid retention power [6,7]. The irregular geometry of the pores should be taken into account in any experimental or theoretical modeling work. The residual oil saturation in a circular capillary tube exists only as a thin film while in non-circular capillary tubes the residual or remaining oil saturation is present as layers in their angular zones [6].

Square and triangular capillary tubes are examples of non-circular geometries which have been used to model porous media instead of circular tubes. Although their representation of porous media is restricted to a single pore system rather than capturing the complex nature of pore network, they are preferred as they provide visual data that are useful for understanding multiphase flow characteristics. One of the earliest studies on non-circular capillary tubes was done by Singhal and Somerton [8]. They derived equations for the shapes of fluid-fluid interfaces as a function of the contact angle and fluid saturations and focused mainly on triangular geometry. They pointed out the need for experimental work at the pore scale to validate their theoretical expressions for relative permeabilities.

3.1.2 Background and solution methodology

In the present research, square capillary tubes were chosen as the pore model to study the gravity drainage dominated flow in a heavy-oil reservoir at different temperature conditions. Reviewing the specialized literature, one finds that the investigations of multiphase flow in square channels or square capillaries such as the displacement of a liquid by a gas phase are really few compared to those on circular capillaries [5]. Works on air bubbles-liquid displacements in square capillary tubes were presented by Dong and Chatzis [7], Thulasidas et al [9], Ratulowski and Chang [10], Kolb and Cerro [11,12] and Kamişli [13]. However, except the study done by Dong and Chatzis [7], these studies focused on applications different from the fluid flow in an oil

reservoir. It is generally assumed that capillary number is less than $1.0E-4$ at reservoir conditions [14,15]. Note that all these studies were conducted for light oil systems whereas the focus in the present study is the development of Sor in heavy oil reservoirs.

Dong and Chatzis [7] carried out experimental research to analyze the behavior of the retention of liquids in the corners of a square capillary tube of 0.03 cm in width in the range of the capillary numbers existing in a reservoir from $1.0E-3$ to $1.0E-6$ in two and three phase horizontal displacements using air as the displacing phase. In two phase displacements (gas-wetting liquid), they observed that for $Ca > 5.0E-4$, the retention of the wetting liquid diminished with decreasing capillary number. For $Ca < 1.0E-4$, the retention of the wetting liquid was observed to be dependent on the capillary forces and the rate effect was negligible.

In the case of three phase displacements (as a double displacement process: air displaces oil which in turn displaces water), Dong and Chatzis [7] stated that the total retention of water and oil vs. the capillary number curve had the same trend as the retention of the wetting phase for the case of two phase displacements. However, with a decreasing capillary number (up to very low values) or increasing viscous forces, the water retention decreased and the oil retention increased.

To date, the investigation of Dong and Chatzis [7] has been the only one focused on the analysis of the developed Sor in square capillaries and it was restricted to light mineral oils and room conditions. In this paper, the liquid retention characteristics in square capillary tubes during two and three phase gravity drainage experiments were investigated at different temperature using heavy crude oil, water and air. The findings and observations will help understanding the development of residual oil and water saturations during isothermal and non-isothermal oil recovery processes (such as SAGD and steamflooding) and oil remediation from soils. Also, the results will shed light on further modeling studies attempting to clarify the physics of three phase flow of heavy oil, water and gas in more complex pore networks.

3.2 Experimental Work

3.2.1 Set up

An experimental setup used in this study is illustrated in **Figure 3-1**[5]. A square capillary tube was placed over a millimeter ruler to measure the change of slug length during the vertical gravity drainage displacements. This assembly was placed inside an oven for a stabilized and constant temperature. To take snapshot photos and videos of the flow, a camera (Canon EO7D) with a macro lens (Canon EF100mm f/2.8L Macro IS USM) was used. A syringe pump (Kent Scientific Corporation), which provided a wide interval of flow rates, was used to achieve displacement tests. In order to eliminate external forces other than the gas injection, the whole setup was placed on a vibration free table.

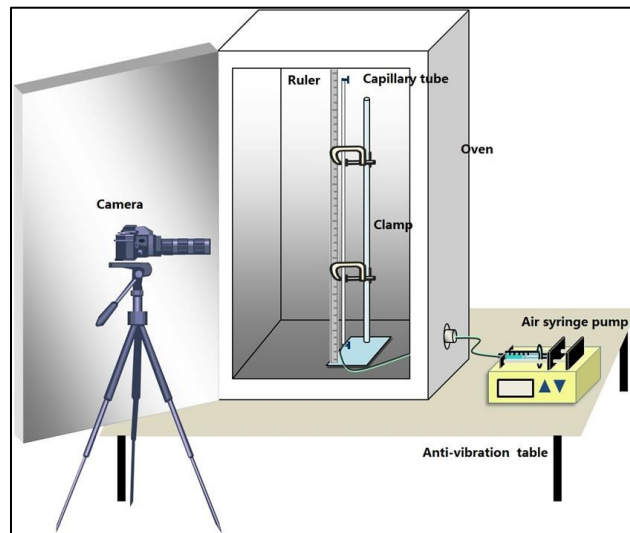


Figure 3-1: Experimental Setup [5].

3.2.2 Fluid properties

Air was used as the gas phase for all experiments. Heavy oil obtained from a field in Alberta Canada (Heavy Oil A) was used as the oil phase. The oil viscosity, the surface tension of the oil and the contact angles between the heavy oil A and the Pyrex glass at the required temperatures were taken from Argüelles and Babadagli [5]. **Table 3-1** shows the fluid properties at the temperatures of the experimental runs.

Table 3-1: Fluids properties (taken from [5], except σ_{ow})

Fluid	T °C	σ_{a-o} (mN/m)	σ_{ow} (mN/m)	θ_{a-o-s} (°)	μ_o (cP)
Heavy Oil A	55	26.5	21.6	24.3	289.8
Heavy Oil A	85	24.3	22.6	0	67.3

a: air, o: oil, w: water, s: glass surface

3.2.3 Capillary tubes

Square capillary tubes (Friedrich & Dimmock, Inc) 0.03 cm in width (W) were used in the two and three phase flow gravity experiments. For free fall gravity drainage experiments, tubes of different sizes (W=0.01, 0.05 and 0.08 cm) were also tested. The length of the capillaries was around 70 cm. **Figure 3-2** shows the cross sectional area of the 0.03 cm square capillary tube as compared to a circular capillary with a diameter (D) of 0.032 cm. One may observe through the photo on the left side that the wall thickness of the circular capillary tube is much bigger than the diameter of the capillary. The cross sectional area of the square capillary can be clearly seen in the right image.

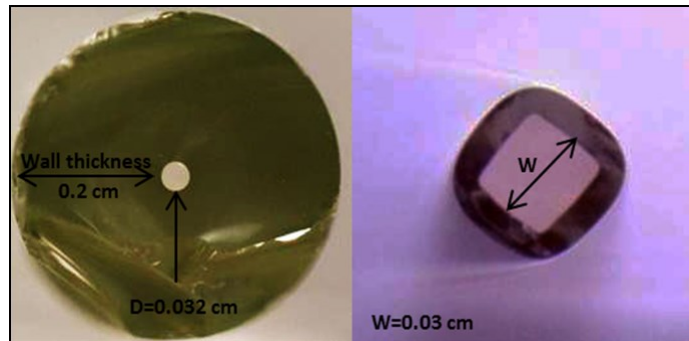


Figure 3-2: Cross sectional area of a circular capillary tube with D=0.032 cm (left) and square capillary tube with W=0.03 cm.

3.2.4 Experimental procedure

For square capillary tubes, a set of experiments were carried out at two different temperatures: T=55 and 85 °C. For all of the experiments, an initial oil slug was placed inside the capillary tubes at the temperature of the test. To introduce the oil, the capillary tube was placed in vertical position. The bottom end of the tube was slightly immersed in a heavy oil container and the oil was sucked slowly using a syringe with plastic tubing attached to a plastic valve placed in the upper end of the capillary tube. Once the desired slug length was obtained, the suction was stopped and the plastic tubing was removed. Next, the capillary tube was rotated 180° so that the

end containing the oil is at the top. To start the experiment, air was sucked through the same syringe with plastic tubing attached to a plastic valve placed now in the bottom end of the capillary tube. The slugs were moved approximately 50 cm. A camera was used to record the whole process. The initial length of the slugs was between 5 and 6 cm for most of the tests. For three phase flow experiments, the initial water slug was also introduced using the same procedure described. For an accurate determination of the lengths of the slugs, the images were further processed.

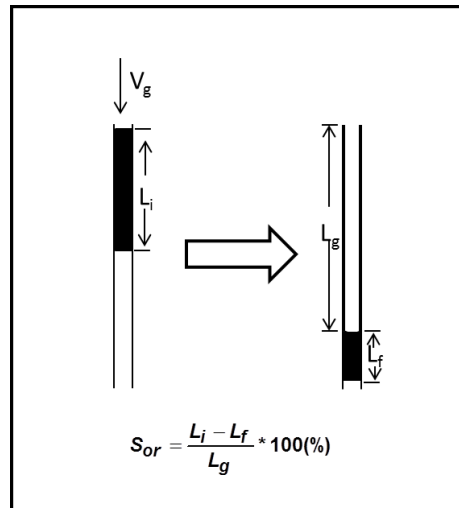


Figure 3-3: Description of the residual oil saturation measurements (taken and modified from Ref. [5]).

The average residual liquid saturations left behind after the displacement with air was calculated by using an approach utilized in a previous publication [5]. This approach was based on dividing the difference between the initial and final lengths of the liquid slug by the distance that the liquid slug was drained by the air bubble. This method to measure the liquid retention was previously used by others [4,7,14]. **Figure 3-3** shows this procedure schematically. In this figure, V_g is the air injection velocity, L_i and L_f are the initial and final length of the liquid slug and L_g is the ‘length of the air bubble’, which is actually the length traveled by the liquid slug, where the residual oil is held. Note that, the residual oil saturation is the volume of oil lost in the slug divided by the volume of tube that the oil passed through, which gives a volumetric residual oil in this section.

After each experimental run, the square capillary tubes were cleaned with heptane, toluene and methanol. Then, a sulfuric chromic solution was used to make the tubes water-wet again. Finally the tubes were washed with water thoroughly and dried with air. In the case of wettability tests,

the square capillaries were treated with a solution of Surfasil™ to alter the wettability of the tubes to oil-wet.

3.3 Results and Discussion

To analyze the behavior of residual oil and water saturation development, the trapping number, NT, was used [16]. This dimensionless number encompasses the competition among the viscous, gravity and capillary forces. Jin [16] derived it to study oil removal using surfactants in polluted soils. It has been used for analysis of oil trapped as globules in porous media [16,17,18].

For air-heavy oil or air-heavy oil-water systems in square capillaries, the trapping number is the summation of the capillary, Ca, [5,19,20,21] and the Bond numbers, Bo [5,10,12,22,23], defined as follows [5]:

$$N_T = |Ca + Bo| \quad (1)$$

$$N_T = \left| \frac{v_a \mu_o}{\sigma_{o-a} \cos \theta} + \frac{\Delta \rho g L^2}{\sigma_{o-a} \cos \theta} \right| \quad (2)$$

where v_a is the air velocity, μ_o is the viscosity of the oil phase, σ_{o-a} is the surface tension of the oil and is the contact angle measured through the wetting phase, $\Delta \rho$ is the density difference between the oil and the air, g is the gravitational constant and L is the characteristic length for each system. The characteristic length of the circular tube was its radius $r=0.016$ cm and for the square capillary tube was half of its width $L=W/2=0.015$ cm.

A more detailed discussion about the use of the trapping, capillary and Bond number to interpret these experiments can be found in Appendix A.

3.3.1 Two phase flow system: Air – heavy oil

3.3.1.1 Gravity drainage experiments at different trapping numbers and temperatures

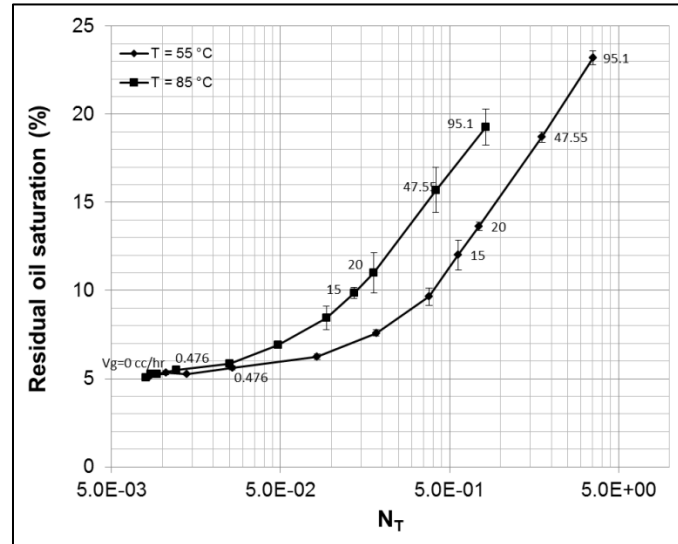


Figure 3-4: Residual oil saturation (heavy oil) vs. trapping number in a square capillary tube ($W=0.03$ cm) at high temperatures.

Figure 3-4 shows the residual oil saturation vs. trapping number for the square capillary tube of 0.03 cm in width at two different temperatures. It should be made clear at this point that, for the same gas injection rate at different temperatures, a lower trapping number was obtained at higher temperatures. Hence, to compare both curves, the S_{or} values must be read in horizontal manner at the same gas flow rate and from the lower to the higher temperature curve. Fluid injection in a reservoir is generally applied at a constant flow rate, so that it is possible to have different trapping numbers at different reservoir depths with the same flow rate and, even more, if there is a considerable geothermal gradient. **Figure 3-4** revealed that:

- 1) For $N_T < 2.7E-2$, the temperature and thereby the viscosity practically did not have influence on the S_{or} during the air assisted gravity drainage. Also, gravity did not affect the amount of retained oil. At these low trapping numbers, the S_{or} was controlled by capillary forces. The difference between the contact angles (24.3° and 0°) did not have a noticeable impact in the difference of the residual oil saturation for both curves.
- 2) For $N_T > 2.7E-2$, the viscous, capillary and gravity forces started to influence the amount of S_{or} left behind for both temperatures. The difference in the S_{or} increased as the trapping

number increased for the same gas flow rate at different temperatures. For example, for a gas flow rate of 2 ml/hr corresponding to trapping numbers of 8.23E-2 and 2.51E-2 at 55 °C and 85 °C respectively, the residual oil saturations were 6.2±0.2 % and 5.9±0.1 %. For a gas flow rate of 95.10 ml/hr corresponding to trapping numbers of 3.53 and 0.82 at 55 °C and 85 °C, respectively, S_{or} were 23.2±0.4 % and 19.3±1.0 %.

- 3) One may question if those were valid trapping numbers considering the capillary numbers reported in the literature for reservoirs applications [14,15]. To clarify this, free fall gravity drainage (FFGD) experiments corresponding to $N_T=0.01$ ($Ca=0$ and $Bo=0.01$) were carried out. S_{or} were 5.1±0.1 % at 55 °C and 85 °C. Hence, for very low trapping numbers ($N_T=1.1E-2$; or $Ca<1.0 E-3$), S_{or} values were obtained between 5.0% and 5.3%, being practically constant and was not controlled by temperature, at least up to 85 °C.

It is worth noting that, in this research, the retention of real heavy oil as the wetting phase began to be constant around $NT<2.7E-2$ ($Ca<1.7E-2$) for both temperatures while in the case of horizontal displacement for lighter oils started around $Ca < 5.0E-4$ [7].

The limit value around 5.0% for both curves at low Ca seemed to be near 6.0% theoretical equilibrium saturation of a wetting fluid surrounding a stationary air bubble in a square capillary tube with perfect corners obtained in earlier studies [7,24]:

$$S_w = \frac{(\cos \theta - \sqrt{\pi / 4 - \theta + \sin \theta \cos \theta})^2}{\theta + \cos^2 \theta - \pi / 4 - \sin \theta \cos \theta} \quad (3)$$

This was demonstrated for the case of liquid displacement in horizontal square capillaries [7]. The deviation with respect to 6.0% for the equilibrium saturation was attributed to the existence of roundness in the corners of the capillary tube [7]. As the same square capillary tube size ($W=0.03$) was used in the present work and that of Dong and Chatzis [7], such explanation also applies for the present research. However, it was found that the approximation to the equilibrium saturation of a wetting fluid surrounding a stationary air bubble in a square capillary tube with perfect corners was only valid for $W=0.03$ cm (as shown in the section for FFGD experiments with different width of square capillary).

Figure 5 shows a comparison of the results for the square ($W=0.03$ cm) and circular ($D=0.03$ cm) capillary tubes (curves for circular capillary tubes were taken from Argüelles and Babadagli [5]). It is known that non-circular geometries, like a square capillary, have a higher wetting phase retention than circular capillary tubes [6,7]. For these tubes and temperature ranges, the square capillary tube retained almost twice ($S_{or} \sim 5.0\%$) the amount retained by the circular tube ($S_{or} \sim 2.6\%$) for ($N_T < 2.7E-2$). It is noteworthy that the difference in the retained oil saturation between both geometries decreased for $N_T > 2.7E-2$ at the same temperature. Therefore, the geometry became less influential as the capillary number increased (through viscous forces).

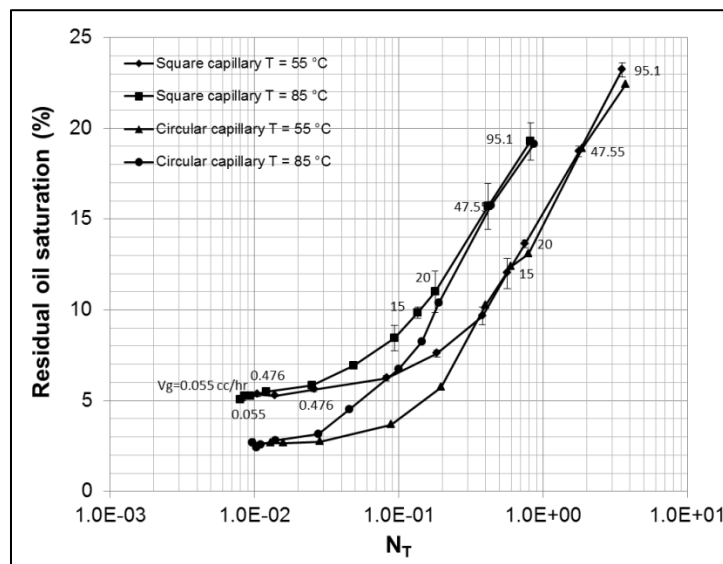


Figure 3-5: Comparison of the residual oil saturations in the square ($W=0.03$ cm) and circular ($D=0.032$ cm) capillary tubes (data of the circular tube experiments taken from Argüelles - Vivas and Babadagli [5]).

After the displacement of the oil slug by air, the residual oil will occur as thin films in the circular capillary tubes and as layers in the angular zones of the non-circular geometries such as square capillary tubes. Note that the drainage of the residual oil formed as layers or films is a very slow process controlled by gravity. The flow of oil in films and layers has been studied by Blunt et al. [6] Ransohoff and Radke [25], Dong and Chatzis [26], Zhou et al. [27], Dong and Chatzis [28] and Dehghanpour et al. [29] for isothermal (and low temperature) systems. However, the removal of the oil films or layers in high temperature systems has not been clarified yet.

Figure 3-6 shows a FFGD experiment in a square capillary tube at 85 °C. In **Figure 3-6-b**, the

rear meniscus of the oil slug and the oil layers on the angular zones are identifiable. In Figures 3-6-c and 3-6-d, the oil layers from 4 cm and 37 cm behind the rear meniscus are clearly seen.

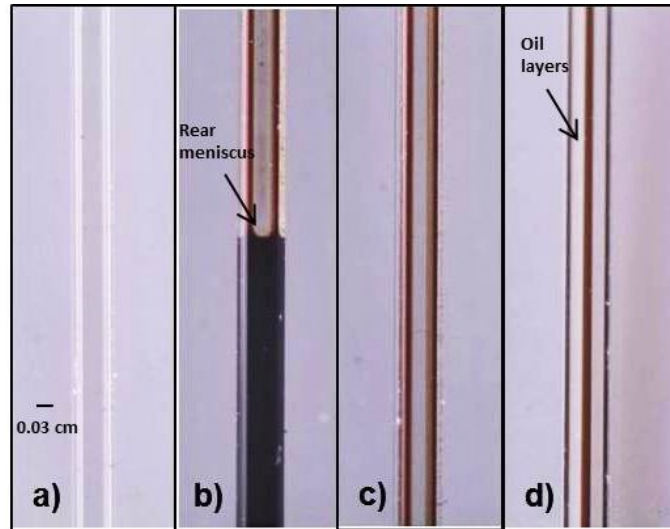


Figure 3-6: Pictures of the square capillary tube ($W=0.03\text{ cm}$): a) before the displacement, b) rear meniscus of the oil slug in FFGD at $85\text{ }^{\circ}\text{C}$, c) oil layers in the angular zones 4 cm behind the rear meniscus, d) oil layer in the angular zones at 37 cm behind the rear meniscus.

Figure 3-7 illustrates the cross sectional area of the square capillary tube at two different times in a FFGD experiment. These photos were taken to capture the shape of the oil-air interface in the cross sectional area after the movement of the oil slug. In **Figure 3-7-b**, the oil layers in the angular zones of the square capillary are well defined.

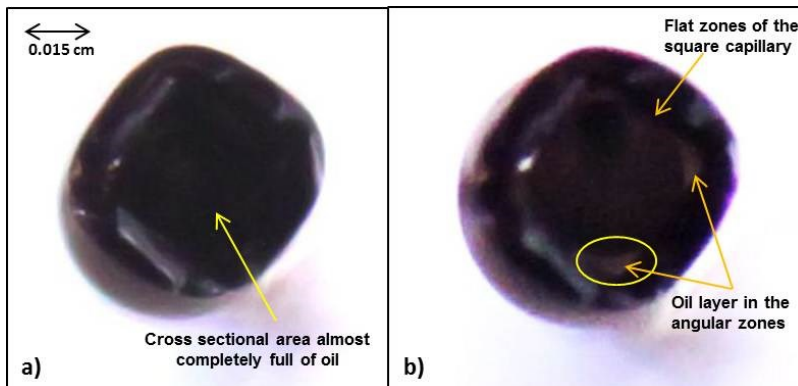


Figure 3-7: Cross sectional area of the square capillary tube ($W=0.03\text{ cm}$) : a) beginning the free fall gravity drainage b) after the oil slug moved 7 mm.

3.3.1.2 Effects of travel distance by the liquid phase (heavy oil) on S_{or} during FFGD

Experiments to clarify the effects of the distance traveled by the oil slug on S_{or} development during FFGD in a square capillary tube of $W=0.03\text{ cm}$ were carried out. The length of the liquid

slug was around 5 and 6 cm for all the experiments and the experimental procedure was exactly the same explained in the previous section. As seen in **Figure 3-8**, the distance traveled by the oil slug did not affect the amount of S_{or} left behind during a FFGD at different temperatures.

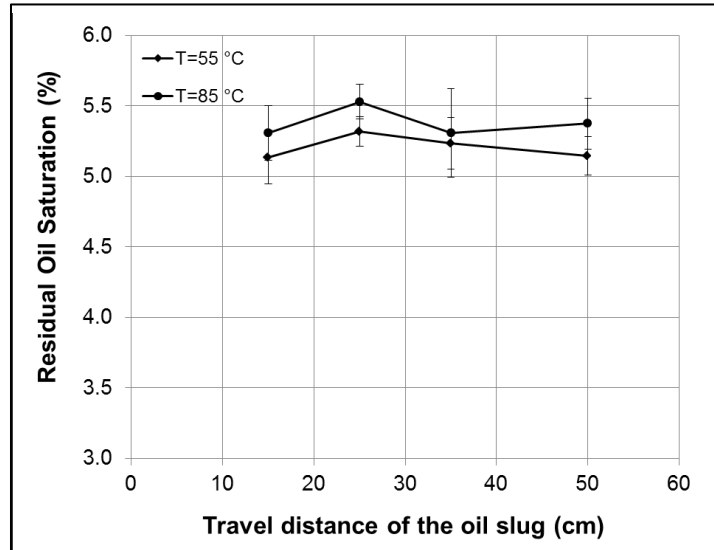


Figure 3-8: Effects of the travel distance on the oil slug on the S_{or} during FFGD experiments.

3.3.1.3 Effects of oil slug length on S_{or} during FFGD

The effects of oil slug length on the S_{or} during FFGD in a square capillary tube of $W=0.03$ cm were also evaluated.

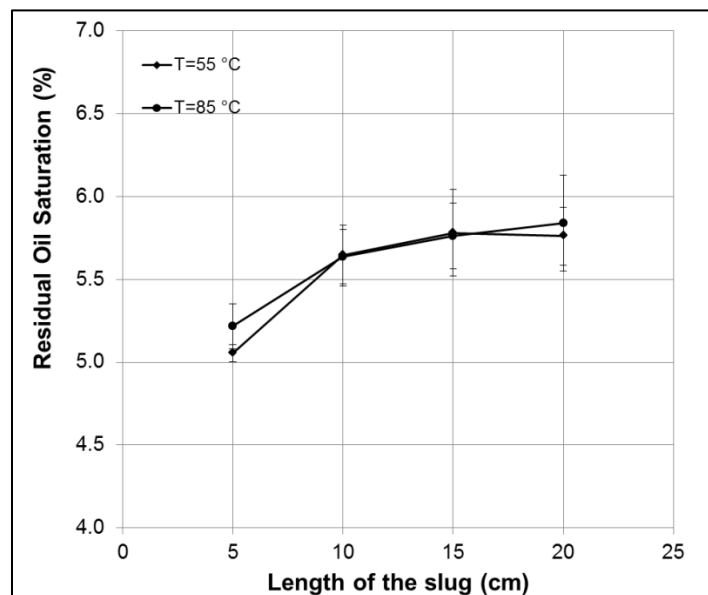


Figure 3-9: Effects of the slug size on the S_{or} during FFGD experiments.

From **Figure 3-9** it can be observed that the amount of residual oil saturation left behind as layer in the corners of a square capillary tube was independent of the oil slug length during FFGD and also did not depend on the temperature.

3.3.1.4 Effects of characteristic length of square capillaries on S_{or} during FFGD

FFGD experiments ($N_T=Bo$) were carried out to investigate the effects of characteristic length of square capillary tube on the development of S_{or} .

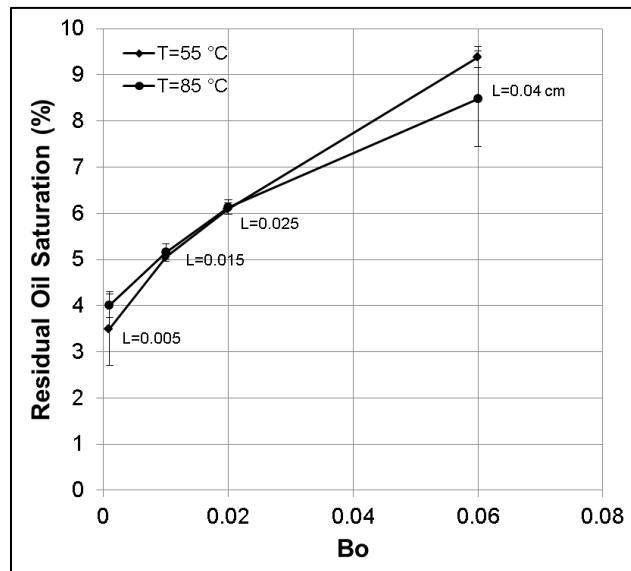


Figure 3-10: Effects of characteristic length (or width) through Bond number on S_{or}

According to **Figure 3-10**, there was a linear relationship between the Bond number and the amount of retained oil during FFGD. The S_{or} increased as the Bond number increased. It is noticeable that an increment in the width meant an increment in the Bond number. The trends shown in **Figure 3-4** and **Figure 3-10** demonstrated the following:

- For FFGD and low trapping number gravity drainage experiments, S_{or} depended on the capillary forces (for the same width of capillaries), and
- For different widths, on the other hand, in the low N_T and FFGD experiments ($N_T=Bo$), the S_{or} depended on the competition between capillary and gravity forces, namely, the Bond number.

Although forced gravity drainage experiments were not carried out for different widths of square

capillaries, the results in **Figure 3-4** and **Figure 3-5** suggested that there was a wide range of N_T where the viscous forces did not influence the S_{or} 's significantly for $W=0.03$ cm ($L=0.015$ cm). An empirical equation was obtained to determine the S_{or} (in %) as a function of the Bond number from **Figure 3-10** (with $R^2=0.98$).

$$S_{or} = 83.367Bo + 4.0786 \quad (4)$$

Equation (4) could fit well to forced gravity drainage experiments at low N_T and to FFGD for different pore size of square shape.

It is clear from **Figure 3-10** that the S_{or} values were different from that of a square capillary tube with perfect corners (around 6.0%) having a wetting fluid surrounding a stationary air bubble [7,24]. This is mainly due to some assumptions that Legait [24] did in order to develop a laminar flow equation for square capillaries:

- a) Thin enough horizontal capillary tube to neglect gravity effects;
- b) Flow did not affect the curvatures of the interfaces between fluids.

Such assumptions are not met for these experiments.

3.3.1.5 Layer thickness of S_{or} in FFGD experiments

The layer thickness for the FFGD experiments at 55 and 85 °C were measured. Although the adjustment of the light source and the use of proper lens to create clear images were done, the shadow in the middle was unavoidable. Therefore, the edges had to be cleared. The width of the empty square capillaries was measured as an initial test to make sure that it was exactly 0.03 cm at every point of the capillary (this was a way to check the size of the tube given by the supplier).

Comparing the images of the empty tube and the ones with oil, the difference in the thickness on each side of the tube was obtained. The empty region above or beneath the oil layer in each image was due to the reflection under the microscope and occurred in the images of empty tubes as well. **Figure 3-11** shows the empty and filled square capillary tubes for an FFGD experiment at 85 °C.

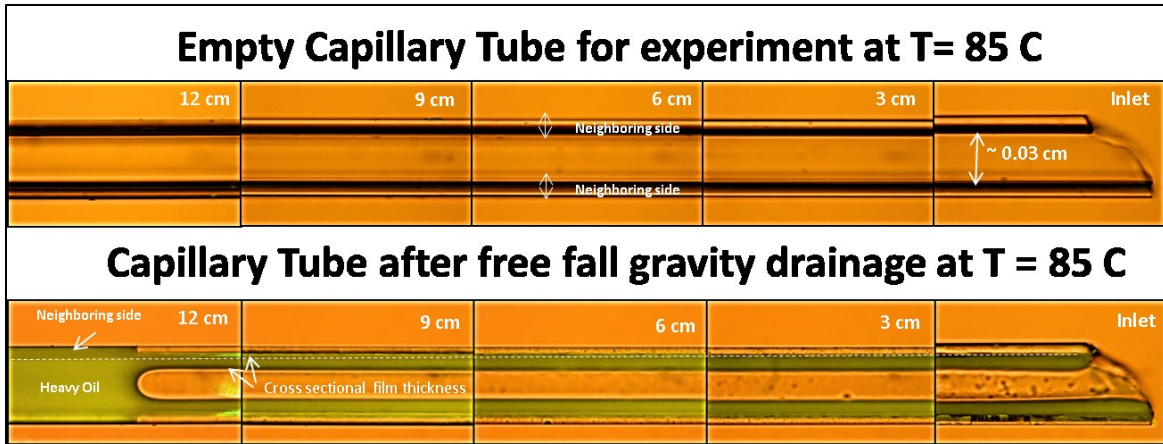


Figure 3-11: Measurements of layer thickness in a square capillary tube ($W=0.03$ cm)

Figure 3-12 and **13** show the layer thickness along the length of the square capillary tubes for $W=0.03$ cm at 55 and 85 °C, respectively. From these figures, the average thickness was obtained to be 0.005 cm (50 μ m) for both temperatures.

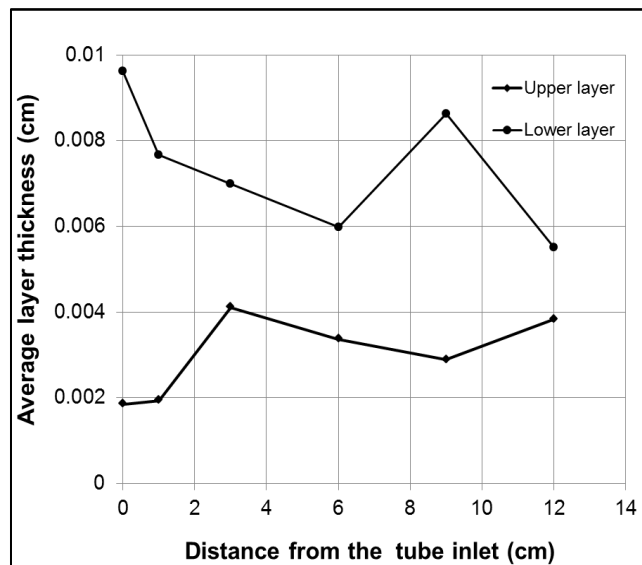


Figure 3-12: Average layer thickness in square capillary tube of $W=0.03$ cm during a free fall gravity drainage at $T=55$ °C.

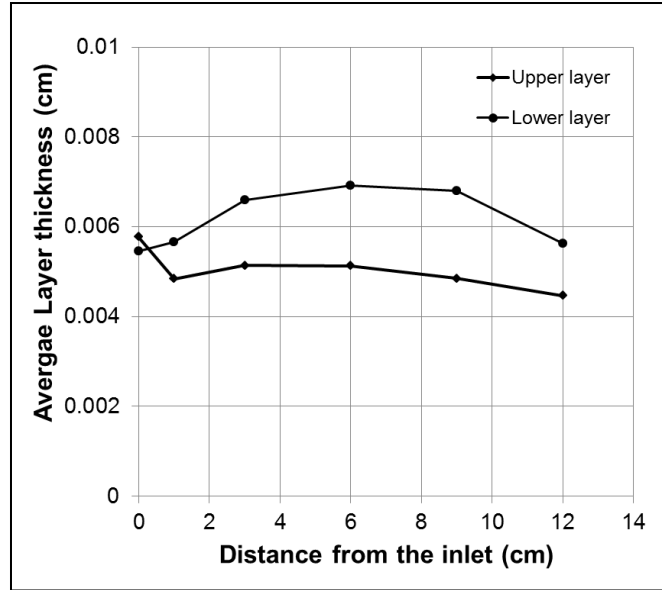


Figure 3-13: Average layer thickness in square capillary tube of $W=0.03$ cm during a free fall gravity drainage at $T=85$ °C.

3.3.2 Three phase flow system: Air – heavy oil – water

3.3.2.1 Gravity drainage experiments at different trapping numbers and temperatures

In order to evaluate the effects of initial water saturation (S_{wi}) on the S_{or} during the gravity drainage experiments, a water slug with a length similar to that of the oil was placed in front of the oil slug. The purpose was to form water film covering along the walls (flat part) and corners of the square capillary tube and the subsequent development of residual oil over this water. Attempts were made to place water first through air-water displacement and then to carry out the air-heavy oil displacements but it was not possible. The saturation curves vs. N_T are displayed using the capillary number based on the air-oil interface as for two phase experiments for ease of interpretation. The water saturation curve could also be expressed based on the water-oil interface and this would just shift it to the left of the graph.

Figure 3-14 and **Figure 3-15** show the S_{or} 's for two (air-heavy oil) and three phase (air-heavy oil-initial water) gravity drainage experiments for $N_T \leq 5.64E-1$ at 55 °C and for $N_T \leq 1.36E-1$ at 85 °C. **Figure 3-16** and **Figure 3-17** display the total saturation, S_{total} , residual oil saturation, S_{or} , and initial water saturation, S_{wi} , during gravity drainage experiments at 55 and 85 °C, respectively.

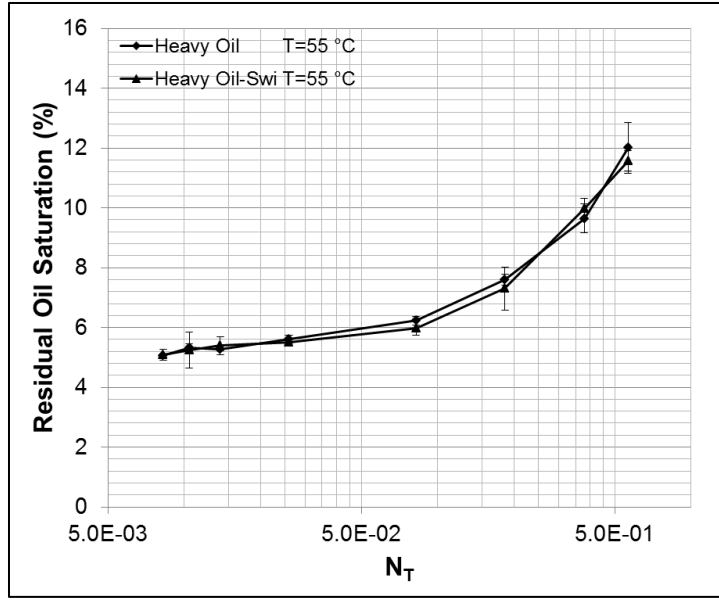


Figure 3-14: Comparison of residual oil saturation between air – heavy oil and air-heavy oil – initial water systems at $T=55\text{ }^\circ\text{C}$ in a square capillary ($W=0.03\text{ cm}$).

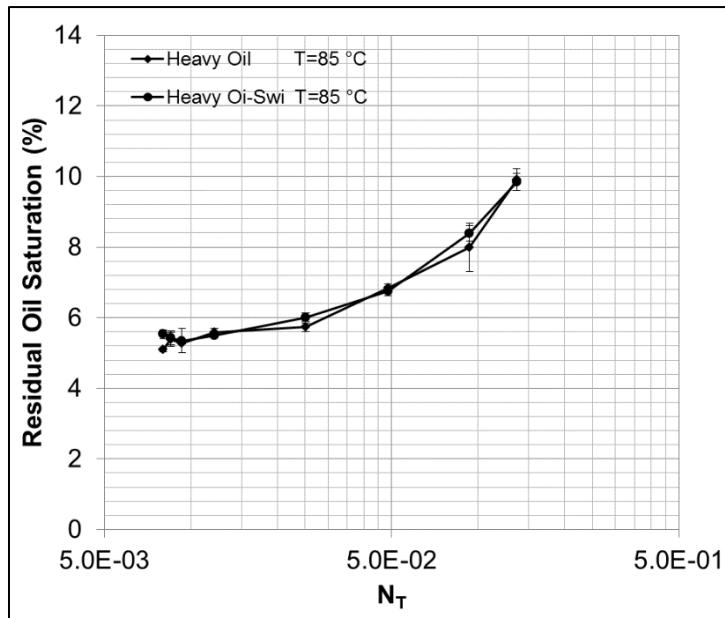


Figure 3-15: Comparison of residual oil saturation between air – heavy oil and air-heavy oil – initial water systems at $T=85\text{ }^\circ\text{C}$ in a square capillary ($W=0.03\text{ cm}$).

The presence of water did not modify the amount of retained heavy oil for all the N_T ranges at both temperatures in two phase flow experiments (air-heavy oil). Also, the retention of water was constant for all N_T ranges at both temperatures. Since oil and water saturations were constant at low N_T values (low Ca numbers), the total saturation was obviously constant, as it can be observed from **Figure 3-16** and **Figure 3-17**. However, these total saturations were characteristically higher than the theoretical equilibrium saturation for a square capillary tube

[24]. These results differ from those of Dong and Chatzis [7] where it was observed that total saturation (oil phase + water phase) at very low Ca is constant and corresponds to the equilibrium saturation of oil surrounding a stationary gas bubble taking into account the rounded corners for horizontal displacements. Therefore, a reduction or augmentation in the retained oil (depending of Ca range) is compensated by an increment or decrement of the retained water, resulting always in the same equilibrium saturation value [7].

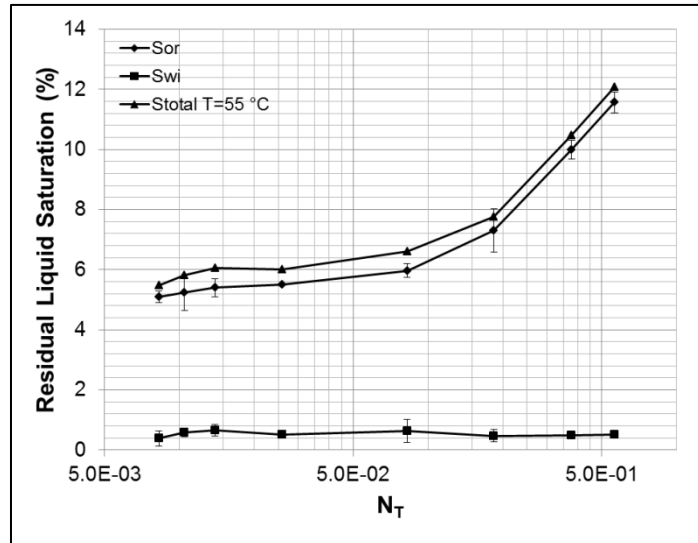


Figure 3-16: Total oil and water saturation during air-heavy oil – water gravity drainage experiments at $T=55\text{ }^\circ\text{C}$ in a square capillary ($W=0.03\text{ cm}$).

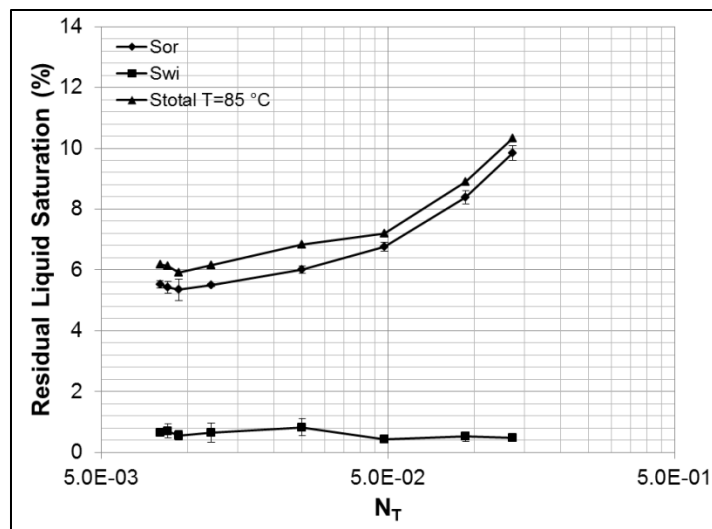


Figure 3-17: Total oil and water saturation during air-heavy oil – water gravity drainage experiments at $T=85\text{ }^\circ\text{C}$ in a square capillary ($W=0.03\text{ cm}$).

In this study, the S_{or} for two and three phase gravity drainage experiments at low N_T (low Ca) at both temperatures would represent such theoretical equilibrium saturation with an ‘extra’ and constant retention of water during air-heavy oil-water experiments. There was no change in water saturation slopes with respect to the N_T number for all the gravity drainage experiments. In contrast to these observations, Dong and Chatzis [7] found that for $Ca < 1.0E-4$ there is a change in the slopes of water saturation curves against the Ca number, and water retention decreased with decreasing Ca (with a corresponding augmentation of oil retention).

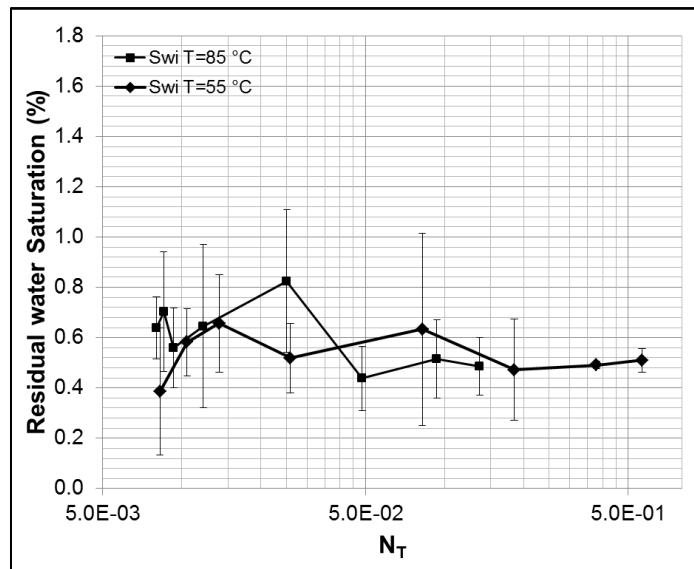


Figure 3-18: Water saturation during air-heavy oil – water gravity drainage experiments at $T=55\text{ }^\circ\text{C}$ and $T=85\text{ }^\circ\text{C}$ in a square capillary ($W=0.03\text{ cm}$).

It is interesting to notice that, with such high viscosities of heavy oil, water was not completely swept from the capillaries. In their horizontal displacement experiments, Dong and Chatzis [7] observed that water saturation was reduced from 1.5%, the equilibrium saturation (discounting the roundness of the tube), to 0.7 % when kerosene (1.94 cP) was introduced. In our case (heavy oil), although the viscosities were very different at 55 and 85 °C, the retained water was the same for the entire N_T range for both temperatures (**Figure 3-18**). These observations suggest the following:

- a) There is an oil viscosity range where minimum residual water saturation exists and cannot be displaced from the square capillary tube;
- b) There is a minimum viscosity value at which the S_{or} becomes constant;

- c) The water retention decreases as the oil viscosity increases until the irreducible water saturation is reached. Experiments carried out with a lighter real oil of 12 cP in the FFGD experiments supported these suggestions ($S_{or}=4.2\%\pm 0.3$ and $S_{wi}=1.4\%\pm 0.2$).

As seen, there is a certain amount of water that could never completely be removed (irreducible water saturation). This was attributed to water wet nature of the capillary tubes. Note that the capillary tubes were treated with a sulfuric chromic solution, which made the tubes strongly water-wet.

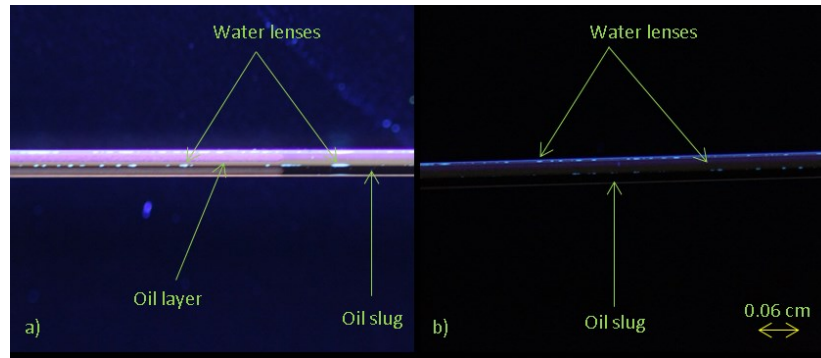


Figure 3-19: Photos of water and oil in a square capillary ($W=0.03$ cm) after a FFGD at 55 °C for air – heavy oil – water system: a) rear meniscus b) oil slug over water saturation.

Photos were taken after displacements to investigate the geometrical shapes of the retained water. In ideal square capillaries with perfect corners, it is expected to have layers of water and oil in the corners. However, layers of water were not observed, at least not with the camera we used. It is highly likely that, due to high viscous forces caused by the heavy nature of the oil, water did not form a layer but a nano film instead. **Figure 3-19** shows the oil layers (in the corners and flat parts of the tube –as thin films) and water as disconnected lenses. This is in agreement with previous observations [30,31]. It was proposed that, for the case of Athabasca oil sands, the connate water saturation occurs as pendular rings, trapped in fines clusters and as thin films in the order of 10-15 nm [30].

3.3.2.2 Effects of fluid distribution on the residual liquids saturation during Free Fall Gravity Drainage (FFGD)

Since more than two phases in different configurations could exist in gravity drainage processes, the behavior of residual liquid saturation left behind under different fluid distributions during FFGD experiments was studied for four different cases (**Figure 3-20**):

- a) air-heavy oil,
- b) air-heavy oil-water,
- c) air-water-heavy oil, and
- d) air-water-heavy oil-water

Square capillaries were 0.03 cm in width and water wet for all these experiments.

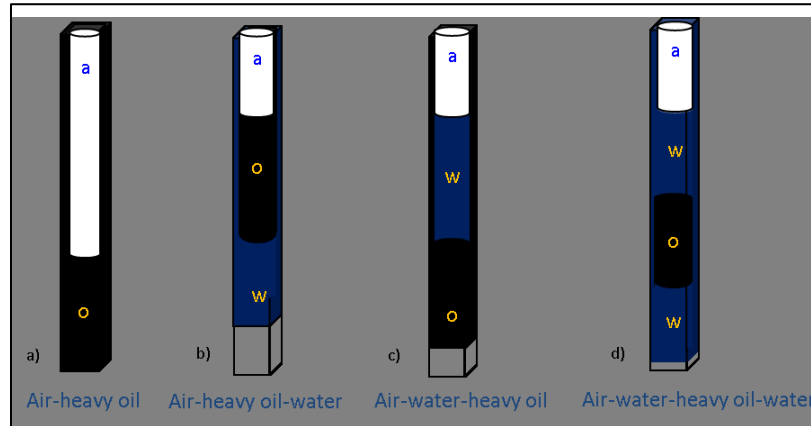


Figure 3-20: Different fluid distribution during FFGD experiments in square capillary ($W=0.03$ cm).

A comparison of S_{or} and S_{wi} for different configurations (illustrated in **Figure 3-20**) is shown in **Figure 3-21** and **Figure 3-22**. As seen, fluid distribution affected the retention of liquids. The first two configurations, Cases *a* and *b*, were analyzed in the previous sections. The third configuration (air–water-heavy oil) could exist in non-isothermal processes where steam condensation occurs or in double displacement processes where gas is injected after water for oil recovery. Higher S_{or} and S_{wi} values were observed for this arrangement compared to Case *b*. Note that in this particular configuration, a less viscous liquid displaced a more viscous liquid, which is opposite to Case *b*. As a consequence of this, water tended to finger more through the center of the capillary where it found less resistance, deforming the water-heavy oil interface and creating a more bullet shape instead of a flatter one. Thereby, the S_{or} increased mainly in the corners of the tube, which explains the increment of S_{or} compared to Case *b*.

A limited number of works on immiscible liquid-liquid displacements in horizontally placed circular capillary were reported [32,33,34]. These studies demonstrated that residual liquid saturation increased as the viscosity ratio of the displaced to displacing phase was decreased by increasing the latter. Soares et al. [34] reported the following three major observations:

- a) For a fixed Ca, the film thickness augmented as the displacing liquid became more viscous,
- b) As the Ca diminished, the interface front became flatter and,
- c) As the viscosity of displacing fluid increased, the interface front became less flat.

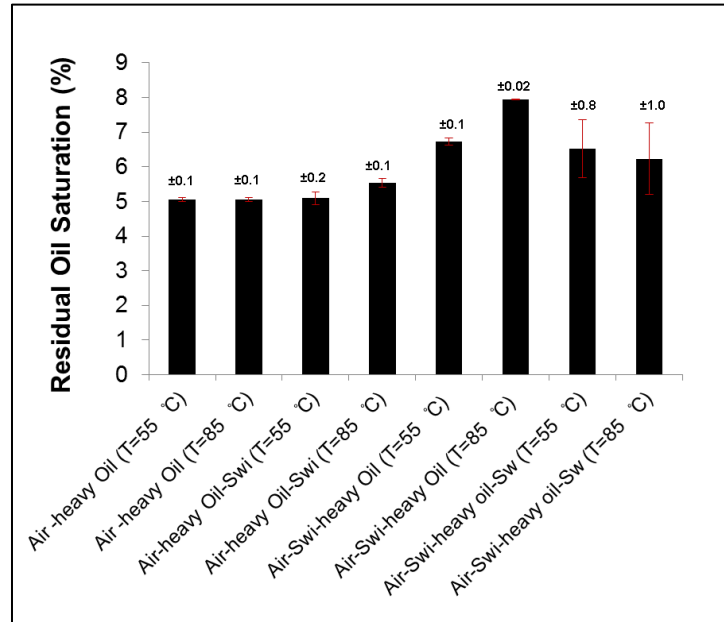


Figure 3-21: Residual oil saturation under different fluid configurations in square capillary tubes (W=0.03 cm).

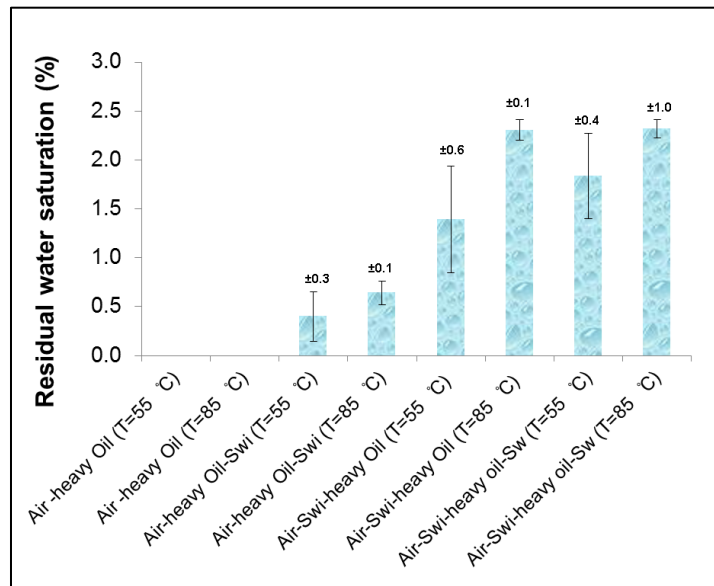


Figure 3-22: Residual water saturation under different fluid configurations in square capillary tubes (W=0.03 cm).

Case *c* experiments (air-water- heavy oil) were carried out as FFGD, where $N_T=0.01$ ($Ca=0$ and $Bo=0.01$). It was observed that the oil retention was much higher at 85 °C in this configuration. Although the competition was between gravity and capillary forces, the viscosity ratio played a more important role in obtaining different S_{or} 's at different temperatures. The viscosity ratio decreased from 579.6 at 55 °C to 196.9 at 85 °C. This kind of high viscosity ratio resulted in a deformation at the water-heavy oil interface. At the higher temperature, FFGD was faster. This resulted in water (displacing fluid) fingering through the interface. Increasing temperature (85 °C) caused a more bullet shape displacement at the interface compared to the lower temperature case (55 °C), where a flatter interface existed. A more bullet shape displacement resulted in a thicker layer around the corners.

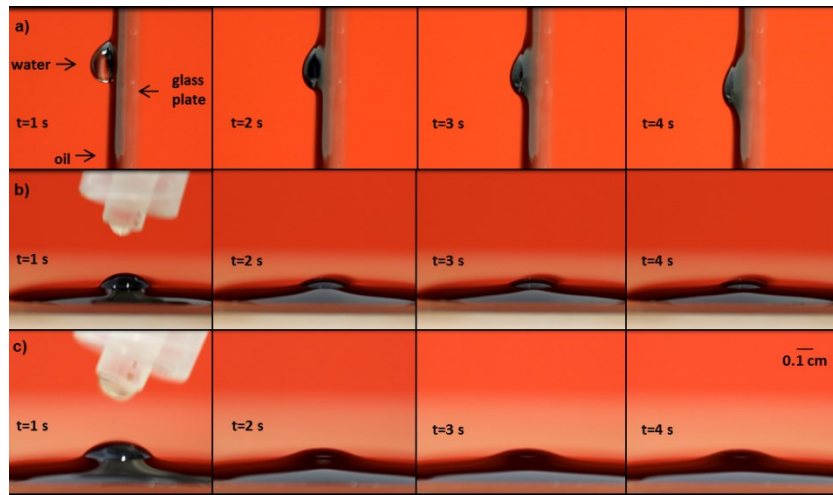


Figure 3-23: Engulfment of water in heavy oil: a) $T=25$ °C, b) $T=55$ °C, c) $T=85$ °C.

Case *c* showed higher water retention at 85 °C than at 55 °C. The retention of water was also higher for Case *c* compared to Case *b*. The negative spreading coefficient of water on oil in the presence of air and a high viscosity ratio explain all these results reasonably well. A negative spreading coefficient means oil does not spread spontaneously between a flat gas–water interface [35] and remains as a bulk lens [4,36,37]. Also, if the initial spreading coefficient is positive but the final spreading coefficient is negative, the equilibrium state will be a monolayer of oil over water with lens of oil [38].

Three experiments on glass plates were carried out to understand this fluid distribution and the effect of spreading coefficient. A layer of heavy oil was placed over the plates and drops of water were carefully placed over the oil. One glass plate was placed vertically at room temperature and

the other two were placed in a heating plate at 55 and 85 °C horizontally. The negative spreading coefficients of water on oil were -67.1 and -70.3 mN/m at 55 and 85 °C, respectively. In the three experiments, it was observed that once the drops contacted the heavy oil, water-in-oil emulsion was formed. This process was faster at higher temperature as can be observed in **Figure 3-23**. The formation of water lenses on the heavy oil surface or the formation of a water monolayer with lenses was not observed.

This behavior of non – spreading of water in oil can be attributed to the contrast between the surface tensions of water-air and oil-air pairs. The air-oil surface tension and the oil-water interfacial tension are very similar to each other so that the oil can stay between air and water forming the shapes seen in Case *b* of **Figure 3-20**. However, the air-water surface tension and the oil-water interfacial tension are very different, being the former much higher. Then, being away from air is a state of less energy for water and therefore has a tendency to be immersed in oil (**Figure 3-23**). This process was aided by the hydrophilic part of heavy oil, which has natural surfactants to reduce the interfacial tension further.

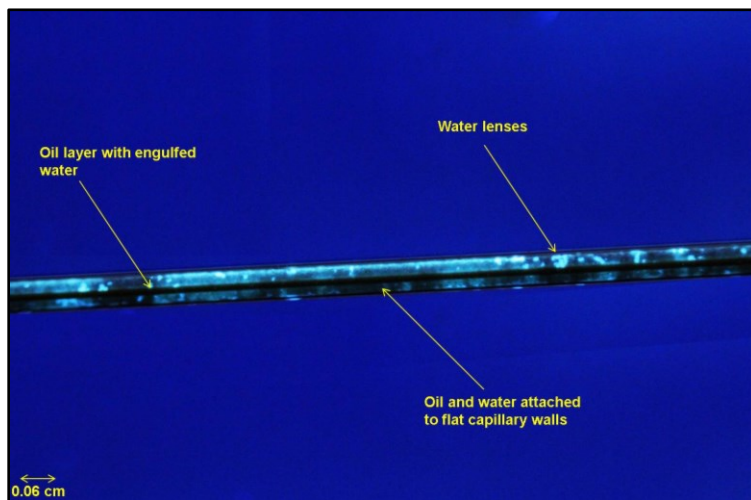


Figure 3-24: Photos of water and oil in a square capillary ($W=0.03$ cm) after a FFGD for air-water – heavy oil configuration at $T=55$ °C.

In this manner, during FFGD, while water saturation develops as layers, some amount of water was gobbled in the oil phase increasing its retention. Since more oil saturation was developed at 85 °C due to the viscosity ratio, more water was engulfed in these thicker oil layers. **Figure 3-24** shows the aspect of residual liquid saturation for Case *c*. In this figure, the oil layers in the corners of the tube are observed. As mentioned earlier, most of the retained water was engulfed

in those layers. In the flat walls of the tube more retained oil mixed with water can be also seen. The bright dots over the surface of the capillary correspond to small water lenses. The retention of fluids for Case c is clearly higher than that observed in **Figure 3-19** for Case b.

The fourth Case d consisted of an oil slug having a water slug in the front and back. In this case, as the FFGD was carried out, the back water slug joined to the water introduced at the front through the existing films of water that created a hydraulic conductivity below the oil phase. As can be observed in **Figure 3-21** and **Figure 3-22**, there was a greater uncertainty in those experiments (see standard deviations for Case d) since this configuration begun as Case d but finished as Case b. At the end, there was a longer front water slug. Measured S_{or} and S_{wi} values were similar to those of Case b but with much greater instability.

3.3.2.3 Effects of wettability on the residual liquids saturation during FFGD

The effects of wettability on the development of S_{or} and S_{wi} were also studied for square capillaries of $W=0.03$ cm with the air-heavy oil-water system (case b) in **Figure 3-20** for FFGD. Residual oil and water saturations values for water-wet (WW) and oil-wet (OW) square capillaries are shown in **Figure 3-25** and **Figure 3-26**, respectively.

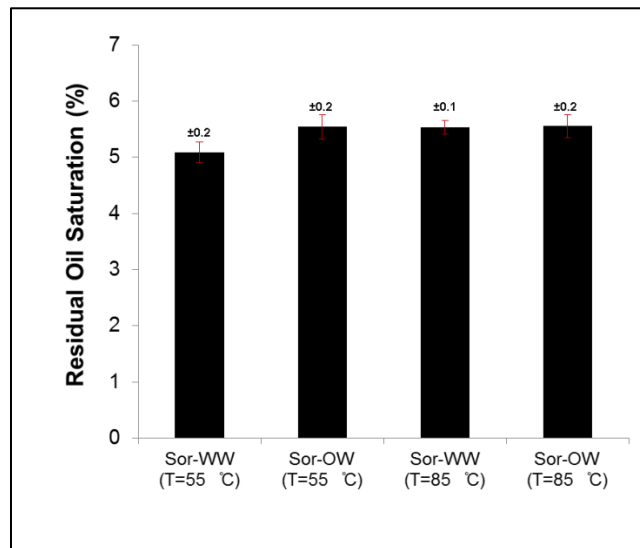


Figure 3-25: Residual oil saturation in WW AND OW square capillary tubes ($W=0.03$ cm) for FFGD experiments.

No significant difference was observed in the S_{or} for different wettability cases. Apparently there was a slight increment in the S_{or} at 55 °C, but this was within limits of the margin of error.

For the experiments at 85 °C, the oil retention was the same for oil and water wet capillaries. There was also not significant change in the water retention for the oil wet case.

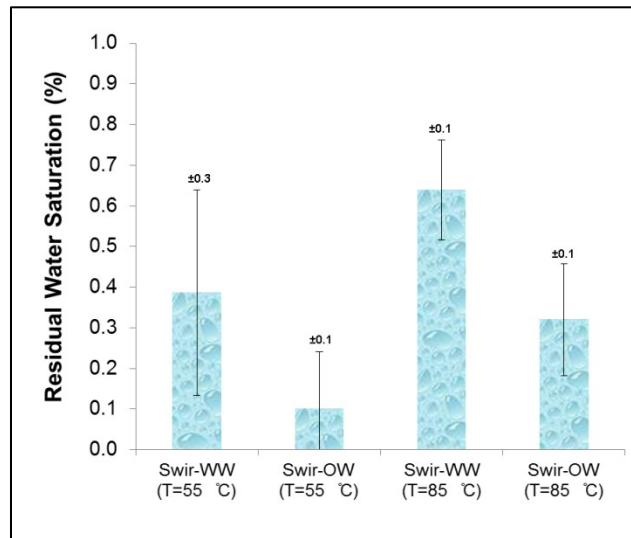


Figure 3-26: Residual water saturation in WW AND OW square capillary tubes ($W=0.03$ cm) for FFGD experiments.

Once again, high viscous forces resulting from heavy oil could explain these behaviors. As it was analyzed in Section 3.2.2.1, the momentum transfer due to viscous forces from heavy oil to water was the dominant mechanism responsible for having very low water retention and the maximum residual oil saturation, even though the square capillaries were water wet. For these experiments with oil wet capillaries, this process was facilitated by oil wetness acting together with the viscous forces but the residual oil saturation was not augmented. These results suggest that, in the case of very viscous oil displacing much less viscous water, the wettability of the square capillary does not influence in the amount of retained oil due to high viscous forces from displacing fluid.

3.4 Conclusions and remarks

The development of residual liquid saturations in square capillaries of $W=0.03$ cm during two and three phase flow under gravity at different temperature conditions was analyzed experimentally. For air-heavy oil gravity drainage experiments (two phases), when the trapping number (N_T) $< 2.7E-2$, S_{or} was independent of viscous and gravity forces and the process was controlled by capillary forces. Therefore, temperature affecting mainly viscous forces did not have influence on S_{or} . In this region of N_T , S_{or} was constant. If $N_T > 2.7E-2$, viscous, capillary

and gravity forces competed, affecting the oil retention. The difference in the S_{or} increased as the N_T increased for the same gas flow rate at different temperatures. Comparing the circular and square capillary cases of the same cross sectional dimension (diameter and width respectively) at the same temperature, it was found that S_{or} difference between both geometries decreased as the N_T augmented for $N_T > 2.7E-2$. Therefore, the effects of the geometrical shape on S_{or} diminished at high N_T values.

In the FFGD experiments, it was demonstrated that the S_{or} was independent of the distance traveled by the oil slug and also independent of the oil slug length. However, the retention of heavy oil was a function of the width of the square capillary and, as a consequence, it depended on the competition between the gravity and capillary forces (defined as the Bond number). An empirical linear correlation was developed by fitting the data, which was independent of temperature. Although this equation was obtained for the FFGD experiments, it can be used for forced (low N_T) gravity drainage displacements as the retention of oil was constant for a wide N_T number interval. It was also demonstrated that constant S_{or} for different width of square capillary in FFGD did not correspond to the equilibrium saturation of a wetting phase surrounding a stationary gas bubble, except for a 0.03 cm square capillary.

In the case of air-heavy oil-water experiments (three phases) in square capillaries of $W=0.03$ cm at 55 and 85 °C, the presence of initial water did not alter the amount of retained oil. The retention of water was also constant for all gravity drainage experiments including the free fall ones. Therefore, the total saturation of retained fluids was constant but higher than the theoretical equilibrium saturation predicted for water surrounding a stationary slug of heavy oil in a water-wet square capillary. This retention beyond the equilibrium saturation corresponded to water that was not completely swept due to water wetness of the tube despite high viscous forces due to heavy oil. It was precisely the high viscosity of the oil that explains why there was no change in the saturation of oil during these three phase gravity drainage experiments. Based on these results and the given discussion, it is suggested that:

- 1) a heavy oil viscosity interval exists where water saturation cannot be completely swept from tubes,
- 2) a minimum heavy oil viscosity exists at which S_{or} is constant, and

- 3) S_{wi} diminishes as the oil viscosity augments until irreducible water saturation is reached.

The amount of retained fluids in FFGD experiments at $T=55$ and 85 °C varied with the fluid distribution in the capillaries. The configuration air-water-heavy oil exhibited the highest oil and water residual saturations among four different fluid distribution configurations. The high oil retention in this case was due to the fact that a much less viscous liquid displaced a very viscous liquid so that it fingered through the center of the tube. The highest S_{or} occurred when the viscosity ratio of displaced to displacing case decreased due to the reduction in heavy oil viscosity. It was also shown that, in this configuration, water is engulfed in the oil due to the negative spreading coefficient of water on oil in the presence of air causing a higher S_{wi} . More water retention occurred at $T=85$ °C due to more available residual oil saturation and more negative spreading coefficient.

Wettability alteration from water-wet to oil-wet did not change the S_{or} for air-heavy oil-water system in the FFGD experiments with square capillaries of 0.03 cm width. In the case of oil-wet state, the oil wettability facilitated the displacement of water by oil through the viscous forces and a mild reduction in S_{wi} was observed due to wettability change.

3.5 References

- [1] O. Mohammadzadeh, I. Chatzis, Pore-Level Investigation of Heavy Oil Recovery Using Steam Assisted Gravity Drainage (SAGD), Paper IPTC 13403 presented at the Int. Petroleum Tech. Conf., Doha, Qatar, 7-9 Dec. (2009).
- [2] Don W. Green, G. Paul Whillhite, Enhanced Oil Recovery, SPE Textbook Series Vol. 6, 1998.
- [3] J. Hagoort, Oil Recovery by Gravity Drainage, Soc. Pet. Eng. J. (1980) 139-150.
- [4] I. Chatzis, A. Kantzas, F.A.L. Dullien, On the Investigation of Gravity Assisted Inert Gas Injection Using Micro-models, Long Berea Sandstone Cores, and Computer-Assisted Tomography, in: Proceedings of the Annual Technical Conference and Exhibition of the Society of Petroleum Engineers, Society of Petroleum Engineering, Houston, TX, 1988, SPE 18284.

- [5] F. J. Argüelles – Vivas, T. Babadagli, Drainage Type Oil and Heavy-Oil Displacement in Circular Capillary Tubes: Two- and Three-Phase Flow Characteristics and Residual Oil Saturation Development in the Form of Film at Different Temperatures. Submitted to Journal of Petroleum Science and Engineering. (2013).
- [6] M. Blunt, D. Zhou, D. Fenwick, Three-Phase Flow and Gravity Drainage in Porous Media, *Transport in Porous Media*. 20 (1995) 77-103.
- [7] M. Dong, I. Chatzis, An Experimental Investigation of Retention of Liquids in Corners of a Square Capillary, *Journal of Colloid and Interface Science*. 273 (2004) 306-312.
- [8] A. K. Singhal, W. H. Somerton, Two-Phase Flow Through a Non – Circular Capillary at Low Reynolds Numbers, *J. Can. Pet. Technol.* 9 (3) (1970) 197-205.
- [9] T. C. Thulasidas, M. A. Abraham, R. L. Cerro, Bubble–Train Flow in Capillaries of Circular and Square Cross Section, *Chemical Engineering Science*. 50 (2) (1995) 183-199.
- [10] J. Ratulowski, H. C. Chang, Transport of Gas Bubbles in Capillaries, *Phys. Fluids A*. 1 (10) (1989) 1642-1655.
- [11] W. B. Kolb, R. L. Cerro, Coating the Inside of a Capillary of Square Cross-Section, *Chemical Engineering Science*. 46 (9) (1991) 2181-2195.
- [12] W. B. Kolb, R. L. Cerro, The Motion of Long Bubbles in Tubes of Square Cross-Section, *Phys. Fluids A*. 5 (7) (1993) 1549-1557.
- [13] F. Kamişli, Flow of a Long Bubble in a Square Capillary, *Chemical Engineering and Processing*. 42 (2003) 351-363.
- [14] L.W. Schwartz, H.M. Princen, A.D. Kiss, On the motion of bubbles in capillary tubes, *Journal of Fluid Mechanics*. 172 (1986) 259-275.
- [15] F.A.L. Dullien, *Porous Media: Fluid Transport and Pore Structure*, second ed., Academic Press, San Diego, 1992.
- [16] M. Jin, A Study of Non-Aqueous Phase Liquid Characterization and Surfactant

Remediation, PhD dissertation, The U. of Texas. Austin, Texas (1995).

[17] K.D. Pennell, G.A. Pope, L.M. Abriola, Influence of Viscous and Buoyancy Forces on the Mobilization of Residual Tetrachloroethylene During Surfactant Flushing, *Environmental Science & Technology*, 30(4) (1996) 1328-1335.

[18] G.A. Pope, W. Wu, G. Narayanaswamy, M. Delshad, M.M. Sharma, P. Wang, Modeling Relative Permeability Effects in Gas-Condensate Reservoirs with a New Trapping Model, *SPE Reservoir Eval. & Eng.* 3 (2) (2000) 171-178.

[19] F. Fairbrother, A.E. Stubbs, Studies in Electroendosmosis. Part VI. The 'Bubble Tube' Method of Measurement, *Journal of Chemical Society*. 1 (1935) 527-529.

[20] F.P. Bretherton, The Motion of Long Bubbles in Tubes, *Journal of Fluid Mechanics*. 10 (1961) 166-188.

[21] M.D. Giavedoni, F.A. Saita, The Axisymmetric and Plane cases of a Gas Phase Steadily Displacing a Newtonian Liquid – A Simultaneous Solution of the Governing Equations, *Phys. Fluids*. 9(8) (1997) 2420-2428.

[22] A. L. Hazel, M. Heil, The Steady Propagation of a Semi-infinite Bubble into a Tube of Elliptical or Rectangular Cross-Section, *Journal of Fluid Mechanics*. 470 (2002) 91-114.

[23] V. S. Ajaev, G. M. Homsy, Modeling Shapes and Dynamics of Confined Bubbles, *Annu. Rev. Fluid. Mech.* 38 (2006) 277-307.

[24] B. Legait, Laminar Flow of Two Phases through a Capillary Tube with Variable Square Cross-Section, *Journal of Colloid and Interface Science*. 96 (1) (1983) 28-38.

[25] T. C. Ransohoff, C. J. Radke, Laminar Flow of a Wetting Liquid along the Corners of a Predominantly Gas-Occupied Noncircular Pore. *Journal of Colloid and Interface Science* 121 (1988) 392-401.

[26] M. Dong, I. Chatzis, The Imbibition and Flow of a Wetting Liquid along the Corners of a Square Capillary Tube, *Journal of Colloid and Interface Science*. 172 (1995) 278-288.

- [27] D. Zhou, M. Blunt, JR. F. M. Orr, Hydrocarbon Drainage along Corners of Noncircular Capillaries, *Journal of Colloid and Interface Science*. 187 (1997) 11-21.
- [28] M. Dong, I. Chatzis, Oil Layer Flow Along the Corners of Non-Circular Capillaries by Gravity Drainage, *Journal of Canadian Petroleum Technology*. 42 (2003) 9-11.
- [29] H. Dehghanpour, B. Aminzadeh, M. Mirzaei, D. A. DiCarlo, Flow Coupling During Three Phase Gravity Drainage, *Physical Review E*. 83 (2011).
- [30] K. Takamura, Microscopic Structure of Athabasca Oil Sand, *The Canadian Journal of Chemical Engineering*. 60 (1982) 538-545.
- [31] J. Czarnecki, B. Radoev, L. L. Schramm, R. Slavchev, On the Nature of Athabasca Oil Sands, *Advances in Colloid and Interface Science*. 114-115 (2005) 53-60.
- [32] H. L. Goldsmith, S. G. Mason, The Flow of Suspensions through Tubes, *Journal of Colloid Science*. 18 (1963) 237-261.
- [33] G. F. Teletzke, H. T. Davis, L. E. Scriven, Wetting Hydrodynamics. *Rev. Phys. Appl.* 23 (1988) 989-1007.
- [34] E. J. Soares, M. S. Carvalho, P. R. Souza Mendes, Immiscible Liquid-Liquid Displacement in Capillary Tubes, *Journal of Fluids Engineering*. 127 (2005) 24-31.
- [35] V. Mani, K. K. Mohanty, Effect of the Spreading Coefficient on Three-Phase Flow in Porous Media, *Journal of Colloid and Interface Science*. 187 (1997) 45-56.
- [36] O. Vizika, J. M. Lombard, Wettability and Spreading: Two Key Parameters in Oil Recovery With Three-Phase Gravity Drainage, *SPE Reservoir Engineering*. 11 (1996) 54-60.
- [37] J. Berg, *An Introduction to Interfaces & Colloids , The Bridge to Nanoscience*, World Scientific Publishing Co. Pte. Ltd, Singapore, 2010.
- [38] A.W. Adamson, A.P. Gast, *Physical Chemistry of Surfaces*, sixth ed., A Wiley – Interscience Publication, USA, 1997.

3.6 Appendix

Essentially, the capillary (Ca) and Bond (Bo) numbers result from the balance of the forces at the fluid-fluid interface. Ca represents the ratio of flow forces (velocity from the fluid causing the deformation multiplied by the viscosity of the deformed fluid) over the surface tension (which is the force resisting against the deformation). Bo represents the ratio of gravity force over the surface tension. A detailed treatment of the continuity and momentum equations with the boundary conditions during a gas-liquid immiscible displacement in circular and square capillaries can be found elsewhere [13,20].

The use of the Ca and Bo numbers is founded on the first investigations on the gas-liquid immiscible displacement in a circular capillary tube to determine the residual liquid saturation as a film adhered to the walls of the tube [19, 20]. Fairbrother and Stubbs [19] empirically found that the fraction of fluid retained on the walls of tube depended on the magnitude of the capillary number. They established an empirical equation valid for $1.0E-3 < Ca < 1.0E-2$:

$$W = \sqrt{\frac{\mu U_b}{\sigma}} = Ca^{1/2} \quad (A1)$$

Where μ is the viscosity of the displaced liquid, U_b is the velocity of the displacing air bubble and σ is the liquid surface tension. Bretherton [20] theoretically formalized the solution of the problem using the lubrication theory. He also found that the thickness of the film was a function of the capillary number:

$$\frac{h}{r} = 0.643(3Ca)^{2/3} \quad (A2)$$

Where r is the radius of the tube and h is the film thickness. In the model it is assumed that the bubble is of constant curvature except very close to the wall, where the meniscus is distorted by viscous forces. Eq. (A2) applies for $Ca > 1.0E-4$. Bretherton [20] also analyzed the motion of a long bubble under gravity ascending in a vertical tube filled with a liquid and sealed at one end. The bubble will not ascend if:

$$\frac{\Delta\rho gr^2}{\sigma} < 0.842 \quad (A3)$$

The expression of the left side is the Bond number. $\Delta\rho$ is the density difference between the liquid and the bubble. A very recent literature review on the gas – liquid immiscible displacement in a circular capillary tube can be found in Argüelles and Babadagli [5].

Based on the above derivations, one can justify the use of the trapping number, N_T , showed in Eq. (1) and (2), since three forces are involved in the development of residual liquids saturation in our experiments as well as new parameters such as viscosity of the displaced fluid (heavy oil in our case). Even though the retained liquids are in the form of layer or films, these are also a kind of trapped oil to be encountered especially in unconsolidated oil sands where steam injection is widely applied, or very high permeability soil susceptible to oil spill.

Chapter 4 : Gas-Heavy Oil Displacement in Capillary Media at High Temperatures: A CFD Approach to Model Microfluidics Experiments

This paper was submitted to Microfluidics and Nanofluidics

Displacement of heavy-oil by gas at elevated temperatures and residual oil saturation (S_{or}) development on the walls of a square capillary were investigated through computational fluid dynamics (CFD). The displacements were carried out at 55 and 85 °C and compared to experimental data showing good quantitative and qualitatively agreement. On the basis of these results, the behavior of S_{or} was explored at 200 °C, a typical temperature of thermal oil recovery (steam injection) applications. It is shown that S_{or} decreases at higher temperatures for a fixed air injection velocity. This numerical study suggests that the S_{or} diminishes exponentially with time until it reaches a constant value along the square capillary during the displacements. It also indicates that when the contact angle is increased, the retention of oil decreases lineally. Above 60°, oil is completely swept at 85 and 200 °C.

This is the first attempt with CFD to analyze the retention of oil in the pores of a reservoir after the application of thermal methods. CFD approach to model this microscopic phenomenon is promising to carry out further research at temperature and pressure conditions that are very difficult to generate at the microscopic scale in laboratory experiments.

4.1 Introduction

Films and layers are some of the geometrical forms of residual oil saturation (S_{or}) in reservoirs (Blunt et al., 1995; Dong and Chatzis, 2003). The development and mobilization of them within the pores strictly control the recovery mechanisms during isothermal and non-isothermal gravity drainage processes (Walls et al., 2003; Mohammadzadeh and Chatzis, 2009 and 2010). Although there are techniques to estimate S_{or} at different scales (reservoir, well or core), its quantification at the pores' (microscopic) scale is still complicated, especially for non-isothermal applications. To imitate the behavior of S_{or} in a single pore (or throats) of reservoirs, an acceptable option is to use capillary tubes.

The behavior of the thickness of a wetting film or layer adhered at the walls of a tube during the displacement of a liquid with an air bubble is a classical problem that started with circular capillaries. Pioneering works are those of Fairbrother and Stubbs (1935), Taylor (1961), and Bretherton (1961). Fairbrother and Stubbs (1935) observed that an air bubble moves faster than the displaced liquid due to the adhesion of a wetting film on the walls of the tube. The interplay between viscous and capillary forces was responsible for the amount of retained liquid. They

expressed this relationship through the capillary number:

$$Ca = \frac{\mu U_b}{\sigma} \quad (1)$$

Where μ is the viscosity of the displaced fluid, U_b is the bubble velocity, and σ is the surface tension. They also found an empirical relationship to calculate the fraction of the liquid left behind as a film adhered to the wall of the tube:

$$W = \frac{U_b - U_m}{U_b} = Ca^{1/2} \quad (2)$$

Where U_m is the average velocity of the liquid. This equation is valid for $1.0E-3 < Ca < 1.0E-2$ and bubble lengths three times larger than the radius of the capillary. Taylor (1961) found that Eq. (2) can be used up to $Ca=0.09$ and that W has an asymptotic value of 0.56. Bretherton (1961) assumed that the bubble profile has constant curvature, except very close to the wall, to calculate the film thickness h through an equation developed with the lubrication theory:

$$\frac{h}{r} = 0.643Ca^{2/3} \quad (3)$$

Bretherton (1961) stated that Eq. (3) is valid for $Ca > 1.0E-4$. For lower gas velocities the theoretical value underestimates the experimental film thickness and for lowest capillary numbers ($Ca < 1.0E-6$), the difference between experiments and theory involves a factor of 8.

Although the circular capillary tube has been employed to mimic reservoir properties as permeability or porosity, it is too simple to represent the real residual oil saturation characteristics (Blunt et al., 1995; Dong and Chatzis, 2004). A recent critical literature review on the gas-liquid displacements in a circular capillary tube can be found in Argüelles-Vivas and Babadagli (2014).

The angular nature of the pores of a reservoir suggests that non-circular capillaries are more realistic models to analyze the retention of oil in a porous medium. Therefore, square geometry has received attention for modeling fluid flow in porous media (Dong and Chatzis, 2004; Argüelles-Vivas and Babadagli, 2015) and other applications (Ratulowski and Chang, 1989; Kolb and Cerro, 1991 and 1993; Thulasidas et al., 1995; Kamişli, 2003). The difference in the

applications lies on the range of the capillary number and the type of fluids employed.

Ratulowski and Chang (1989) studied the motion of isolated bubbles and train of bubbles in circular and square capillaries. They obtained the fraction of liquid left as a film and the pressure drop across the front of the bubble. Kolb and Cerro (1991) analyzed isothermal gas-liquid displacement in a square capillary and found that fraction of the liquid adhered to the walls increased with the augmentation of the capillary number approaching to an asymptotic value of 0.64. Up to $Ca=0.1$ the bubble is not axisymmetric and adopts a superellipse shape with flattening on the walls far from the corners. For $Ca>0.1$, the shape of the bubble is cylindrical and axisymmetric. Later, Kolb and Cerro (1993) extended their previous work for capillary numbers between 0.7 and 2. The film thickness was calculated as a function of the capillary number and the velocity of the flowing liquid was monitored. They used a lubrication approximation and found a good agreement with the experimental results.

Thulasidas et al. (1995) experimentally determined bubble shape and size, velocity of the bubble, and the fraction of liquid as a function of capillary number in circular and square capillaries on the basis of the superficial flow rates of liquid and gas in feed. In order to develop a mass balance model, they also examined train of bubbles in the capillaries at a large range of capillary numbers.

Kamişli (2003) determined theoretically the fraction of a Newtonian liquid deposited in a square capillary during the passage of a long air bubble using a stream function to eliminate the pressure from the motion equation. The resulting fourth-order differential equation was solved analytically to obtain an eigenfunction solution through the assumption that the angle between the normal gas-liquid interfacial and the axial direction was $\pi/2$. The deviation of the fraction of the liquid left behind between the analytical solution and the experimental work ranged from 9 to 20% (percentage of liquid retained) depending on the capillary number.

In reference to oil recovery applications (the focus of this paper), Dong and Chatzis (2004) experimentally studied the retention of light oils in the corners of a square capillary (0.03 cm in width) as a function of the capillary numbers from $1.0E-3$ to $1.0E-6$ during two and three phase horizontal displacements. In two phase displacements (air-light oil), the retention of the wetting liquid decreased with diminishing capillary number for $Ca>5.0E-4$. In three phase displacements

(air displacing oil, which in turn displaces water), they found that the total retention of oil and water against the capillary number had the same trend as the case with two phase displacements. However, for very low capillary numbers values, the water retention decreased and the oil retention increased.

Recently, Argüelles-Vivas and Babadagli (2014, 2015) analyzed the development of residual oil saturation during air-heavy oil and air-heavy oil-water gravity drainage displacements in cylindrical and square capillaries at different high temperature conditions. In two phase flow experiments (air-heavy oil) they stated that S_{or} is constant and independent of temperature at low values of the trapping number. However, beyond certain trapping numbers, S_{or} varied with temperature and its magnitude depends of the interplay among viscous, capillary, and gravity forces.

For free fall gravity drainage experiments (gas-heavy oil) and changing the radius or width of the capillary, they found that S_{or} increased lineally at higher Bond numbers. In the case of three phase displacements (air displacing heavy oil which in turn displaces water), Argüelles-Vivas and Babadagli (2015) found that the water did not alter the amount of retained oil. Water retention was constant for all the trapping number range. For free fall gravity drainage experiments with three fluids (air, heavy oil and water), the retention of oil was higher when air displaced water, which in turn displaced oil. When the wettability of the square capillaries was changed from water to oil wet, they observed that the S_{or} did not change for the system air-heavy oil-water (since the viscous forces of heavy oil were dominant). They affirmed that the change of wettability facilitated the displacement of water.

Although Argüelles-Vivas and Babadagli (2014, 2015) addressed their research toward the application of thermal methods where high temperatures exist, it was limited to temperatures up to 85 °C due to the difficulties of handling higher temperatures and pressures with capillaries. Furthermore, in thermal methods, temperature conditions are non-isothermal rather than isothermal. However, keeping a temperature gradient at pore scale in lab is also very difficult.

An alternative approach to analyze the behavior of gas-heavy oil displacement at high temperature conditions is computational fluid dynamics (CFD). To date, there is no numerical research through CFD focusing on investigating the dynamics of residual oil saturation formation

as layers deposited in a square capillary during the displacement gas-heavy oil at different temperature conditions. Numerous papers investigated the Taylor flow (slug flow) in circular and square channels using numerical techniques. Taylor flow consists on the motion of train of bubbles filling almost the entire channel, separated from each other by slugs of liquid and from the wall by a liquid film (Taha and Cui, 2006). An extensive literature review about Taylor flow in microchannels was published by Gupta et al. (2009).

In the present study, the liquid phase (heavy oil) was displaced by an ‘endless bubble’ (continuous injection of air) and the contact angle played an important role in the development of the layer adhered to the walls of the tube. In the case of Taylor flow, as pointed out by Gupta et al. (2009), the contact angle is not relevant once the slug flow has been developed since the wall adhesion does not play a role in defining the bubble shape.

In this paper, we carried out 3D numerical simulations using Ansys’ CFX 14.5 to evaluate the behavior and dynamics of the residual oil saturation in the corners of a square capillary during a gas-heavy oil displacement at different temperatures. First, the numerical simulations were carried out at 55 and 85 °C, temperatures at which there are published experimental data. Then, the displacements were extrapolated to 200 °C, a common temperature in thermal methods (steam injection). A sensitivity analysis of the mesh was done at the different temperatures while keeping the same air injection velocity for all the cases on the basis that, in an oil reservoir, the injection rate can be constant during the application of a thermal recovery method. In general, numerical simulations reproduced the fluid dynamics reported in experiments but slightly overestimated the amount of retained heavy oil after the passing of the air. A discussion of the factor causing the discrepancies with the experimental results and recommendations are included. The effects of wettability and the behavior of S_{or} with respect to the time are scrutinized.

4.2 Numerical modeling in CFX

4.2.1 Multiphase flow equations

Air-heavy oil displacement in a square capillary is a time-dependent free surface problem. Since the displacements are in the low capillary number region, the surface tension strongly affects the

interface curvature and thus the boundary conditions (Peterson, 1999). In modeling homogeneous multiphase model by CFX, a common flow field is shared by all phases so that the ‘one fluid transport equations’ are solved instead of individual phasic transport equations.

Equation of continuity:

$$\frac{\partial \rho}{\partial t} + \nabla \cdot (\rho U) = 0 \quad (4)$$

Equation of momentum:

$$\frac{\partial(\rho U)}{\partial t} + \nabla \cdot (\rho U \otimes U) = -\nabla p + \nabla \cdot (\mu(\nabla U + \nabla U^T)) + F_{st} + \rho g \quad (5)$$

Equation of volume fraction:

$$\frac{\partial \alpha}{\partial t} + U \cdot \nabla \alpha = 0 \quad (6)$$

Where U is the velocity vector, p is the pressure, ρ is the density, and μ is the dynamic viscosity of the fluid. Eq. (6) is the advection equation to capture and determine the air – heavy oil interface. α is the volume fraction of the heavy oil or air. F_{st} represents the body force due to surface tension. g is the gravity vector.

The average fluid density and viscosity are obtained from the volume fraction weighted average properties of the gas and liquid:

$$\rho = \alpha \rho_1 + (1 - \alpha) \rho_2 \quad (7)$$

$$\mu = \alpha \mu_1 + (1 - \alpha) \mu_2 \quad (8)$$

4.2.2 Surface Tension and Wettability Model

Surface tension and wettability effects are included in Eq. (5) through the continuum surface force (CSF) model proposed by Brackbill et al. (1992). This model approaches the surface tension as a body force concentrated at a small region surrounding the fluid-fluid interface:

$$F_{st} = (-\sigma \kappa n + \nabla_s \sigma) \delta \quad (9)$$

Where σ is the surface tension coefficient, n is the interface normal vector (estimated from the gradient of a smoothed volume fraction), ∇_s is the gradient operator on the interface, κ is the curvature of the interface, and δ is the Dirac delta function. The two terms on the right side of Eq. (9) represent the normal and tangential components of surface tension, respectively. To account for wettability, the contact angle θ is measured through the liquid. The interface normal vector and the curvature of the interface are calculated to satisfy the given contact angle.

4.2.3 Volume of Fluid Method (VOF)

In CFX 14.5, the VOF method (Hirt and Nichols, 1981) was implemented to discretize the transport equations. Compared with other methods, the VOF method has an inherent nature to conserve the volume (Ferziger and Peric, 2002). The gas-liquid interface is captured by solving Eq. (6) for the gas or liquid fraction. If $\alpha_l=1$, the liquid is fully occupying a computational cell, otherwise the cell is shared with the gas volume fraction, α_g . The gas-liquid interface is located where α_g and α_l lie between 0 and 1. A geometric reconstruction scheme is used to delimit the interface through a piecewise-linear approach (Youngs, 1982). Under appropriate boundary conditions, Eqs. (4) - (9) are solved iteratively to calculate the gas and liquid volume fractions and the velocity field solution.

4.3 Solution methodology

4.3.1 Body diagram of the problem and geometry

A square capillary is initially filled with heavy oil, as depicted on the left side of **Figure 4-1**. Then, air is injected at the inlet to displace the heavy oil at a specific velocity, which is calculated with the following definition of the capillary number (Ca):

$$Ca = \frac{U_z \mu_{heavyoil}}{\sigma_{air-heavyoil} \cos \theta} \quad (10)$$

where U_z is the air velocity, $\mu_{heavyoil}$ is the viscosity of the heavy oil, $\sigma_{air-heavyoil}$ is the surface tension of the oil, and θ is the contact angle. During the displacement some of the heavy oil is retained at the walls of the capillary. This is called residual oil saturation (S_{or}). This amount of

liquid deposited depends on the interplay of viscous, capillary, and gravity forces. The ratio of the gravity and capillary forces is called Bond number (Bo):

$$Bo = \frac{\Delta\rho l^2}{\sigma_{air-heavyoil} \cos \theta} \quad (11)$$

where $\Delta\rho$ is the density difference between air and the heavy oil and l is the characteristic length, which is half of capillary width $l=W/2$. Since the displacement is vertical and the gravity is acting at the four corners of the square capillary, it is possible to model just a quarter of the capillary along the length and to apply symmetry in two boundaries of the model. This is illustrated on the right side of **Figure 4-1**.

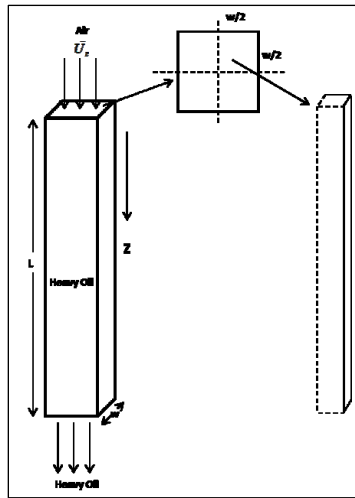


Figure 4-1: Body diagram and selection of geometry.

The S_{or} is constant along the length of the capillary after the transition zone and the cap of the endless bubble (the name of the regions were defined by Bretherton [1961] for a cylindrical capillary). This implies that the S_{or} seen in cross-sectional planes along the capillary is also constant as depicted in **Figure 4-2**. As it was established above, only $1/4$ of the capillary along the length was simulated.

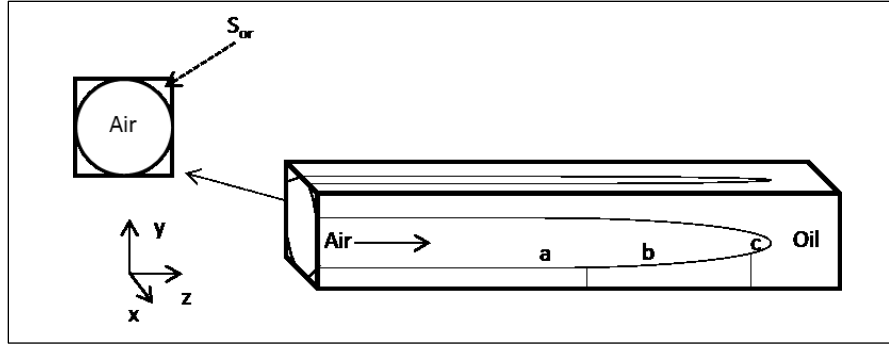


Figure 4-2: Profile of the air-heavy oil displacements and zones of the interface: a) constant thickness region, b) transition zone, c) cap region.

4.3.2 Meshing

The 3D geometries and the meshes were generated using the ANSYS Workbench and the ANSYS CFX-Mesh, respectively. Six different meshes were tested for each temperature. The first mesh for all the cases was a structured coarse cubic grid used as a reference and to start the grid-independency analysis. Since this is a time-dependant free surface-multiphase problem, the use of a very fine grid is costly from computation time point of view. Hence, a compromise between computational efficiency and accuracy must be established.

Table 4-1: Mesh information for the simulations runs.

	Mesh Data					
	I	II	III	IV	V	VI
Nodes	13056	28866	28866	36771	36771	49419
Growth Rate (GR)	-	1.1	1.2	1.1	1.2	1.1
Inflation layers	-	10	10	15	15	23

Table 4-1 shows the mesh information. Structured mesh with inflation layers were generated to minimize artificial diffusion and to have grid surfaces nearly aligned with the flow. The total thickness of the inflation layers was set to 50 μm , based on the experimental thickness reported by Argüelles-Vivas and Babadagli (2015). The use of fine hexahedron elements permitted to capture the oil thickness in the flat zone of the walls and its curvature near the center of the tube, which was not observed with the coarse homogeneous grid. Two Growth Rates (1.1 and 1.2) were tested for the same number of nodes. In ANSYS Workbench the Growth Rate refers to the augmentation of the edge length with each sequent layer of elements to match the larger length scale employed for the rest of the domain. An approximate refinement ratio of $1.3^{1/3}$ was used to

generate the meshes. All the grids had the quality parameters within the known acceptable range for hexahedrons elements.

4.3.3 Fluids and properties

The properties for the heavy oil and air at the simulated temperatures are shown in the **Table 4-2**. The values for the heavy oil as well as the wettability and surface tension measurements were taken from Argüelles-Vivas and Babadagli (2014; 2015).

Table 4-2: Air and heavy oil properties used in the simulations runs.

Fluid	Temperature (°C)	Viscosity (kg/m s)	Density (kg/m ³)	Surface tension (N/m)	Contact angle (°)
Heavy oil	55	0.2898	904.9	0.0265	24.3
	85	0.0673	883.9	0.0243	0
	200	0.0038	803.4	0.0159	0
Air	55	2.00E-5	1.0852		
	85	2.14E-5	0.9802		
	200	2.62E-5	0.7451		

4.3.4 Boundary conditions

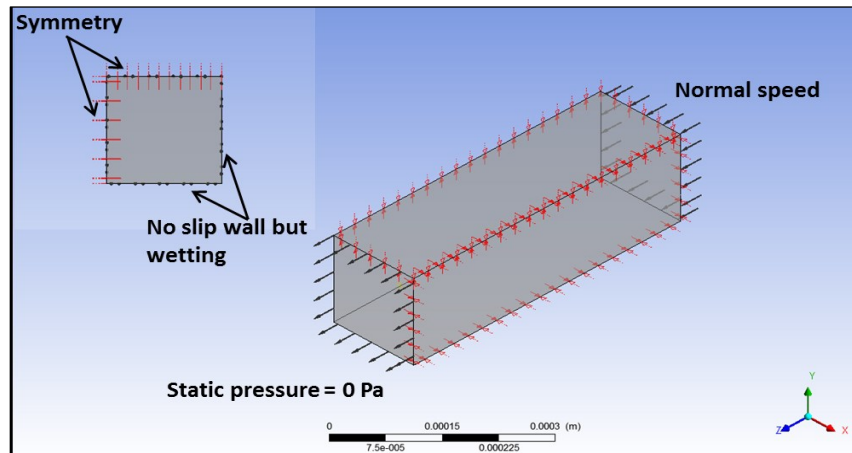


Figure 4-3: Boundary conditions for the simulations cases.

Air was injected at the inlet at constant velocity and a static pressure of 0 Pa was fixed at the outlet. This is known to be a very robust boundary condition configuration. The walls of the corners were modeled using a no slip condition but with adhesion to mimic wettability. Symmetry was established in the other two walls, which meet each other in what would be the

contact line of the four symmetry planes along the length of a square capillary. **Figure 4-3** shows the boundary conditions schematically.

At the beginning of each displacement, the capillary was completely filled with heavy oil and the simulation stopped when the air-heavy oil interface reached the outlet of the tube.

4.3.5 Simulations cases

A square capillary of $3E-4$ m in width (W) and length of $1.67W$ was used for the simulations. The displacements were carried out at three temperatures. For all the cases, the same air injection velocity was employed. The reason for this is that in an oil reservoir the displacing fluid can be injected at constant rate while the reservoir is subjected to a temperature gradient. **Table 4-3** shows the different scenarios as well as the characteristic dimensionless numbers. Reynolds numbers clearly indicate that the displacements are Stokes flow type.

Table 4-3: Simulation cases and dimensionless numbers.

T (°C)	Air velocity (m/s)	Re	Ca	Bo
55	0.0062	6.42E-06	7.40E-02	0.01
85	0.0062	2.76E-05	1.71E-02	0.01
200	0.0062	4.89E-04	1.47E-03	0.04

The simulations at 55 and 85 °C were compared with experimental data reported by Argüelles-Vivas and Babadagli (2015). The displacement at 200 °C is the numerical experiment to investigate the behavior at real thermal conditions of non-isothermal applications as SAGD or steamflooding.

4.3.6 Solver solution technique

The simulations were performed under transient conditions. A second order backward time discretization scheme for the transient terms and high resolution scheme for the advection term were chosen. Since these displacements are Stoke flow type, the stability criterion must be the following dimensionless parameter (Ferziger and Peric, 2002):

$$\frac{\Gamma \Delta t}{\rho (\Delta x)^2} < 0.5 \quad (12)$$

Where Γ represents the diffusive term, Δt is the time step used in the simulation, Δx is the size of the grid, and ρ is the density of the fluid. Taking as a base case the coarse grid size of $1E-5$ m and the viscosity and density values of the heavy oil, this criterion indicates that the time step should be less than $1E-7$ s. Due to the variability of the element size in the grids, we set an initial time step of $1E-7$ s and let CFX 14.5 to automatically adjust the time step. Convergence criteria of $1E-6$ were specified for the RMS. The time step remained between $1E-7$ and $1E-10$ s for all the simulations. The running time was 4 days for the meshes with 10 layers and 20 days for the meshes with 23 layers.

4.4 Results and Discussion

In the post-processor of CFX, the distinction between phases is determined through contours of colors. By default, in CFX the red or orange color represents 100 % of liquid ($\alpha_l=1$) and blue color represents 100% of gas ($\alpha_g=1$). Nested contours can be found between the two fluids, which is the region of the interface indicating that one cell is computationally filled with both fluids. In this paper, the interface was delimited in the region of 100% of heavy oil for calculations and visualization analysis. In Taha and Cui (2006) and Gupta et al. (2009), this approximation was taken for Taylor flow studies. Ashish et al. (2009) chose the isocontour of 0.5 to identify the interface and for the analysis of their results.

4.4.1 Development of S_{or} along the square capillary

As explained in the section 4.3.1, after the passing of the air bubble the fraction of the fluid left behind as a layer along the swept zone is constant, except near the interface between both fluids. The S_{or} in experimental displacements at 55 and 85 °C were 6.2 and 5.9% respectively (Argüelles-Vivas and Babadagli, 2015), at the same air injection velocity of the simulations (**Table 4-3**). The experimental S_{or} was determined as the difference between the initial and final length of a heavy oil slug divided by the distance that the slug was displaced by the injection of air. Since the fraction of the liquid is constant along the length of the capillary, the experimental average S_{or} is also constant at each cross sectional plane along the square capillary.

In **Figure 4-4** and **Figure 4-5**, the profiles of the numerical S_{or} along the length of the tube once that the air is about to reach the outlet of the capillary are shown for the different meshes at 55

and 85 °C, respectively. The points on the graphs represent the average S_{or} at cross-sectional planes along the length of the capillary. This is illustrated in the image to the right of **Figure 4-4** to better visualize the S_{or} profiles along the capillary. The right image of **Figure 4-4** applies also for **Figure 4-5** and **Figure 4-7**. The experimental average S_{or} 's are also shown as single points for 55 and 85 °C.

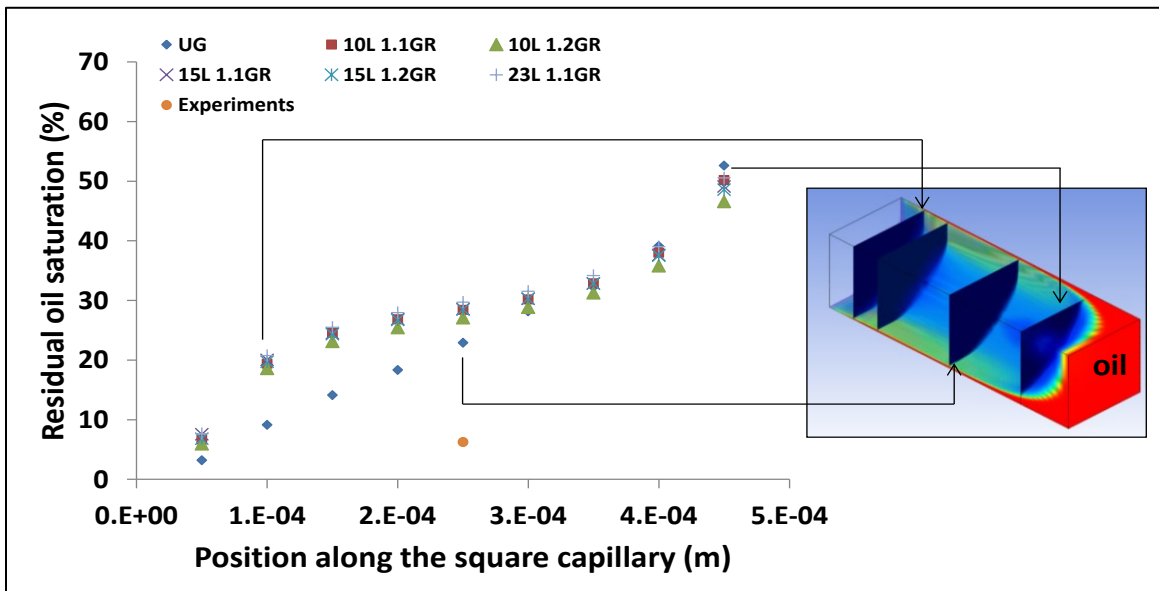


Figure 4-4: Residual oil saturation in cross sectional planes along the square capillary at 55 °C. (UG: Uniform Grid, 10L 1.1GR:10 Inflation layers with 1.1 Growth Rate, 10L 1.1GR:10 Inflation layers with 1.2 Growth Rate, 15L 1.1GR:15 Inflation layers with 1.1 Growth Rate, 15L 1.2GR:15 Inflation layers with 1.2 Growth Rate, 23L 1.1GR:23 Inflation layers with 1.1 Growth Rate).

To compare the simulations results of S_{or} with the experimental data, the flattest S_{or} region in the numerical domain was identified. In the **Figure 4-4** and **Figure 4-5** it can be noticed that the change of S_{or} in the middle zone of the capillary is smooth and small, especially for the case at 85 °C but without having a plateau. This interval lied between 1.5E-4 and 3E-4 m.

Apparently, the uniform grid (UG) was closer to the experimental values for both temperatures. However, this mesh did not capture well the ‘numerically’ retained oil near the flat zone of the wall and in the air-heavy oil interface. This can be seen in **Figure 4-6** where a comparison of the S_{or} of the different meshes at 85 °C is shown for a cross sectional plane located at the middle of the tube (2.5E-4 m in **Figure 4-4**).

On the other hand, the values of the S_{or} along the tube for the other meshes indicated that our results can be considered within the grid independence region since the variations were not

significant when the number of nodes was increased from 13056 (10 inflation layers) to 49419 (23 inflation layers). Also, the growth rate of the mesh did not affect the results significantly.

The simulations at 55 °C had a S_{or} of 27.5%, a difference of 21% with respect to the experimental value. In the case of 85 °C, the S_{or} was 13.5%, a difference of 7.6% with the experimental S_{or} . As seen, the deviation from experimental results was higher at lower temperatures.

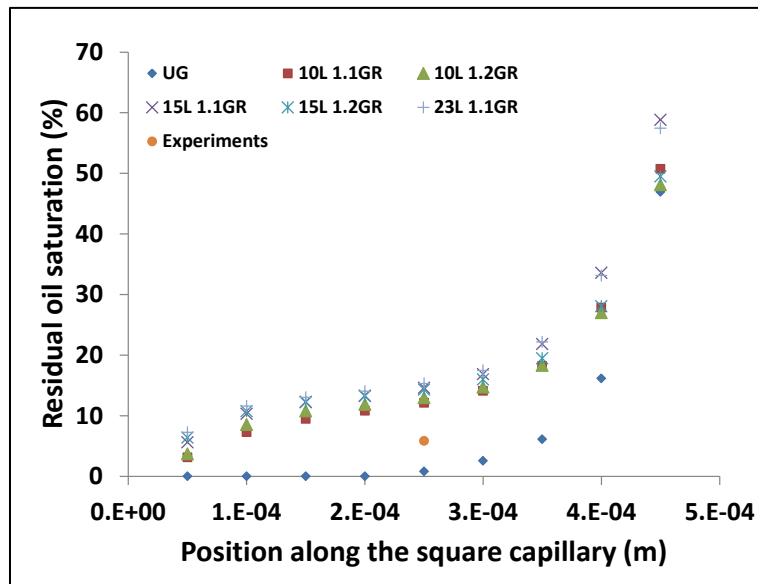


Figure 4-5: Residual oil saturation in cross sectional planes along the square capillary at 85 °C. (UG: Uniform Grid, 10L 1.1GR:10 Inflation layers with 1.1 Growth Rate, 10L 1.1GR:10 Inflation layers with 1.2 Growth Rate, 15L 1.1GR:15 Inflation layers with 1.1 Growth Rate, 15L 1.2GR:15 Inflation layers with 1.2 Growth Rate, 23L 1.1GR:23 Inflation layers with 1.1 Growth Rate).

As a numerical experiment, one more case was carried out at 200 °C, a common temperature in thermal recovery processes considering the specific case of steam assisted gravity drainage process (SAGD) at which the S_{or} can be developed as layers in the crevices of the pores. The results are shown in **Figure 4-7** for different meshes. The uniform grid was not able to capture any residual oil left behind in the tube during the displacements. For the other grids, it is interesting to observe that the region of the constant S_{or} along the capillary is much flatter for this case compared to those at 55 and 85 °C. The S_{or} had an average value of 4.9%.

Although there is a quantitative difference with the experimental values, the numerical simulations of the air – heavy oil displacements are acceptable and in qualitative agreement with the physics of the real process. In the research of Argüelles-Vivas and Babadagli (2015) it

was found that the S_{or} diminishes at higher temperature for the same air injection velocity (different Ca). In this numerical work the S_{or} is decreasing from 55 to 200 °C at the same air velocity.

The quantitative difference cannot be attributed to the mesh refinement or quality. It is clear from **Figure 4-6** that as the mesh was finer more S_{or} was captured by the numerical solution in the flat zones of the tube and toward the center of the capillary, near the air-heavy oil interface. As a result, the numerical S_{or} 's were farther from the experimental ones. Increasing the resolution mesh would be unnecessary and more costly computationally. It is true that the refinement of the mesh shrank the interface error (compare **Figure 4-6-I** and **Figure 4-6-VI**), but this resulted in a decrement of the air saturation and in an augmentation of the S_{or} .

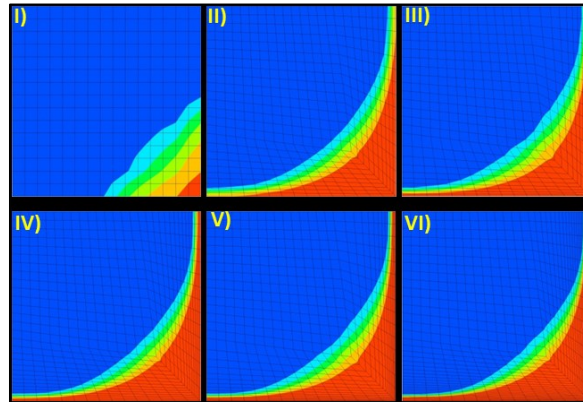


Figure 4-6: Comparison of the S_{or} in a cross sectional plane at $2.5E-4$ for the tested grids at 85 °C. (red color is heavy oil, the rest is air: I: Uniform Grid, II: 10 Inflation layers with 1.1 Growth Rate, III: 10 Inflation layers with 1.2 Growth Rate, IV: 15 Inflation layers with 1.1 Growth Rate, V: 15 Inflation layers with 1.2 Growth Rate, VI: 23 Inflation layers with 1.1 Growth Rate).

The problem with the overestimation of the liquid retained in the capillary can be due to the numerical and mathematical treatment of the gas-liquid interface. Kamişli (2003) also found that his analytical model overestimated the fraction of the fluid left behind in the tube with respect to the experimental results of Kolb and Cerro (1991). The deviation of the percentage of liquid retained was of 20% at low capillary numbers and 8% at high capillary numbers. He attributed the deviation to the assumptions behind his analytical model. He assumed the gas-liquid interface parallel to the walls of the square capillary, which implies that the shape of the nose of the bubble (the cap of the bubble) was not considered in the mathematical analysis. The interface shape and specifically the cap of the bubble should be considered in the solution since it influences the distribution and amount of retained oil in square capillary.

Unlike Kamişli's (2003) research, in numerical simulations the entire interface shape including the nose is reconstructed and tracked. However, in CFD, the numerical treatment of the interface and the phenomena related to capillarity are known to be a challenging problem. In this work, we hypothesize that the overestimation of S_{or} can be mainly due to the limitations of the CSF model of Brackbill et al. (1992) to model the surface tension and the wettability (wall adhesion).

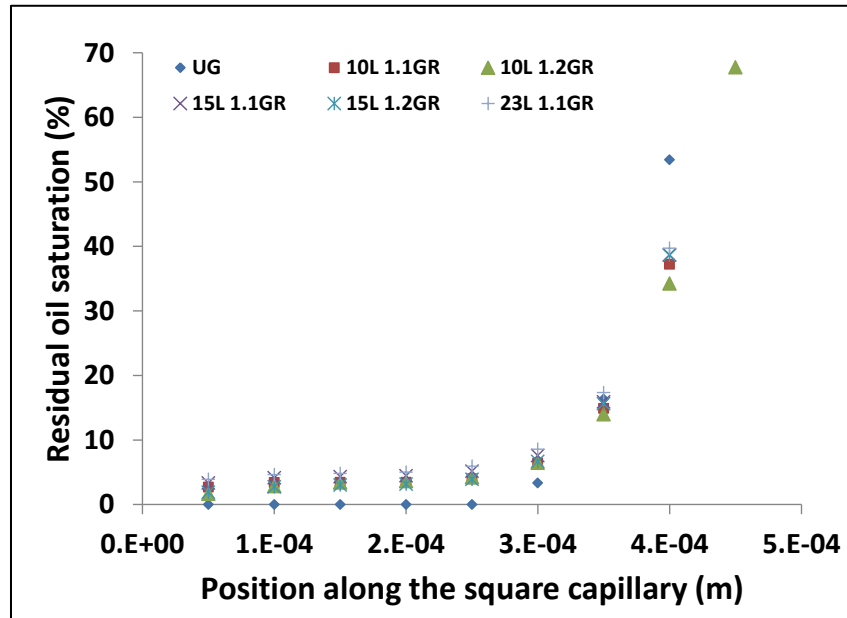


Figure 4-7: Residual oil saturation in cross sectional planes along the square capillary at 200 °C. (UG: Uniform Grid, 10L 1.1GR:10 Inflation layers with 1.1 Growth Rate, 10L 1.1GR:10 Inflation layers with 1.2 Growth Rate, 15L 1.1GR:15 Inflation layers with 1.1 Growth Rate, 15L 1.2GR:15 Inflation layers with 1.2 Growth Rate, 23L 1.1GR:23 Inflation layers with 1.1 Growth Rate).

In the CSF model, the normal boundary condition is solved for interfaces between inviscid and incompressible fluids ($\mu=0$) so that the viscous stress tensor containing the viscosity of the fluids and the partial derivatives of the velocity with respect to the normal direction is vanished. In the heavy oil displacement, these terms could be important especially considering that this is creeping flow. The heavy oil- air viscosity ratio, $\mu_{\text{heavy oil}}/\mu_{\text{air}}$, was 14490 at 55 °C and 3145 at 85 °C. These are much higher than some cases published in the literature where the viscosity ratio is about 50 and the liquid is water (e.g. Gupta et al., 2009). Furthermore, it was also reported that the implementation of this surface tension model induces spurious currents in the flow field, which could be larger than the physical flow, particularly at low capillary numbers (Raeini et al., 2012). Another numerical issue that could influence the shape of the interface and thus the amount of retained oil is the scheme for the reconstruction of the interface.

The probable existence of the Marangoni effect in the experiments provoking a variation of the surface tension along the interface due to the natural surfactants in the heavy oil is another factor for the discrepancy. CFX permits surface tension changes through an expression given by the user. However, we ran the simulations assuming that surface tension is constant since no mathematical behavior of the Marangoni effect is known.

Also, some concerns with respect to the inclusion of the contact angle could explain in part the difference between the experimental and numerical results. In CFX, the contact angle is specified and then the normal vectors at the interface are estimated to calculate the curvature and satisfy such contact angle. Hence, there is a modified surface tension force F_{st} . However, the contact angle not only depends on the fluid properties but also in a complex manner on the smoothness of the wall and the geometry (Huang et al., 2005; Hoffman, 1975).

In this work, we used the static contact angle provided in the references of the experimental data to run our simulations. Although CFX also permits to add equations for dynamic contact angles, the behavior of advancing or receding contact angles is not known for heavy oil. Through hydrodynamics analysis, it was shown that the viscous effects are responsible for dynamic wetting behavior and are negligible for $Ca < 1E-5$ or $1E-6$ (Berg, 2010). Also, Ma (2012) demonstrated that the flow resistance of a liquid plug in a capillary tube is significantly affected by the advancing contact angle. This in turn should affect the shape and curvature of the interface.

4.4.2 Visualization of the S_{or} formation

Regardless of the quantitative difference between the numerical and the experimental results, the physical behavior was reproduced with simulations. In **Figure 4-8**, the displacements at 55, 85, and 200 °C are shown in 3D and 2D for the same time 0.025 s. The yz plane at $x=3E-5$ m is near the wall of the capillary whereas the yz plane at $x=15E-5$ m is very close to the symmetry plane. In these images the shape of the air-heavy oil interfaces are seen easily.

Looking at the yz planes at $x=15E-5$ m, one may notice that the interface at 55 °C has a more bullet shape compared to those interfaces at 85 and 200 °C. Consequently, its nose was ahead during the displacement at the same time (see the vertical dashed line for reference). The

interface in the yz plane at $x=3E-5$ m for 55 °C (near wall) was more inclined with respect to the bottom wall, indicating that during the development of the S_{or} the air tended to bypass the oil located close to the corners, where a higher resistance exists to displace the oil. Contrary to this, a better sweeping of the oil close to the corner was achieved at 85 and 200 °C, as it can be observed in the yz planes at $x=3E-5$ m. Also, the interfaces were flatter close to the symmetry plane (center of the capillary).

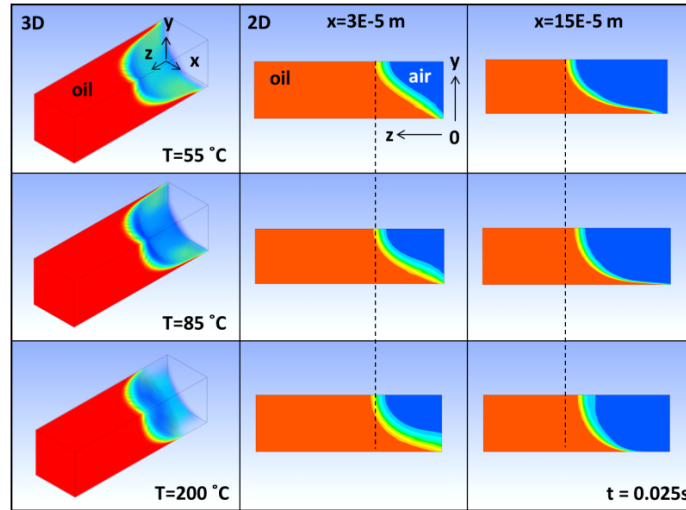


Figure 4-8: 3D and 2D air - heavy oil displacements at 55, 85, and 200 °C.

Although the capillary forces are the ‘retaining forces,’ their magnitude cannot alone explain the difference in the S_{or} at these temperatures. The higher oil retention at 55 °C was due to the high viscosity ratio, $\mu_{heavy\ oil}/\mu_{air}$, and it can be explained as follows. Since the air velocity was the same in the three displacements and the air viscosity did not vary significantly with temperature, the momentum transfer due to the viscous forces of the air on the heavy oil-air interface was practically of the same magnitude. A similar situation occurred with the gravity force. However, the change of heavy oil viscosity with temperature was much more severe. This means that the viscous forces needed to mobilize the heavy oil and overcome the combined effect of the capillary forces and the resistance to flow due to the corner effect being higher at lower temperature (higher heavy oil viscosity). As a result, the air with its low viscous force was only able to displace the oil located at the center of the tube and near the flat zones of the wall where it found less resistance to flow. The air tended to ‘finger’ through the center of the tube, especially at 55 °C.

4.4.3 Change of S_{or} with time

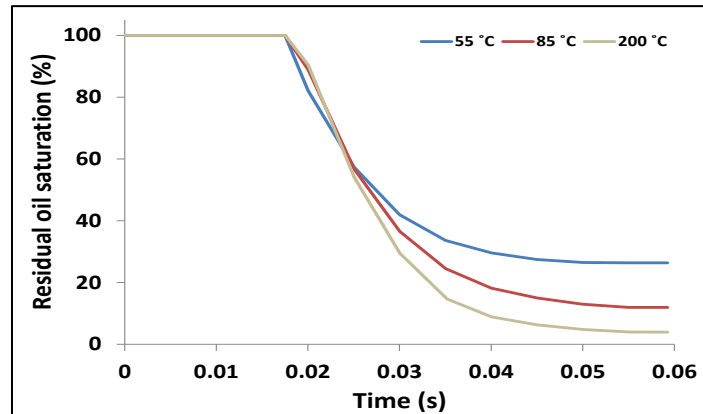


Figure 4-9: Change of S_{or} with respect to time in a cross sectional plane located at the middle of the square capillary for 55, 85, and 200 °C.

After the heavy oil is displaced by the passing of the air it is assumed that the S_{or} becomes immediately constant at each cross sectional plane of the square capillary. However, in CFX we were able to capture in the order of hundredths of seconds the dynamics of S_{or} until it reached the constant value.

In **Figure 4-9**, the change of S_{or} with respect to time in a cross sectional plane at the middle of the square capillary is shown for the three temperatures. It can be inferred from **Figure 4-9** that the same cross sectional plane was reached by the air almost at the same time for the three different displacements. When the S_{or} started decreasing (~ 0.018 s) the decrement for 55 °C was faster compared to the other two temperatures. This is explained by the bullet shape of the interface at the center of the capillary at 55 °C (as it was shown in the previous section) that it is sweeping the oil of this region faster due to the “fingering” compared to the other two cases.

At a characteristic time (~ 0.025 s), the curves crossed each other and the curves started showing different behavior depending on temperature. After about 0.05 s, the S_{or} values stabilized and the retained oil for each temperature case was determined. The air at 55 °C mainly swept the oil located at the center and near flat zones of the walls but bypassed the oil closer to the square corner, leaving a higher amount of S_{or} . In this situation, the interface in a cross sectional plane looks more axisymmetric. On the other hand, the sweeping of oil near the corners was improved at 85 and 200 °C, temperatures at which the air-heavy oil interface was flatter and looks more

non-axisymmetric if it is seen at a cross sectional plane. The simulations suggest that the S_{or} decays exponentially with time at different temperatures.

4.4.4 Wettability effects

The effects of the wettability on the S_{or} were investigated while keeping the other variables constant. For the displacements at 85 and 200 °C, the retention of oil was nil above 60°, as seen in **Figure 4-10**. The numerical simulations suggest that the S_{or} decreases lineally with the increment of the contact angle for all the temperatures. However, the variation in the oil retention was more abrupt at lower temperatures, based on the pendant of the trend.

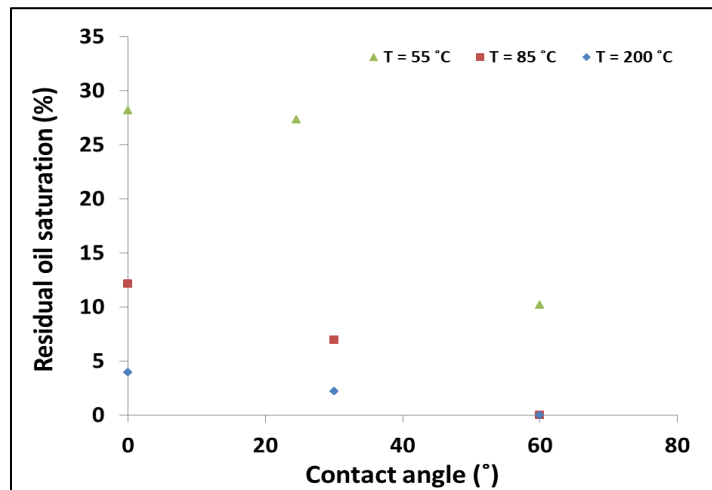


Figure 4-10: Change of S_{or} with respect to the contact angle at different temperatures.

4.5 Conclusions

The 3D behavior of residual oil saturation during the displacement of heavy oil by a gas phase (air) in a square capillary at different temperatures was investigated using CFD approach. The numerical simulations showed that S_{or} diminished at higher temperature at the same air injection velocity and agreed well with published experiments at 55 and 85 °C. For a better matching, it is recommended to investigate the effects of dynamic contact angles models and the Marangoni effect. The simulations indicated that the decrement of S_{or} with respect to time during the displacements obeys an exponential function until getting a constant value. When the contact angle was increased, the S_{or} diminished lineally for all the temperatures but the decrement was

more severe at lower temperatures. All the oil was completely swept for contact angles above of 60° at 85 and 200°C .

4.6 References

1. Argüelles–Vivas, F.J. and Babadagli, T. 2014. Drainage Type Oil and Heavy-Oil Displacement in Circular Capillary Tubes: Two- and Three-Phase Flow Characteristics and Residual Oil Saturation Development in the Form of Film at Different Temperatures. *Journal of Petroleum Science and Engineering* **118**: 61-73.
2. Argüelles–Vivas, F.J. and Babadagli, T. 2015. Residual Liquids Saturation Development During Two and Three Phase Flow under Gravity in Square Capillaries at Different Temperatures. *Int. J. of Heat and Fluid Flow* **52**: 1-14.
3. Berg, J. 2010. *An Introduction to Interfaces & Colloids, The Bridge to Nanoscience*. World Scientific Publishing Co. Pte. Ltd, Singapore.
4. Blunt, M., Zhou, D., and Fenwick, D. 1995. Three-Phase Flow and Gravity Drainage in Porous Media. *Transport in Porous Media* **20**:77-103.
5. Brackbill, J.U., Kothe, D.B. and Zemach, C. 1992. A Continuum Method for Modeling Surface Tension. *Journal of Computational Physics*. **100**: 335-354.
6. Bretherton, F.P. 1961. The Motion of Long Bubbles in Tubes. *Journal of Fluid Mechanics* **10**: 166-188.
7. Dong, M. and Chatzis, I. 2003. Oil Layer Flow along the Corners of Non-Circular Capillaries by Gravity Drainage. *JCPT* **42**: 9-11.
8. Dong, M. and Chatzis, I. 2004. An Experimental Investigation of Retention of Liquids in Corners of a Square Capillary. *Journal of Colloid and Interface Science* **273**: 306-312.
9. Fairbrother, F. and Stubbs, J. 1935. Studies in Electroendosmosis. Part VI. The 'Bubble Tube' Method of Measurement. *Journal of Chemical Society* **1**: 527-529.
10. Ferziger, J.H. and Perić, M. 2002. *Computational Methods for Fluid Dynamics*, third edition. Berlin Heidelberg New York. Springer.
11. Hirt, C.W. and Nichols, B.D. 1981. Volume of Fluid (VOF) Method for the Dynamics of Free Boundaries. *Journal of Computational Physics* **39**: 201-225.
12. Hoffman, R. 1975. A study of the Advancing Interface 1. Interface Shape in Liquid-Gas Systems. *J. Colloid Interface Sci.* **50** (2): 228-241.
13. Huang, H., Meakin, P., and Liu, M.B. 2005. Computer Simulation of Two-Phase Immiscible Fluid Motion in Unsaturated Complex Fractures Using a Volume of Fluid Method. *Water Resources Research* **41**(12): W12413.
14. Kamişli, F. 2003. Flow of a Long Bubble in a Square Capillary. *Chemical Engineering and Processing* **42**: 351-363.
15. Kolb, W.B. and Cerro, R.L. 1991. Coating the Inside of a Capillary of Square Cross-Section. *Chemical Engineering Science* **46** (9): 2181-2195.
16. Kolb, W.B. and Cerro, R.L. 1993. The Motion of Long Bubbles in Tubes of Square Cross-Section. *Phys Fluids A* **5** (7): 1549-1557.
17. Ma, Y.D. 2012. Motion Effect on the Dynamic Contact Angles in a Capillary Tube. *Microfluid Nanofluid, Short Communication* **12**: 671-675.

18. Mohammadzadeh, O. and Chatzis, I. 2009. Pore-Level Investigation of Heavy Oil Recovery Using Steam Assisted Gravity Drainage (SAGD). Paper IPTC 13403 presented at the Int. Petroleum Tech. Conf., Doha, Qatar, Dec 7-9.
19. Mohammadzadeh, O. and Chatzis, I. 2010. Pore-Level Investigation of Heavy Oil Recovery Using Steam Assisted Gravity Drainage (SAGD). *Oil & Gas Science and Technology – Rev. IFP Energies Nouvelles* **65** (6): 839-857.
20. Peterson, R.C. 1999. The Numerical Solution of Free-Surface Problems for Incompressible, Newtonian Fluids. PhD dissertation. The University of Leeds, England.
21. Raeini, A.Q., Blunt, M.J., and Bijeljic, B. 2012. Modelling Two-Phase Flow in Porous Media at the Pore Scale Using the Volume-of-Fluid Method. *Journal of Computational Physics* **231**: 5653-5668.
22. Ratulowski, J. and Chang, H.C. 1989. Transport of Gas Bubbles in Capillaries. *Phys. Fluids A* **1** (10): 1642-1655.
23. Taha, T. and Cui, Z.F. 2006. CFD Modeling of Slug Flow inside Square Capillaries. *Chemical Engineering Science* **61**(2): 665-675.
24. Taylor, G.I. 1960. Deposition of a Viscous Fluid on the Wall of a Tube. *Journal of Fluid Mechanics* **10**: 161-165.
25. Thulasidas, T.C., Abraham, M.A., and Cerro, R.L. 1995. Bubble-Train Flow in Capillaries of Circular and Square Cross Section. *Chemical Engineering Science* **50** (2): 183-199.
26. Walls, E., Palmgren, C., and Kisman, K. 2003. Residual Oil Saturation Inside the Steam Chamber During SAGD. *JCPT* **42** (1): 39-47
27. Youngs, D.L. 1982. Time-Dependent Multi-Material Flow with Large Fluid Distortion In: Morton, K.W., Baines, M.J. (Eds.), *Numerical Methods for Fluid Dynamics*. Academic, New York. 273-285.

Chapter 5 : Analytical Solutions and Derivation of Relative Permeabilities for Water–Heavy Oil Displacement and Gas–Heavy Oil Gravity Drainage Under Non-Isothermal Conditions

This paper was submitted to SPE Reservoir Evaluation & Engineering

Analytical models were developed for non-isothermal gas–heavy oil gravity drainage and water–heavy oil displacements in round capillary tubes including the effects of a temperature gradient throughout the system. Using the model solution for a bundle of capillaries, relative permeability curves were generated at different temperature conditions.

The results showed that water/gas–heavy oil interface location, oil drainage velocity, and production rate depend on the change of oil properties with temperature. The displacement of heavy oil by water or gas was accelerated under a positive temperature gradient, including the spontaneous imbibition of water. Relative permeability curves were greatly affected by temperature gradient and showed significant changes compared to the curves at constant temperature. Clarifications were made as to the effect of variable temperature compared to the constant (but high) temperatures throughout the bundle of capillary tube system.

5.1 Introduction

In the field of flow in porous media, non-isothermal conditions are encountered in many applications. The most common case is thermal methods such as steam and hot water injection in heavy-oil reservoirs. When these methods are applied in the form of steam assisted gravity drainage (SAGD) to recover heavy oil or bitumen, gravity controls the flow process and the development of residual phase saturations is typically in the form of film due to low capillary pressure caused by high permeability.

The influence of heat transfer in fluid dynamics is one of the controversial topics in SAGD. It has been pointed out that steam injection can be analyzed at three different scales (Satik and Yortsos, 1995). (1) Pore scale: where processes such as condensation, displacement, wetting and phase distributions need to be considered. (2) Networks of pores: where the events are analyzed as a result of the interaction between pores. (3) Macro scale (well or field scale): where the systems are analyzed based on averaged properties and variables such as permeabilities, temperatures, or fluid saturations.

For practicality's sake, most of the attention has been given to macro scale. The process modeling is achieved by incorporation of relative permeability curves into numerical models for a grid block size on the order of 10-100 meters. Rock–fluid properties and their interactions

used in this type of models such as the relative permeability, capillary pressure, and residual saturations are typically taken from analyses performed under isothermal conditions (Satik and Yortsos, 1995; Yortsos, 1999).

A very common assumption in steam drive process, dominated by viscous displacement, is negligible residual oil saturation (Satik and Yortsos, 1995). The same assumption is made for SAGD in which the main drive mechanism is gravity segregation based on laboratory scale observations (Chung and Butler, 1987; Sasaki et al., 1999; Mohammadzadeh et al., 2012). An extensive review of field scale applications by Jimenez (2008) showed that pilot and field results may result in high residual oil saturation variable between 60% and 80% even at the mature stages. For thermal methods, these recovery factors are considered low, making the process highly inefficient due to the extreme cost of steam.

In analytical models of SAGD (Butler, 1991), the estimations of residual oil saturation, S_{or} , are based on an equation derived by Cardwell and Parson (1949) in their free fall gravity drainage theory for isothermal applications:

$$S_{or} = \frac{(b-1)}{b} \left(\frac{v_s \phi Y}{b k g t} \right)^{1/(b-1)} \quad (1)$$

where v_s is the kinematic viscosity of the oil, ϕ is the porosity, Y is the drainage height, k is the absolute permeability, g is the gravity constant and t is the time. In this equation, parameter b —used to compute relative permeabilities—is obtained from isothermal displacement experiments in sand packs. Furthermore, data fed to SAGD reservoir simulators, such as relative permeabilities, residual oil saturations, and mobile oil are based also on liquid–gas and liquid–liquid systems for isothermal processes where the mechanisms could be different from non-isothermal conditions.

The main problem with the use of isothermal relative permeability for non-isothermal applications is that they do not take into account the effects of heat transfer rates, phase change, and complex flow/displacement configurations, such as water–heavy oil displacement, steam–oil gravity drainage, double displacements (steam–water–oil), and, even, emulsion formation, which was observed in capillaries recently (Argüelles-Vivas and Babadagli, 2015). Beyond all these complexities with non-isothermal relative permeabilities, the controversy respect to the effect of

temperature (at isothermal conditions) on the behavior of heavy oil – water relative permeabilities and the shifts of fluid saturations are still alive as it can be concluded from the work of Ashrafi et al. (2014). Hence, relative permeability, as an average property (since it is integrated for a network of interconnected pores) representing transport phenomena at the micro level, needs more research at the pore scale. Although the coupling of all pore scale events and field scale modeling is still an open question (Joekar-Niasar et al., 2012), the unresolved issues in isothermal and non-isothermal models obligate to return to the analysis in a single pore, the basic cell of an oil reservoir, where momentum, heat and mass transfers start.

However, including all these factors in a single research is not a simple challenge. Studies on simplified conditions—incorporation of a temperature gradient to study the pore scale behavior of non-isothermal processes—are very limited. Medina et al. (2003) theoretically studied the spontaneous imbibition in a cylindrical capillary tube under a constant longitudinal temperature gradient. They found that the interface location depended markedly on the liquid surface tension and viscosity behavior with temperature and that spontaneous imbibition was accelerated when the temperature gradient was negative. Later, Sanchez et al. (2004) studied imbibition process in a Hele-Shaw model under a temperature gradient, theoretically and experimentally. They stated that the evolution of the fluid interface will depend on how the surface tension and viscosity changes with temperature. Sanchez et al. (2005) studied the effects of a longitudinal temperature gradient on the spontaneous imbibition process in a Berea Sandstone. This study showed that the averaged imbibition front was affected by the temperature gradient.

In this paper we carried out a fundamental analysis of the water—heavy oil displacement and gas—heavy oil gravity drainage under a temperature gradient using the classical capillary tube model. First, the momentum equations for both processes were developed with the inclusion of a temperature gradient and its effects on the fluids. Then, the exact solutions were obtained to describe the time-space fluid–fluid interface location and the application of the models was demonstrated in a single capillary tube. Finally, relative permeability curves were obtained for bundles of non-interconnected capillary tubes. A discussion on the limitations of the relative permeability curves and the non-isothermal models is included.

5.2 Theoretical work: development of non – isothermal models

5.2.1 Non-isothermal water–heavy oil displacement

This model mimics steam drive or condensed water drive as typically encountered during steam flooding.

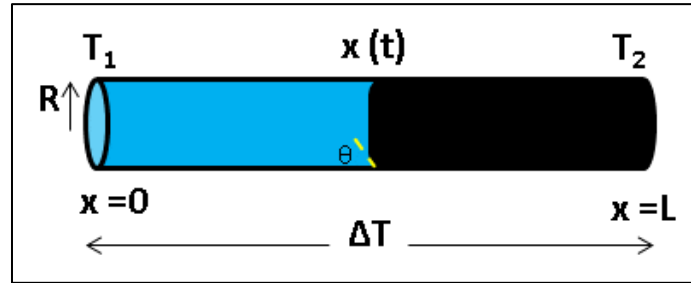


Figure 5-1: Non-isothermal water–heavy oil displacement in a single capillary tube.

Consider that a horizontal cylindrical capillary tube of length L is initially filled with heavy oil and subjected to a longitudinal temperature gradient $\Delta T = T_2 - T_1$ between $x = 0$ and $x = L$, as depicted in **Figure 5-1**. Water is injected at $x = 0$ and penetrates into the tube due to the favorable capillary pressure ($\theta < 90^\circ$, water wet capillary). A small pressure drop is also imposed between $x = 0$ and $x = L$. The total pressure drop and the interface velocity are so small that the magnitude of the Reynolds number permits the assumption that a Hagen-Poiseuille flow occurs during the displacement. To describe the fluid dynamics of this system, the momentum equation will be obtained through a balance between the molecular forces (due to the viscous forces and the external imposed pressure drop) (Bird et al., 2002) and the capillary forces:

$$\int_0^{x(t)} \tau_{w-w} dA + \int_{x(t)}^L \tau_{w-o} dA - \Delta p \pi R^2 = 2\pi \sigma_{wo}(x(t)) R \cos \theta \quad (2)$$

This method of force balance was previously used to analyze the spontaneous imbibition of a liquid into a vertical capillary tube filled with air (Medina et al., 2003) and the spontaneous imbibition of glycerol into a vertical Hele-Shaw model also filled with air (Sanchez et al., 2004), both under a longitudinal temperature gradient.

The first two terms in the integrals represent the internal shear stresses on the wall (White, 2008) at the area covered by water and oil respectively, defined as:

$$\tau_{w-w} = \frac{4\mu_w \bar{v}_x}{R} \quad (3a)$$

$$\tau_{w-o} = \frac{4\mu_o \bar{v}_x}{R} \quad (3b)$$

Where \bar{v}_x is the average interface velocity. These forces that must be integrated from 0 to $x(t)$ in the case of invading water and from $x(t)$ to L for the outgoing oil are effective for each differential area, $dA = 2\pi R dx$. The pressure forces, Δp , act perpendicularly onto the cross sectional area πR^2 whereas the capillary force works on the liquid–liquid interface area, given also by πR^2 but at $x = x(t)$.

By substituting Eqs. (3a), (3b) and the expressions for the areas into Eq. (2), this becomes:

$$\int_0^{x(t)} \frac{4\mu_w \bar{v}_x}{R} (2\pi R dx) + \int_{x(t)}^L \frac{4\mu_o \bar{v}_x}{R} (2\pi R dx) - \Delta p \pi R^2 = 2\pi \sigma_{wo}(x(t)) R \cos \theta \quad (4)$$

Since a temperature gradient is imposed through the capillary tube, this can result in variations of the fluids properties, which depend on temperature such as the viscosity and the interfacial tension. In this paper, it is accepted that the fluid properties can exhibit a linear behavior with temperature (Medina et al., 2003). Furthermore, since the temperature changes through the length, the viscosities of the fluids are also modified along the capillary tube. Linear equations for oil and water viscosity taking into account the temperature and the spatial change are, respectively:

$$\mu_o = \mu_{o0} + \left(\frac{d\mu_o}{dT} \right) \frac{\Delta T}{L} x \quad (5)$$

$$\mu_w = \mu_{w0} + \left(\frac{d\mu_w}{dT} \right) \frac{\Delta T}{L} x \quad (6)$$

The change of viscosity is especially notable for heavy oil (Argüelles-Vivas et al., 2012). In the case of the interfacial tension, the variations with respect to temperature depend just on the location of the interface front $x(t)$:

$$\sigma_{wo} = \sigma_{wo0} + \left(\frac{d\sigma_{wo}}{dT} \right) \frac{\Delta T}{L} x(t) \quad (7)$$

The subscript 0 in Eqs. (5) to (7) denotes oil viscosity, μ_o , water viscosity, μ_w and water-heavy oil interfacial tension, σ_{wo} at the reference temperature T_0 .

The interfacial tension between water and heavy oil can change at the first contact between both fluids due to the existence of natural surfactants in the heavy oil (Argüelles-Vivas et al., 2012) so that a dynamic interfacial tension is created. Here, we assumed that the change in the interfacial tension due to the natural surfactants of the oil occurs as soon as the water contacts the oil at the inlet of the capillary tube, which imply that the reference value σ_{wo0} corresponds to this value. Thus, the change in the interfacial tension along the capillary is just due to the temperature and the spatial change of the interface.

It is important to emphasize that in the development of the non-isothermal model, it is assumed that the diffusive time $t_{\text{Diff}} = R^2/\alpha_l$ is very small compared to the traveling time of the fluid interface, $t = R/(dx/dt)$. This means that as the interface is progressing and the fluids are moving, these acquire immediately the temperature distribution of the capillary wall (Medina et al., 2003).

Substituting Eqs. (5) and (7) into Eq. (4), one obtains:

$$8\pi \bar{v}_x \int_0^{x(t)} \left(\mu_{w0} + \left(\frac{d\mu_w}{dT} \right) \frac{\Delta T}{L} x \right) dx + 8\pi \bar{v}_x \int_{x(t)}^L \left(\mu_{o0} + \left(\frac{d\mu_o}{dT} \right) \frac{\Delta T}{L} x \right) dx - \Delta p \pi R^2 = 2\pi \left(\sigma_{wo0} + \left(\frac{d\sigma_{wo}}{dT} \right) \frac{\Delta T}{L} x(t) \right) R \cos \theta \quad (8)$$

As mentioned, \bar{v}_x is the average interface velocity and is also represented as dx/dt . Solving the integrals in Eq. (8) results in:

$$\left[\frac{\left(\mu_{w0} \left(1 + \left(\frac{d\mu_w}{dT} \right) \frac{\Delta T}{2\mu_{w0}L} x(t) \right) x(t) + \left(\mu_{o0} \left(1 + \left(\frac{d\mu_o}{dT} \right) \frac{\Delta T}{2\mu_{o0}L} (L + x(t)) \right) (L - x(t)) \right) \right)}{\left(\Delta p + \frac{2\sigma_{wo0} \cos \theta}{R} \left(1 + \left(\frac{d\sigma_{wo}}{dT} \right) \frac{\Delta T}{\sigma_{wo0}L} x(t) \right) \right)} \right] \frac{dx}{dt} = \frac{R^2}{8} \quad (9)$$

Equation (9) represents the average interface front velocity as the interface is progressing along the capillary tube under a linear temperature gradient. To solve this nonlinear differential equation, the following dimensionless variables are defined:

$$x_D = \frac{x}{L} \quad (10)$$

$$M_1 = \left(\frac{d\mu_w}{dT} \right) \frac{\Delta T}{2\mu_{w0}} \quad (11)$$

$$M_2 = \left(\frac{d\mu_o}{dT} \right) \frac{\Delta T}{2\mu_{o0}} \quad (12)$$

$$\Gamma_{wo} = \left(\frac{d\sigma_{wo}}{dT} \right) \frac{\Delta T}{\sigma_{wo0}} \quad (13)$$

$$Ca = \frac{\Delta p R}{\sigma_{wo0} \cos \theta} \quad (14)$$

$$\lambda = \frac{\mu_{o0}}{\mu_{w0}} \quad (15)$$

$$t_D = \frac{t(\sigma_{wo0} \cos \theta)}{8\mu_{w0}R} \quad (16)$$

$$l_0^2 = \left(\frac{R}{L} \right)^2 \quad (17)$$

where M_1 , M_2 and Γ_{ow} are the dimensionless parameters that contain the variations of fluid properties with temperature.

Substituting Eqs. (10) - (17) in Eq. (9), its dimensionless form is obtained as follows:

$$\left[\frac{(M_1 - \lambda M_2)x_D^2 + (1 - \lambda)x_D + (1 + M_2)\lambda}{2(\Gamma_{wo}x_D + 1) + Ca} \right] \frac{dx_D}{dt_D} = l_0^2 \quad (18)$$

Separating variables, integrating x_D from 0 to 1 and t_D from 0 to t_D and applying the initial conditions ($x_D = 0$ at $t_D = 0$), the exact solution for Eq. (18) can be obtained:

$$\frac{(M_1 - \lambda M_2)}{4\Gamma_{wo}} x_D^2 + \frac{(2\Gamma(1-\lambda) - (M_1 - \lambda M_2)(Ca+2))}{4\Gamma_{wo}^2} x_D + \left[\frac{\lambda(M_2+1)}{2\Gamma_{wo}} - \left(\frac{(2\Gamma_{wo}(1-\lambda) - (M_1 - \lambda M_2)(Ca+2))}{2\Gamma_{wo}} \right) \left(\frac{Ca+2}{4\Gamma_{wo}^2} \right) \right] \left(\ln \left| \frac{2(\Gamma_{wo} x_D + 1) + Ca}{Ca+2} \right| \right) = \frac{1}{\rho} t_D \quad (19)$$

If $\Delta T = 0$ (i.e., $M_1 = M_2 = 0$), the natural logarithm is expanded in a Taylor series and $\Gamma_{wo} = 0$, the known Washburn-Darcy equation (Berg 2010) is obtained:

$$(1-\lambda)x_D^2 + 2\lambda x_D - 2(Ca+2)\rho^2 t_D = 0 \quad (20)$$

5.2.2 Non-isothermal gas-heavy oil gravity drainage

This model mimics steam drive process driven by gravity (as typically encountered during the SAGD process).

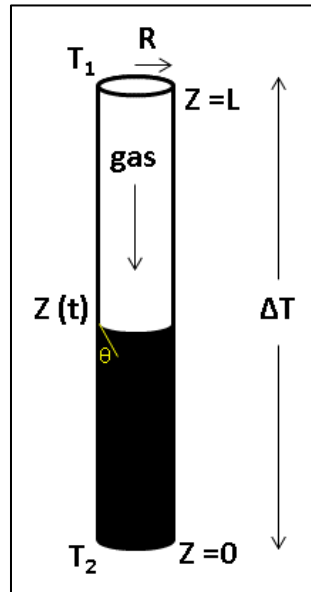


Figure 5-2: Non-isothermal gas-heavy oil gravity drainage displacement in a single capillary tube.

Suppose that a vertical capillary tube of length L is filled with heavy oil and that a longitudinal temperature gradient $\Delta T = T_2 - T_1$ is imposed between $z = 0$ and $z = L$. Then, gas is injected at the upper inlet at $z = L$ provoking a forced gravity drainage that it is controlled by a small and constant pressure drop set between $z = 0$ and $z = L$. The displacement is carried out at low velocity so that a Hagen-Poiseuille flow can be assumed. In the development of this model, it is

also assumed that as the oil slug is moving downward, it achieves the capillary temperature distribution (diffusive time is dominant). The capillary tube is assumed to be oil-wet ($\theta < 90^\circ$). This process is schematically shown in **Figure 5-2**.

Similar to the water–heavy oil displacement given above, this system can be also described through balance of forces. The balance is between the molecular forces (viscous forces and the external imposed pressure drop), the gravity, and the capillary forces:

$$\int_0^{z(t)} -\tau_w dA = \int_0^{z(t)} \rho g dV + \Delta p \pi R^2 - 2\pi\sigma(z(t))R \cos \theta \quad (21)$$

The integrand term τ_w at the left side of the equation corresponds to the internal viscous forces acting on each differential cylindrical area $dA = 2\pi R dz$ and it must be integrated from $z = 0$ to the moving interface front $z(t)$. This term is similar to Eq. (3b) but should be written for the axis z :

$$\tau_w = \frac{4\mu_o \bar{v}_z}{R} \quad (22)$$

In this system, \bar{v}_z in Eq. (22) represents the average gas–heavy oil interface velocity. The gravity force in the first term of the right side of Eq. (21) works on the differential cylindrical volume of fluid given by $dV = \pi R^2 dz$ and it must be integrated from 0 to the current interface position $z(t)$. The pressures forces, as it was explained before, work on the cross-sectional area πR^2 and the capillary force acts on the gas–liquid interface area, πR^2 at $z = z(t)$. Introducing Eq. (22) and the equations for the differential area and volume into Eq. (21), we obtain:

$$\int_0^{z(t)} -\frac{4\mu_o \bar{v}_z}{R} (2\pi R dz) = \int_0^{z(t)} \rho g \pi R^2 dz + \Delta p \pi R^2 - 2\pi\sigma(z(t))R \cos \theta \quad (23)$$

As it was applied for the previous modeling, the non-isothermal conditions are established through a temperature gradient affecting the fluid properties. For this system, oil viscosity and the gas–heavy oil surface tension are given by the next equations:

$$\mu_o = \mu_{o0} - \left(\frac{d\mu_o}{dT} \right) \frac{\Delta T}{L} z \quad (24)$$

$$\sigma = \sigma_0 - \left(\frac{d\sigma}{dT} \right) \frac{\Delta T}{L} z(t) \quad (25)$$

As can be observed from Eq. (24), oil viscosity changes linearly with temperature and with respect to the position along the capillary tube. Surface tension changes with temperature at the interface front $z(t)$ as it is stated at Eq. (25). Gas density is negligible in comparison to density of the oil, which in turn is assumed constant. Introducing Eqs. (24) and (25) into Eq. (23):

$$-8\pi \bar{v}_z \int_0^{z(t)} \left(\mu_0 - \left(\frac{d\mu}{dT} \right) \frac{\Delta T}{L} z \right) dz = \int_0^{z(t)} \rho g \pi R^2 dz + \Delta p \pi R^2 - 2\pi \left(\sigma_0 - \left(\frac{d\sigma}{dT} \right) \frac{\Delta T}{L} z(t) \right) R \cos \theta \quad (26)$$

Solving the integrals in Eq. (26), this results in:

$$\frac{\left(z(t) - \left(\frac{d\mu}{dT} \right) \frac{G}{2\mu_0} z^2(t) \right) dz}{\left[\frac{\rho_0 g R z(t)}{\sigma_0} + \frac{\Delta p R}{\sigma_0} - 2 \left(1 - \left(\frac{d\sigma}{dT} \right) \frac{G}{\sigma_0} z(t) \right) \right]} dt = - \frac{\sigma_0 R}{8\mu_0} \quad (27)$$

Next, Eq. (27) should be transformed into dimensionless variables:

$$z_D = \frac{z}{L} \quad (28)$$

$$M = \left(\frac{d\mu}{dT} \right) \frac{\Delta T}{2\mu_0} \quad (29)$$

$$\Gamma = \left(\frac{d\sigma}{dT} \right) \frac{\Delta T}{\sigma_0} \quad (30)$$

$$Ca_{go} = \frac{\Delta p R}{\sigma \cos \theta} \quad (31)$$

$$Bo = \frac{\rho g R L}{\sigma \cos \theta} \quad (32)$$

$$t_D = \frac{t(\sigma \cos \theta)}{8\mu_{o0} R} \quad (33)$$

Here, M and Γ are the non-isothermal dimensionless parameters. Introducing Eq. (17) and Eqs. (28) - (33) into Eq. (27) and re-arranging it becomes:

$$\frac{z_D - Mz_D^2}{(Bo + 2\Gamma)z_D + (Ca_{go} - 2)} \frac{dz_D}{dt_D} = -l_0^2 \quad (34)$$

Equation (34) is solved through the separation of variables, integrating from $z_D = 1$ to $z_D = z_D$ and from $t_D = 0$ to $t_D = t_D$ and applying the initial condition of $z_D = 1$ at $t_D = 0$. The exact solution for Equation (34) is:

$$\left(\frac{(Bo + 2\Gamma) + M(Ca_{go} - 2)}{(Bo + 2\Gamma)^3} \right) \left((Bo + 2\Gamma)(1 - z_D) + (Ca_{go} - 2) \ln \left(\frac{(Bo + 2\Gamma)z_D + (Ca_{go} - 2)}{(Bo + 2\Gamma) + (Ca_{go} - 2)} \right) \right) - \frac{M}{2(Bo + 2\Gamma)}(1 - z_D^2) = l_0^2 t_D \quad (35)$$

If $\Delta T = 0$ ($M = 0$) and $\Gamma = 0$ we then get the isothermal gas-liquid displacement equation:

$$\frac{1}{Bo^2} \left[Bo(1 - z_D) + (Ca_{go} - 2) \ln \left| \frac{Boz_D + Ca_{go} - 2}{Bo + Ca_{go} - 2} \right| \right] = l_0^2 t_D \quad (36)$$

Note that Eq. (36) was derived by Youngs (1960) to develop a model of porous medium in order to predict the production of a liquid at different times during free fall gravity drainage.

5.3 Results and Discussion: Application of non-isothermal models

In this section, the behavior of non-isothermal models is explored in comparison with the isothermal case. First, the effects of a temperature gradient on the interface location and velocity were analyzed for a single capillary tube and were applied to a bundle of capillary tubes. Then, the influence of a temperature gradient on the relative permeability curves was studied for both systems using a bundle of parallel non-interconnected capillary tubes. The size of the single capillary tube was 0.00005 m. For the bundle of capillary tubes, a uniform size distribution was chosen from 0.0001 m to 0.00001 m having a total of 100 cylindrical capillaries. The length of the capillaries was 1 m. For the single tube the diffusive time was around 0.037 s. For the bundle of capillaries, it was from 0.14 s (for 0.0001 m) to 0.001 s (for 0.00001 m). The transit time of the interfaces changed during the displacement but remained bigger than the diffusive time. The data of the thermal properties of the oil were taken from Butler (1991). In the non-isothermal water-heavy oil displacements, the capillaries are assumed water wet, whereas in the non-

isothermal gas-heavy oil gravity drainage displacements, the capillaries are oil wet. Most of the results are shown in dimensionless variables.

5.3.1 Fluid properties

Fitted equations were obtained based on published measurements to extrapolate data at high temperature conditions. The density and viscosity of heavy oil and the interfacial tension data were taken from Argüelles-Vivas et al. (2012) and the gas-heavy oil surface tension from Argüelles-Vivas and Babadagli (2015). Water viscosities were taken from Perry and Green (1984). It was assumed that the absolute pressure of the systems is high enough to avoid boiling or condensation. It was also considered that the fluid properties are not modified by pressure significantly. The magnitudes of the temperature are those typically encountered during thermal methods.

Figure 5-3 shows the viscosity behavior of heavy oil and water with temperature. Water-heavy oil interfacial tension and gas-heavy oil interfacial tension are shown in **Figure 5-4**. The ranges of temperature were selected from the linear behavior.

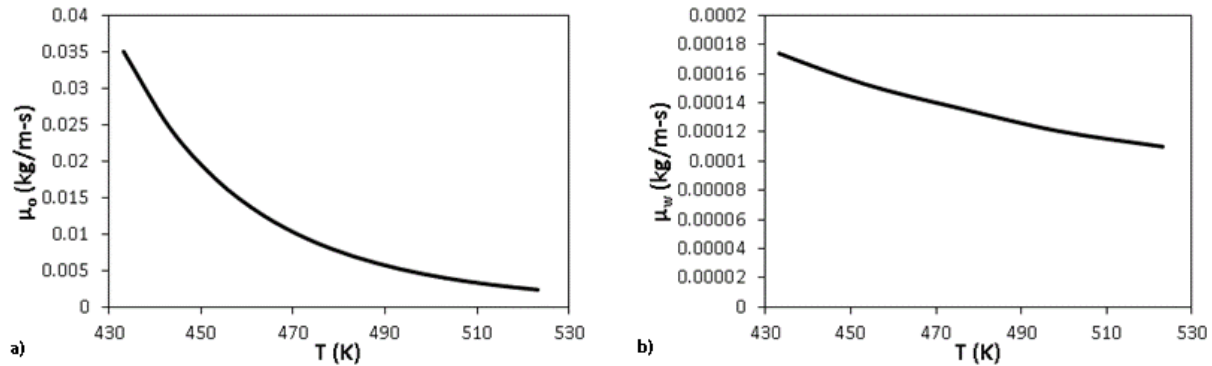


Figure 5-3: Viscosity behavior with respect to temperature: a) heavy oil viscosity, b) water viscosity.

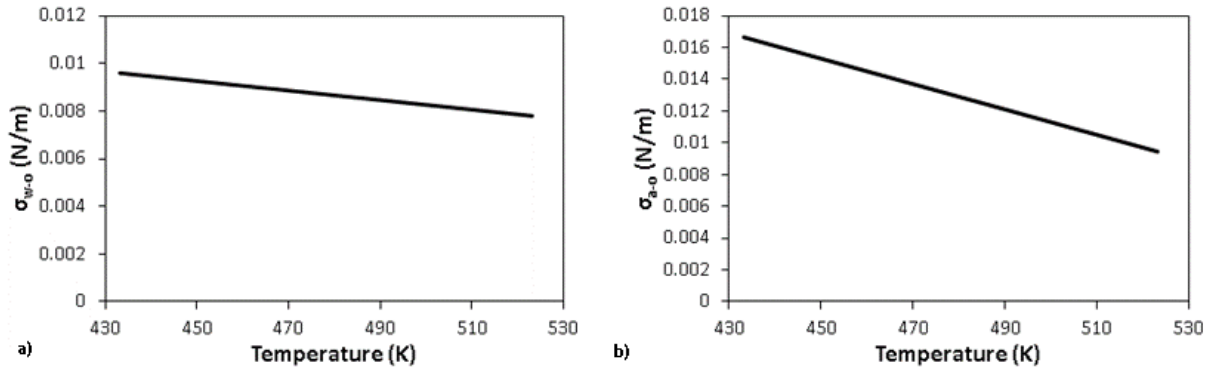


Figure 5-4: Interfacial tension behavior with respect to temperature: a) water–heavy oil, b) air–heavy oil.

5.3.2 Non – isothermal water – heavy oil displacements

The imposed pressure drop during the displacement was set at 10 Pa. The dimensionless interface location of isothermal and non-isothermal displacements is illustrated in **Figure 5-5**, which also indicates the comparisons of constant temperature displacements at $T=523.15$ K and $T=433.15$ K with temperature gradient displacements at $\Delta T=523.15-433.15=90$ K and $\Delta T=433.15-523.15=-90$ K (refer to **Figure 5-1** keeping in mind that $\Delta T=T_2-T_1$). The displacement at $T=523.15$ K is the fastest while the slowest occurred at $T=433.15$ K.

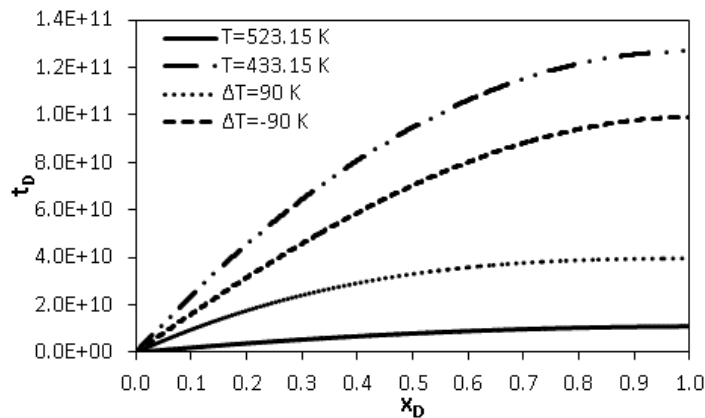


Figure 5-5: Location of the water–heavy oil interface in a capillary tube of $R = 0.00005$ m for isothermal and non-isothermal cases.

An interesting finding from this analysis is that the heavy oil displacement with a positive temperature gradient was accelerated compared to a displacement under a negative one, which is much slower. To be clear, considering the same absolute temperature gradient, the displacement of heavy oil was faster when water was injected at a temperature colder than that at the outlet of the capillary tube. When the temperatures were inverted (i.e., the higher temperatures were at the

inlet), the displacement was slowed down as can be observed in **Figure 5-5**. This behavior is also noticeable in **Figure 5-6** (the interface velocity accelerated at $\Delta T=90$ K and was closer to the interface velocity profile at $T=523.15$ K).

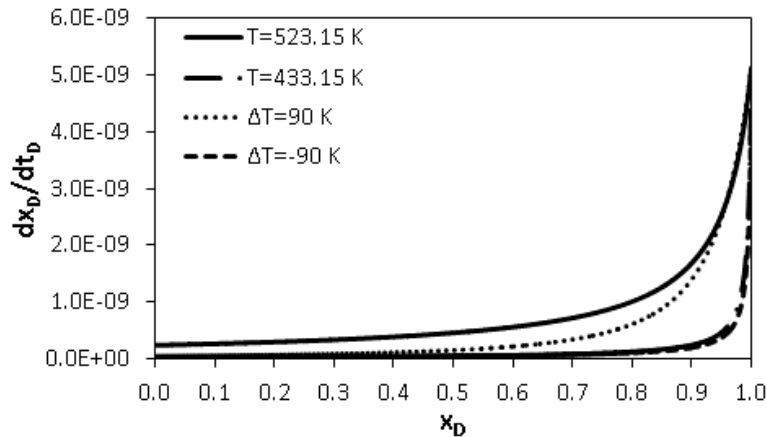


Figure 5-6: Dimensionless velocity of the water-heavy oil interface in a capillary tube of $R = 0.00005$ m for isothermal and non-isothermal cases.

When $\Delta p=0$ corresponding to a pure spontaneous imbibition process, the behavior was similar to the previous displacements; the imbibition was accelerated with a positive temperature gradient (**Figure 5-7**, the case of $\Delta T=\pm 40$ K).

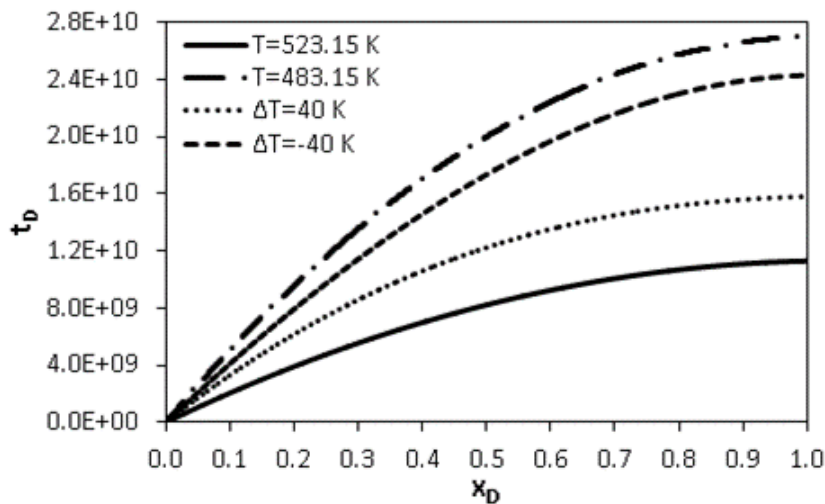


Figure 5-7: Location of the water-heavy oil interface in a capillary tube of $R = 0.00005$ m in a spontaneous imbibition process for isothermal and non-isothermal cases.

These results can be explained based on the variations of the fluids properties with temperature and the effects of such properties on the forces competing during the displacement. When the temperature increases, the viscosity decreases and the flow is enhanced. Conversely, if the

temperature rises, the interfacial tension decreases and the displacement tends to be slower (a higher capillary pressure is favorable to the water penetration since the capillary is water-wet). In this system, the decrease of the dynamic oil viscosity was more severe than the change of dynamic water viscosity and interfacial tension when temperature augmented. Therefore, it dominated the flow and the displacements at the highest temperatures were the fastest.

In the positive temperature gradient case, water drove the oil to a warmer region where higher temperatures exist. Then, oil viscosity was diminished along the oil slug as well as the interfacial tension of the fluid interface. As the displacement progressed, not only the smaller viscosities but also the decrement in the oil slug accelerated the flow overcoming the dampening effect of the interfacial tension. In the negative temperature gradient case, the viscosity profile values augmented, slowing down the flow and surpassing the favorable augmented interfacial tension. These behaviors are depicted in **Figure 5-8** for $\Delta T = \pm 90$ K. **Figure 5-8a1** and **Figure 5-8a2** reveal that displacement is accelerated under a positive temperature gradient at two different dimensionless times. In turn, **Figure 5-8b1** and **Figure 5-8b2** display how the displacement is slowed down under a negative temperature gradient for the same two dimensionless times. Interestingly, note how both interfaces are close each other at the beginning of the water penetration. As the time progresses, the distance between such interfaces increases notably.

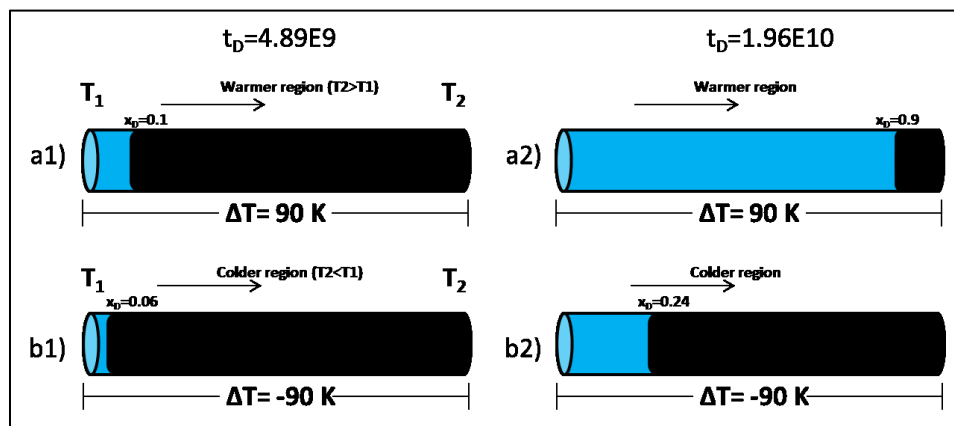


Figure 5-8: An illustrative example of the effects of: a) positive temperature gradient, b) negative temperature gradient.

The location of the interfaces for a bundle of capillary tubes is shown in **Figure 5-9** for two different times. Note that the progress of the interface at $T = 523.15$ K is much faster than the others. At $t = 1000$ s, the displacements are close to each other for $T = 433.15$ K and $\Delta T = \pm 90$ K but then they are markedly different at $t = 4000$ s, becoming faster with $\Delta T = 90$ K.

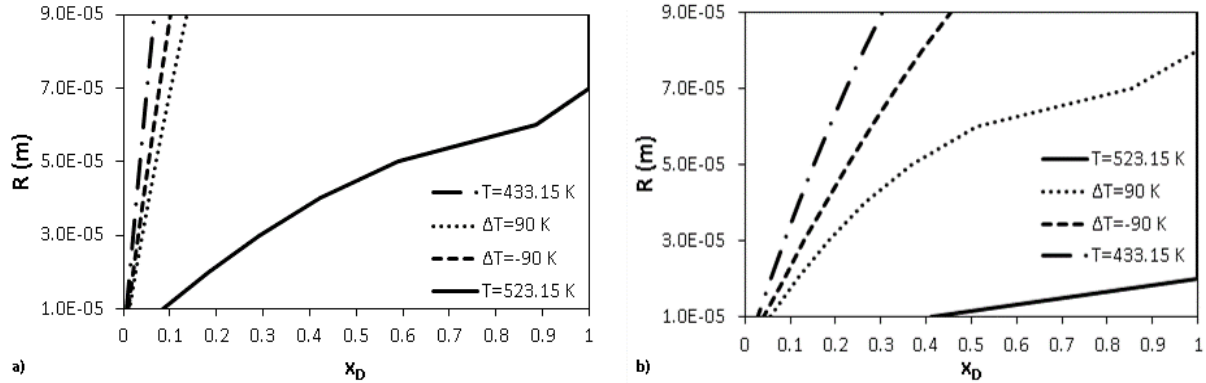


Figure 5-9: Positions of water – heavy oil interfaces in a bundle of capillary tube for isothermal and non-isothermal cases: a) 10000 s b) 40000 s.

5.3.3 Non – isothermal gas – heavy oil gravity drainage displacements

For this process, the capillary radius was also taken as 0.00005 m. The selected pressure drop was 5 Pa. Dimensionless gas-heavy oil front changes are shown in **Figure 5-10**. Non-isothermal gravity drainage displacements were carried out at $\Delta T = \pm 90$ K and compared to the isothermal cases at $T = 523.15$ K and $T = 433.15$ K. It was also found that under a positive temperature gradient, the gravity drainage process was faster compared to that with a negative temperature gradient, as observed in **Figure 5-9**. This can also be confirmed in **Figure 5-11** where it is observed that the velocity for $\Delta T = 90$ K is accelerated and the one for $\Delta T = -90$ K is slowed down.

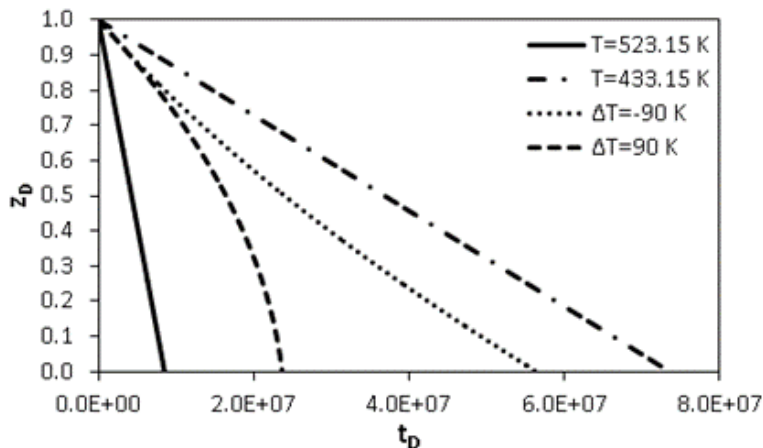


Figure 5-10: Location of the gas-heavy oil interface in a capillary tube of $R = 0.00005$ m for isothermal and non-isothermal cases.

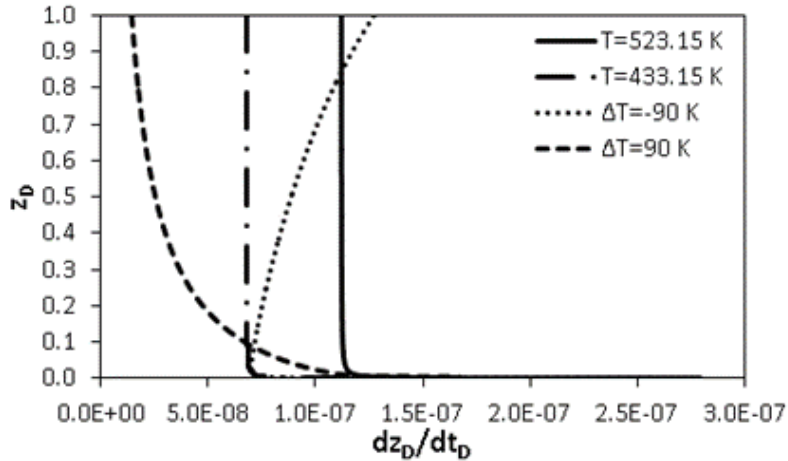


Figure 5-11: Dimensionless velocity of the gas-heavy oil interface in a capillary tube of $R = 0.00005$ m for isothermal and non-isothermal cases.

A similar explanation given for the water-heavy displacements is made for the gas-heavy oil case. In the case with positive temperature gradient, the gas displaced the oil to a zone of higher temperature where both oil viscosity and surface tension were diminished. However, unlike the water-heavy oil displacements, the decrement of both properties was found to be favorable for the acceleration of the interface (since the capillary is oil-wet). With a negative gradient, both the viscosity and the surface tension increased, together causing a retarding effect on the flow. The positions of the gas-heavy oil interfaces in the bundle of capillary tubes case are shown in **Figure 5-12** at two different times to compare the constant temperature and temperature gradient cases.

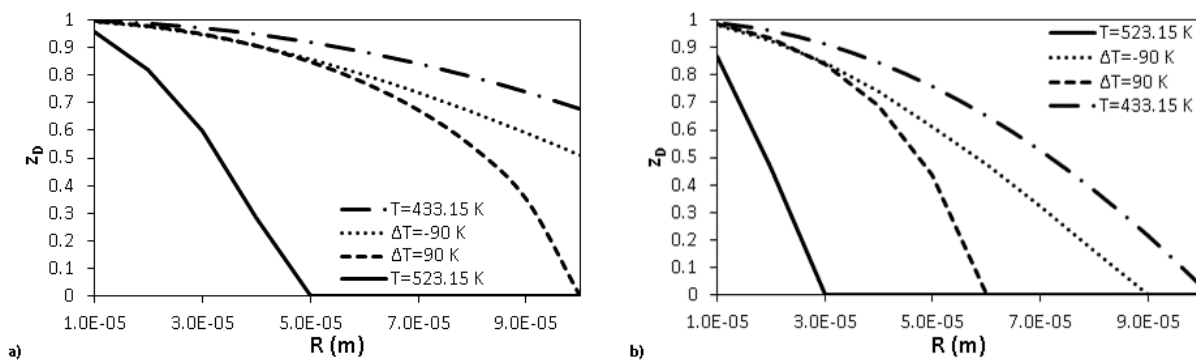


Figure 5-12: Positions of gas-heavy oil interfaces in a bundle of capillary tubes for isothermal and non-isothermal cases: a) $t = 1000$ s, b) 3000 s.

5.3.4 Effects of non – isothermal conditions on relative permeability curves

We investigated the influence of non-isothermal conditions on water–heavy oil and gas–heavy oil relative permeability curves using the bundle of parallel and non-interconnected capillary tubes. This model ideally represents unconsolidated (very high permeability of up to 10 Darcies) oil sands filled with very heavy oil as typically encountered in Alberta, Canada (**Figure 5-13**).

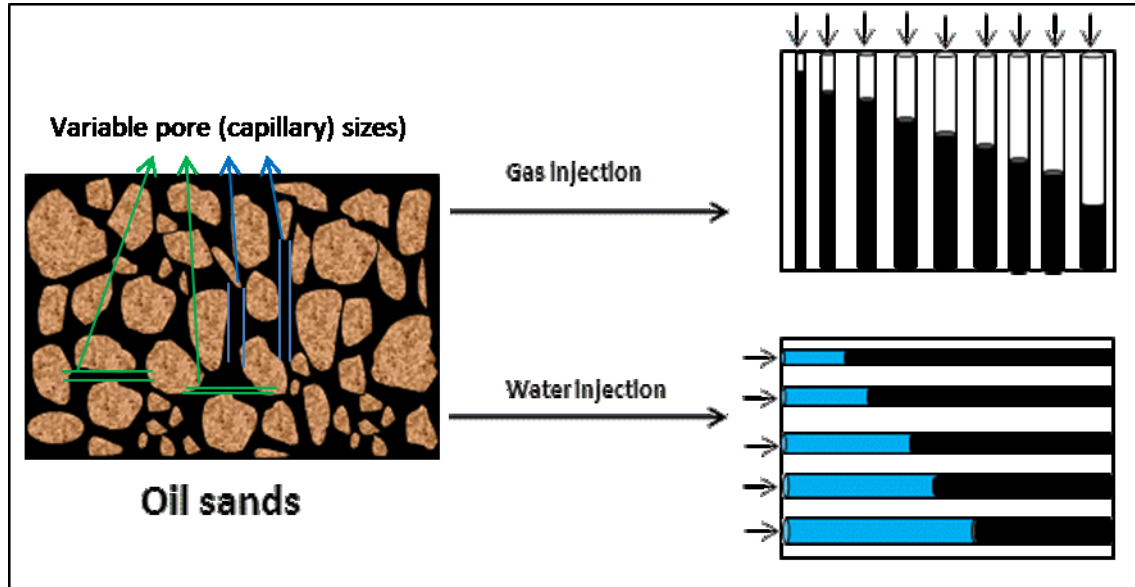


Figure 5-13: Representation of oil sands as bundles of capillaries tubes during gas and water injection.

The JBN method (acronym from Johnson et al., (1959), its developers) was used to calculate both sets of unsteady-state relative permeability curves. To apply this method, two physical conditions have to be met: (1) the overall pressure drop must be higher than capillary pressure and (2) both phases must act as immiscible and incompressible fluids.

In the case of water–heavy oil, the capillary pressure was set to zero and the applied external pressure drop was 10 Pa. For gas–heavy oil, the external pressure drop was 5 Pa over the capillary pressure in each capillary so that the net pressure drop was 5 Pa. Thus, unsteady-state displacements were carried out at a constant pressure drop. Due to the restrictions of the method, the analysis was focused on the effects of oil/displacing fluid viscosity ratio on relative permeabilities at isothermal and non-isothermal conditions.

Data taken from the displacements for the calculation of relative permeability curves were the production times, the water, oil, and gas volumes at the outlet of the bundle of capillaries. The non-isothermal equations developed previously were used for this purpose.

It must be noted that when using the JBN method (or the alternative method of Jones and Roszelle [1978]) the relative permeabilities are calculated at the exit face of bundle. The sequence of calculations is as follows:

The average saturation of the displacing phase, \bar{S}_d , is given by:

$$\bar{S}_d = S_{di} + \frac{N_p}{V_p} \quad (37)$$

The subscript d can be water or gas. S_{di} is the initial saturation of the displacing phase in the porous medium. The fractional flow of oil at the exit face, $(f_o)_2$, is defined by:

$$(f_o)_2 = \frac{d\bar{S}_d}{dQ_i} \quad (38)$$

Where Q_i is the number of injected pore volumes. The saturation of the displacing phase at the outlet is defined by:

$$S_{d2} = \bar{S}_d - Q_i (f_o)_2 \quad (39)$$

The oil relative permeability is calculated as:

$$k_{ro} = \frac{(f_o)_2}{d(q_{ti} / Q_i q_t) / d(1 / Q_i)} \quad (40)$$

where q_{ti} is the total flow rate at the very beginning of the flooding and q_t is the total flow rate at different times. Finally, relative permeability of the displacing phase is defined as:

$$k_{rd} = \frac{1 - (f_o)_2}{(f_o)_2} \frac{\mu_d}{\mu_o} k_{ro} \quad (41)$$

Where μ_d is the viscosity of the displacing phase. For simplification, in these displacements the oil is considered to be completely swept from the capillaries and the initial water saturation is zero. However, recently, Argüelles-Vivas and Babadagli (2014; 2015) showed that the development of residual heavy oil saturation in circular and square capillaries depends of the magnitude of the capillary and Bond numbers and the temperature conditions. In the case of gas-heavy oil displacements under gravity drainage at low velocities in round capillaries, the residual oil saturation, in the form of film, is around 2.5 % for 300 μm in diameter and decreases linearly for smaller pore sizes. At higher Capillary and Bond numbers, the residual heavy oil may even increase (Argüelles–Vivas and Babadagli, 2014 and 2015).

To mimic non-isothermal conditions the unsteady–state, displacements were carried out with $\Delta T = \pm 90$ K and compared to the isothermal displacements at $T = 523.15$ K and $T = 433.15$ K. **Figure 5-14** and **Figure 5-15** show the resulting sets of water–heavy oil and gas–heavy oil relative permeability curves, respectively.

Figure 5-14a and **Figure 5-15a** show the relative permeabilities directly obtained from the application of the JBN method to the water–heavy oil and gas heavy–oil displacements in bundles of parallel non-connected capillaries tubes. A pitfall with the JBN method (Johnson et al. 1959) or the technique of Jones and Roszelle (1978) is that it is not possible to obtain the relative permeability curves between the initial water saturation (zero in our case) and the water saturation at the breakthrough time (no point between in the water saturation range of 0 and 0.57), as observed in these graphs. This complicates the determination of the shape of the curves between these two points of saturation. As a first attempt, the points were connected using a spline (**Figure 5-14a** and **Figure 5-15a**). Although **Figure 5-14a** shows expected values of relative permeabilities being below “1”, one point corresponding to water saturation value of ~ 0.57 appeared to be above “1” for the case $\Delta T = 90$ K. This could be an indication of the strong effect of viscosity variations on oil relative permeability (in this case viscosity reduction). This point corresponds to water saturation of ~ 0.57 , where the water breakthrough occurred, which means the total flow rate suddenly changed (increasing faster due to the water flow at the outlet of the bundle). This, and the additional effect of severe viscosity reduction due to positive temperature gradient ($\Delta T = 90$ K) provoked that an oil relative permeability value above one is obtained.

As a second attempt, the cubic spline method was applied to fill the points to obtain a best fitting and curves having an upward concave shape (hump shape) were obtained (**Figure 5-14b and Figure 5-15b**).

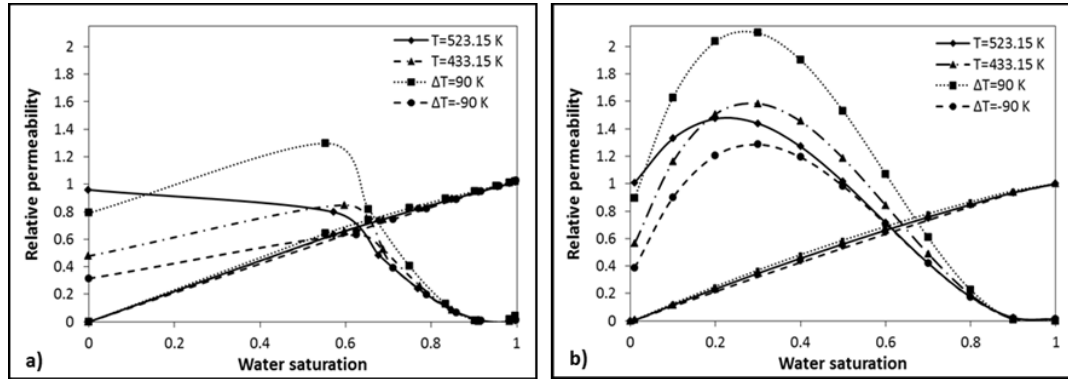


Figure 5-14: Water –heavy oil relative permeability curves at isothermal and non–isothermal conditions for a bundle of parallel and non-interconnected capillary tubes.

Further analysis of the relative permeabilities will be done based on these latter curves. First focusing the attention to the isothermal cases at T=523.15 K and T=433.15 K, it was observed that the relative permeabilities varied with temperature and, as a consequence, with the viscosity ratio μ_o/μ_d . These curves at constant temperature with a defined μ_o/μ_d ratio were consistent with those published by Bartley and Ruth (1999) and Dong et al. (2006) for the same type of parallel and non-interconnected capillary tubes (Dong et al. [2006] called it the non-interacting capillary bundle model). These studies, however, did not discuss the underlying physics that yield “hump shape” oil relative permeabilities.

In the case of the gas–heavy oil relative permeability curves at a constant temperature, we did not find similar curves in the published literature; however, they followed a similar trend to that of isothermal water–heavy oil curves shown in **Figure 5-14** and in the works of Bartley and Ruth (1999) and Dong et al. (2006). In certain range of water saturation, oil relative permeability is above unity. This can be explained through physical reasons behind it and attributed to the notorious effect of oil viscosity changes and the abrupt increment of total flow rate (gas flowing much faster than oil) at the outlet of the porous medium affecting then the saturations and fluids distribution.

In this kind of capillary tube bundle models, low values of oil relative permeabilities are found as μ_o/μ_w is higher at very low water saturation, as it can be observed in **Figure 5-14** for T=433.15

K or in Bartley and Ruth (1999) and Dong et al. (2006). Then, at intermediate water saturation the oil relative permeability becomes higher as μ_o/μ_w is higher. This is still satisfied at high water saturation but the difference in the oil relative permeability values among the curves decrease (see curves at $T=523.15$ K and $T=433.15$ K in **Figure 5-14**). This is also applicable to gas-heavy oil relative permeability curves as it is shown in **Figure 5-15**.

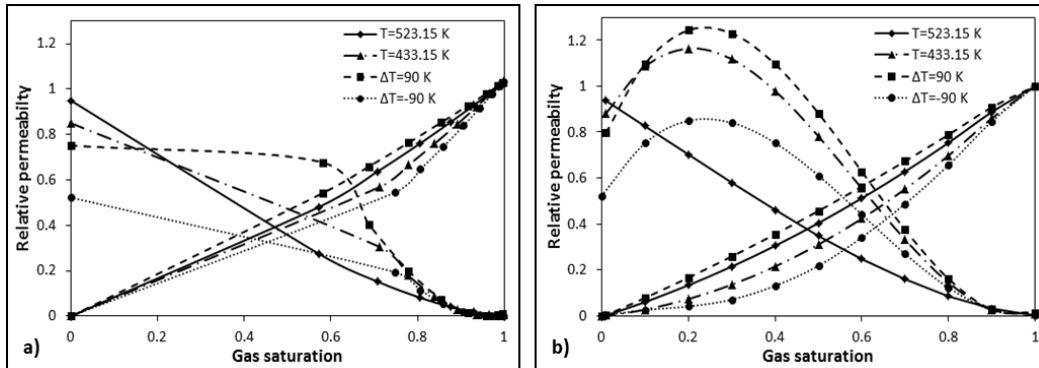


Figure 5-15: Gas-heavy oil relative permeability curves at isothermal and non-isothermal conditions for a bundle of parallel and non-interconnected capillary tubes.

As pointed out by Bartley and Ruth (1999), the variations in the points of origin on the oil relative permeability when using the JBN method are caused by the increment of the total flow rate q_t (oil flow plus water flow), as the interface front progresses in the tube (**Figure 5-5**, **Figure 5-7**, and **Figure 5-10**), since this variable is directly related to the oil permeability calculation (Eq. [40]). This effect is exacerbated as the μ_o/μ_w increases. It can be observed in **Figure 5-14** and **Figure 5-15** that the water and gas relative permeability curves are less affected by the variations of the viscosity ratio and the oil flow rate. This occurs since a limit is reached in the fractional flow ratio of the displacing phase and oil as the μ_o/μ_d augments (Bartley et al. 1999).

In relation to the displacements under non-isothermal conditions, we found that the oil relative permeability curves were greatly affected by the temperature gradient and were noticeably different to the constant temperature ones. These cases of constant temperature corresponded to the extreme values of the temperature gradient (remember that $\Delta T=523.15-433.15=90$ K and $\Delta T=433.15-523.15=-90$ K). Higher values of oil relative permeabilities were found for the positive temperature gradient $\Delta T=90$ K with respect to the negative gradient case and even with respect to the isothermal case at $T=433.15$ K, except at very low water or gas saturation, as observed in **Figure 5-14** and **Figure 5-15**.

With a negative temperature gradient ($\Delta T = -90$ K) the oil relative permeability resulted smaller than those determined for the isothermal cases at $T = 523.15$ K and for that with a positive gradient in the water–heavy oil system. For the gas–heavy oil system, it was found that the oil relative permeability with the negative temperature gradient was smaller than those for the positive temperature gradient, and for the isothermal case at $T = 433.15$ K but bigger than the oil relative permeability for the constant temperature case at $T = 523.15$ K. Similar to what occurred in the systems at constant temperature, the changes of the water and gas relative permeability curves with temperature gradient were much smaller than the changes of the oil relative permeability curves. We also hypothesize that under a negative temperature gradient, the variations of oil relative permeability in a certain range of saturations are due to the influence of the changes of oil viscosity. However, since the oil is flowing toward a colder region, the oil relative permeability becomes smaller compared to that of the cases with a positive temperature gradient due to augmented viscosity.

It should be iterated that the JBN or Jones and Roszelle (1978) methods determine the relative permeabilities at a point of the porous medium (the exit face) based on the average saturation history (Welge, 1952), the average relative injectivity (Johnson et al., 1959) or the overall pressure/rate (Jones and Roszelle, 1978). When using one of these methods, the relative permeabilities in a system with a temperature gradient must be interpreted as the relative permeabilities at an isothermal fixed plane with constant fluids properties affected by the average behavior inside the porous medium where the fluids have variable properties due to the temperature gradient.

It should also be emphasized that there is no general consensus about the behavior of the relative permeabilities curves for high viscosity ratios and variable temperature. Most of the earlier works (i.e., Johnson et al., 1959; Leverette, 1939; Schneider and Owens, 1970) did not find effects of the viscosity ratio on these curves. On the contrary, Odeh (1959) and Danis and Jacquin (1983) showed that when water is flowing as thick films adhered to the walls of the pores and oil is flowing over the water, there is a strong hydraulic coupling at the low water saturation range causing an apparent slip of the oil, which results in an increase of the oil relative permeability as the viscosity ratio μ_o/μ_w augments. Odeh (1959) found no alteration of the water relative permeability, as similar to our observations.

Dullien (1992) stated that if one of the fluids is very viscous and is introduced in the porous medium first, the less viscous fluid will flow at the center of the pores no matter if it is the wetting fluid or not. In such situation, the viscosity ratio becomes a crucial parameter. Wang et al. (2006) analyzed water-oil relative permeabilities in a wide range of oil viscosity (0.43 Pa.s to 13.55 Pa.s). They stated that water and oil relative permeabilities curves shifted to lower values with the increase of oil viscosity.

In a single capillary, Yuster (1951) demonstrated that oil relative permeability depended on the viscosity ratio. Using parallel and serial capillary tubes models, Ruth and Bartley (1999) demonstrated that the viscosity ratio μ_o/μ_w affected the relative permeability curves so that a unique set of relative permeabilities was not obtained. Dong et al. (2005; 2006) created an interacting capillary bundle model and found that the relative permeability is independent of the viscosity ratio μ_o/μ_w (tested in a range from 1 to 100).

With respect to the influence of the temperature on the relative permeabilities, there are also controversial observations in literature. As reported by Ashrafi et al. (2014), some researchers observed changes of the end point saturations and the relative permeabilities with temperature (Edmonson, 1965; Lo and Mungan, 1973; Bennion et al., 1985). However, Wilson (1956), Sufi (1982), and Miller and Ramey (1985) did not find any effects of temperature on relative permeability and end point saturations. In relation to heavy oils, Poston et al. (1970) found changes on relative permeabilities and in the water and oil residual saturations. Maini and Batycky (1985) found changes of oil relative permeability with temperature. Sola et al. (2007) observed through their experimental and numerical test in using carbonate rocks that relative permeabilities depend on temperature in the range from 310.9 K to 533.15 K.

The shifts of the relative permeabilities with temperature were attributed to instabilities, capillary end effects, and viscous fingering rather than to fundamental flow properties governing multiphase flow (Ashrafi et al., 2014; Miller and Ramey, 1985; Sufi et al., 1982; Maini and Okazawa, 1987). The last published investigation at the time of this work was that of Ashrafi et al. (2014). Based on their literature review, analysis, and experiments they stated that it is not possible to justify a unique trend of the relative permeabilities even though the range of water

saturation changes and, therefore, the relative permeability behavior depends on the particular system.

Since the temperature conditions in the reservoirs and during the thermal methods are rather non-isothermal, we focused our research on the behavior of relative permeability curves in an ideal porous medium under a temperature gradient. We found only one study on the effects of a steep temperature gradient on relative permeability. Watson and Ertekin (1988), using Berea Sandstones with Soltrol 170 and CaCl₂ brine, observed that the oil and water relative permeability diminished as the injection temperature increased.

5.3.5 Limitations of the model, potential improvements and considerations for field scale modeling

In this paper, the effects of a temperature gradient on the oil displacement by water or gas in cylindrical capillaries were analyzed through a newly developed analytical model. The analysis was limited to the cases where the fluid properties exhibit a linear behavior with respect to the temperature gradient. For a wider temperature ranges, new equations for the properties have to be developed and the solutions of the models derived in this work should also be modified.

Part of the ingenuity of this kind of models (originated from Medina et al., 2003) was to include combined effects of temperature, temperature gradient and distance on the properties of the fluids. One of the concerns in this type of approach is to obtain suitable formulas that take into account all of these parameters, especially the treatment of the derivatives over wider temperature ranges. However, our modeling approach was able to capture the effect of viscosity change due to temperature and the impact of temperature gradient. The extension of this work would be to use more sophisticated pore systems. Our model did not consider the inherent connectivity among the pores, which could modify the behaviors explained in this paper. In this case, a different modeling approach can be proposed and the temperature gradients can be included in the interacting capillary bundle (Dong et al., 2005, 2006), the bundle of serial tubes (Bartley and Ruth, 1999), or the cross flow (Ruth and Bartley, 2002) models.

Although our curves were obtained for bundles of parallel and non-interconnected capillary tubes, they showed that actual relative permeability curves in non-isothermal processes could be

different from the conventional ones used in reservoir simulation studies. Hence, practitioners working in field scale modeling of thermal methods should be careful when they selected or match the relative permeability curves. For example, in the case of SAGD, the relative permeabilities inside the chamber could be different than those in the edge of chamber or in the ceiling part. On the other hand, as mentioned in the introduction part, the residual oil saturation inside the chamber is determined using the equation of Cardwell and Parson (1949) which was derived for isothermal free fall gravity drainage. A temperature gradient affecting oil trapping deserves more attention. In the scaling process or in the design of experiments, a temperature gradient and its effects on properties have to be analyzed. The notoriously different behavior with positive or temperature gradient could bring ideas for new well pattern designs or improved recovery processes.

5.4 Conclusions

- Closed-form analytical solutions, including a temperature gradient that affects fluid properties, were developed to analyze the displacement of heavy oil by water and gas in capillary tubes. When $\Delta T=0$, the Washburn–Darcy equation is recovered for the water–heavy oil displacement. In the same manner, the isothermal gravity drainage equation for gas–heavy oil is obtained.
- For both systems (water-heavy oil and gas-heavy oil), the fluid–fluid interface location depended on the behavior of interfacial/surface tension and fluid viscosity with temperature. Since the change of heavy oil viscosity with temperature was stronger, it became the dominant variable during the non-isothermal displacements.
- The displacement of heavy oil during the water or gas invasion was accelerated when the temperature gradient was positive (i.e., when the temperature at the inlet of the capillary was smaller than temperature at the exit face). This included spontaneous imbibition of water ($\Delta p=0$).
- Applying the non-isothermal models to a bundle of parallel non-interconnected capillary tubes demonstrated that a temperature gradient could modify the behavior of the relative permeability curves, making it different to that of relative permeability curves determined at constant temperature.

5.5 Nomenclature

A	enveloping cylinder area, m ²
dx/dt	water – heavy oil interface velocity, m/s
dz/dt	gas – heavy oil interface velocity, m/s
(f _o) ₂	fractional flow of oil at the exit face of the bundle of capillaries
g	gravity constant, kg m/s ²
k	absolute permeability in equation (1), m ²
k _{ro}	oil relative permeability
k _{rw}	water relative permeability
L	length of the capillary, m
x	horizontal coordinate direction
x(t)	water–heavy oil interface location, m
Δp	pressure drop imposed between the inlet and outlet of the capillary
N _p	heavy oil production at different times, m ³
V _p	pore volume, m ³
\overline{dS}_d/dQ_i	derivative of the average displacing fluid saturation with respect to the injected pore volumes
Q _i	injected pore volumes
q _{ti}	total flow rate at the very beginning of the displacement, m ³ /s
q _t	total flow rate at different times, m ³ /s
R	radius of the capillary, m
S _{d2}	displacing fluid saturation at the outlet of the bundle of capillaries
\overline{S}_d	average displacing fluid saturation inside the bundle of capillaries
S _{di}	initial displacing fluid saturation inside the bundle of capillaries
S _{or}	residual oil saturation in equation (1)
T ₁ , T ₂	temperature at the inlet and outlet of the capillary, K
ΔT	temperature gradient, K
t _{diff}	diffusive time, s

t	time, s
Y	drainage height in equation (1), m
z	vertical coordinate direction
z(t)	gas – heavy oil interface location, m

Greek letters

α_l	<i>thermal diffusivity of a liquid, m^2/s</i>
μ_{o0}	<i>oil viscosity at the reference temperature, $kg/m-s$</i>
μ_w	<i>water viscosity, $kg/m-s$</i>
μ_{w0}	<i>water viscosity at the reference temperature, $kg/m-s$</i>
μ_d	<i>displacing fluid viscosity, $kg/m-s$</i>
ν_s	<i>kinematic viscosity in equation (1), m^2/s</i>
ρ	<i>oil density, kg/m^3</i>
σ_{wo}	<i>water – heavy oil interfacial tension, N/m</i>
σ_{wo0}	<i>water – heavy oil interfacial tension at the reference temperature, N/m</i>
σ	<i>gas – heavy oil surface tension, N/m</i>
σ_0	<i>gas – heavy oil surface tension at the reference temperature, N/m</i>
τ_{w_w}	<i>wall shear stress at the area covered by water, N/m^2</i>
τ_{w_o}	<i>wall shear stress at the area covered by oil, N/m^2</i>
τ_w	<i>wall shear stress at the area covered by oil in the gas – heavy oil system, Pa</i>
φ	<i>porosity in equation (1)</i>
θ	<i>contact angle</i>
$d\mu_o/dT$	<i>derivative of oil viscosity with temperature, $kg\ m^{-1}s^{-1}/K$</i>
$d\mu_w/dT$	<i>derivative of water viscosity with temperature, $kg\ m^{-1}s^{-1}/K$</i>
$d\sigma_{wo}/dt$	<i>derivative of water – heavy oil interfacial tension with temperature, Nm^{-1}/K</i>

Dimensionless numbers

x_D	<i>dimensionless water – heavy oil interface location</i>
M_1	<i>dimensionless parameter containing the change of water viscosity with temperature</i>
M_2	<i>dimensionless parameter containing the change of heavy oil viscosity with temperature</i>
Γ_{wo}	<i>dimensionless parameter containing the change of water – heavy oil interfacial tension with temperature</i>
Γ	<i>dimensionless parameter containing the change of gas – heavy oil surface tension with temperature</i>
Ca	<i>dimensionless capillary number in the water – heavy oil displacement</i>
Ca_{go}	<i>dimensionless capillary number in the gas – heavy oil gravity drainage displacement</i>
λ	<i>dimensionless oil – water viscosity ratio</i>
t_D	<i>dimensionless time</i>
dx_D/dt_D	<i>dimensionless water – heavy oil interface velocity</i>
dz_D/dt_D	<i>dimensionless gas – heavy oil interface velocity</i>
l_0	<i>dimensionless ratio between the radius and the length of the capillary</i>
z_D	<i>dimensionless gas – heavy oil interface location</i>
M	<i>dimensionless parameter containing the change of heavy oil viscosity with temperature in the gas – heavy oil gravity drainage displacement</i>
Bo	<i>Bond number</i>

5.6 References

1. Argüelles–Vivas, F.J. and Babadagli, T. 2014. Drainage Type Oil and Heavy-Oil Displacement in Circular Capillary Tubes: Two- and Three-Phase Flow Characteristics and Residual Oil Saturation Development in the Form of Film at Different Temperatures. *Journal of Petroleum Science and Engineering* 118: 61-73.
2. Argüelles–Vivas, F.J. and Babadagli, T. 2015. Residual Liquids Saturation Development During Two and Three Phase Flow under Gravity in Square Capillaries at Different Temperatures. *Int. J. of Heat and Fluid Flow* 52: 1-14.

3. Argüelles–Vivas, F.J., Babadagli, T., Little, T., et al. 2012. High Temperature Density, Viscosity and Interfacial Tension Measurements of Bitumen-Pentane-Biodiesel and Process Water Mixtures. *Journal of Chemical & Engineering Data* 57 (10): 2878-2889.
4. Ashrafi, M., Souraki, Y., and Torsaeter, O. 2014. Investigating the Temperature Dependency of Oil and Water Relative Permeabilities for Heavy Oil Systems. *Transport in Porous Media* 105: 517-537.
5. Bartley, J.T. and Ruth, D.W. 1999. Relative Permeability Analysis of Tube Bundle Models. *Transport in Porous Media* 36: 161-187.
6. Bennion, D.W., Moore, R.G., and Thomas, F.B. 1985. Effect of Relative Permeability on the Numerical Simulations of the Steam Stimulation Process. *J Can Pet Technol* 24 (2): 40-44.
7. Berg, J. 2010. *An Introduction to Interfaces & Colloids: The Bridge to Nanoscience*. Singapore: World Scientific Publishing Co. Pte. Ltd.
8. Bird, R.B., Stewart, E.N., and Lightfoot, E.N. 2002. *Transport Phenomena*, second edition. New York: John Wiley & Sons.
9. Butler, R.M. 1991. *Thermal Recovery of Oil and Bitumen*. Prentice Hall Inc., New Jersey, 1991.
10. Cardwell, W.T. and Parsons, R.L. 1949. Gravity Drainage Theory, *Trans. AIME* 179: 199-211.
11. Chung, K.H. and Butler, R.M. 1987. Geometrical Effect of Steam Injection on the Formation of Emulsions in the Steam-Assisted Gravity Drainage Process. Paper 87-38-22 presented at the 38th Annual Technology Meeting of the Petroleum Society of CIM, Calgary, AB, Canada, 7-10 June.
12. Danis, M. and Jacqui, C. 1983. Influence du Contraste de Viscosité sur les Permeabilités Relatives Lors du Drainage: Experimentation et Modelisation. *Rev dl'IFT* 38.
13. Donaldson, E.C., Lorenz, P.B., and Thomas, R.D. 1966. The Effects of Viscosity and Wettability on Oil and Water Relative Permeabilities. *Proc: 41st Annual SPE Meet., Dalas, TX, 2-5 October, SPE* 1562.
14. Dong, M., Dullien, F.A.L., Dai, L., et al. 2005. Immiscible Displacement in the Interacting Capillary Bundle Model Part I. Development of Interacting Capillary Bundle Model. *Transport in Porous Media* 59: 1-18.
15. Dong, M., Dullien, F.A.L., Dai, L., et al. 2006. Immiscible Displacement in the Interacting

- Capillary Bundle Model Part II. Applications of Model and Comparison of Interacting and Non-Interacting Capillary Bundle Models. *Transport in Porous Media* 63: 289-304.
16. Dullien, F.A.L. 1992. *Porous Media: Fluid Transport and Pore Structure*, second edition. San Diego: Academic Press.
 17. Edmonson, T.A. 1965. Effect of Temperature on Waterflooding. *J Can Pet Technol* 4 (4): 236-242.
 18. Geffen, T.M., Owen, W.W., D.R. Parris., et al. 1951. Experimental Investigation of Factors Affecting Laboratory Relative Permeability Measurements. *Transactions AIME* 192: 99-110.
 19. Jimenez, J. 2008. The Field Performance of SAGD Projects in Canada. Paper IPTC 12860 presented at the Int. Petroleum Tech. Conf., Kuala Lumpur, Malaysia, 3-5 December.
 20. Joekar-Niasar, V., van Dijke, M.I.J., and Hassanizadeh, S.M. 2012. Pore-Scale Modeling of Multiphase Flow and Transport: Achievements and Perspectives. *Transport in Porous Media* 94: 461-464.
 21. Johnson, E.F., Bossler, D.P., and Naumann, V.O. 1959. Calculation of Relative permeability from Displacement Experiments. *Petroleum Transactions AIME* 216: 370-372.
 22. Jones, S.C. and Roszelle, W.O. 1978. Graphical Techniques for Determining Relative permeability from Displacement experiments. *Journal Pet Technol* 5: 807-817.
 23. Leverett, M.C. 1939. Flow of Oil-Water Mixtures through Unconsolidated Sands. *Petroleum Transactions AIME* 132: 149-171.
 24. Lo, H.Y. and Mungan, N. 1973. Temperature Effect on Relative Permeability and Residual Oil Saturations. Oral presentation RR-19 given at the Petroleum Recovery Institute, Calgary, AB.
 25. Maini, B.B. and Batycky, J.P. 1985. The Effect of Temperature on Heavy Oil/Water Relative Permeabilities in Horizontally and Vertically Drilled Core Plugs. *JPT* 37 (8): 1500-1510.
 26. Maini, B.B. and Okazawa, T. 1987. Effect of Temperature on Heavy Oil-Water Relative Permeability of Sand. *J Can Pet Technol* 26 (3): 33-41.
 27. Medina, A., Pineda, A., and Treviño, C. 2003. Imbibition Driven by a Temperature Gradient. *Journal of the Physical Society of Japan* 75 (2): 979-982.
 28. Miller, M.A. and Ramey Jr, H.J. 1985. Effect of Temperature on Oil/Water Relative Permeabilities of Unconsolidated and Consolidated Sands. *SPE J* 25 (6): 945-953.
 29. Mohammadzadeh, O., Rezaei, N., and Chatzis, I. 2002. Production Characteristics of the

- Steam-Assisted Gravity Drainage (SAGD) and Solvent-Aided SAGD (SA-SAGD) Processes Using a 2-D Macroscale Physical Model. *Energy & Fuels* 26: 4346-4365.
30. Odeh, A.S. 1959. Effect of Viscosity Ratio on Relative Permeability. *Petroleum Transactions AIME* 216: 346-353.
 31. Osoba, J.S., Richardson, J.G., and Blair, P.M. 1951. Laboratory Measurements of Relative Permeability. *Transactions AIME* 192: 47-56.
 32. Perry, R.H. and Green, D.W. 1984. *Perry's Chemical Engineers' Handbook*, sixth edition. New York: McGraw-Hill.
 33. Poston, S.W., Ysrael, S., Hossain, A.K.M.S., et al. 1970. The Effect of Temperature on Irreducible Water Saturation and Relative Permeability of Unconsolidated Sand. *SPE J* 10 (2): 171-180.
 34. Richardson, J.G. 1957. Calculation of Waterflooding Recovery from Steady State Relative Permeability Data. *J Pet Technol* 19 (5): 64-66.
 35. Ruth, D.W. and Bartley, J.T. 2002. A Perfect-Cross-Flow Model for Two phase Flow in Porous Media. In: *Proceedings of the 2002 International Symposium of the Society of Core Analysts*, Monterrey, California, SCA2002-05 (2002) 12.
 36. Sanchez, M. and Medina, A. 2005. Spontaneous Imbibition in a Porous Medium under Longitudinal Temperature Gradients. *Revista Mexicana de Física* 51 (4): 349-355.
 37. Sanchez, M., Sanchez, F., Pérez-Rosales, A., et al. 2004. Imbibition in a Hele-Shaw Cell Under a Temperature Gradient. *Physics Letters, Section A: General, Atomic and Solid State Physics* 324 (1): 14-21.
 38. Sandberg, C.R., Gournay, L.S., and Sippel, R.F. 1958. The effect of Fluid Flow Rate and Viscosity on Laboratory Determination of Oil/Water Relative Permeability. *Transactions AIME* 213: 36-43.
 39. Sasaki, K., Akibayashi, S., Yazawa, N., et al. 1999. Experimental Modeling of the SAGD process – Enhancing SAGD Performance with Periodic Stimulation of the Horizontal Producer. Paper SPE 56544 presented at the SPE Annual Technical Conference and Exhibition, Houston, TX, USA, 3-6 October.
 40. Satik, C. and Yortsos, Y. 1995. Pore-Network Studies of Steam Injection in Porous Media. Paper SPE 30751 presented at the SPE Annual Technical Conference & Exhibition, Dallas, TX, USA, 22-25 October.

41. Schneider, F.N. and Owens, W.W. 1970. Sandstone and Carbonate Two and Three Phase Relative Permeability Characteristics. SPE J. 10: 75-84.
42. Sola, S.B., Rashidi, F., and Babadagli, T. 2007. Temperature Effects on the Heavy Oil/Water Relative Permeabilities of Carbonate Rocks. J Petr Sci and Eng 59: 27-42.
43. Sufi, A.H. 1982. Temperature Effects on Oil-Water Relative Permeability for Unconsolidated Sands. PhD Thesis, Stanford University, Stanford, California.
44. Sufi, A.H., Ramey Jr, H.J., and Brigham, W.E. 1982. Temperature Effects on Relative Permeabilities of Oil-Water Systems. Paper SPE 11071 presented at the 57th Annual Technical Conference and Exhibition of Society of Petroleum Engineers, New Orleans, USA, 26-29 September.
45. Wang, J., Dong, M., and Asghari K. 2006. Effect of Oil Viscosity on Heavy Oil/Water Relative Permeability Curves. Paper SPE 99763 presented at the SPE/DOE Symposium in IOR, Tulsa, Oklahoma, USA, 22-26 April.
46. Watson, R.W. and Ertekin, T. 1988. The Effect of Steep Temperature Gradient on Relative Permeability Measurements. Paper SPE 17505 presented at the SPE Rocky Mountain Regional Meeting, Casper, WY, 11-13 May.
47. Welge, H.J. 1952. A Simplified Method for Computing Oil Recovery by Gas or Water Drive. Petroleum Transaction AIME 195: 91-98.
48. White, F.M. 2008. Fluid Mechanics, sixth edition. New York: McGraw-Hill.
49. Wilson, J.W. 1956. Determination of Relative Permeability Under Simulated Reservoir Conditions. AIChE J. 2 (1): 94-100. DOI: 10.1002/aic.690020120.
50. Yortsos, Y. 1999. Displacement Regimes in Fully-Developed Steam Injection. Paper SPE 54117 presented at the SPE International Thermal Operations and Heavy Oil Symposium, Bakersfield, CA, 17-March.
51. Youngs, E.G. 1960. The Drainage of Liquids from Porous Materials. Journal of Geophysical Research 65 (12): 4025-4030.
52. Yuster, S.T. 1951. Theoretical Considerations of Multiphase Flow in Idealized Capillary Systems. Proc: 3rd World Petroleum Congress, Section II, The Hague: 437-445.

Chapter 6 : Pore Scale Investigations on the Dynamics of Gravity Driven Steam Displacement Process for Heavy Oil Recovery and Development of Residual Oil Saturation: A 2-D Visual Analysis.

A version of this chapter was submitted to Colloids and Surface A: Physicochemical and Engineering Aspects

The dynamics of gravity driven injection process for heavy oil recovery at the pore scale and the mechanisms leading to the formation of residual oil saturation were investigated. 10 x 15 cm and 5 x 5 cm 2-D visual sand pack models (a single layer of sintered micro scale glass beads) were prepared and placed into a transparent vacuum chamber to prevent heat loss. The processes were recorded using a high speed camera to obtain visual data at the pore scale. This process represents the lateral spreading of steam chamber (half symmetric chamber growth) during steam assisted gravity drainage (SAGD) process for heavy-oil recovery.

Oil trapping mechanisms yielding to the formation of residual oil saturation were described and analyzed due to (1) lateral expansion, (2) simultaneous vertical and lateral expansion, (3) pore and particle size, (4) heterogeneities (pore and particle size distribution), and (5) wettability. Attention was also given to the ceiling region of the steam chamber and its interaction with the mobilized region at the lateral boundaries of the chamber.

6.1 Introduction

Due to the unavoidable depletion of conventional oil reservoirs and the growing demand of energy in the world, the exploitation of bitumen and heavy oil fields is crucial to meet future energy needs. Thermal and miscible methods are considered the best options to recovery bitumen and heavy oil. While miscible injection is not a commercial technology yet, thermal methods (mainly in the form of steam assisted gravity drainage, SAGD), have been widely applied to produce bitumen and heavy oil in Canada since late 1980s and recently in Venezuela.

Steam assisted gravity drainage (SAGD) process has been demonstrated to be an effective heavy oil and bitumen recovery method (Butler 1991, 1994a, 1994b). However, its efficiency has been questioned due to lower ultimate recoveries than expected (averaging around 50%), even under optimal geological and petrophysical conditions (Al-Bahlani and Babadagli, 2009). On the other hand, the dynamics of this displacement process still unclear due to the multiple parameters involved. Although analytical and numerical investigations partially supported by field data exist in literature, detailed experimental analyses of high residual oil saturations under gravity (SAGD) are limited.

Heavy-oil recovery by SAGD is achieved through injecting steam at a constant pressure in a upper horizontal well located close to the bottom zone of the reservoir and producing oil in another horizontal well placed below (5-10 meters) the injection well. This process develops through four subsequent stages (Mohammadzadeh and Chatzis, 2009): (1) Communication between injection and producing wells, (2) vertical growing of steam chamber, (3) lateral expansion of steam chamber, and (4) falling-down of steam chamber conducting to depletion.

Even though SAGD was conceived to recovery bitumen or heavy oil more efficiently than other thermal processes, there are still many challenges to solve at the micro and macro scale to make this method technically and economically viable (Al-Bahlani and Babadagli, 2009). It is possible to group the existing challenges of SAGD into five categories (Al-Bahlani and Babadagli, 2009): (1) Mechanics of SAGD, (2) reservoir properties, (3) SAGD operation, (4) numerical modeling, and (5) improvements. One of the critical issues that has received very little attention is the development of residual oil saturation (S_{or}). Al-Bahlani and Babadagli (2009) stressed that it is actually a problem that it is influenced by the mechanics, the reservoir properties and the operation of SAGD.

This paper investigates the dynamics of SAGD at pore scale leading to the formation of residual oil saturation (S_{or}). We begin with a detailed analysis of residual oil saturation concept and a review of earlier publications on the subject. Then, we introduce our experimental approach of visual trials on 2-D glass bead models. Drainage mechanism and trapping of oil are visualized and analyzed during the lateral expansion of the SAGD chamber. Also, the effects of pore and particle size, heterogeneities, and wettability on the development of S_{or} are clarified.

6.2 Background of Residual Oil Saturation Development in SAGD

Jimenez (2008) concluded from the analysis of SAGD field projects that reservoir properties and geology are by far the most dominant features for successful SAGD operation. The highest ultimate recovery at field scale have been around 60-70% OOIP, assuming that the above mentioned features are met. However, the average recovery factor lies between 30-40%. Later, Baker et al. (2010) analyzed two field scale SAGD trials using injection pressure, seismic, and temperature logs and concluded that oil recovery of thermal projects strongly depends on the displacement and volumetric sweep efficiencies. They also pointed out that heterogeneity and

fluid dynamics affect the steam chamber shape.

Volumetric sweep efficiency is a macroscopic parameter that depends on flooding pattern design, number of injection wells, heterogeneity, and continuity of the reservoir whereas displacement efficiency is a microscopic parameter that indicates the interplay of gravity, capillary, and viscous forces. The role of capillary forces is the most difficult to analyze since it comprises wettability and interfacial tensions, particle and pore size distribution, microscopic heterogeneities, and pore structure issues.

Although global macroscopic behavior in porous media is the result of microscopic transport mechanisms, experimental and theoretical works of the mechanics of SAGD at pore scale are scarce. Argüelles-Vivas and Babadagli (2014) pointed out that, up to date, it is not well understood how and to what extent phenomena at pore scale such as counter- and co-current flow, trapping of phases, pore structure, phase distribution due to wettability, flow of emulsion, organic precipitation, and heat transfer mechanisms play a role on the SAGD performance, more specifically the development of residual oil saturation (S_{or}). This is a crucial issue especially in accurate description of relative permeability curves to predict the performance of field scale SAGD. **Figure 6-1** schematically displays the SAGD concept.

In the original conception of SAGD it was assumed that the oil is swept through chamber growth, immediately reaching the stage of residual oil (Butler, 1991). During such a process average residual oil saturation can be initially estimated for air – liquid free fall gravity drainage using the following equation (Cardwell and Parsons, 1949):

$$\bar{S}_{or} = \frac{(b-1)}{b} \left(\frac{v_s \phi Y}{bkgt} \right)^{1/(b-1)} \quad (1)$$

Where \bar{S}_{or} is the average residual oil saturation after time, t , Z is the drainage height, k is the absolute permeability, b is an exponent for relative permeability (typically 3.5 as determined empirically for unconsolidated sands) and v_s is the kinematic viscosity of the oil at the steam temperature. Eq. 1 is limited in incorporating the complex nature of the evolution of the residual oil saturation during SAGD due to its highly empirical nature.

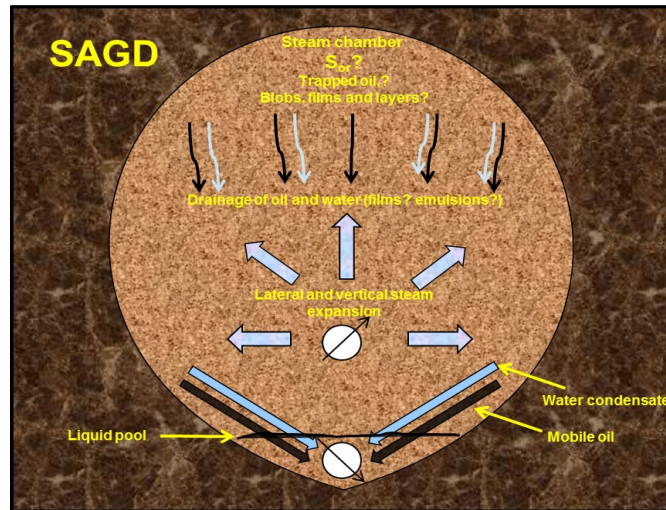


Figure 6-1: Theorized SAGD concept.

Studies on S_{or} development during SAGD are very limited and are mainly defined at the macro-scale. Pooladi-Darvish and Mattar (2002) pointed out that high residual oil saturation can be formed if steam pressure is high due to less latent head (more heat will leave the reservoir with the produced fluid). Walls et al. (2003) carried out a sensitivity study on the shapes and end points of relative permeability curves and then adjusted oil-gas relative permeability curves using a theoretical S_{or} determined by Eq. (1).

In a pioneering study, Mohammadzadeh and Chatzis (2009, 2010) studied the SAGD process at the pore scale. Using glass micromodels, they analyzed the development of S_{or} at the micro scale and stated that there are three fluid regions in a SAGD process at the pore scale: (a) Steam chamber, where the dominant existing phase is the steam, (b) bitumen filled pores, the inactive region where the bitumen is stagnant due to its high viscosity, and (c) mobilized region, where mobile oil, steam and water are flowing simultaneously. They also observed that there are two drainage mechanisms responsible for oil mobilization: (1) capillary drainage displacement and (2) flow of films. The capillary drainage displacement consists of the direct displacement of a small amount of mobile oil (covering 1-5 pores) in the mobilized zone by the steam phase, with the aid of the gravity in the presence of negligible viscous forces. A water slug can be formed due to the periodic steam condensation which in turn is displaced by the steam, improving the mixing of water and oil in the pores. In the case of film-flow mechanism, the high level of

mixing in the mobile zone does not permit an extended hydraulic continuity of the films, causing a detriment on the contribution to the total drainage of oil.

Mohammadzadeh and Chatzis (2009, 2010) also observed the emulsification phenomenon at the interface caused by local steam condensation. Due to the non-spreading characteristics of water on oil (negative spreading coefficient), very fine water droplets are engulfed within the bulk oil at the interface resulting in water-in-oil emulsification. In several earlier experimental studies, similar emulsification process during oil recovery was observed for SAGD (Chung and Butler, 1987; Sasaki et al., 2002), and steamflooding (Kong et al., 1992).

In reference to S_{or} , Mohammadzadeh and Chatzis (2012) observed through homogeneous micromodels that the residual oil exists as thin pendular rings covering some of the solid grains and as tiny spots that are trapped within the rough sites of the glass beads. The recovery factor of their models depended mainly on permeability and ranged between 33% (34.13 D) and 80% (94.61 D). They also observed lower S_{or} at higher temperatures.

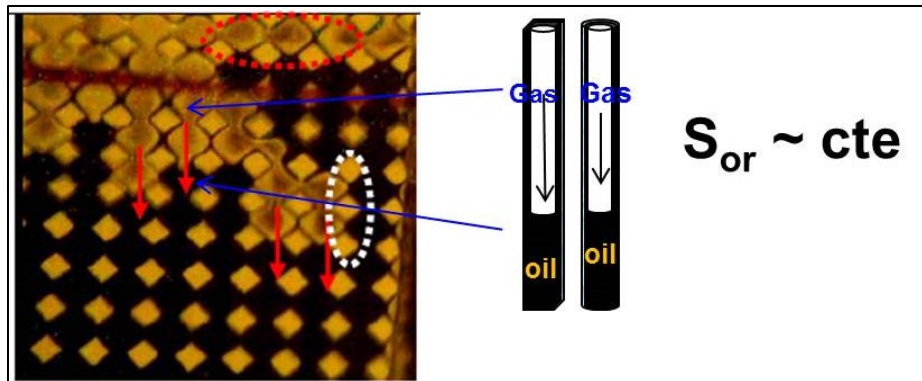


Figure 6-2: Relationship of S_{or} in capillaries with SAGD (Figure in left side taken from Mohammadzadeh and Chatzis, 2009; 2010; 2012).

Argüelles-Vivas and Babadagli (2014, 2015) analyzed the development of S_{or} in cylindrical and square capillaries formed as films and layers during forced and free fall 2-and 3-phase gravity drainage displacement of heavy oil at different temperatures. For higher trapping numbers (N_T), S_{or} changed with temperature due to the interplay among viscous, capillary and gravity forces. They also observed that, for free fall gravity drainage experiments, S_{or} increases with the augmentation of the Bond number in the form of films and layers.

As mentioned above, Mohammadzadeh and Chatzis (2009, 2010) observed that mobile oil is

displaced directly by steam or through a double displacement where the oil is displaced by a water slug (originated from condensation). Argüelles-Vivas and Babadagli (2014, 2015) observed and analyzed these types of distributions and displacements in capillaries. **Figure 6-2** shows the similarities between the capillaries and porous medium in terms of S_{or} development during the capillary drainage mechanism described by Mohammadzadeh and Chatzis (2009). The engulfment process of water in oil to form an emulsion on a surface (left side) and in porous media (right side) is shown in **Figure 6-3**.

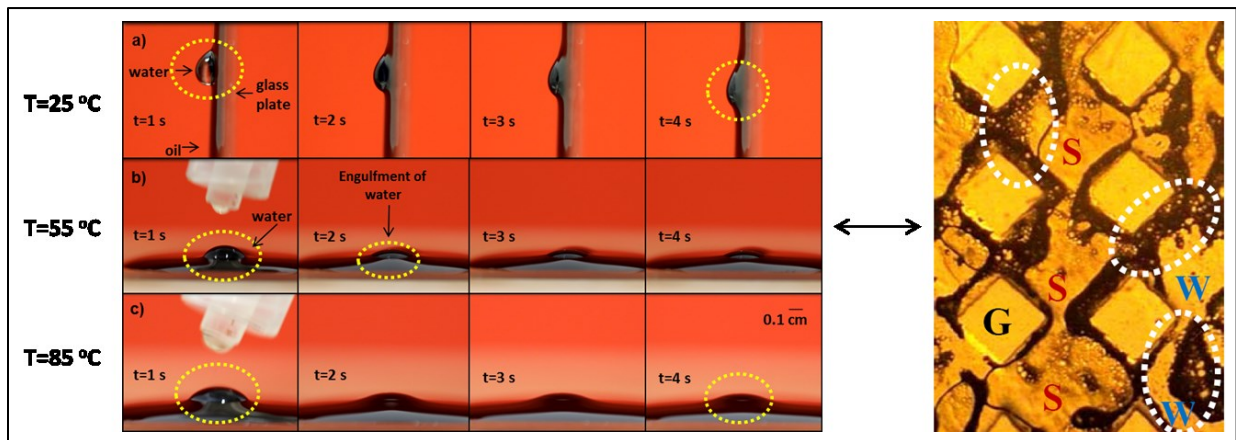


Figure 6-3: Emulsion formation observed by Arguelles and Babadagli (2015, Figure in left side) and Mohammadzadeh and Chatzis (2009, Figure in right side,) at different scales.

6.3 Experimental Work

2-D visual glass bead models were used to study the (a) development of S_{or} at pore scale during SAGD, (b) simultaneous expansion of SAGD chamber (half symmetric steam chamber) vertically and laterally, and (c) effect of pore/particle size, heterogeneities and wettability on the dynamics of SAGD and development of S_{or} .

6.3.1 Models and materials

The glass beads ranging between 3 mm to 0.2 mm diameter were packed between two 9 mm thick plexi-glass plates. The experiments were carried out with two different visual models of 10 x 15 cm and 5 x 5 cm. This latter was used to study effect of pore size, heterogeneities (pore and particle size distribution), and wettability. **Figure 6-4** shows the former (10 x 15 cm) model.

One port at the top and three ports at the bottom of the model were placed to create different injection/production schemes. The porosity of the model varied between 35% and 40%. The permeability estimated through the Kozeny-Carman equation was ~ 7200 D for 3 mm, 3200 D for 2 mm, 803 D for 1 mm, and 32 D for 0.2 mm. To study the wettability effect, more oil-wet Teflon beads were used.

The oil used was naturally transparent but dyed with a compatible colorant. The viscosity of the oil was 113,000 cP at 20 °C, which was viscous enough to be immobile at our lab conditions. This value is compatible with the heavy-oil encountered in many fields under SAGD in Alberta. **Figure 6-5** shows the viscosity behavior with respect to temperature.

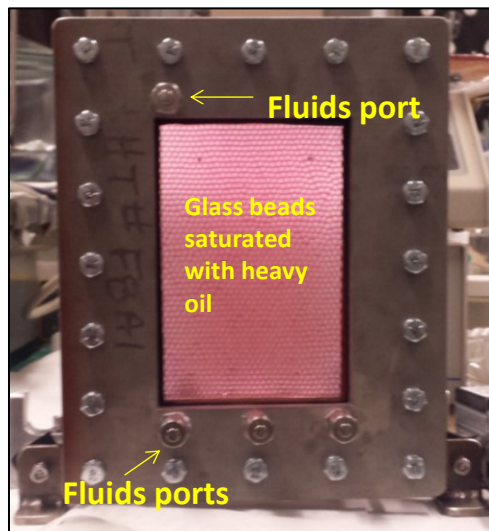


Figure 6-4: Framework and glass beads model to carry out the steam injection experiments.

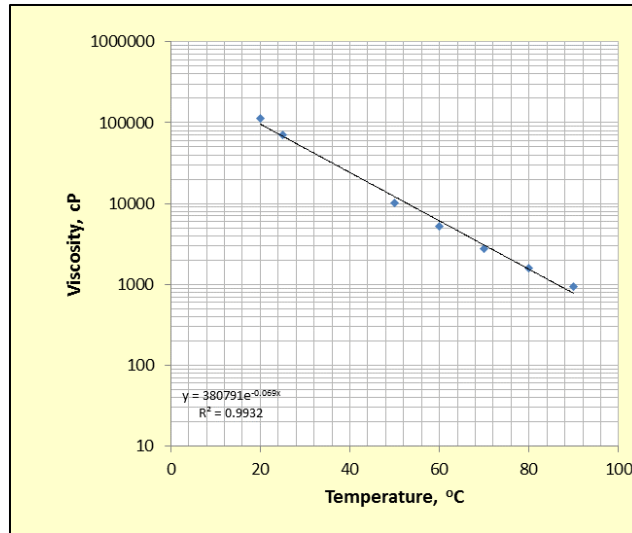


Figure 6-5: Heavy oil viscosity behavior with temperature.

6.3.2 Setup

The experimental system is shown in **Figure 6-6** and consists of (a) an oven with stainless containers, (b) steam lines, (c) temperature controller, (d) inlet valve and manometer (e) a vacuum chamber, (f) the glass beads model, (g) a production port, (h) data acquisition system, and (i) a camera to record pore scale events.

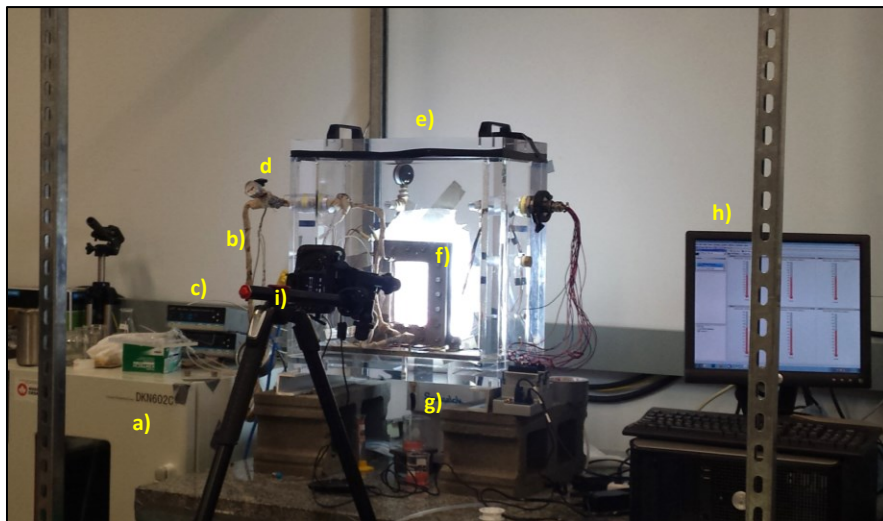


Figure 6-6: Experimental system a) oven with container, b) steam lines, c) temperature controller, d) inlet valve and manometer, e) a vacuum chamber, f) glass beads model, g) production port, h) data acquisition system, and i) a camera to record pore scale events.

6.3.3 Procedure

Steam generated in a steel container located inside an oven at 110°C-130 °C was transferred to insulated and heated tubing at 130 °C to supply superheated steam and to avoid condensation along the pipe. Steam generation and experiments were carried out at atmospheric conditions. To minimize excessive heat losses by convection from the model to the surroundings, the experiments were conducted in a vacuum chamber as suggested and applied by Mohammadzadeh and Chatzis (2009).

Different combinations of injection/production ports were used depending on the application type. For example, to study the lateral expansion of chamber, steam was injected from the upper port of the model while it was vertically situated as seen in **Figure 6-4**. A “fracture like” channel was created between the injection and production points to facilitate the communication between these ports. The produced fluids were collected through the valve located below and outside of the vacuum chamber.

To mimic half of a steam chamber, the model shown in **Figure 6-4** was positioned horizontally (turning it to right 90°). Steam was injected in the middle port located at the left side of the model and all the fluids were produced from the lower most one the three ports. Details are given in the results and discussions section.

6.4 Results and discussion

6.4.1 Dynamics of S_{or} and trapping mechanisms during the lateral expansion of steam chamber

The progress of the **lateral** growth of the SAGD chamber and the formation of S_{or} is shown in **Figure 6-7**. Three distinct regions can be identified as similar to Mohammadzadeh and Chatzis’ (2009) observations: a) Steam chamber (steam is the dominant phase) with condensate and residual oil, b) bitumen-filled zone (oil is stagnant and cold), and c) mobilized zone (steam, condensate, and oil flow together). These regions are pointed in **Figure 6-7d**.

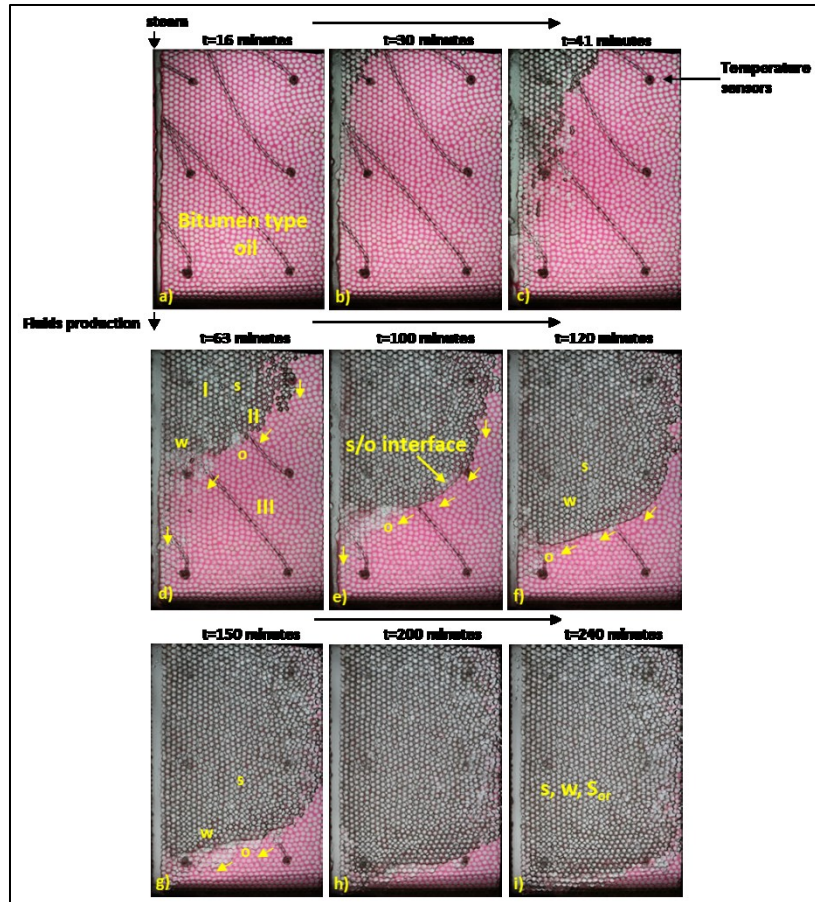


Figure 6-7: Steam chamber lateral growth (s: steam, w: water, o: oil).

Steam injected from top of the model flows through the channel towards the production end and starts heating the oil. During this process, the viscosity of oil is reduced and a steam (or heat) chamber develops as similar to the SAGD chamber. Then, oil is drained from the upper pores of the model under gravity. Oil drainage started twenty minutes after the beginning of the experiment. **Figure 6-8** displays the temperature profiles during the lateral expansion experiment shown in **Figure 6-7**. The figure on the left in **Figure 6-7** shows the location of the thermocouples. In four thermocouples (T1, T2, T4 and T5) the temperature reached 100°C eventually during the experiments whereas the ones at the bottom of the model (T3 and T6), the temperature was less than 100°C.

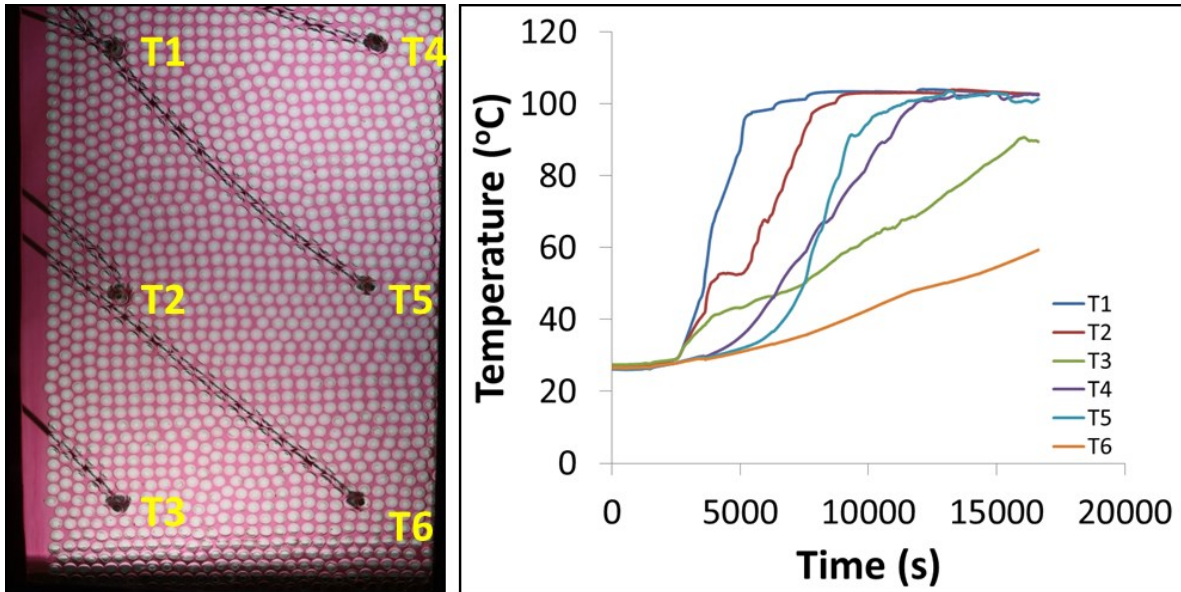


Figure 6-8: Temperature profiles during the lateral expansion of the steam chamber experiment.

As seen in **Figure 6-9**, steam and drops of water condensate enter into the channel (pointed by a dashed yellow circle). At the very early stage of chamber growth, steam invaded porous medium only in a horizontal manner (while oil was flowing in the gravity direction).

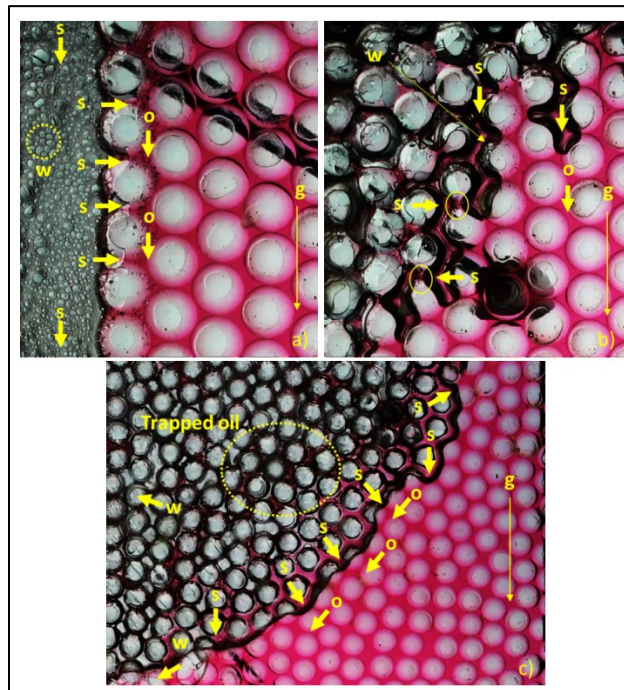


Figure 6-9: Dynamics at pore scale during the lateral expansion of SAGD (s: steam, w: water, o: oil).

Water-in-oil emulsification process can also be seen in **Figure 6-9a**. Once steam contacted oil, it condensed forming drops of water near the interface due to the heat transfer. These drops were

immediately engulfed by oil to form an emulsion (right of the first column of beads in **Figure 6-9a**), where the oil mixed with the foggy-looking droplets. That is to say, the negative spreading coefficient of water on oil in the presence of a vapor phase (or a gas) caused emulsification. Negative spreading coefficient also implies that a liquid does not spread spontaneously between the gas-liquid interface and remains as bulk lenses (Adamson and Gast, 1997). This non-spreading behavior of water on oil can be explained through the surface/interfacial tension. Steam-water surface tension is much higher than steam-oil surface tension and water-oil interfacial tension. Then, it is expected that water tends to be away from gas and, due to the existence of compounds with a hydrophilic part in oil, water-oil emulsion develops.

As seen in **Figure 6-9b**, as steam penetrated into the pores in the top portion of the model, the free fall gravity drainage process started. One may also observe through the same image that, as steam invaded vertically, it also moved horizontally assisting the gravity on the thinning of the oil which connects two adjacent beads (see solid yellow circles). Formation of water droplets near the steam-oil interface (indicated by dash yellow arrow) is also obvious.

As the chamber grows, the movement of steam/condensate at the interface with heavy oil (in the mobilized zone) becomes more complex since the local interface in the pores, besides moving horizontally and vertically, can also advance with an inclined angle with respect to the gravity force (**Figure 6-9c**). One may also infer from the same figure that, while oil and water flow towards the production port through the channel and the chamber grows, trapped oil exists inside the steam chamber (circled areas) in the form of ganglia.

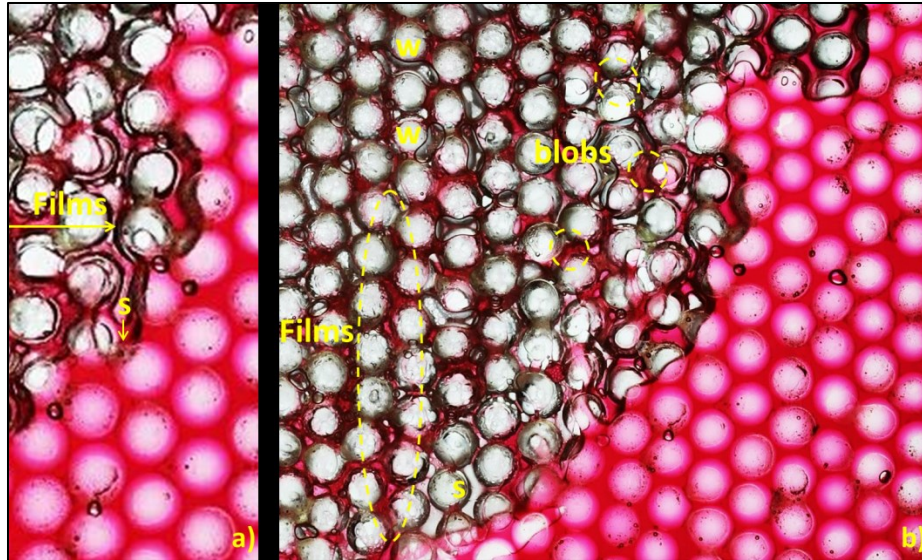


Figure 6-10: (a) Direct steam displacement and flow of film; (b) existence of films, water (w), trapped blobs and steam (s) within steam chamber (s: steam, w: water).

Based on these observations through the visual data provided so far, one may state that S_{or} and the growth of steam chamber are consequences of these local combined movements of the steam/condensate-oil interface within the pores. Once oil gets mobile after being heated, it is drained by gravity along a short series of pores and throats through direct displacement with steam (**Figure 6-9b** and **Figure 6-10a**) or condensate and by the simultaneous flow of films (**Figure 6-10**), whose hydraulic continuity depends on the existence of blobs between adjacent grains (**Figure 6-10**). This is called capillary drainage and film-flow type drainage mechanisms (Mohammadzadeh and Chatzis, 2009).

During the process described above, i.e., once the drainage has been activated, the S_{or} is formed through two mechanisms: (1) breaking or snap-off of the oil blobs between glass beads (grains), which leads to the formation of trapped films of short length within the chamber, and (2) bypassing the oil contained in the cluster of smaller throats and pores due to the preferential flow of the non-wetting steam through bigger space.

In **Figure 6-10b**, one may observe films of oil with a limited extension toward the mobilized zone (yellow dashed ellipse), insulated drops of water, steam and trapped oil in the form of blobs. **Figure 6-11** shows a close-up of different shapes of the residual oil (orange color between the beads) at the end of the experiment. The remaining oil as well as produced oil during the experiment contacted by steam/condensate was found in emulsified form. The yellow dashed

ellipse on the left side of **Figure 6-11a** shows the residual oil as a short film connected by blobs between the beads. The yellow dashed ellipse in **Figure 6-11b** shows the trapped oil in the form of an island bypassed by the steam. Next to the island some oil blobs between the beads can be observed.

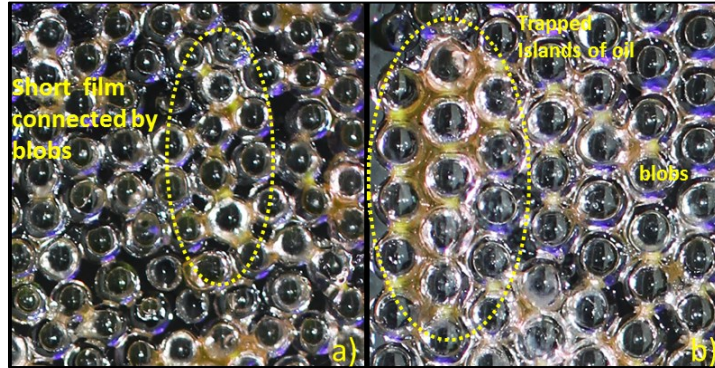


Figure 6-11: Shapes of residual oil: (a) films connected by blobs, (b) islands of oil and blobs.

6.4.2 Dynamics of S_{or} and trapping mechanisms during half symmetric SAGD chamber growth

A new injection scheme was designed to reproduce half of a steam chamber and to analyze the simultaneous vertical and lateral growth of the steam chamber. The model shown in **Figure 6-4** was placed in horizontal position so that the bottom ports were on the left side. The images acquired through the experiment are shown in **Figure 6-12**. Steam was injected in the middle port at 130 °C and fluids were produced at the bottom port (**Figure 6-12a**). A vertical channel between the injector and producer port accelerated the communication between them as similar to the previous experiment given in **Figure 6-7**. Similar to the lateral expansion experiments, the production valve was opened intermittently and a column of produced oil and condensate were retained in the production tubing to minimize steam channeling.

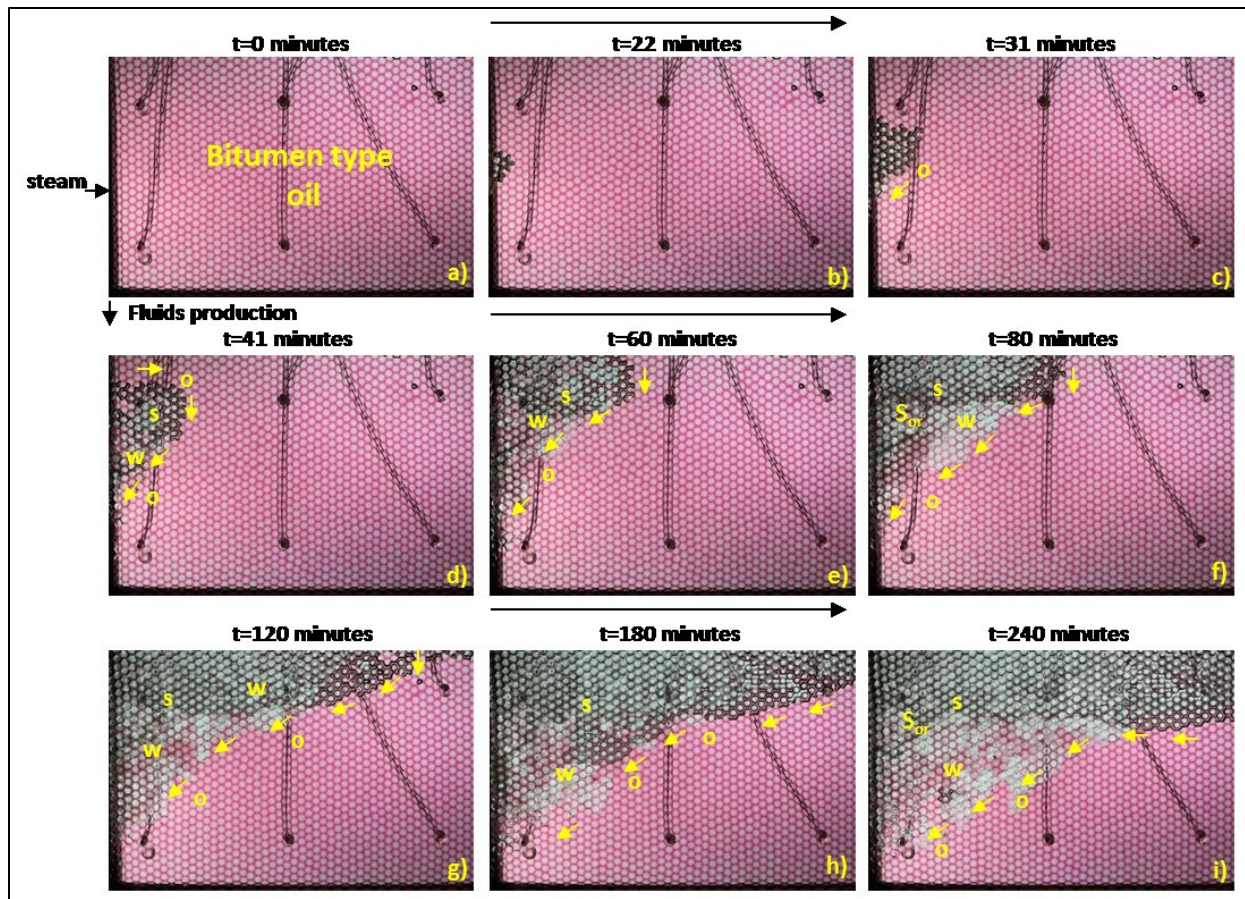


Figure 6-12: Half symmetric SAGD chamber growth (s: steam, w: water, o: oil).

The birth of the SAGD chamber was observed twenty minutes after the experiment was started (**Figure 6-12**). At the scale given in **Figure 6-12**, we observe that the steam chamber grew as an inverted pear with an almost flat bottom (ceiling part). This can be seen best in **Figure 6-12d** through **Figure 6-12f**. This chamber shape is mainly controlled by the permeability of the model, which was isotropic and viscous forces due to steam injection was minimally low (the purpose was to create a pure steam assisted gravity drainage process). Note that if pressurized steam had been injected, the ceiling part would have had a more downwardly concave shape with noticeable fingers as observed by Sasaki et al. (2001).

It is interesting to note that the region of the lateral expansion connecting with the ceiling part kept a vertical interface (while steam/condensate move horizontally) with an approximate constant length during almost all the growth. This is clearly observed in **Figure 6-12c** through **Figure 6-12g**. Once the steam chamber has reached the right side (boundary) of the model, steam/water-oil interface moved downward and laterally (**Figure 6-12h** and **Figure 6-12i**). It is

also noticeable that almost half of the interface became flatter (the right side) while the other half kept a pronounced inclination (**Figure 6-12h**). At the end of this experiment (**Figure 6-12i**), one third of the interface was horizontal and flat and the rest kept an inclination toward the production port. In **Figure 6-12d–Figure 6-12i**, the formation of the emulsified residual oil saturation within the steam chamber can be observed.

The growth of the chamber was very regular and homogeneous during the whole process. However, more observations can be made at a smaller (pore) scale. In **Figure 6-13**, the birth of the steam chamber is shown. It was observed that the steam expanded locally in all directions condensing and forming water-in-oil emulsions (w-o).

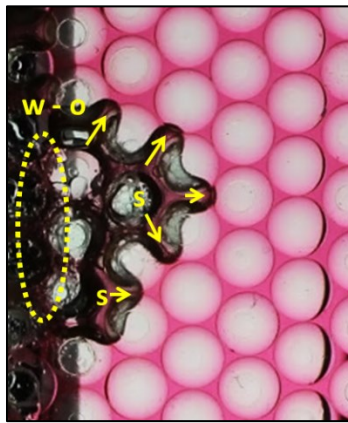


Figure 6-13: The birth of the steam chamber (s: steam, w-o: water in oil emulsion).

After the birth, the spreading of the steam chamber was not very regular (**Figure 6-14**) and the movement of steam was in all direction. Steam invaded first the bigger throats obeying the classical rules of drainage of a wetting phase displaced by a non-wetting phase. Water was also observed within the chamber and flowing to the production port. In the mobile zone, there is emulsified oil (w-o) since little drops of water are engulfed in oil.

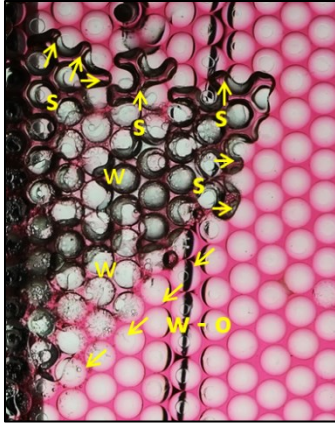


Figure 6-14: Early spreading of the steam chamber showing irregular interface at pore scale (s: steam, w: water, w-o: water in oil emulsion).

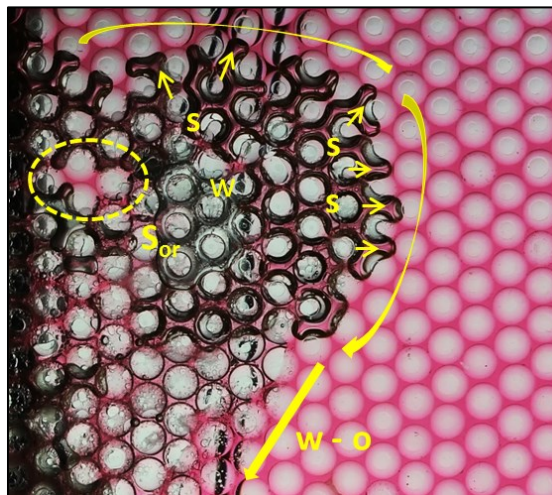


Figure 6-15: Residual oil saturation formation during the upward and outward growing of the steam chamber (s: steam, w: water, w-o: water in oil emulsion).

The steam chamber kept growing vertically and laterally (**Figure 6-15**) and oil was trapped in the steam chamber due to differences in the throat and pore size (dashed yellow circle in **Figure 6-15**). As the process continued, this oil could drain later through connection with adjacent films or be displaced directly by steam and only some portion could be trapped as thin films on the beads or as blobs.

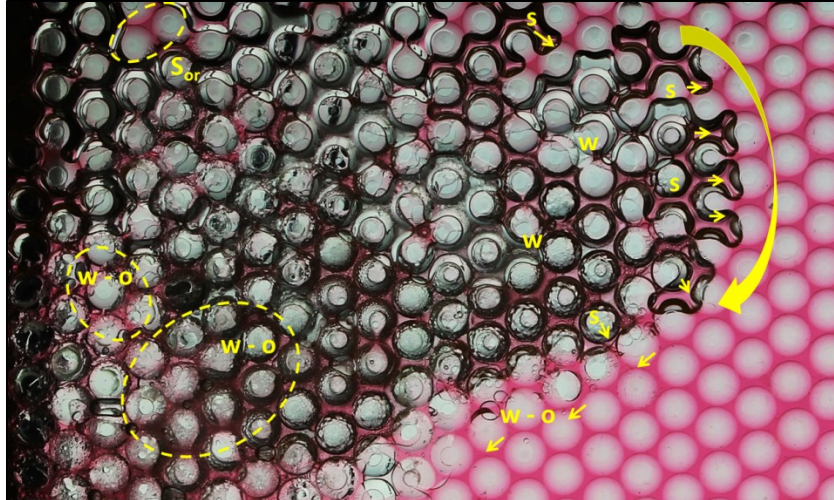


Figure 6-16: Residual oil saturation formation during the expansion of the steam chamber (s: steam, w: water, w-o: water in oil emulsion).

Once that the steam reached the top of the model, the expansion occurred laterally (**Figure 6-16**). Steam displaced the oil directly in a horizontal manner. The interface of water/steam-heavy oil also moved with an inclined angle toward the production port. However, the downward movement of this region of the interface was slower since it was fed by the oil draining from the lateral expansion of the upper part (thick yellow arrow in **Figure 6-16**). Some residual oil was observed at the top of the model due to overpassing through bigger throats and due to the snap-off of the blobs between the glass beads. Close to the injection port, the heavy oil was much emulsified (w-o).

Besides the three distinct fluid regions identified in the lateral expansion experiments, one more flow zone exists during the growth of the steam chamber and before reaching the top of the model (the ceiling part). In this region, the upward steam, aiding the gravity, “displaces” the mobilized oil sideways to feed the lateral boundaries of the steam chamber. The steam, once condensed, is engulfed as tiny droplets of water in the salient mobile oil and it is not observed the formation of a continuous phase of water flowing sideways next to the oil (**Figure 6-15**). Therefore, the only pore scale drainage mechanism in this part of the chamber occurred through direct displacement with steam.

In conjunction with these observations, Butler (1994b) noticed that oil flows preferentially on the chamber sideways instead of into it. He hypothesized that the reasons for this are the low S_{or} in the chamber and the support that the water condensate between steam and oil, the water

imbibition and the interfacial tension exert on oil to drain laterally. Then, Al-Bahlani and Babadagli (2009) discussed whether or not counter-current movement also happens within a pore and whether or not oil drains down through the sides closer to the grain due to wettability and connate water issues. This requires further discussion on the dynamics of the process questioning the counter-current nature of the displacement.

In the ceiling part of the chamber, we did not observe counter-current flow of oil into the steam chamber within the same pore (steam moving up while oil is drained downward in a single pore). On the basis of our visual experiments, we affirm that the reason for not having this type of counter-current flow is the loss of capillary continuity of the oil along the pores (hydraulic continuity of oil phase) within steam chamber due to the snap-off of the oil blobs between grains and the bypass of islands of oil. The hydraulic continuity would enable oil to have an area to flow down while the steam goes up in the center of the pore. In the opposite case, the steam occupies all the area and drives the flow upward. Consequently, we can state that if the steam goes up and there is upward movement of the chamber is not mainly due to the rising nature of the steam but rather due to the hydraulic connectivity of the mobile oil with the lateral boundaries of the chamber through the upper edges that extends to the region of the production well.

In **Figure 6-17** shows the sequence of the flow of mobilized oil and the invasion of steam(s) replacing it in a local region of the ceiling part. In **Figure 6-17a**, the oil lost part of its capillary continuity with the beads inside of the steam chamber (yellow dashed ellipse). The blue arrows represent the direction and flow of oil and the yellow arrows indicate the invasion and direction of steam. We also observe how oil phase lost its continuity between two grains while it was flowing up and then sideways towards the lateral boundaries (yellow dashed circles in **Figure 6-17b** and **Figure 6-17c**). As steam kept invading the pores, the oil covering two different grains also lost the hydraulic continuity due to the thinning oil blob between them (the yellow dashed circle with the yellow arrow inside in **Figure 6-17d-Figure 6-17f**). Oil continued flowing in the ceiling part toward the lateral boundaries to drain down while steam was replacing it.

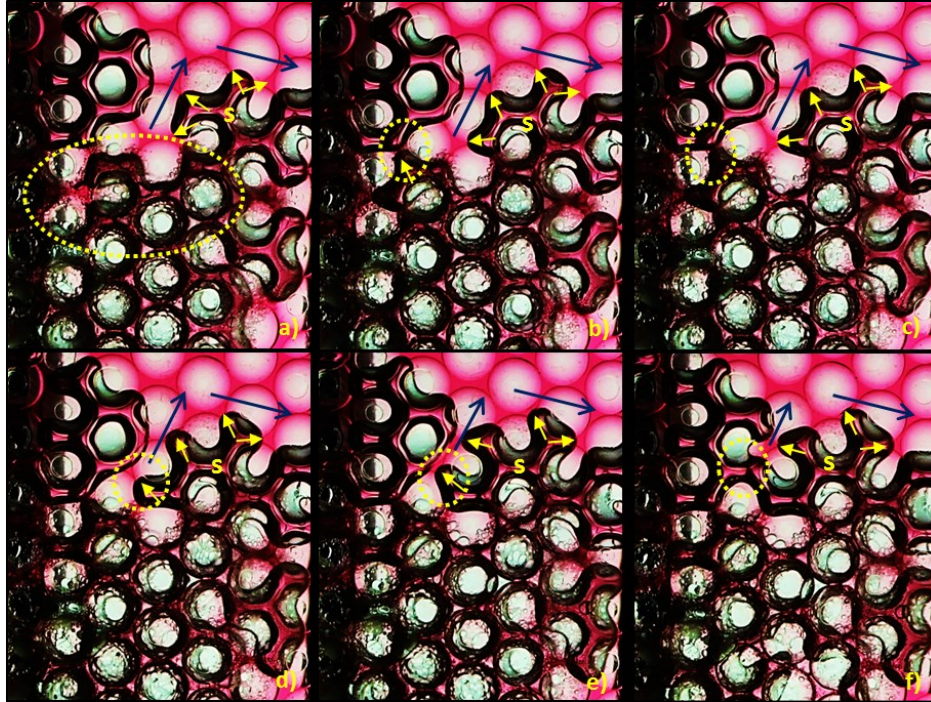


Figure 6-17: Sequence of capillary (hydraulic) continuity lost in the ceiling part of the steam chamber (s: steam).

To further clarify the concept of hydraulic continuity, another experiment was performed using capillary tubes. In **Figure 6-18**, the capillary is shown where there was no counter-current flow. Initially, an oil slug was placed in one of the ends of the tube (**Figure 6-18a**) and this end was sealed and a capful was formed with resistant glue. Below the oil slug, the wall of the capillary tube was completely dried without any thin layer of oil. The bottom end was connected to a syringe to inject air. Air was injected from the bottom at different pressures (**Figure 6-18b**). The highest possible pressure was applied manually to move the oil, expecting that this would flow down. However, the flow direction of air and oil was upward (indicated by the blue and yellow arrows in **Figure 6-18b**). Finally, due to the excessive hand pressure, the seal at the top was broken and the oil and air escaped (**Figure 6-18c**). The reason of this phenomenon is that the air occupied all the flow area at the interface and drove the flow upward as there was no film or layer connected to the upper oil slug in order for a counter-current (downward) flow of oil takes place.

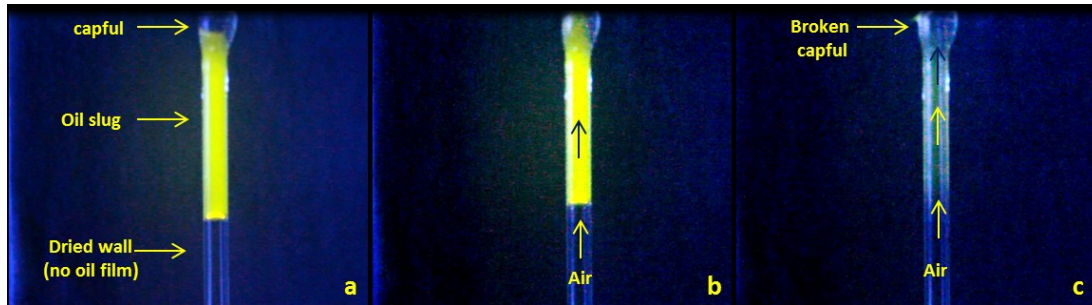


Figure 6-18: Capillary tube experiment where there is not hydraulic continuity and thus there is not counter-current flow.

The opposite situation is shown in the experiment of **Figure 6-19**. In this case, an oil slug was placed inside the capillary tube and was displaced along all the length of the capillary to lubricate the wall of the tube and create a layer of oil. Then, the oil slug was placed again at the initial end, which was sealed with resistant glue. The oil slug was set upside down as shown in **Figure 6-19a**. Unlike the previous experiment, fluids moved by free fall gravity drainage. It can be seen in **Figure 6-19b** that the length of the oil slug decreased due to the flow of oil downward through the falling oil layer while the air was flowing upward through the center of the capillary. In this case, oil flowed in a counter-current manner. The explanation for this phenomenon is the existence of hydraulic continuity between the oil slug and the falling films of oil, which occupy some area inside the capillary tube and let the upper oil to flow down.

In **Figure 6-19c–Figure 6-19e** the evolution of the counter-current flow is shown. One may observe the appearance of an oil slug at the bottom of the capillary due to the accumulation of oil coming from the falling layers (**Figure 6-19d–Figure 6-19e**). Finally, as shown in **Figure 6-19f**, there is no oil slug at the top of the capillary since all the oil flowed down through the connected falling films. A big oil slug with almost the length of the initial oil slug was observed. The rest of oil was in the form of layers.

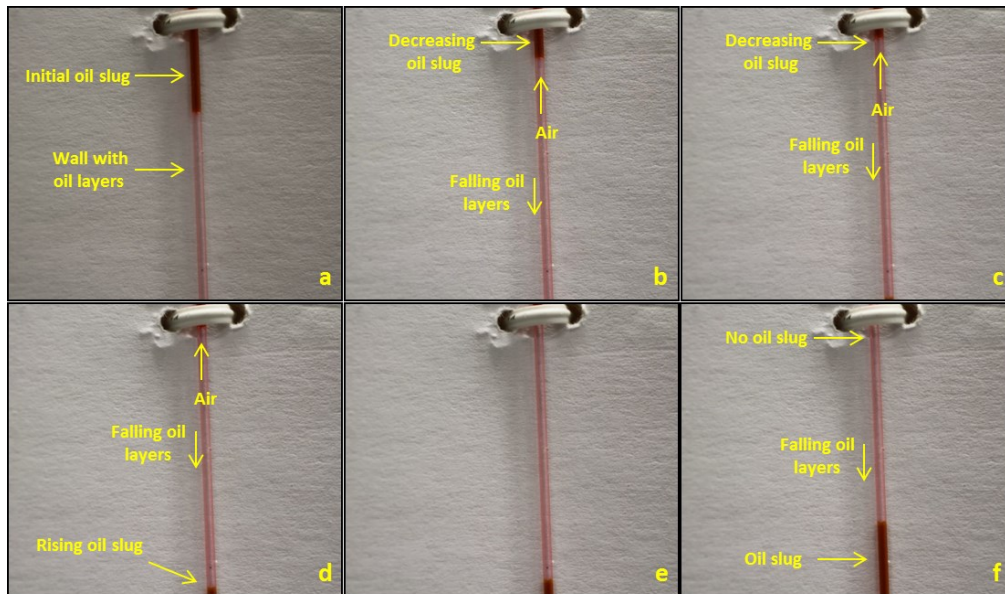


Figure 6-19: Capillary tube experiment where hydraulic continuity exists and there is counter-current flow.

In specific regions inside the steam chamber, especially close to the lateral expansion, counter-current flow could occur once the film of short length had been formed and started flowing toward the mobilized region to contribute to the production (as also shown in section 6.4.1 for lateral expansion). However, since the steam moves through the pores in all directions depending on the aspect ratio of the pore and throats (in a sense, we could say steam moves in a chaotic way in the pores), it is difficult to predict the length of the films and the time it could flow before breaking off.

Counter-current flow is also understood as the flow of steam upward in the entire chamber (macro scale) with respect to the downward flow of oil and water at the mobilized regions (chamber edge). In this case, each fluid flows through its own pore network without interacting each other. The exception occurs in a series of developed short films near the steam chamber, as explained before. We did not observe a clear counter-current flow at the lateral edges of the steam chambers since a horizontal displacement occurred first.

6.4.3 Shape of the steam chamber

Further speculations can be made with respect to the shape of the chamber before reaching the top of the reservoir from our visual experiments. As mentioned, due to the isotropic permeability and the absence of significant viscous forces, the shape of the chamber in our experiment was

that of an inverted pear with an almost flat bottom. If the viscous forces exist, the ceiling part could acquire a dome shape. It would be expected that (in the case of higher vertical permeability than the horizontal one) the chamber would grow upward, with the lateral boundaries expanding slower due to the smaller permeability and to the oil flowing from the ceiling part. The shape in this case would be an inverted and elongated “water droplet” (or teardrop).

On the contrary, if the vertical permeability was lower than the horizontal one, the chamber would grow outwards, with the lateral boundaries expanding faster than the ceiling part. The oil production would be from the lateral sides mainly and the ceiling part would have a long horizontal length. The shape in this case would be a “flat-bottomed teardrop.”

6.4.4 Effects on porous medium characteristics on S_{or}

In this section, the influence of permeability, wettability, and pores scale heterogeneity S_{or} development during the lateral expansion of SAGD was analyzed and visualized. The size of the model in these experiments was 5 x 5 cm. Steam was injected at 130 °C at atmospheric pressure and the procedure is as described in section 6.3.3.

6.4.4.1 Effects on permeability on S_{or}

Two homogeneous models with glass beads of 3 and 1 mm were used to study the effects of permeability on S_{or} developed during the lateral expansion of SAGD. The same pore geometry as in the previous experiments was kept. **Figure 6-20** illustrates the S_{or} for the 3 mm glass beads model at the end of the experiment (after two hours of steam injection). S_{or} after two and seven hr of steam injection is shown in **Figure 6-20b1** and **Figure 6-20b2** for 1 mm glass beads model, respectively. In these three images, one may observe residual oil (reddish areas) and water inside of the chamber.

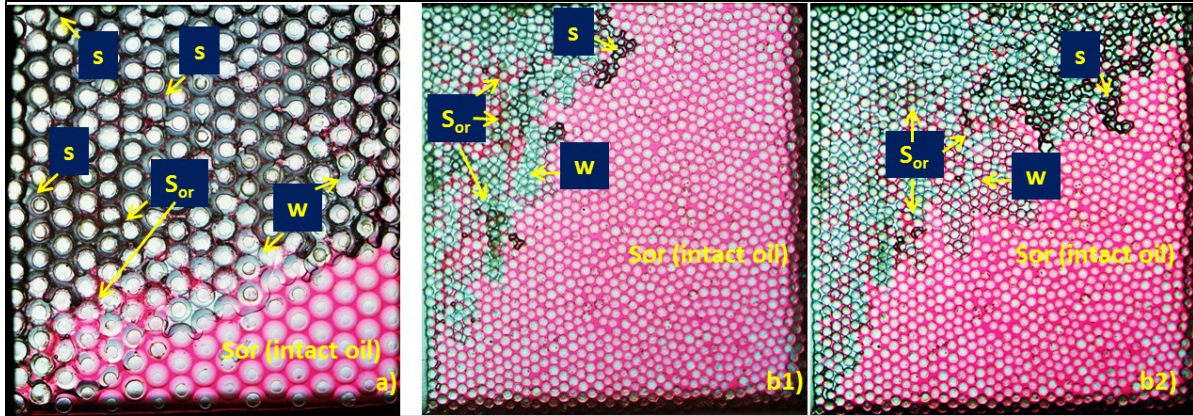


Figure 6-20: Permeability effects on S_{or} during lateral expansion of steam chamber: (a) 3 mm model (2 hours), (b1) 1 mm model (2 hours) and (b2) 1 mm model (7 hours). (s: steam, w: water, o: oil).

These experiments show the effect of permeability on the dynamics of the process and the development of residual oil saturation. The main difference between these two models was the amount of intact residual oil that had not been swept. In 2 hours, the model of 3 mm glass beads was almost depleted (**Figure 6-20a**) whereas the area swept in the model of 1 mm glass beads was much smaller for the same time period (**Figure 6-20b1**).

A close up image of **Figure 6-20** is shown in **Figure 6-21**. For the model of 3 mm glass beads, more S_{or} in the form of blobs between the beads was found in the steam chamber region (dashed yellow circles and ellipse in **Figure 6-21a1** and **Figure 6-21a2**). In **Figure 6-21a2**, the S_{or} is clearly seen in the emulsified state.

In the case of 1 mm glass beads model, the S_{or} at the end of the experiment (7 hours) was also found as islands of trapped oil within the steam chamber (dashed yellow circles of **Figure 6-21b1** and **Figure 6-21b2**). The solid yellow circle of **Figure 6-21b1** shows that the S_{or} existed also as single oil blobs. The formation of S_{or} as a cluster of oil in the 1 mm model is due to the presence of stronger capillary forces compared to the 3 mm model glass beads and unfavorable pore throat aspect ratios at the boundaries of such clusters.

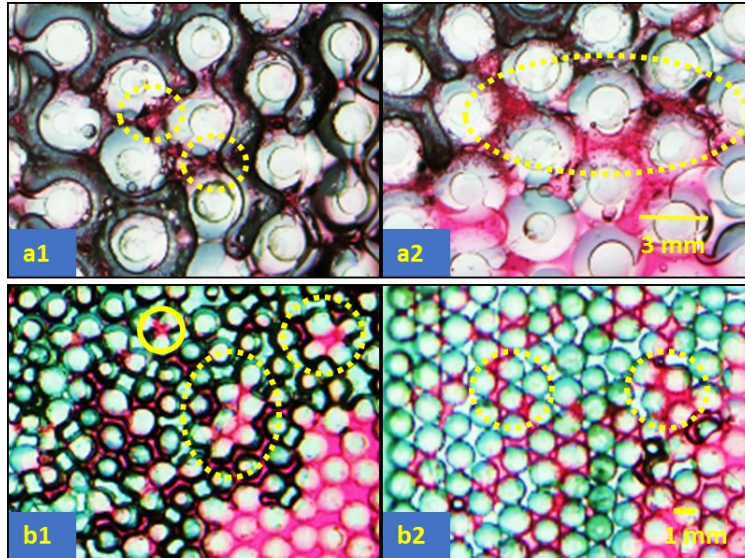


Figure 6-21: Close up of the S_{or} shapes of (a) 3 mm model and (b) 1 mm model of Figure 6-20.

6.4.4.2 Effects of pore scale heterogeneities on S_{or}

Since the arrangements of pores and grains in an oil sand reservoir are not homogeneous and do not have the same pore and particle size distributions, we analyzed the effects of pore and grain size heterogeneities on the development of S_{or} during the lateral expansion of steam chamber. These porous media models are highly idealized but they show how the pores are drained and how the trapping of oil occurs in heterogeneous models. Different configurations of heterogeneity are tested and presented in the next two subsections.

6.4.4.2.1 Small glass beads surrounded by big glass beads

In this case clusters of small beads of 0.2, 1, and 2 mm were surrounded by big glass beads of 3 mm. In **Figure 6-22a** through **Figure 6-22f**, a sequence of stages during the experiment is shown. Yellow arrows indicate steam and condensate direction and black arrows show oil flow direction. The steam and condensate started invading the model in a horizontal manner, mixing with the oil to form emulsions (dashed elongated ellipse in **Figure 6-22a**), as also described in section 6.4.1.

Figure 6-22b and **Figure 6-22c** show that steam penetrated through the big glass beads trying to surround the upper left cluster of small particles first since there was higher resistance in the throats and pores due to the higher capillary pressure. However, steam and tiny drops of water

started to interact with the oil in this cluster as pointed out with small yellow arrows around the cluster. The change of color to a darker one is an indication of the mixing and the emulsion formation.



Figure 6-22: Sequence of stages during the lateral expansion of steam in a model of small beads clusters surrounded by big beads (s: steam, w:water, o:oil).

Later, steam and water continued to invade preferentially through the big glass beads (**Figure 6-22d** and **Figure 6-22e**) while water and steam kept penetrating and interacting with the oil in the cluster of the small particles. However, these clusters of small beads were never drained. In this system, oil and water are the wetting phases and the steam is the non-wetting phase. The small black arrows in the upper part of the clusters (see **Figure 6-22c** –**Figure 6-22e**) indicate oil flowing from the big beads. This oil replenished the oil that was flowing down through the bottom part of the same clusters. The flow through the clusters of small particles will occur as long as those particles keep the capillary continuity with the surrounding big beads.

Also, notice that all the pores of the bottom part of the left upper cluster kept draining down (**Figure 6-22d**). However, those pores lost the continuity with the big beads due to the snap-off of the films as indicated by the left arrows in the bottom of the same cluster (**Figure 6-22e**). The loss of the continuity also depends on the aspect ratio between these two different pore and throat size systems (Chatzis et al., 1983). **Figure 6-22f** shows the final state of the model after the completion of the experiments. A considerable amount of oil was retained even in the bigger size glass bead regions.

Although glass is more water-wet than oil, a clear imbibition in the clusters or in the big beads was not observed. Oil covered all the surfaces of the glass beads (no film of water) due to its more viscous nature and the absence of initial film of water, imbibition between two distinct permeability media did not occur. In the case of one of the fluids is very viscous, the capillary forces are not dominant and the less viscous fluid (although it is a wetting phase) flowed through the center of the pores as also reported by Dullien (1992).

Hence, one may conclude that the clusters of small particles surrounded by bigger particles retain heavy oil during the invasion of condensate (wetting phase) and steam (non-wetting phase) if the capillary continuity is lost between the small grains of the cluster and the bigger beads surrounding them due to the snap-off of the films. **Figure 6-23** shows the final state of the Sor under fluorescent light. It is noticeable how the connectivity was lost between the “islands” of small particles surrounded by the bigger particles (dark dashed ellipses). In certain regions the continuity was conserved as it is pointed out in the solid black ellipse. It must be emphasized that the S_{or} is in the emulsified form, especially in the clusters of the middle part. The pink color in the center of the image is the cluster of 0.2 mm glass beads. This zone was not completely swept since the pores were too small.

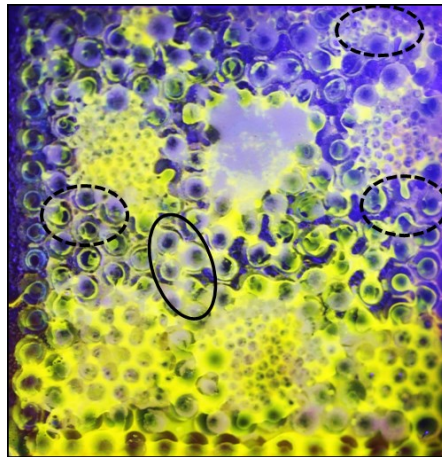


Figure 6-23: Final state of the residual oil saturation in the model of small beads clusters surrounded by big beads.

6.4.4.2.2 *Big glass beads surrounded by small glass beads*

In this experiment, the clusters of beads of 2 and 3 mm were surrounded by smaller size glass beads (1 mm) as shown in Figure 6-24.

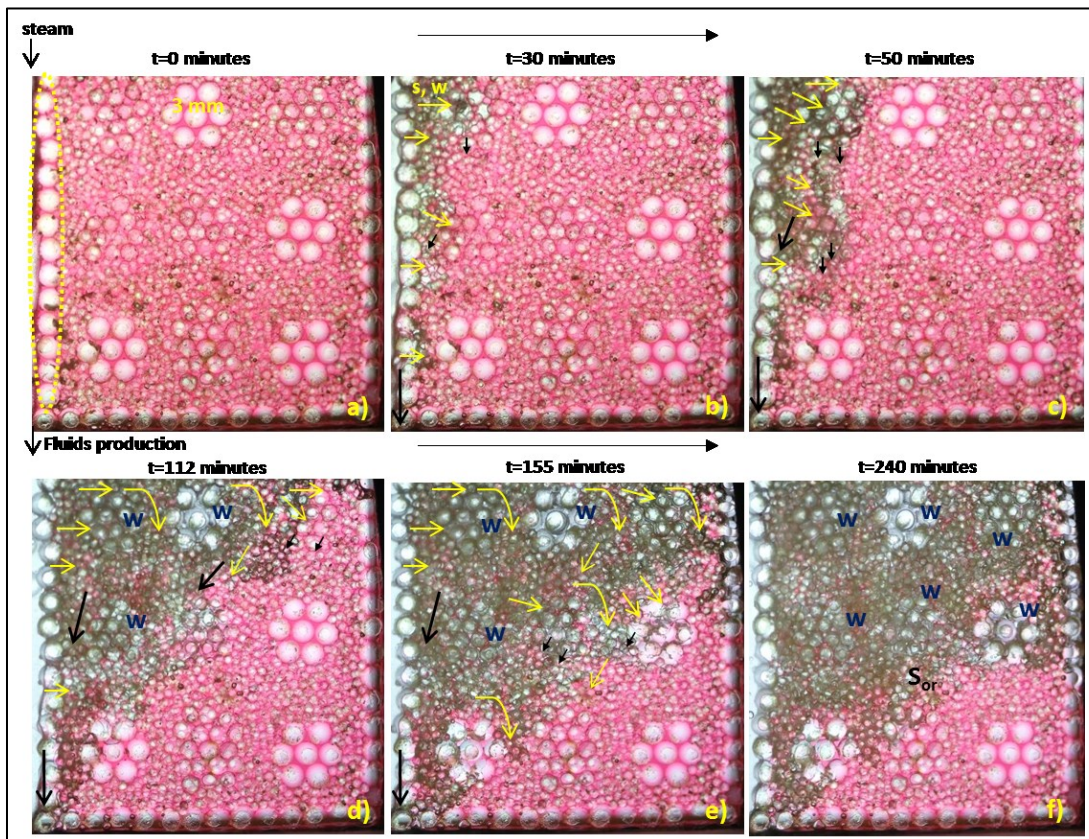


Figure 6-24: Sequence of stages during the lateral expansion of steam in a model of big beads clusters surrounded by small beads (w: water).

The sequence of the lateral expansion of steam injection is shown through **Figure 6-24a-Figure 6-24f**. Steam was injected in the upper part and the fluids were produced in the bottom as shown in **Figure 6-24a**. As in the previous model, the yellow arrows represent the steam and condensate direction and the black arrows are for the flow of oil. In this system, once steam and condensate reached the cluster of big beads, they both started penetrating into them easily (**Figure 6-24b** and **Figure 6-24c**). The oil, represented by the small black arrows, drained from the upper left clusters of big glass beads. In these “islands” of big glass beads, the capillary forces were low so that the oil was not retained and there was no replenishment from the upper pores.

As the invasion of steam and water continued, they entered into the other “islands” of big beads as shown in **Figure 6-24d** and **Figure 6-24e**. When the clusters were out of oil, water (indicated by “w” in **Figure 6-24d-Figure 6-24f**) was trapped in these clusters. Water was not able to flow down out of the cluster or imbibe into the surrounding small beads of 1 mm despite its wetting nature (depending of temperature and the stage of the steam chamber development, this water could be steam). The last stage of the experiment is shown in **Figure 6-24f**. In the large size glass bead clusters of the two upper rows, water was trapped and oil in the clusters of the bottom rows was not drained at all.

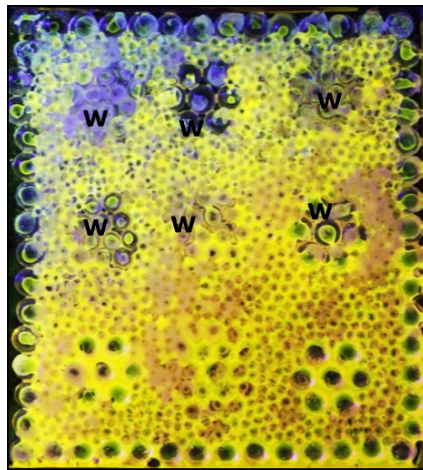


Figure 6-25: Final state of the residual oil saturation in the model of big beads clusters surrounded by small beads (w: water).

From these observations, one may conclude that it is unlikely that islands of big particles surrounded by smaller particles retain oil since it is displaced easier by invading steam (non-wetting phase) and the condensate (wetting phase). Furthermore, the low capillary pressure in

these beads facilitates the drainage of oil. It is expected that in this type of distribution, most of the oil will be drained but requires longer time. Although water wets the glass (at least more than oil), oil covered the entire surface of the beads due to the absence of initial film of water, the viscous forces overcame the capillarity that promotes imbibition.

Figure 6-25 shows the final S_{or} distribution under fluorescent light. In this case, there is no trapped oil due to the configuration of beads. The oil was retained in the surrounding small beads but more oil could have been drained if the experiment was continued for more hours. According to the observations in the sections 6.4.1 and 6.4.2, the S_{or} will be located inside of the steam chamber as short films due to snap-off or as oil blobs due to local bypassing through the neighboring bigger pore. Hence, the aspect ratio also plays an important role.

One may also notice that the intensity of the yellow color in **Figure 6-25** show what type of residual oil is located in the different regions of the model. At the bottom part, the oil has an intense yellow color, this was the virgin oil not contacted by the steam and condensate. In the upper part the yellow color is less bright indicating the emulsified state (water-in-oil emulsion).

6.4.4.3 Effects of wettability

Three states of wettability were compared during the lateral expansion of the steam chamber: (1) water wettability, (2) strongly oil wettability, and (3) mixed wettability. The models are shown in **Figure 6-26**. Teflon beads were used to mimic the strongly wettability state. The intermediate wettability was achieved mixing -one by one- glass and Teflon beads.

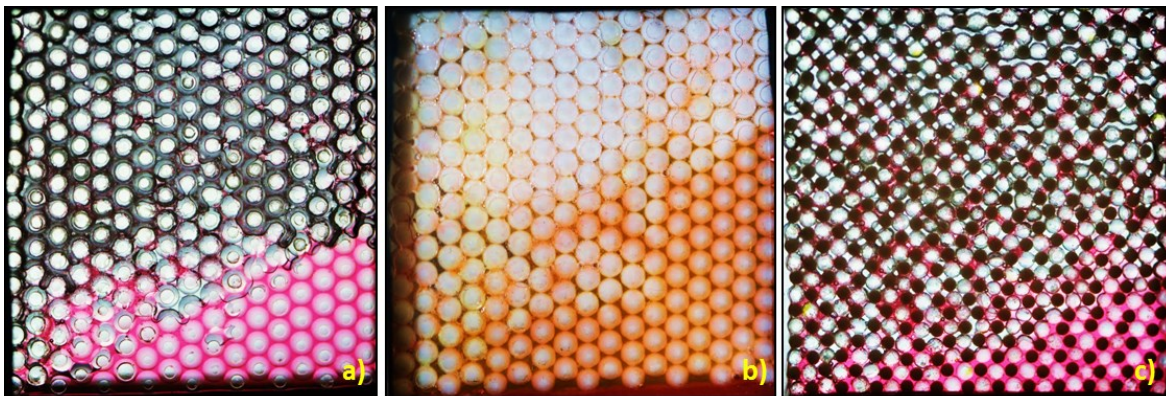


Figure 6-26: Wettability effects on S_{or} : (a) 3 mm water wet model, (b) 3 mm strongly oil wet model, and (c) 2 mm mixed wettability model.

As seen in **Figure 6-26**, the strongly oil wet model retained more oil compared to the water and mixed wettability systems after two hours of steam injection. The mixed wet state gave the lowest S_{or} . A close up image of the S_{or} for the wettability cases of **Figure 6-26** is shown in **Figure 6-27**.

It is noticeable the highest S_{or} for the strongly oil wet model (**Figure 6-27b**). In this case the S_{or} inside the steam chamber appeared in emulsified state as oil blobs connected with layers of oil (dashed blue circle of **Figure 6-27b**). In the case of water-wet model (**Figure 6-27a**), the oil was in the form of singles oil blobs as shown and discussed earlier. For the mixed wettability case (**Figure 6-27c**), the S_{or} existed also as isolated oil blobs between the glass and Teflon beads (dashed yellow circles).

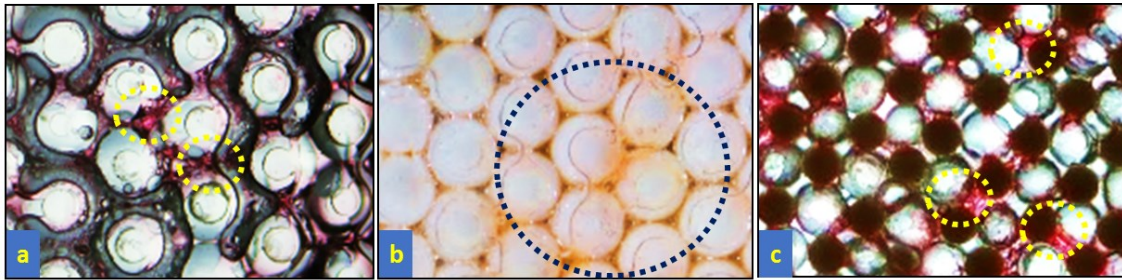


Figure 6-27: Close up of the S_{or} shapes for the wettability cases shown in Figure 6-26.

6.5 Conclusions

The dynamics of SAGD and formation of S_{or} during the process were analyzed visually at the pore scale. This was achieved for two different process dynamics: (1) lateral expansion of the steam chamber and (2) growth of half of steam chamber, which implies simultaneous vertical and lateral spreading of the chamber. The effects of heterogeneities (pore and particle distribution) and wettability were also investigated.

The following conclusions can be withdrawn from the observations through this paper:

Lateral Expansion of the Steam Chamber

- Once oil is mobile due to the heat transfer from the steam and condensate, two pore scale drainage mechanisms were observed: (1) direct displacement by steam and condensate and (2) concurrent flow of films along the pores while local direct displacement are

occurring.

- The flow of films on the grains and the direct displacement of mobile oil are actually driven by gravity since there is absence of viscous forces.
- Trapping mechanisms responsible for the formation of residual oil saturation were (i) bypassing of oil, as a consequence of the preferential flow of the steam (non-wetting phase) and condensate in bigger pores, and (ii) film snap-off due to the thinning of the oil blobs between adjacent grains that join the oil covering the grains. Those trapping mechanisms arose as a consequence of the activation of the drainage mechanisms.
- The phenomenon of emulsification was clearly visualized at the moment that the tiny droplets of water were engulfed by oil, confirming the previous investigations published in the literature. The negative spreading coefficient of water and the existence of hydrophilic components in the oil promote the formation of water in oil emulsions. Produced oil and the residual oil saturation are found in emulsified form.
- The S_{or} exists within the steam chamber as isolated films of short length, disperse blobs and trapped islands of oil.

Half Symmetric SAGD Chamber Growth

Drainage and trapping mechanisms.

- Besides the three fluid regions during the lateral expansion (mobile, stagnant, and steam chamber), the ceiling part was also identified as a mobilized zone in the growing chamber.
- In the ceiling part, steam “displaces” the mobile oil sideways to feed the lateral boundaries of the steam chamber. Since the viscous forces are not critically effective, this displacement must be understood as an aid to the gravity which is in fact a driving force.
- Unlike the lateral expansion, the only drainage mechanism in the ceiling part was the direct displacement with steam, driven by gravity (that pulls the oil to the lateral boundaries). If a film is formed along a series of pores, it is highly probable that it loses its capillarity continuity due to the disordered movement of steam which can break it. As the steam chamber grows, the possibility of films drainage contributing to the production through the lateral mobile regions decreases with the time.

Counter-current flow.

- The counter-current flow of oil within the same pore inside the chamber was not observed while steam was moving upward. The main reason is the loss of hydraulic continuity of the oil along the pores in the steam chamber, caused by the breaking of the oil blobs between the grains and bypass of oil (oil blob). The loss of hydraulic continuity was demonstrated visually (**Figure 6-17**).
- The capillary continuity is very important during the SAGD process. Actually, the capillary continuity along the ceiling part to the production well through the lateral boundaries is a necessary condition for the upward movement of the steam and even in the formation of more protruding fingers in the ceiling part.
- Counter-current flow can be interpreted at different scales. At the macro scale, it refers to the whole upward growing of the steam chamber with respect to the descending flow of condensate and oil at the lateral mobilized regions. At this scale, the gas and liquids flow in their own network of pores and do not interact with each other.
- At the pore scale, the counter-current flow occurs along a series of developed short films near the lateral mobilized regions until the film breaks.

Effects of Porous Medium Characteristics during Lateral Expansion of Steam Chamber

Pore and particle size (permeability in homogeneous models).

- In the case of homogeneous models, permeability impacts the amount of intact residual oil (sweep) more than the S_{or} inside of the steam chamber (pore scale entrapment). However, it was observed that in the case of the 3 mm glass beads model the S_{or} was found as single oil blobs whereas in the 1 mm glass bead models, the S_{or} was also in the form of clusters of trapped oil. The reason for having this kind of S_{or} in the 1 mm models is the presence of stronger capillary forces and unfavorable aspect ratio at the pore and throats located at the boundaries of such cluster of oil.
- Homogeneous models with different permeabilities could also have the same final residual oil saturation structure if the aspect ratio between the pores and throat were the same or if the formed cluster of oils were connected with the rest of the oil in form of layers and films. Of course, the models with less permeability would need longer times to

drain and reach the same S_{or} .

Pore Scale Heterogeneity

Small glass beads surrounded by big glass beads.

- Clusters of small grains surrounded by large grains retain heavy oil during the injection of steam (non-wetting phase) and condensate (wetting phase) if the capillary continuity is lost between the small and large particles due to the breaking of the films. Aspect ratio in the boundaries between both systems of beads can be the controlling parameter in this process.
- Water is not able to imbibe into the clusters of small beads to displace the oil since oil may cover the surface of the beads in the absence of initial water film. However, if this invasion is carried out at higher temperature and the oil gets more mobile and removed from the surface of the grain, imbibition of water could be a possibility.
- Although there is bypassing, the main trapping mechanisms in this type of pore configuration is the snap-off of connecting films between both (small and large size grains) systems.

Big glass beads surrounded by small glass beads.

- The clusters of big grains surrounded by smaller ones do not retain oil since the invading steam (non-wetting phase) and condensate (a less wetting phase in this system) displace the heavy oil easier in the pores of the big beads once they have reached the clusters. Depending on the temperature and stage of the process, water or steam can be found in these “islands” of big beads.
- In this type of configuration, S_{or} can be very low if enough time is given for draining during the steam injection since the heavy oil is also a wetting phase which is covering all the grains and its viscosity overcomes the capillarity which could promote the imbibition of water.

Wettability.

- For the same time of steam injection during the lateral expansion, strongly oil wet porous

medium has more S_{or} compared to water and intermediate wettability systems.

- For the water wet case, the S_{or} was found as single oil blobs whereas for the strongly oil wet model the S_{or} existed as oil blobs connected with layers of oil covering the surface of the Teflon beads. The mixed wettability model had the highest oil recovery.

6.6 References

1. Adamson, A.W. and Gast, A.P. 1997. Physical Chemistry of Surfaces. sixth ed., A Wiley – Interscience Publication, USA.
2. Al-Bahlani, A.M. and Babadagli, T. 2009. SAGD Laboratory Experimental and Numerical Simulation Studies: A Review of Current Status and Future Issues. *J. Petr. Sci. and Eng.*, 68 (3-4): 135-150.
3. Argüelles-Vivas, F. J. and Babadagli, T. 2014. Drainage Type Oil and Heavy – Oil Displacement in Circular Capillary Tubes: Two and Three – Phase Flow and Residual Oil Saturation Development in the Form of Film at Different Temperatures. *Journal of Petroleum Science and Engineering* 118: 61-73.
4. Argüelles-Vivas, F. J. and Babadagli, T. 2015. Residual Liquids Saturation Development during Two and Three-Phase Flow under Gravity in Square Capillaries at Different Temperatures. *Int. J. of Heat and Fluid Flow* 52: 1-14.
5. Butler, R.M. 1991. Thermal Recovery of Oil and Bitumen. Prentice Hall Inc., New Jersey, 285-359.
6. Butler, R.M. 1994a. Horizontal Wells for the Recovery of Oil, Gas and Bitumen: Petroleum Society Monograph Number 2, Canadian Institute of Mining Metallurgy & Petroleum.
7. Butler, R.M. 1994b. Steam-Assisted Gravity Drainage: Concept, Development, Performance and Future. *JCPT* 32 (2).
8. Cardwell, W.T. and Parsons, R.L. 1949. Gravity Drainage Theory. *Trans. AIME* 179: 199-211.
9. Chatzis, I., Morrow, N.R. and Lim, H.T. 1983. Magnitude and Detailed Structure of Residual Oil Saturation. *Soc. Pet. Eng. J.* 23(2): 311-326.
10. Chung, K.H. and Butler, R.M. 1987. Geometrical Effect of Steam Injection on the Formation of Emulsions in the Steam-Assisted Gravity Drainage Process: Paper 87-38-22., 398th Ann.

Tech. Meet. of the Pet. Soc. Of CIM, Calgary, June.

11. Dullien, F.A.L. 1992. Porous Media: Fluid Transport and Pore Structure. Academic Press, San Diego.
12. Jimenez, J. 2008. The Field Performance of SAGD Projects in Canada. Paper IPTC 12860 presented at the Int. Petroleum Tech. Conf., Kuala Lumpur, Malaysia, 3-5 Dec.
13. Kong, X., Haghghi, M. and Yortsos, Y.C. 1992. Visualization of steam displacement of heavy oils in a Hele-Shaw cell. Fuel 71: 1465-1471.
14. Mohammadzadeh, O. and Chatzis, I. 2009. Pore-Level Investigation of Heavy Oil Recovery Using Steam Assisted Gravity Drainage (SAGD). Paper IPTC 13403 presented at the Int. Petroleum Tech. Conf., Doha, Qatar, 7-9 Dec.
15. Mohammadzadeh, O. and Chatzis, I. 2010. Pore-Level Investigation of Heavy Oil Recovery Using Steam Assisted Gravity Drainage (SAGD). Oil & Gas Science and Technology – Rev. IFP Energies Nouvelles. 65 (6): 839-857.
16. Mohammadzadeh, O. and Chatzis, I. 2012. SAGD Visualization Experiments: What Have We Learned From the Pore-Level Physics of This Process? Paper WHOC12-421 presented at the World Heavy Oil Congress, Aberdeen, Scotland, 2012.
17. Sasaki, K., Akibayashi, S., Yazawa, N. and Kaneko, F. 2002. Microscopic Visualization with High Resolution Optical-Fiber Scope at Steam Chamber Interface on Initial Stage of SAGD Process. SPE 75241, SPE/DOE Imp. Oil Rec. Sym., Tulsa USA.
18. Sasaki, K., Akibayashi, S., Yazawa, N., Doan, Q.T. and Kaneko, F. 2001. Experimental Modeling of the SAGD Process – Enhancing SAGD Performance with Periodic Stimulation of the Horizontal Producer. SPEJ March: 89-97.

Chapter 7 : Summary, Contributions and Recommendations

7.1 Summary of the research

Steam Assisted Gravity Drainage (SAGD) field applications performed over the last twenty years showed that oil recovery is not as high as predicted by laboratory and numerical model studies. Considering the cost of steam injection, the reasons behind the high residual oil should be clarified to improve the efficiency of the process. This thesis targeted this and investigated the physics behind the development of residual oil saturation (S_{or}) during SAGD (or non-isothermal recovery processed in general terms) at the pore scale. First, capillary tubes to imitate the pore of an unconsolidated reservoir were used to study the development of S_{or} as a film or layer at variable temperatures. Then, computational fluid dynamics (CFD) approach was employed to analyze the S_{or} at temperatures and pressures that are difficult to simulate through physical experiments. Using the observations from these studies, the effects of a temperature gradient on oil recovery and relative permeabilities were investigated analytically using a cylindrical capillary tube model. Finally, SAGD process was mimicked on a 2-D glass beads model, and the dynamics of SAGD and oil trapping mechanisms were visually analyzed for different reservoir conditions.

7.2 Limitations and applicability of this research

The present research is one of the very few works devoted to investigate the development of residual oil saturation during thermal techniques. The biggest challenge in this type of work is to carry out experimental (and even theoretical) works under high temperature and non-isothermal conditions at the pore scale. As explained at the beginning of the thesis, most of the previous work focused the problem at the macro scale. In general, the SAGD process, as a whole, has been better understood at the macro than the pore scale. However, the evident discrepancy between the low oil recovery factor of finished SAGD field projects and the very optimistic high recovery factor determined from physical-scaled SAGD lab experiments obligated the researchers to go in depth, to the fundamentals, in order to unveil the reasons behind the low recovery factor of field SAGD projects.

The experiments and modeling of this thesis were carried out under controlled conditions and attempts were made to apply realistic conditions. In the initial part of this research, the pores and crevices of oil sands were imitated with circular and square capillaries. In this sense, the scale is

the same as that of the pores in reservoirs and it is well recognized that capillary tubes are the best manner to represent them. Although the oil was not bitumen, heavy oil (~2800 cP at room temperature) was used and the existing velocities in the real pores were also simulated. If the trapping numbers in the reservoirs are in the ranges where S_{or} is independent of temperature, the set of S_{or} curves of this work can be used as a reasonable approach to estimate the residual oil as layers of films.

If the trapping numbers are out of the range where S_{or} is constant and the temperature is much higher, new capillary tubes must be designed for high pressures but the methodology is essentially the same as the one developed in this research. In the case of capillaries of different geometry (i.e. triangular shape), the same methodology can be employed and this was done in the analytical modeling part of the thesis as given in Chapter 5.

On the other hand, the CFD simulations of the fourth chapter of this thesis show a promising option to determine the S_{or} for typical temperatures and pressures of real thermal methods as SAGD and steamflooding. However, more research is needed to improve the modeling of interfacial phenomena and the tracking of the interface to delimit the location of gas and liquid since. These factors could be the reason for the overestimation of the residual oil saturation in square capillaries. Another pitfall with the simulations is the computational cost to carry out a single simulation. For the finest meshes, the real simulation time was around 20 days for a length displacement of 0.05 cm. Each point of the curves NT versus S_{or} requires a mesh independency analysis to get a rigorous and trustable value of residual oil saturation, which is impractical.

The investigations presented in the fifth chapter about the effects of non-isothermal conditions during the displacement of heavy oil and water can initiate a new line of research on the dynamics of displacements, oil trapping and relative permeability curves. This work must be extended to more complex pore networks. The inclusion of the natural connectivity of oil sands could lead to different results to those found in this research. This chapter highlights the importance of considering a temperature gradient in the analysis and simulation of thermal methods. For example, the relative permeability within the steam chamber could be different to those in the edges of the chamber or in the ceiling part. The effects of a temperature gradient on the trapping of oil and in the scaling process deserve more research.

In the sixth chapter of this thesis, a visualization study of the dynamics of SAGD and the development of S_{or} at pore scale was presented. It must be clear that the main objective of this thesis was to study the interaction of the fluids and the transport phenomena in the pores or networks of pores rather than the up-scaling and the simulation in the lab of SAGD along years. It is known from the vast literature that the scaling of thermal methods is a big challenge due to the difficulty to satisfy all variables involved in the accomplishment of the similarity between the physical scaled model and the particular field or prototype. Therefore, a compromise must be established giving priority to the particular aspects or variables of interest of the research.

In the last stage of the research, the main priority was the visualization of the S_{or} . Therefore, the oil had to be transparent enough to properly make observations of the process. Although bitumen was not used for this stage (since is completely dark), standard transparent oil was employed with a viscosity behavior similar to that of bitumen. At 20 °C the viscosity was 113, 000 cP and was immobile and stagnant as bitumen at the moment to start the steam injection and the warming up period. The permeability of the homogeneous models was much higher than that of homogeneous oil sands. In the case of heterogeneous models, the permeability of the clusters of beads was smaller and ranged from 32 to 7200 D for 0.2 and 3 mm glass beads, respectively. The porosity of the models was between 35–40%, very similar to the porosity of oil sands.

To avoid excessive viscous forces and to be the closest as possible to SAGD, characterized theoretically by “free fall gravity drainage,” the steam was generated and injected at atmospheric pressure and temperature around 130 °C. In this way, the steam entered into the model due to natural movement inside the insulated and heated stainless steel tubing. Also, with the channel created between the injector and production port, any excessive viscous force was weakened by the presence of such channel. Besides, all the selected photos shown in chapter 6 and those not published clearly show that the steam expansion was fairly homogeneous without the presence of viscous fingering.

It is evident that the temperature was well below the common temperature in SAGD processes, which is around 200–220 °C. The main reasons for this were the limitations of the lab materials and the creation of excessive viscous forces.

The study of the influence of heterogeneities, pore structure, and wettability was clearly under

controlled conditions. The method developed to create these heterogeneous glass beads models required attaching each of the glass beads one-by-one to the surface of the Plexiglass plates. This was done so that the construction of these plates could take several weeks if too small beads were used and the probability to block the pores and throats was higher as the beads were smaller. The wettability was artificially imitated using Teflon beads for the strongly oil-wet state and Teflon and glass beads to create an idealistic 50-50% mixed wettability model. As seen, certain conditions (pore size, oil viscosity and process dynamics) can meet reservoir conditions but up-scaling requires more realistic representation of permeability and oil chemistry (real crude oil). Therefore, up-scaling from pore scale study presented in this thesis to reservoir conditions was not the main target.

In short, this study can be considered as a fundamental research study about the formation of S_{or} at the micro scale. The dynamics of the SAGD process and the trapping mechanisms were described and analyzed. Also presented were the visualizations and demonstrations of how the heterogeneities, size, and pore structure contribute to the trapping of oil and thus to the behavior of S_{or} , which is a dynamic property. General rules about the trapping of oil were proposed as it was done in the literature for gas and water flooding.

However, this work can be extended to more realistic conditions to strengthen the findings and to make new contributions. A new study on micro models with controlled pore and grain size must be carried out. The temperature must be increased to 200–220 °C, at high pressures and controlled steam injection rate. The effects of different temperature and injection rates on the residual oil saturation need to be evaluated. The behavior and stability of emulsions at higher temperatures must also be investigated. New micro models with pore size distribution based on oil sands characterization have to be used for a new experimental program.

7.3 Scientific and practical contributions to the literature and industry

Chapter 2:

- The physics of the formation of S_{or} in pores were investigated on circular capillaries for horizontal and vertical displacements at high temperature conditions (55 and 85 °C). Gas

injection rate was the changing variable and the capillary number was used to analyze the displacements.

- In general it was found that for heavy oil there is a critical capillary number around $1E-2$ over which the S_{or} depends on temperature (and thus of the fluid and capillary properties). At lower capillary numbers, the S_{or} is a function of capillary forces in the case of horizontal displacements, and a function of Bond number in Free Fall Gravity Drainage (FFGD). Empirical correlations between S_{or} and dimensionless numbers were proposed.

Chapter 3:

- Fluid retention characteristics were determined at different temperatures under gravity drainage conditions for two phase (air and heavy oil) and three phases (air, water, heavy oil) in square capillaries, representing the pores and crevices of unconsolidated sands more realistically.
- Trapping number, N_T , (summation of capillary and Bond number) was proposed for the analysis of the experiments. In the case of two phase flow (air – heavy oil), the findings are that the S_{or} is constant and does not depend on temperature for $N_T < 2.7E-2$ in a square capillary of 0.03 cm in width. In the same range, S_{or} is determined by the capillary forces, including FFGD (for a pore size). Above this N_T , the competition between gravity, viscous and capillary forces dictate the S_{or} . At different temperatures for the same gas injection rate, S_{or} is bigger at lower temperature. Comparing at the same N_T , S_{or} is bigger at higher temperatures. With respect to the pore size and for FFGD cases, it was found that the oil retention in square capillaries depends on the Bond number and S_{or} increases linearly for higher Bond numbers.
- In the case of three phases (air displaces oil which in turn displaces water) the S_{or} does not decrease with a thin layer of water on the surface of the tube for the entire range of N_T at 55 and 85 °C. Viscous forces of the heavy oil are responsible for this behavior. However, water is not completely removed from the tube due to water wettability.
- S_{or} depends on how the fluids are distributed each other in the capillary tubes. Higher water and oil retention was found for air – water – heavy oil distribution (air displacing water which in turn displaces oil) at higher temperatures. The unfavorable viscosity ratio

oil/water, the negative spreading coefficient of water in oil in presence the air and the natural surfactants in the oil explain this behavior. The wettability (water or oil) does not change the S_{or} but the water saturation decreases slightly in the oil wettability state (for the distribution air-heavy oil – water).

- For both types of capillary tubes, empirical correlations are provided to be used in the simulation of gravity drainage processes.

Chapter 4:

- CFD approach was used to analyze the retention of heavy oil in a reservoir. The displacement of heavy oil by gas at high temperature conditions in a square capillary was investigated. The objective was to simulate conditions that are not easy to reproduce in a laboratory.
- CFD agrees well with the experimental data at 55 and 85 °C. A numerical experiment was carried out at 200 °C and the results show that S_{or} decreases at higher temperatures for a fixed injection rate.
- S_{or} decreases exponentially with respect to time until it gets a constant value along the square capillary during the displacements.
- S_{or} diminishes lineally if the contact angle is augmented. For the 85 and 55 °C cases, above 60°, oil is completely swept from the capillaries.

Chapter 5:

- The effects of a temperature gradient on the displacement of heavy oil by water or gas (steam) in a cylindrical capillary tube were studied analytically. Solving the momentum equations, the exact solutions were derived to describe the oil recovery during the water – heavy oil immiscible displacement and the free and forced gas – heavy oil gravity drainage. The solutions were applied to a bunch of non - connected capillaries to obtain the relative permeability curves.
- It was found that the location of the interface depends on the capillary behavior and fluid viscosity with temperature. Since the change of the viscosity of the oil is more severe with temperature, viscous forces become dominant during the non-isothermal displacements.

- The displacement of heavy oil with water or gas is accelerated under a positive temperature gradient (inlet temperature smaller than outlet temperature), including spontaneous imbibition of water.
- Temperature gradient could potentially modify the behavior and shape of the permeability curves, and as a consequence, they could be different to those curves at constant temperature.

Chapter 6:

- The mechanisms leading to the formation of S_{or} due to the nature of the reservoir and the dynamics of SAGD are studied at the micro scale. Experiments were carried out in 2D glass beads models to visualize the lateral expansion of the steam chamber and the growth of a half symmetric SAGD chamber. Effects of heterogeneities, pore size and wettability on S_{or} were clarified.
- It was observed that in SAGD the trapping mechanisms responsible for the development of S_{or} are the bypassing of the oil and the breaking of oil films. Both mechanisms arise as a consequence of the drainage mechanisms driven by gravity, which are the direct displacement of oil by steam and/or condensate and the simultaneous flow of films.
- The bypass of oil occurs due to the preferential flow of non-wetting - steam and/or condensate in bigger pores. The snap-off of films is due to the thinning of the oil blobs that are found between adjacent beads. The emulsification phenomenon was clearly visualized at the moment that the drops of water moved into the oil. This confirms previous observations in the literature. The negative spreading coefficient of water in oil in the presence of steam and the hydrophilic components of the oil propitiate the formation of water in oil emulsion. Both, S_{or} and produced oil are found highly emulsified. In general the S_{or} exists as isolated short films, disperses blobs and trapped clusters of oil within the chamber.
- In addition to the three fluid regions recognized during the lateral expansion in the literature, the ceiling part is also identified as a mobilized region in the complete SAGD process. Dissimilar to the lateral expansion, the only drainage mechanism in the ceiling part is the direct displacement with steam, driven by gravity that “pulls” the oil sideways to feed the lateral boundaries of the steam chamber. Due to the disordered movements of

steam (proved visually), it is very unlikely that the formation of films occurs at the ceiling part of the chamber. If it does, the films undergo snap-off. As the steam chamber grows the chance of these possible films to contribute to the production of oil will decrease with the time.

- Counter current flow of oil within the chamber with respect to the steam was not observed at the ceiling part. This was attributed to the loss of hydraulic continuity of the oil along the pores inside the steam chamber due to the snap-off of the oil blobs between grains and the bypassing of clusters of oil. The hydraulic continuity would assure an area for the oil located at the top to flow down in the same pores (or others) where the steam ascends through the center. Otherwise, steam occupies all the area and drives the flow upward. On the basis of this statement, it can be emphasized that hydraulic continuity is critical in the SAGD process. The hydraulic continuity from the ceiling part to the production well along the lateral boundaries is necessary for the upward movement of steam and in the formation of protruding fingers in the ceiling part.
- At the pore scale, the counter – current flow occurs along a series of developed short films close to the lateral mobilized regions until the film snaps off.
- Homogeneous models with the same pore structure but different permeability could have the same final S_{or} but the difference is the time required to drain the oil. In the case of heterogeneities, however, a cluster of small particles surrounded by big ones retain heavy oil if the hydraulic continuity is lost between both systems of particles due to the breaking of the films during the injection of steam (non-wetting phase) and condensate (wetting phase). The aspect ratio in the boundaries between both systems is critical in this process. Since the oil viscosity is dominant over the capillary properties water does not imbibe in the islands of small beads to remove the oil. However, higher temperature and similitude of water and oil viscosity could make possible the water imbibition.
- On the other hand, clusters of big particles surrounded by small particles do not retain oil since the penetrating steam (non-wetting phase) and condensate (wetting phase) remove the heavy oil easier in the pores of the cluster of big beads. Water or steam can be found in these islands of particles. S_{or} can be very low in this distribution if enough time is given for draining during the steam injection. From these experiments it can be affirmed

that different pore and particle size distributions will lead to variations in the amount of S_{or} due to this kind of heterogeneities.

- With respect to the wettability, using the same time of steam injection, the S_{or} is much higher for the strongly oil wet porous medium compared to the water and mixed wettability reservoir models. The mixed wettability model has the lowest S_{or} even though the size of the beads was 30% smaller.
- The findings and observations of this final chapter contribute to enhance the understanding of the SAGD process. The details about the formation of residual oil saturation can be helpful in making decisions when those values are assigned in different regions of the oil sands to simulate the SAGD process at the field scale.

7.4 Suggested future work

- 1) The experimental data for heavy oil in cylindrical capillaries can be modeled extending or modifying the classical Bretherton model for horizontal displacements and simple fluids.
- 2) The models including the temperature gradients to get the relative permeabilities can be extended to connected capillary tubes models to evaluate if the temperature gradient influences or not the relative permeability curves in more complex system.
- 3) Another challenging research is to improve the numerical model to simulate surface tension and wettability effects in multiphase flow. Challenging problems in CFD are the tracking, location and shape of the interface between fluids. The interpolation scheme of reconstruction of the interface must be investigated and improved.
- 4) Following the same experimental methodology, the SAGD experiments can be tested at higher temperatures and pressures. Experiments with specific and low steam injection rates will definitively improve the estimation of the S_{or} at different temperatures. For these experiments, the design of special micro models is needed.

BIBLIOGRAPHY

Adamson, A.W., and Gast, A. P. 1997. *Physical Chemistry of Surfaces*. A Wiley – Interscience Publication, USA.

Ajaev, V.S., and Homsy, G.M. 2006. , Modeling Shapes and Dynamics of Confined Bubbles. *Annu. Rev. Fluid. Mech.*, 38: 277-307.

Al-Bahlani, A.M. and Babadagli, T. 2009. SAGD Laboratory Experimental and Numerical Simulation Studies: A Review of Current Status and Future Issues. *J. Petr. Sci. and Eng.*, **68** (3-4): 135-150.

Arguelles, F. and Babadagli, T. 2012. Pore Scale Modeling of Gravity Drainage Dominated Flow under Isothermal and Non-Isothermal Conditions. Paper SPE 153591 presented at the SPE Latin American and Carib. Petr. Eng. Conf. (LACPEC), Mexico City, Mexico, April 16-18.

Argüelles–Vivas, F.J. and Babadagli, T. 2014. Drainage Type Oil and Heavy-Oil Displacement in Circular Capillary Tubes: Two- and Three-Phase Flow Characteristics and Residual Oil Saturation Development in the Form of Film at Different Temperatures. *Journal of Petroleum Science and Engineering*, **118**: 61-73.

Argüelles–Vivas, F.J. and Babadagli, T. 2015. Residual Liquids Saturation Development During Two and Three Phase Flow under Gravity in Square Capillaries at Different Temperatures. *Int. J. of Heat and Fluid Flow*, **52**: 1-14.

Argüelles–Vivas, F.J., Babadagli, T., Little, T., et al. 2012. High Temperature Density, Viscosity and Interfacial Tension Measurements of Bitumen-Pentane-Biodiesel and Process Water Mixtures. *Journal of Chemical & Engineering Data*, 57 (10): 2878-2889.

Ashrafi, M., Souraki, Y., and Torsaeter, O. 2014. Investigating the Temperature Dependency of Oil and Water Relative Permeabilities for Heavy Oil Systems. *Transport in Porous Media*, 105: 517-537.

Baker, R.O., Rodrigues, K., Sandhu, K.S. and Jong, E.S.W. 2010. Key Parameters in Steam Chamber Development. Paper SPE 138113-MS presented at the Canadian Unconventional Resources and International Petroleum Conference, Calgary, Alberta, Canada. October 19-21.

Bartley, J.T. and Ruth, D.W. 1999. Relative Permeability Analysis of Tube Bundle Models. *Transport in Porous Media*, 36: 161-187.

Bennion, D.W., Moore, R.G., and Thomas, F.B. 1985. Effect of Relative Permeability on the Numerical Simulations of the Steam Stimulation Process. *J Can Pet Technol.*, 24 (2): 40-44.

Berg, J. 2010. *An Introduction to Interfaces & Colloids, The Bridge to Nanoscience*. World Scientific Publishing Co. Pte. Ltd, Singapore.

Bird, R.B., Stewart, E.N., and Lightfoot, E.N. 2002. *Transport Phenomena*, second edition. New York: John Wiley & Sons.

- Blunt, M., Zhou, D. and Fenwick, D. 1995. Three-Phase Flow and Gravity Drainage in Porous Media. *Transport in Porous Media*, **20**:77-103.
- Brackbill, J.U., Kothe, D.B. and Zemach, C. 1992. A Continuum Method for Modeling Surface Tension. *Journal of Computational Physics*, **100**: 335-354.
- Bretherton, F.P. 1961. The Motion of Long Bubbles in Tubes. *Journal of Fluid Mechanics*, **10**: 166-188.
- Butler, R.M. 1987. Rise of Interfering Steam Chambers. JCPT, Paper 87-03-07.
- Butler, R.M. 1991. *Thermal Recovery of Oil and Bitumen*. Prentice Hall Inc., New Jersey, 285-359.
- Butler, R.M. 1994a. *Horizontal Wells for the Recovery of Oil, Gas and Bitumen: Petroleum Society Monograph Number 2*, Canadian Institute of Mining Metallurgy & Petroleum.
- Butler, R.M. 1994a. Steam-Assisted Gravity Drainage: Concept, Development, Performance and Future. JCPT, **32** (2).
- Cardwell, W.T. and Parsons, R.L. 1949. Gravity Drainage Theory. *Trans. AIME*, **179**: 199-211.
- Chatzis, I., Kantzas, A. and Dullien, F.A.L. 1988. On the investigation of gravity assisted inert gas injection using micro-models, long Berea sandstone cores, and computer assisted tomography. Paper SPE 18284 presented at the SPE Annual Tech. Conf. and Exh., Houston, TX.
- Chatzis, I., Kuntamukkula, M. and Morrow, N. 1988. Effect of Capillary Number on the Microstructure of Residual Oil in Strongly Water Wet Sandstones. *Soc. Pet. Eng. Reservoir Engineering*, **3**(3): 902-912.
- Chatzis, I., Morrow, N.R. and Lim, H.T. 1983. Magnitude and Detailed Structure of Residual Oil Saturation. Paper SPE 10681 presented at the 1982 SPE/DOE Enhanced Oil Recovery Symposium, Tulsa, OK.
- Chen, J. D. 1986. Measuring the film thickness surrounding a bubble inside a capillary. *Journal of Colloid and Interface Science*, **109**: 34-39.
- Chung, K.H. and Butler, R.M. 1987. Geometrical Effect of Steam Injection on the Formation of Emulsions in the Steam-Assisted Gravity Drainage Process. Paper 87-38-22 presented at the 38th Annual Technology Meeting of the Petroleum Society of CIM, Calgary, AB, Canada, 7-10 June.
- Churaev, N. V. and Derjaguin, B.V. 1985. Inclusion of Structural Forces in the Theory of Stability of Colloids and Films. *Journal of Colloid and Interface Science*, **103** (2): 542-553.
- Cox, B.G. 1962. On Driving a Viscous Fluid Out of a Tube. *Journal of Fluid Mechanics*, **14**:81-96.
- Czarnecki, J., Radoev, B., Schramm, L.L., and Slavchev, R. 2005. On the Nature of Athabasca Oil Sands. *Advances in Colloid and Interface Science*, 114-115: 53-60.

- Danis, M. and Jacqui, C. 1983. Influence du Contraste de Viscosité sur les Permeabilités Relatives Lors du Drainage: Experimentation et Modelisation. Rev dl'IFT, 38.
- Dehghanpour, H., Aminzadeh, B., Mirzaei, M., and DiCarlo, D.A. 2011. Flow Coupling During Three Phase Gravity Drainage. Physical Review E, 83: 1-4.
- Donaldson, E.C., Lorenz, P.B., and Thomas, R.D. 1966. The Effects of Viscosity and Wettability on Oil and Water Relative Permeabilities. Proc: 41st Annual SPE Meet., Dalas, TX, 2-5 October, SPE 1562.
- Dong, M. and Chatzis, I. 2003. Oil Layer Flow along the Corners of Non-Circular Capillaries by Gravity Drainage. JCPT, 42: 9-11.
- Dong, M. and Chatzis, I. 2004. An Experimental Investigation of Retention of Liquids in Corners of a Square Capillary. Journal of Colloid and Interface Science, 273: 306-312.
- Dong, M., and Chatzis, I. 1995. The Imbibition and Flow of a Wetting Liquid along the Corners of a Square Capillary Tube. Journal of Colloid and Interface Science, 172: 278-288.
- Dong, M., Dullien, F.A.L., Dai, L., et al. 2005. Immiscible Displacement in the Interacting Capillary Bundle Model Part I. Development of Interacting Capillary Bundle Model. Transport in Porous Media, 59: 1-18.
- Dong, M., Dullien, F.A.L., Dai, L., et al. 2006. Immiscible Displacement in the Interacting Capillary Bundle Model Part II. Applications of Model and Comparison of Interacting and Non-Interacting Capillary Bundle Models. Transport in Porous Media, 63: 289-304.
- Dong, M. 1995. A study of Film Transport in Capillaries with an Angular Cross-Section. *Ph.D. thesis*, University of Waterloo.
- Dullien, F.A.L. 1992. Porous Media: Fluid Transport and Pore Structure. Academic Press, San Diego.
- Edmonson, T.A. 1965. Effect of Temperature on Waterflooding. J Can Pet Technol., 4 (4): 236-242.
- Fairbrother, F. and Stubbs, J. 1935. Studies in Electroendosmosis. Part VI. The 'Bubble Tube' Method of Measurement. Journal of Chemical Society. 1: 527-529.
- Ferziger, J.H. and Peric, M. 2002. Computational Methods for Fluid Dynamics, third edition. Berlin Heidelberg New York. Springer.
- Gauglitz, P. A. and Radke, C.J. 1988. An Extended Evolution Equation for Liquid Film Breakup in Cylindrical Capillaries. Chemical Engineering Science, 43 (7): 1457-1465.
- Geffen, T.M., Owen, W.W., D.R. Parris., et al. 1951. Experimental Investigation of Factors Affecting Laboratory Relative Permeability Measurements. Transactions AIME, 192: 99-110.
- Giavedoni, M.D. and Saita, F.A. 1997. The Axisymmetric and Plane Cases of a Gas phase Steadily Displacing a Newtonian liquid – A simultaneous solution of the governing equations. Phys. Fluids, 9(8): 2420-2428.

- Ginley, G.M. and Radke, C.J. 1989. The Influence of Soluble Surfactants on the Flow of the Long Bubbles through a Cylindrical Capillary. ACS Symposium Series, **396**: 480-501.
- Goldsmith, H.L., and Mason, S.G. 1963. The Flow of Suspensions through Tubes. Journal of Colloid Science, **18**: 237-261.
- Green, D.W., Whillhite, G.P. 1998. Enhanced Oil Recovery. SPE Textbook Series Vol. 6.
- Gregory, J. 1969. The Calculation of Hamaker Constants. Advan. Colloid Interface Sci., **2**: 396-417.
- Hagoort, J. 1980. Oil Recovery by Gravity Drainage. Paper SPE 7424 presented at the SPE 53rd Annual Fall Tech. Conf. and Exh., Houston, TX, Oct. 1-3.
- Hazel, A.L., and Heil, M. 2002. The Steady Propagation of a Semi-infinite Bubble into a Tube of Elliptical or Rectangular Cross-Section. Journal of Fluid Mechanics, **470**: 91-114.
- Hirasaki, G.J. and Lawson, J.B. 1985. Mechanisms of Foam Flow in Porous Media: Apparent Viscosity in Smooth Capillaries. SPEJ, **25**: 176-190.
- Hirt, C.W. and Nichols, B.D. 1981. Volume of Fluid (VOF) Method for the Dynamics of Free Boundaries. Journal of Computational Physics, **39**: 201-225.
- Hoffman, R. 1975. A study of the Advancing Interface 1. Interface Shape in Liquid-Gas Systems. J. Colloid Interface Sci., **50** (2): 228-241.
- Huang, H., Meakin, P., and Liu, M.B. 2005. Computer Simulation of Two-Phase Immiscible Fluid Motion in Unsaturated Complex Fractures Using a Volume of Fluid Method. Water Resources Research, **41**(12): W12413.
- Jimenez, J. 2008. The Field Performance of SAGD Projects in Canada. Paper IPTC 12860 presented at the Int. Petroleum Tech. Conf., Kuala Lumpur, Malaysia, 3-5 Dec.
- Jin, M. 1995. A Study of Non-Aqueous Phase Liquid Characterization and Surfactant Remediation. PhD dissertation, The U. of Texas. Austin, Texas.
- Joekar-Niasar, V., van Dijke, M.I.J., and Hassanizadeh, S.M. 2012. Pore-Scale Modeling of Multiphase Flow and Transport: Achievements and Perspectives. Transport in Porous Media, **94**: 461-464.
- Johnson, E.F., Bossler, D.P., and Naumann, V.O. 1959. Calculation of Relative permeability from Displacement Experiments. Petroleum Transactions AIME, **216**: 370-372.
- Jones, S.C. and Roszelle, W.O. 1978. Graphical Techniques for Determining Relative permeability from Displacement experiments. Journal Pet Technol., **5**: 807-817.
- Kamath, J., Nakagawa, F., Meyer, R., Kabir, S. and Hobbet, R. 2001. Laboratory Evaluation of Waterflood Residual Oil Saturation in Four Carbonate Cores. Paper SCA 2001-12. Proc. SCA Symposium Technical Programme, Edinburgh, Scotland, September 16-19.

- Kamişli, F. 2003. Flow of a Long Bubble in a Square Capillary. *Chemical Engineering and Processing*, **42**: 351-363.
- Kolb, W.B. and Cerro, R.L. 1991. Coating the Inside of a Capillary of Square Cross-Section. *Chemical Engineering Science*, **46** (9): 2181-2195.
- Kolb, W.B. and Cerro, R.L. 1993. The Motion of Long Bubbles in Tubes of Square Cross-Section. *Phys Fluids A*, **5** (7): 1549-1557.
- Kong, X., Haghghi, M. and Yortsos, Y.C. 1992. Visualization of steam displacement of heavy oils in a Hele-Shaw cell. *Fuel*, **71**: 1465-1471.
- Legait, B. 1983. Laminar Flow of Two Phases through a Capillary Tube with Variable Square Cross-Section. *Journal of Colloid and Interface Science*, **96** (1): 28-38.
- Leverett, M.C. 1939. Flow of Oil-Water Mixtures through Unconsolidated Sands. *Petroleum Transactions AIME*, **132**: 149-171.
- Lo, H.Y. and Mungan, N. 1973. Temperature Effect on Relative Permeability and Residual Oil Saturations. Oral presentation RR-19 given at the Petroleum Recovery Institute, Calgary, AB.
- Ma, Y.D. 2012. Motion Effect on the Dynamic Contact Angles in a Capillary Tube. *Microfluid Nanofluid*, Short Communication, **12**: 671-675.
- Maini, B.B. and Batycky, J.P. 1985. The Effect of Temperature on Heavy Oil/Water Relative Permeabilities in Horizontally and Vertically Drilled Core Plugs. *JPT*, **37** (8): 1500-1510.
- Maini, B.B. and Okazawa, T. 1987. Effect of Temperature on Heavy Oil-Water Relative Permeability of Sand. *J Can Pet Technol.*, **26** (3): 33-41.
- Mani, V., and Mohanty, K.K. 1997. Effect of the Spreading Coefficient on Three-Phase Flow in Porous Media. *Journal of Colloid and Interface Science*, **187**: 45-56.
- Martinez, M.J. and Udell, K.S. 1989. Boundary Integral Analysis of the Creeping flow of Long Bubbles in Capillaries. *Journal of Applied Mechanics*, **56**: 211-217.
- Medina, A., Pineda, A., and Treviño, C. 2003. Imbibition Driven by a Temperature Gradient. *Journal of the Physical Society of Japan*, **75** (2): 979-982.
- Miller, M.A. and Ramey Jr, H.J. 1985. Effect of Temperature on Oil/Water Relative Permeabilities of Unconsolidated and Consolidated Sands. *SPE J*, **25** (6): 945-953.
- Mohammadzadeh, O. and Chatzis, I. 2009. Pore-Level Investigation of Heavy Oil Recovery Using Steam Assisted Gravity Drainage (SAGD). Paper IPTC 13403 presented at the Int. Petroleum Tech. Conf., Doha, Qatar, 7-9 Dec.
- Mohammadzadeh, O. and Chatzis, I. 2010. Pore-Level Investigation of Heavy Oil Recovery Using Steam Assisted Gravity Drainage (SAGD). *Oil & Gas Science and Technology – Rev. IFP Energies Nouvelles*, **65** (6): 839-857.
- Mohammadzadeh, O., Rezaei, N. and Chatzis, I. 2012. SAGD Visualization Experiments: What

Have We Learned From the Pore-Level Physics of This Process? Paper WHOC12-421 presented at the World Heavy Oil Congress, Aberdeen, Scotland.

Mohammadzadeh, O., Rezaei, N., and Chatzis, I. 2002. Production Characteristics of the Steam-Assisted Gravity Drainage (SAGD) and Solvent-Aided SAGD (SA-SAGD) Processes Using a 2-D Macroscale Physical Model. *Energy & Fuels*, 26: 4346-4365.

Odeh, A.S. 1959. Effect of Viscosity Ratio on Relative Permeability. *Petroleum Transactions AIME*, 216: 346-353.

Oshita, T., Okabe, H. and Namba. 2000. Early Water Breakthrough – X-ray CT Visualizes How It happens in Oil-Wet Cores. Paper SPE 59426 presented at the 2000 SPE Asia Pacific Conference on Integrated Modeling for Asset Management, Yokohama, Japan, April 25-26.

Osoba, J.S., Richardson, J.G., and Blair, P.M. 1951. Laboratory Measurements of Relative Permeability. *Transactions AIME*, 192: 47-56.

Park, C.W. and Homsy, G.M. 1984. Two Phase Displacement in Hele-Shaw cell: Theory. *Journal of Fluid Mechanics*, **139**: 291-308.

Pennell, K. D., Pope, G. A. and Abriola, L.M. 1996. Influence of Viscous and Buoyancy Forces on the Mobilization of Residual Tetrachloroethylene during Surfactant Flushing. *Environmental Science & Technology*, **30** (4): 1328-1335.

Perry, R.H. and Green, D.W. 1984. *Perry's Chemical Engineers' Handbook*, sixth edition. New York: McGraw-Hill.

Peterson, R.C. 1999. The Numerical Solution of Free-Surface Problems for Incompressible, Newtonian Fluids. PhD dissertation. The University of Leeds, England.

Pooladi-Darvish, M. and Mattar, L. 2002. SAGD Operations in the presence of overlaying gas cap and water layer-effect of shale layers. *JCPT*, **41** (6).

Pope, G.A., Wu, W., Narayanaswamy, G., Delshad, M., Sharma, M.M. and Wang, P. 2000. Modeling Relative Permeability Effects in Gas-Condensate Reservoirs With a New Trapping Model. *SPE Reservoir Eval. & Eng.*, **3** (2): 171-178.

Poston, S.W., Ysrael, S., Hossain, A.K.M.S., et al. 1970. The Effect of Temperature on Irreducible Water Saturation and Relative Permeability of Unconsolidated Sand. *SPE J*, 10 (2): 171-180.

Raeini, A.Q., Blunt, M.J., and Bijeljic, B. 2012. Modelling Two-Phase Flow in Porous Media at the Pore Scale Using the Volume-of-Fluid Method. *Journal of Computational Physics*, **231**: 5653-5668.

Ransohoff, T.C., and Radke, C.J. 1988. Laminar Flow of a Wetting Liquid along the Corners of a Predominantly Gas-Occupied Noncircular Pore. *Journal of Colloid and Interface Science*, 121: 392-401.

- Ratulowski, J. and Chang, H.C. 1989. Transport of Gas Bubbles in Capillaries. *Phys. Fluids A*, **1**(10): 1642-1655.
- Ratulowski, J. and Chang, H.C. 1990. Marangoni Effects of Trace Impurities on the Motion of Long Gas Bubbles in Capillaries. *Journal of Fluid Mechanics*, **210**: 303-328.
- Reinelt, D.A. and Saffman, P.G. 1985. The Penetration of a Finger into a Viscous Fluid in a Channel and Tube. *SIAM J. Sci. Stat. Comput.*, **6** (3): 542-561.
- Richardson, J.G. 1957. Calculation of Waterflooding Recovery from Steady State Relative Permeability Data. *J Pet Technol.*, **19** (5): 64-66.
- Rusanov, A. I. 2007. Equilibrium Thin Liquid Films. *Colloid Journal*, **69** (1): 39-49.
- Ruth, D.W. and Bartley, J.T. 2002. A Perfect-Cross-Flow Model for Two phase Flow in Porous Media. In: *Proceedings of the 2002 International Symposium of the Society of Core Analysts*, Monterrey, California, SCA2002-05 (2002) 12.
- Sanchez, M. and Medina, A. 2005. Spontaneous Imbibition in a Porous Medium under Longitudinal Temperature Gradients. *Revista Mexicana de Física*, **51** (4): 349-355.
- Sanchez, M., Sanchez, F., Pérez-Rosales, A., et al. 2004. Imbibition in a Hele-Shaw Cell Under a Temperature Gradient. *Physics Letters, Section A: General, Atomic and Solid State Physics*, **324** (1): 14-21.
- Sandberg, C.R., Gournay, L.S., and Sippel, R.F. 1958. The effect of Fluid Flow Rate and Viscosity on Laboratory Determination of Oil/Water Relative Permeability. *Transactions AIME*, **213**: 36-43.
- Sasaki, K., Akibayashi, S., Yazawa, N. and Kaneko, F. 2002. Microscopic visualization with high resolution optical-fiber scope at steam chamber interface on initial stage of SAGD process. *SPE 75241, SPE/DOE Imp. Oil Rec. Sym., Tulsa USA*.
- Sasaki, K., Akibayashi, S., Yazawa, N., et al. 1999. Experimental Modeling of the SAGD process – Enhancing SAGD Performance with Periodic Stimulation of the Horizontal Producer. Paper SPE 56544 presented at the SPE Annual Technical Conference and Exhibition, Houston, TX, USA, 3-6 October.
- Satik, C. and Yortsos, Y. 1995. Pore-Network Studies of Steam Injection in Porous Media. Paper SPE 30751 presented at the SPE Annual Technical Conference & Exhibition, Dallas, TX, USA, 22-25 October.
- Schneider, F.N. and Owens, W.W. 1970. Sandstone and Carbonate Two and Three Phase Relative Permeability Characteristics. *SPE J*, **10**: 75-84.
- Schwartz, L.W., Princen, H.M. and Kiss, A.D. 1986. On the motion of Bubbles in Capillary Tubes. *Journal of Fluid Mechanics*, **172**: 259-275.
- Shen, E. I. and Udell, K. S. 1985. A Finite Element Study of Low Reynolds Number Two-Phase Flow in Cylindrical Tubes. *Journal of Applied Mechanics*, **52**: 253-256.

- Singhal, A.K., and Somerton, W.H. 1970. Two-Phase Flow Through a Non – Circular Capillary at Low Reynolds Numbers. *J. Can. Pet. Technol.*, 9 (3): 197-205.
- Soares, E.J., Carvalho, M.S., and Souza Mendes, P.R. 2005. Immiscible Liquid-Liquid Displacement in Capillary Tubes. *Journal of Fluids Engineering*, 127: 24-31.
- Sola, S.B., Rashidi, F., and Babadagli, T. 2007. Temperature Effects on the Heavy Oil/Water Relative Permeabilities of Carbonate Rocks. *J Petr Sci and Eng.*, 59: 27-42.
- Sufi, A.H. 1982. Temperature Effects on Oil-Water Relative Permeability for Unconsolidated Sands. PhD Thesis, Stanford University, Stanford, California.
- Sufi, A.H., Ramey Jr, H.J., and Brigham, W.E. 1982. Temperature Effects on Relative Permeabilities of Oil-Water Systems. Paper SPE 11071 presented at the 57th Annual Technical Conference and Exhibition of Society of Petroleum Engineers, New Orleans, USA, 26-29 September.
- Taha, T. and Cui, Z.F. 2006. CFD Modeling of Slug Flow inside Square Capillaries. *Chemical Engineering Science*, 61(2): 665-675.
- Takamura, K. 1982. Microscopic Structure of Athabasca Oil Sand. *The Canadian Journal of Chemical Engineering*, 60: 538-545.
- Taylor, G.I. 1960. Deposition of a Viscous Fluid on the Wall of a Tube. *Journal of Fluid Mechanics*, 10: 161-165.
- Teletzke, G. F., Davis, H.T. and Scriven L. E. 1988. Wetting Hydrodynamics. *Revue Phys. Appl.*, 23: 989-1007.
- Thulasidas, T.C., Abraham, M.A., and Cerro, R.L. 1995. Bubble–Train Flow in Capillaries of Circular and Square Cross Section. *Chemical Engineering Science*, 50 (2): 183-199.
- Vizika, O., and Lombard, J.M. 1996. Wettability and Spreading: Two Key Parameters in Oil Recovery With Three-Phase Gravity Drainage. *SPE Reservoir Engineering*, 11: 54-60.
- Walls, E., Palmgren, S. and Kisman, K. 2003. Residual oil saturation inside the steam chamber during SAGD. *JCPT*, 42 (1).
- Wang, J., Dong, M., and Asghari K. 2006. Effect of Oil Viscosity on Heavy Oil/Water Relative Permeability Curves. Paper SPE 99763 presented at the SPE/DOE Symposium in IOR, Tulsa, Oklahoma, USA, 22-26 April.
- Watson, R.W. and Ertekin, T. 1988. The Effect of Steep Temperature Gradient on Relative Permeability Measurements. Paper SPE 17505 presented at the SPE Rocky Mountain Regional Meeting, Casper, WY, 11-13 May.
- Welge, H.J. 1952. A Simplified Method for Computing Oil Recovery by Gas or Water Drive. *Petroleum Transaction AIME*, 195: 91-98.
- White, F.M. 2008. *Fluid Mechanics*, sixth edition. New York: McGraw-Hill.

Wilson, J.W. 1956. Determination of Relative Permeability Under Simulated Reservoir Conditions. *AIChE J.*, 2 (1): 94-100. DOI: 10.1002/aic.690020120.

Yang, P., Guo, H. and Yang, D. 2013. Determination of Residual Oil Distribution during Waterflooding in Tight Oil Formations with NMR Relaxometry Measurements. *Energy & Fuels*, **27**(10): 5750-5756.

Yortsos, Y. 1999. Displacement Regimes in Fully-Developed Steam Injection. Paper SPE 54117 presented at the SPE International Thermal Operations and Heavy Oil Symposium, Bakersfield, CA, 17-March.

Youngs, D.L. 1982. Time-Dependent Multi-Material Flow with Large Fluid Distortion In: Morton, K.W., Baines, M.J. (Eds.), *Numerical Methods for Fluid Dynamics*. Academic, New York. 273-285.

Youngs, E.G. 1960. The Drainage of Liquids from Porous Materials. *Journal of Geophysical Research*, 65 (12): 4025-4030.

Yuster, S.T. 1951. Theoretical Considerations of Multiphase Flow in Idealized Capillary Systems. Proc: 3rd World Petroleum Congress, Section II, The Hague: 437-445.

Zhou, D., Blunt, M., and Orr, JR.F.M. 1997. Hydrocarbon Drainage along Corners of Noncircular Capillaries. *Journal of Colloid and Interface Science*, 187: 11-21.